

UC San Diego

UC San Diego Electronic Theses and Dissertations

Title

Carbon dioxide signal transduction in Arabidopsis guard cells

Permalink

<https://escholarship.org/uc/item/0h47q7r1>

Author

Young, Jared

Publication Date

2005

Peer reviewed|Thesis/dissertation

UNIVERSITY OF CALIFORNIA, SAN DIEGO

Carbon Dioxide Signal Transduction in *Arabidopsis* Guard Cells

A dissertation submitted in partial satisfaction of the requirements for the
degree Doctor of Philosophy

in

Biology

by

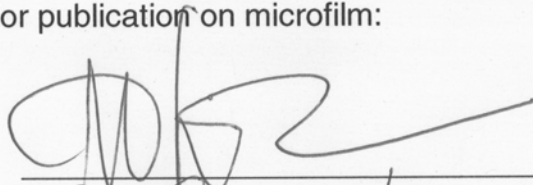
Jared Young

Committee in charge:

Professor Julian I. Schroeder, Chair
Professor Joanne Chory
Professor Maarten J. Chrispeels
Professor Walter Oechel
Professor Nick Spitzer
Professor Roger Y. Tsien

2005

The dissertation of Jared Young is approved, and it is acceptable in quality and form for publication on microfilm:



Richard C. Griffin

Rogery B. ...

Joanne Chouy

McDab

JTS

Chair

University of California, San Diego

2005

DEDICATION

This dissertation is dedicated to my research mentors, Sharron Lin and the late Gethyn Allen.

TABLE OF CONTENTS

Signature Page	iii
Dedication	iv
Table of Contents	v
Acknowledgements	vii
Vita and Publications.....	ix
Abstract	x
I. Introduction	1
II. Carbon dioxide signaling in guard cells via calcium response modulation and CO ₂ insensitivity of <i>gca2</i> mutant	8
A. Manuscript	8
B. Supplementary Data	45
III. Convergence of calcium signaling pathways of pathogenic elicitors and abscisic acid in <i>Arabidopsis</i> guard cells	63
IV. <i>Arabidopsis</i> HT1 kinase controls stomatal pore aperture in response to atmospheric CO ₂	107
A. Manuscript	107
B. Supplementary Data and Methods	125
V. Discussion	131
Appendices	
A. Methods Development	146

B. Phosphatidylinositol 3- and 4-phosphate are required for normal stomatal movements	164
C. Localization, ion channel regulation, and genetic interactions during abscisic acid signaling of the nuclear mRNA cap- binding protein, ABH1	208
D. The nitrate transporter AtNRT1.1 (CHL1) functions in stomatal opening and contributes to drought susceptibility in Arabidopsis	250

ACKNOWLEDGEMENTS

The text of Section A of Chapter II, in full, has been submitted for publication of the material by authors Young, J.J., Mehta, S., Grill, E., and Schroeder, J.I. I generated all data and was the primary writer for this paper.

The text of Chapter III, in full, is a reprint of the material as it appears in *Plant Physiology*, Klüsener, B., Young, J.J., Murata, Y., Allen, G.J., Mori, I.C., Hugouvieux, V., and Schroeder, J.I. (2002). I generated the data for Figures III-7A-C, Fig. III-8 A-D and some of the data for III-8E, and Table II, and was the primary writer for this paper.

The text of Chapter IV, in full, has been submitted for publication of the material by authors Hashimoto, M., Negi, J., Young, J., Schroeder, J.I., and Iba, K. I generated the data for Figure IV-2 A-D.

The text of Section B of the Appendix is a reprint of the material as it appears in *The Plant Cell*, Jung, J.-Y., Kim, Y.-W., Kwak, J.M., Hwang, J.-U., Young, J., Schroeder, J.I., Hwang, I., and Lee, Y. (2002). I generated some of the data for Fig. B-8.

The text of Section C of the Appendix is a reprint of the material as it appears in *Plant Physiology*, Hugouvieux, V., Murata, Y., Young, J.J., Kwak, J.M., Mackesy, D.Z., and Schroeder, J.I. (2002). I generated the data for Fig. C-7B.

The text of Section D of the Appendix is a reprint of the material as it appears in *The Plant Cell*, Guo, F.-Q., Young, J., Crawford, N.M. (2003). I contributed to the data for Figure D-4A.

VITA

- 1995-1997 Undergraduate Research, Dept. of Molecular and Cell Biology, University of California, Berkeley
- 1997 B.A., University of California, Berkeley
- 1997-1999 Research Technician, Edward Hines Jr. Veterans Affairs Hospital
- 1999-2005 Graduate Studies and Research, Division of Biological Sciences, University of California, San Diego
- 2005 Ph.D., University of California, San Diego

PUBLICATIONS

Guo, F.-Q., Young J. and Crawford N.M. The nitrate transporter AtNRT1.1 (CHL1) functions in stomatal opening and contributes to drought susceptibility in Arabidopsis. ***Plant Cell*** 15:107-117 (2003). www.plantcell.org

Klusener B.*, Young J.J.*, Murata Y., Allen G.J., Mori I.C., Hugouvieux V., and Schroeder J.I. Convergence of calcium signaling pathways of pathogenic elicitors and abscisic acid in Arabidopsis guard cells. ***Plant Physiology*** 130:2152-2163 (2002). www.plantphysiol.org

*These authors contributed equally to the paper.

Hugouvieux V., Murata Y., Young J.J., Kwak J.M., Mackesy D.Z., and Schroeder J.I. Localization, ion channel regulation and genetic interactions during abscisic acid signaling of the nuclear mRNA cap binding protein ABH1. ***Plant Physiology*** 130(3):1276-1287 (2002). www.plantphysiol.org

Jung J.-Y., Kim Y.-W., Kwak J.M., Hwang J.-U., Young J., Schroeder J.I., Hwang I. and Lee Y. Phosphatidylinositol 3- and 4-Phosphate are required for normal stomatal movements. ***Plant Cell*** 14:2399-2412 (2002). www.plantcell.org

Dhand R., Young J., Teng A., Krishnasamy S., and Gross N.J. Is dipalmitoylphosphatidylcholine a substrate for convertase? ***Am J Physiol Lung Cell Mol Physiol*** 278:L19-L24 (2000). <http://ajplung.physiology.org>

Gross N.J., Kellam M., Young J., Krishnasamy S., and Dhand R. Separation of Alveolar Surfactant into Subtypes. ***Am J Respir Crit Care Med*** 162:617-622 (2000). <http://ajrccm.atsjournals.org>

Dhand R., Young J., Krishnasamy S., Possmayer F., and Gross N.J. Influence of Phospholipid Composition on the Properties of Reconstituted Surfactants. ***Lung*** 177:127-138 (1999).

ABSTRACT OF THE DISSERTATION

Carbon Dioxide Signal Transduction in *Arabidopsis* Guard Cells

by

Jared Young

Doctor of Philosophy in Biology

University of California, San Diego, 2005

Professor Julian I. Schroeder, Chair

A complex signal transduction network operates in guard cells to regulate stomatal apertures. Though our understanding of this signaling network continues to deepen, many fundamental questions remain regarding the identities of the proteins and second messengers that function in the network and their roles. The work presented in this thesis describes important progress in our understanding of the components and mechanisms of the stomatal signaling network, in the reference plant *Arabidopsis thaliana*. This work is particularly focused on the role of calcium transients in stomatal signaling and on the signaling pathway regulated by carbon dioxide. Experiments were pursued to analyze calcium dynamics using time-lapse

imaging of transgenic guard cells, and stomatal phenotypes using gas exchange and direct microscopic measurements of stomatal apertures. Findings from several studies are reported here. Two of these studies identified important new components in the CO₂ signaling pathway. One suggests a role for calcium transients in stomatal responses to CO₂ and identified the *GCA2* gene as a regulator of CO₂ responses. The second characterized a novel kinase, *HT1*, that mediates guard cell CO₂ responses. A third project revealed common features of the stomatal signaling pathways activated by pathogenic elicitors and by abscisic acid (ABA), a drought stress hormone, and provided new information about calcium transients produced in guard cells in the absence of applied stimuli. Other stomatal signaling advances to which I contributed are also included. The findings presented in this thesis represent a substantial advance in our understanding of stomatal guard cell signal transduction.

CHAPTER I

Introduction

Cells must be able to respond to signals, both internal and external, in a manner consistent with organismal survival and success. The molecular events that enable cells to respond to stimuli collectively represent the process of signal transduction -- a process fundamental to the function of all cells. Signal transduction is widely researched in a variety of cellular contexts. My thesis research utilized the stomatal guard cell of *Arabidopsis thaliana* as a model system for signal transduction research.

Arabidopsis thaliana is the most popular model organism for biological research in the plant kingdom. It is a member of the mustard family native to Eurasia and North Africa. *Arabidopsis* has a number of useful attributes for genetic studies such as a short generation time, small size, prolific seed production, simple genome, and self-fertilization. Its popularity has led to the development of a wide and powerful assortment of molecular and genetic tools, including several mutant collections, efficient transformation techniques, a sequenced genome, and an expanding array of bioinformatics resources. This combination of beneficial research characteristics and useful available tools makes *Arabidopsis* a powerful biological model system.

Stomata are formed by a pair of guard cells surrounding a central pore. These stomatal pores are distributed throughout the epidermis of aerial plant

organs and are the sites of gas exchange between the plant and the atmosphere. Guard cells regulate stomatal pore size to optimize the rate of gas exchange for the prevailing conditions. To accomplish this, guard cells must be able to respond to a variety of signals including light, humidity, and carbon dioxide.

Stomatal aperture is determined by the turgor and shape of the guard cells. Guard cells are specialized for quick movement (quick for plants, that is), which is achieved by modulations in cell volume and turgor. Due to the particular architecture of the rigid cell wall that encloses the guard cell, swelling of the guard cell causes the cell to bow out, widening the stomatal pore. To achieve this swelling, the guard cell accumulates ions (most importantly K^+ and Cl^-), organic solutes (most importantly malate) and water. A drop in cell volume and turgor, achieved by a loss of ions, solutes, and water, causes the guard cell to collapse inward, closing the stomatal pore. Ionic currents in the plasma membrane and vacuole play key roles in accomplishing these turgor alterations. Signal transduction pathways must link the concentration of stimuli that affect guard cell aperture to the regulation of the ion channels that mediate these currents, as well as to metabolic processes that function in guard cell movements, such as metabolism of sugars and cell membrane trafficking.

The result of signal transduction events in guard cells which regulate stomatal aperture can be readily quantified by measuring either stomatal pore

size using a light microscope or the rate of leaf gas exchange using an infrared gas analyzer (IRGA)-based photosynthesis system. Components and mechanisms that function in guard cell signaling pathways can be identified through the use of mutants and pharmacology. The simple, robust methods available for quantifying the output of signal transduction combined with the powerful molecular genetic toolbox developed for Arabidopsis make the Arabidopsis guard cell an effective model system for studying eukaryotic signal transduction.

My thesis research had two related foci, and the majority of my efforts were directed at the intersection of those foci. The first focus was to elucidate the signal transduction pathway for guard cell responses to carbon dioxide. It has been known since the work of Freudenberger and Heath and colleagues in the 1940s and 50s that stomatal aperture is inversely correlated with the CO₂ concentration¹⁻³. Thus high CO₂ closes stomata while low CO₂ opens them. This response is physiologically intuitive, if stomatal aperture is viewed as a balance between maximizing CO₂ uptake for photosynthesis while minimizing water loss via transpiration. In this scenario, as the concentration of CO₂ declines, the stomata must open wider to receive more CO₂. Conversely, when the [CO₂] increases, stomata are given leave to close, since sufficient CO₂ can now be admitted at a lower rate of gas exchange, thus reducing the rate of water loss. In the absence of photosynthesis (i.e. in the dark), the leaf need not acquire CO₂, and the stomata are closed. Although this interpretation

of stomatal control may be oversimplified, it fits very well, to a first approximation, with the many measurements of stomatal conductance that have been reported in diverse plant species.

Understanding the CO₂ signaling pathway is critical due to the rising levels of atmospheric CO₂⁴, the established effect of CO₂ on stomatal apertures, and the central role of gas exchange in plant physiology and plant-environment interactions. Numerous studies have been conducted on the effects of increased CO₂ at the stomatal, whole plant and ecosystem levels⁵⁻¹⁰. These reports show that decreases in stomatal conductance in the range of 20-40% accompany a doubling of atmospheric CO₂. These reductions in stomatal conductance are likely to be largely responsible for the increases in productivity that also accompany growth in enriched CO₂. Since stomatal conductance reductions and productivity increases vary widely among species, increased CO₂ will almost certainly have major impacts on species distributions. Despite these important advances, the guard cell CO₂ signaling pathway is still poorly understood at the molecular level.

The second focus of my research has been to examine the role of cytosolic calcium transients in guard cell signal transduction. In the past decade calcium spiking has been studied in a variety of contexts, leading to an increased appreciation of how these spikes function in signal transduction¹¹⁻¹⁴. Recent work in our lab exploited the Arabidopsis guard cell to contribute to this expanding knowledge base¹⁵⁻¹⁷. I endeavored to further explore, through the

use of our model system, the ways in which cytosolic calcium transients can function in eukaryotic signaling systems. As mentioned, the central interest in my thesis research lay at the intersection of these two main goals: the study of the role of cytosolic calcium transients in CO₂ stomatal signaling.

In this thesis I present the manuscripts, all published in peer-reviewed journals or in the peer review process, that include my major findings. I also include descriptions of some of the techniques I developed during my research and additional supplementary data.

REFERENCES CITED

1. Freudenberg, H. Die Reaktion der Schliesszellen auf Kohlensäure und Sauerstoffentzug. *Protoplasma* **35**, 15-54 (1940).
2. Heath, O. V. S. Control of stomatal movement by a reduction in the normal carbon dioxide content of the air. *Nature* **161**, 179-81 (1948).
3. Heath, O. V. S. in *Handbuch der Pflanzenphysiologie* (ed. Ruhland, W.) 415-64 (Springer-Verlag, Berlin, 1959).
4. Leggett, J., Pepper, W. J. & Swart, R. J. in *Climate Change 1992: The Supplementary Report to the IPCC Scientific Assessment* (ed. Houghton JT, C. B., Varney SK) 69-95 (Cambridge University Press, Cambridge, 1992).
5. Ainsworth, E. A. & Long, S. P. What have we learned from 15 years of free-air CO₂ enrichment (FACE)? A meta-analytic review of the responses of photosynthesis, canopy. *New Phytologist* **165**, 351-371 (2005).

6. DeLucia, E. H., Hamilton, J. G., Naidu, S. L., Thomas, R. B., Andrews, J. A. et al. Net primary production of a forest ecosystem with experimental CO₂ enrichment. *Science* **284**, 1177-9 (1999).
7. LaDeau, S. L. & Clark, J. S. Rising CO₂ levels and the fecundity of forest trees. *Science* **292**, 95-8 (2001).
8. Medlyn, B. E., Barton, C. V. M., Broadmeadow, M. S. J., Ceulemans, R., De Angelis, P. et al. Stomatal conductance of forest species after long-term exposure to elevated CO₂ concentration: a synthesis. *New Phytologist* **149**, 247-264 (2001).
9. Woodward, F. I., Lake, J. A. & Quick, W. P. Stomatal development and CO₂: ecological consequences. *New Phytologist* **153**, 477-484 (2002).
10. Morison, J. I. L. Stomatal response to increased CO₂ concentration. *Journal of Experimental Botany* **49**, 443-452 (1998).
11. Kupzig, S., Walker, S. A. & Cullen, P. J. The frequencies of calcium oscillations are optimized for efficient calcium-mediated activation of Ras and the ERK/MAPK cascade. *Proceedings of the National Academy of Sciences of the United States of America* **102**, 7577-7582 (2005).
12. Borodinsky, L. N., Root, C. M., Cronin, J. A., Sann, S. B., Gu, X. et al. Activity-dependent homeostatic specification of transmitter expression in embryonic neurons. *Nature* **429**, 523-30 (2004).
13. Dolmetsch, R. E., Xu, K. & Lewis, R. S. Calcium oscillations increase the efficiency and specificity of gene expression. *Nature* **392**, 933-6 (1998).
14. Gomez, T. M. & Spitzer, N. C. In vivo regulation of axon extension and pathfinding by growth-cone calcium transients. *Nature* **397**, 350-5 (1999).

15. Allen, G. J., Chu, S. P., Harrington, C. L., Schumacher, K., Hoffman, T. et al. A defined range of guard cell calcium oscillation parameters encodes stomatal movements. *Nature* **411**, 1053-1057 (2001).
16. Allen, G. J., Chu, S. P., Schumacher, K., Shimazaki, C. T., Vafeados, D. et al. Alteration of stimulus-specific guard cell calcium oscillations and stomatal closing in *Arabidopsis det3* mutant. *Science* **289**, 2338-2342 (2000).
17. Klüsener, B., Young, J. J., Murata, Y., Allen, G. J., Mori, I. C. et al. Convergence of calcium signaling pathways of pathogenic elicitors and abscisic acid in *Arabidopsis* guard cells. *Plant Physiol* **130**, 2152-63 (2002).

CHAPTER II

Carbon dioxide signaling in guard cells via calcium response modulation and

CO₂ insensitivity of *gca2* mutant

Section A

Manuscript

ABSTRACT

Leaf stomata close in response to high carbon dioxide levels and open at low CO₂. CO₂ concentrations in leaves are altered by daily dark/light cycles, as well as the continuing rise in atmospheric CO₂. Relatively little is known about the molecular, cellular and genetic mechanisms of CO₂ signaling in guard cells. Interestingly, we report here that repetitive Ca²⁺ transients were observed during the stomatal opening stimulus low [CO₂]. Furthermore, low/high [CO₂] transitions modulated the cytosolic Ca²⁺ transient pattern in *Arabidopsis* guard cells (*Landsberg erecta*). Inhibition of these CO₂-regulated cytosolic Ca²⁺ transients, achieved by loading guard cells with the calcium chelator BAPTA and not adding external Ca²⁺, abolished both high CO₂-induced stomatal closing and low CO₂-induced stomatal opening. Furthermore, the mutant, *gca2*, shows impairment in [CO₂] modulation of the cytosolic Ca²⁺ transient rate and impairment in high CO₂-induced stomatal closing. Our findings provide new insights into guard cell CO₂ signaling mechanisms and demonstrate that calcium elevations can participate in opposed signaling events during stomatal opening and closing. A model is proposed in which CO₂ concentrations modulate Ca²⁺ sensors which can mediate specificity in Ca²⁺ signaling.

INTRODUCTION

Stomatal pores in aerial parts of plants close in response to high carbon dioxide concentrations and open at low $[CO_2]$. These changes in leaf CO_2 concentrations occur as a result of photosynthesis and respiration. Furthermore, atmospheric CO_2 is predicted to double in the present century¹. Numerous studies have been carried out to determine the effects of atmospheric CO_2 increases on plant gas exchange, carbon fixation, and growth, and the resulting impact this will have on natural and agricultural ecosystems²⁻⁶. One of the mechanisms by which increased atmospheric CO_2 affects plants is CO_2 regulation of stomatal apertures. Reports show that a doubling of atmospheric $[CO_2]$ causes significant stomatal closure by 20-40% in diverse plant species⁷⁻⁹.

Stomata experience diurnal changes in $[CO_2]$ inside the leaf during light/dark transitions. In the dark CO_2 is produced in leaves by cellular respiration. The $[CO_2]$ shifts caused by illumination changes are rapid and large, with $[CO_2]$ in the stomatal cavity ranging from 200 ppm to 700 ppm¹⁰.

Stomatal aperture is controlled by the turgor pressure in the guard cells surrounding the stomatal pore. Guard cell turgor pressure is mediated by the ion and organic solute concentration in guard cells. To date little is known about the molecular processes that mediate CO_2 regulation of stomatal apertures. Elevated CO_2 has been shown to enhance potassium efflux

channel and S-type anion channel activities that mediate extrusion of ions during stomatal closure^{11,12}, and chloride release from guard cells is triggered by CO₂ elevation¹³. Furthermore CO₂ activation of R-type anion channel currents was found in a subset of *Vicia faba* guard cells¹².

Little is known about the CO₂ signal transduction mechanisms that function upstream of ion channels in guard cells¹⁴⁻¹⁷. CO₂-induced stomatal movements were previously found to be absent in two mutants that affect the stomatal closure signaling network for the drought stress hormone abscisic acid (ABA): *abi1-1* and *abi2-1*¹⁸. However, CO₂ responsiveness was reported in these mutants using different experimental conditions^{19,20}. Another ABA-insensitive mutant, *ost1*, shows a wildtype response to [CO₂]²¹. Although the *abi1-1* and *abi2-1* mutants can show a conditional effect, no strong CO₂-insensitive stomatal movement response mutant has been reported to date. Characterization of genetic mutants that strongly impair CO₂ modulation of stomatal movements would aid in dissecting the molecular mechanisms of CO₂ signaling.

Studies have suggested a role for Ca²⁺ in mediating CO₂-induced stomatal closing^{22,23}. High [CO₂] induces cytosolic Ca²⁺ elevation in *Commelina communis* guard cells²². Many studies have established that cytosolic calcium functions in mechanisms that mediate stomatal closing^{14-16,24-30}. Furthermore, some studies have also indicated a role for calcium increases in the opposing response of stomatal opening³¹⁻³³. It is unclear how

these opposite responses could be directed via elevations in the same second messenger, Ca^{2+} .

CO_2 is a particularly interesting stomatal stimulus with respect to cytosolic Ca^{2+} responses, as demonstrated in the present study. CO_2 can induce stomatal opening or closing depending on its concentration³⁴. Studies in animal and plant cells have shown that different patterns of repetitive calcium transients could yield distinct responses, and that the frequency of the calcium transients seems particularly relevant for the direction of differing outcomes^{27,35-37}. Although previous studies have shown a role for calcium in CO_2 signaling in guard cells^{22,23}, changes in repetitive calcium transient patterns have not yet been studied in guard cells in response to CO_2 . The present study demonstrates CO_2 -modulation of repetitive calcium transient patterns in *Arabidopsis* guard cells and characterizes roles of Ca^{2+} in CO_2 -regulated stomatal opening and closing. In addition, we show that the abscisic acid-insensitive mutant, *gca2*, exhibits a strong CO_2 insensitivity in cytosolic Ca^{2+} pattern regulation, in stomatal aperture regulation and in CO_2 regulation of stomatal conductance changes in leaves. Furthermore, findings including repetitive cytosolic Ca^{2+} elevations in response to low CO_2 lead us to propose a new model in CO_2 and stomatal signaling, in which CO_2 signal transduction includes modulation of guard cell Ca^{2+} sensors.

MATERIALS AND METHODS

Plant Growth and Calcium Imaging. *A. thaliana* plants were grown in Conviron growth chambers with a 16 hour light/8 hour dark cycle at $75 \mu\text{mol m}^{-2} \text{s}^{-1}$ and 20°C . Cytosolic calcium imaging in guard cells expressing yellow cameleon 2.1 was performed as previously described^{38,39}. Resolution of long term $[\text{Ca}^{2+}]_{\text{cyt}}$ dynamics was achieved by choosing cells with significant fluorescence and limiting epifluorescence excitation. Ca^{2+} imaging data were captured using a 60x Plan Apo oil lens with a n.a. of 1.4 (Nikon, Tokyo, Japan) and a CCD camera (ORCA 100, Hamamatsu Photonics, Hamamatsu City, Japan). 4x pixel binning was used (yielding 16 pixels per bin); each bin measured an area of approximately $0.10 \mu\text{m}^2$. Light was provided by a 75 watt xenon short arc lamp (Osram, Berlin, Germany) and light intensity was reduced 32x using neutral density filters. Guard cells exhibiting an average YFP fluorescence intensity of at least 250 counts per bin during a 200-400 ms exposure time were analyzed.

To analyze guard cells in intact epidermes, leaves were gently pressed abaxial side down onto a coverslip with a very thin coating of medical adhesive (Hollister, Libertyville, IL). Upper cell layers were then carefully removed using a razor blade. Leaf epidermes were preincubated for 2-4 hours in white light ($125 \mu\text{mol m}^{-2} \text{s}^{-1}$) in buffer (10 mM KCl, 50 μM CaCl_2 , 10 mM Mes-Tris pH 6.15) that had been rendered nominally CO_2 -free by bubbling overnight with

air depleted of CO₂ by passage through a CO₂ absorbing mesh (Ascarite II, Thomas Scientific, or soda lime).

For experiments in which BAPTA-AM was used, cells were first imaged in the standard imaging buffer. Then cells were incubated in 10 mM KCl, 10 mM Mes-Tris pH 6.15, 25 μM BAPTA-AM, 300 μM eserine (an esterase inhibitor, Sigma catalog number E-8375), and 0.025% Pluronic F-127 (an amphiphile) at ambient CO₂. The eserine and Pluronic F-127 were added to improve the stability, solubility, and cell loading of the BAPTA-AM⁴⁰.

Uncleaved BAPTA-AM does not bind Ca²⁺ with a high affinity and addition of an esterase inhibitor to the medium aids in ensuring that BAPTA-AM is not cleaved by cell wall esterases prior to cell loading⁴⁰. Finally the cells were exposed to the same buffer with the eserine removed, equilibrated with CO₂-depleted air. In CO₂-controlled buffers the pH did not deviate more than 0.05 pH units from pH 6.15.

CO₂ Application During Calcium Imaging Experiments. Epidermes affixed to coverslips were adhered to a glass slide with a hole drilled in the middle, creating a shallow well (1.22 cm², 200 μl capacity). This well was perfused via a peristaltic pump and Teflon tubing with the same buffer used in the preincubations, pre-bubbled either with CO₂ depleted air, gas from a compressed gas tank containing 740 ppm or 800 ppm CO₂ in air, or air with 800 ppm CO₂ added by a CO₂ mixer using a Li-6400 gas exchange analyzer

(LI-COR Inc., Lincoln, NE). Leaf epidermes were perfused with the buffer that they would be first recorded in (buffer bubbled with the indicated CO₂ concentration) for 10-15 minutes before recordings began. Perfusion rate was 85 seconds per ml, and the buffer transit time (the time from when the buffer was taken from the bubbled CO₂-equilibrated source until the buffer reached the imaging well) was 90 seconds.

Determination of [CO₂] in Perfused Buffers. Buffer equilibrated by bubbling with CO₂-free or high CO₂ air was perfused into the well used for calcium imaging, then collected a short time later (~ 3-5 seconds) in an airtight glass syringe, to estimate the final CO₂ concentration to which stomata were exposed. CO₂-free air was introduced into the syringe, and the [CO₂] in the buffer and air was equilibrated by shaking for 5 minutes. The [CO₂] of the equilibrated air was then measured using a Li-6400 gas exchange analyzer (LI-COR Inc., Lincoln, NE). The CO₂ content of the buffer was calculated by performing calibration measurements and a mass balance as described ⁴¹. The [CO₂] content of buffer equilibrated with 740 ppm [CO₂] was estimated by interpolation from 800 ppm and 0 ppm CO₂ measurements.

Automated [Ca²⁺] Transient Analysis. [Ca²⁺]_{cyt} transients were automatically detected using a modified version of a MATLAB (MathWorks, Natick, MA) program ⁴². The first derivative of 535 nm/480 nm cameleon ratio data was

convolved with a Haar function with a width of 186 seconds. The transformed data traces produced from the convolution were then analyzed for areas with high correlation; i.e. areas that matched the shape of the function. A detection threshold was set for data traces, thus times at which the transformed data exceeded the detection threshold were counted as $[Ca^{2+}]_{cyt}$ transients. A reset threshold of -0.1 was also used for all data traces, requiring that the transients returned to low values before another transient could be counted; this prevented high frequency noise near the detection threshold from being registered as $[Ca^{2+}]_{cyt}$ transients. Programs are available upon request. For wavelet analysis, raw data traces were transformed with the Morlet wavelet using the MATLAB Wavelet Toolbox⁴³. A larger scale value in wavelet analyses corresponds to both wider spikes and longer periodicities. The maximum scale illustrated (Fig. II-1D) corresponds to a waveform spanning approximately 10 minutes.

Gas Exchange. Measurements of stomatal conductance were performed in intact leaves using a Li-6400 infrared gas analyzer (IRGA)-based gas exchange system (LI-COR Inc., Lincoln, NE). The first series of wildtype experiments were performed at 23 °C and a photon flux density of 500 $\mu\text{mol m}^{-2} \text{s}^{-1}$. Experiments analyzing the *gca2* mutant were performed in parallel to additional wildtype experiments at 26.5 °C and 75 $\mu\text{mol m}^{-2} \text{s}^{-1}$. Average gas exchange traces in Fig. II-1B were aligned upon returning to low CO_2 .

Stomatal Aperture Measurements. Leaf epidermes were prepared as described above to maintain an intact leaf epidermal environment using the same conditions as in Ca^{2+} imaging experiments (see Calcium imaging). All assays were performed as double blind experiments, in which both the plant genotype and the CO_2 concentration were unknown or both the \pm BAPTA-AM treatment and the $[\text{CO}_2]$ were unknown to the experimenter. Just prior (~ 2 min) to stomatal aperture measurements, fluorescein diacetate (dissolved in acetone) was added at 0.0007% (w/v) to visualize live cells. Only live stomatal guard cells that were completely surrounded by live pavement cells were chosen for measurements. Control wildtype responses were analyzed within experiment sets. Buffers were identical to those used in calcium imaging experiments for direct comparisons. CO_2 concentrations were imposed by equilibrating solutions with an air stream containing a defined CO_2 concentration. Samples were exposed to a light fluence rate of $130 \mu\text{mol m}^{-2} \text{s}^{-1}$. For BAPTA-AM experiments (Fig. II-2C), buffers and treatments were the same as for calcium imaging (see Calcium imaging): samples were exposed to a 2-4 hour preincubation in control buffer, followed by an additional 10 minute preincubation in either control buffer or BAPTA-AM buffer (containing eserine and Pluronic F-127), and finally a 1 hour incubation in CO_2 -controlled buffer (either control buffer or BAPTA-AM buffer without the eserine) prior to measurements. For experiments with *gca2* (Fig. II-3C), samples were exposed

to a 2-4 hour preincubation in control buffer, followed by a 2 hour incubation in CO₂-controlled buffer prior to measurements.

RESULTS

Cytosolic Calcium Responses to Changes in [CO₂]. To examine the role of calcium in stomatal CO₂ responses, calcium imaging was performed on *Arabidopsis* (cv. Landsberg *erecta*) guard cells expressing the pH and Cl⁻-insensitive GFP-based calcium indicator isoform yellow cameleon 2.1⁴⁴, which allows long-term (> 90 min) ratiometric measurements of changes in free [Ca²⁺]_{cyt} in guard cells^{38,39}. Leaf epidermes were pre-exposed to nominally CO₂-free buffer and then guard cells were analyzed in CO₂-free buffer and then exposed to elevated CO₂ buffer. Interestingly, more [Ca²⁺]_{cyt} transients were produced in the low CO₂ (stomatal opening) buffer than in the elevated CO₂ (stomatal closing) buffer (Fig. II-1A). This CO₂-induced shift in the [Ca²⁺]_{cyt} transient rate was observed in the majority of guard cells (36 of 41; 88%). Leaf epidermes were subsequently returned to CO₂-free buffer again, and the transient rate increased (Fig. II-1A). This reversibility in the [Ca²⁺]_{cyt} transient rate was observed in 78% of cells (32 of 41). Thus in guard cells the rate of [Ca²⁺]_{cyt} transient production decreased after the switch from low CO₂ buffer to high CO₂ and increased after the switch back to low CO₂ buffer (Fig. II-1A), providing evidence that repetitive [Ca²⁺]_{cyt} transients occur

at low CO₂, a condition that mediates stomatal opening. Furthermore, the [Ca²⁺]_{cyt} transient rate is modulated by CO₂ concentration changes. Gas exchange experiments in which a similar series of [CO₂] changes were imposed showed a reduction in stomatal conductance in response to high CO₂ and a subsequent reopening of stomata upon the return to CO₂-free air, showing robust CO₂ responses in *Arabidopsis* (cv. Landsberg *erecta*) leaves (Fig. II-1B).

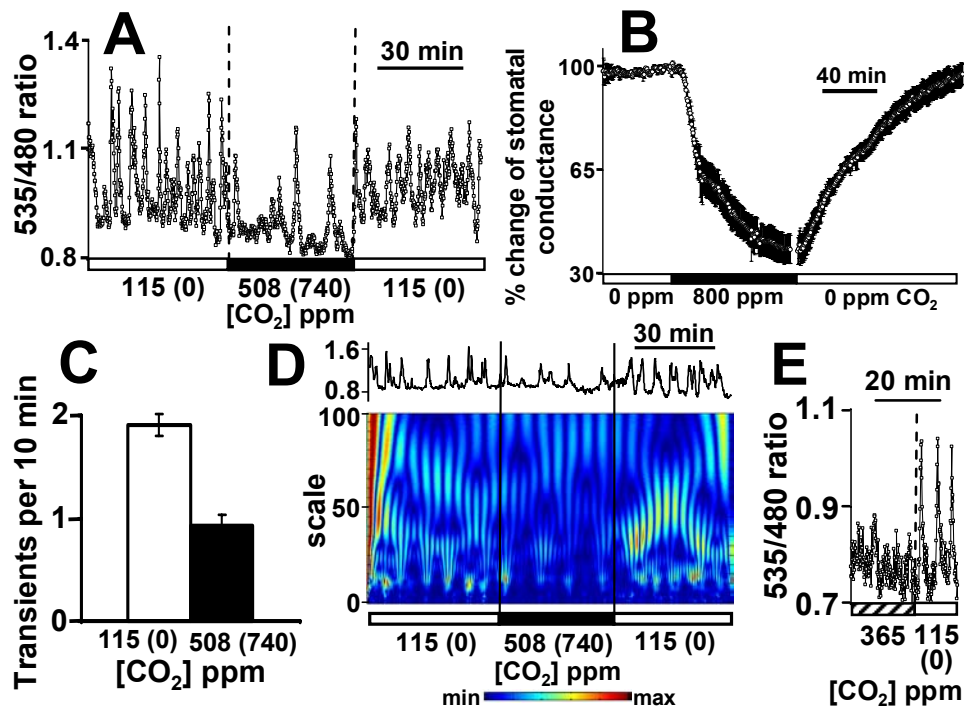


Figure II-1: The rate of cytosolic calcium transient production in guard cells is modulated by an increase in the CO₂ concentration. (A) Cytosolic calcium changes in a guard cell pre-exposed to low CO₂, switched to high CO₂, then returned to low CO₂ as indicated. (B) Stomatal conductance changes in response to similar [CO₂] changes as in (A). (C) Automated [Ca²⁺]_{cyt} transient detection program analysis of [Ca²⁺]_{cyt} transient rates in guard cells first exposed to low CO₂ buffer, then to high CO₂, and subsequently again to low CO₂ (n = 41 cells, values are means ± s.e.m.). A. *thaliana* plants (Landsberg *erecta* ecotype) were grown in Conviron growth chambers with a 16 hour light/8 hour dark cycle at 75 μE m⁻² s⁻¹ and 20 °C. (D) Wavelet analysis shows CO₂-induced alteration of cytosolic Ca²⁺ elevation pattern in guard cells. Top: Raw data trace; Y-axis depicts the cameleon ratio as in (A). Bottom: Corresponding wavelet transformation of the data trace above shows change in Morlet wavelet parameters at high CO₂. Colors represent the strength of the frequency component at a given coordinate. (E) Cytosolic calcium changes in a guard cell pre-exposed to ambient CO₂, then switched to low CO₂ as indicated. Where two CO₂ concentrations are listed, in all figures, the first value is the final [CO₂] bathing the cells, the second value (listed in parentheses) is the [CO₂] of the air bubbled into the buffer source prior to perfusion from the source to the recording chamber (see Materials and Methods).

To pursue standardized analyses of $[Ca^{2+}]_{cyt}$ data, software was developed to analyze $[Ca^{2+}]_{cyt}$ transient rates. $[Ca^{2+}]_{cyt}$ transients were automatically detected based on pre-defined search parameters. This approach allows an automated, consistent basis for $[Ca^{2+}]_{cyt}$ transient analysis throughout experiments. The $[Ca^{2+}]_{cyt}$ transient rate was calculated by determining the number of $[Ca^{2+}]_{cyt}$ transients detected within the time windows analyzed. The average $[Ca^{2+}]_{cyt}$ transient rate under low and elevated CO_2 concentrations was determined for all cells, including non-responsive cells, and found to be significantly different (Fig. II-1C; $P < 0.001$ $n = 41$).

Additional approaches were pursued to further analyze CO_2 modulation of $[Ca^{2+}]_{cyt}$ transient patterns. Wavelet transformation allows data analyses at a range of widths of wavelet functions⁴⁵. This ensures that the results found with the transient detection software are not dependent on the specific function width chosen. Independent wavelet analyses also showed clear reversible changes in the Ca^{2+} elevation pattern in response to CO_2 concentration changes as shown in Fig. II-1D. Ca^{2+} imaging traces were transformed with a Morlet wavelet⁴³. The goodness of fits of the waveform to the imaging trace is depicted by the color scale. The weaker colors in high CO_2 indicate that there are fewer transients in high CO_2 across all function widths (scales) shown. Thus transitions from low $[CO_2]$ to high $[CO_2]$ cause a significant change in the $[Ca^{2+}]_{cyt}$ transient pattern in guard cells (Fig. II-1 C and D). Amplitudes of Ca^{2+} transients were compared at low CO_2 and high CO_2 by analyzing ratio

changes during the initial two CO₂ exposures, before substantial bleaching of the YFP acceptor occurred⁴⁴. Ca²⁺ transient ratios were 0.26 ± 0.02 ratio units at low CO₂ and 0.21 ± 0.02 ratio units at high CO₂ ($P > 0.1$, $n = 11$ guard cells), suggesting no dramatic effects of CO₂ on [Ca²⁺]_{cyt} transient amplitudes under the imposed conditions.

To further investigate [CO₂] modulation of the [Ca²⁺]_{cyt} transient rate, calcium imaging was also performed on cells exposed to the opposite series of [CO₂] regimes. Cells were first exposed to elevated [CO₂], switched to low CO₂ and finally switched back to elevated [CO₂]. In these experiments, 69% (18 of 26) showed an increase in the transient rate upon switching from elevated [CO₂] to low CO₂, and the majority of those cells (15 of 18, 58% of 26 guard cells) showed a decrease in the transient rate when they were returned to elevated CO₂. Automated analyses show a statistically significant difference in the [Ca²⁺]_{cyt} transient rates produced in high and low CO₂ using this protocol (high CO₂: 0.95 ± 0.13 , low CO₂: 1.55 ± 0.16 transients per 10 minutes, $n = 26$ guard cells, $P = 0.005$). Note that, for a given cell, the relative change in [Ca²⁺]_{cyt} transient rate in response to a physiological stimulus may be more relevant than the absolute observed [Ca²⁺]_{cyt} transient rate during stimulation, which can depend on experimental conditions⁴⁶⁻⁴⁹. Experiments were also performed using ambient CO₂. A switch from ambient CO₂ to low CO₂ could enhance [Ca²⁺]_{cyt} transients (Fig. II-1E), but larger CO₂ shifts showed more robust [Ca²⁺]_{cyt} pattern changes.

Analysis of CO₂ Concentrations in Calcium Imaging Experiments. During calcium imaging, epidermes were placed in a shallow well and perfused via a peristaltic pump and Teflon tubing with buffers equilibrated with air containing either 0 ppm CO₂ or high CO₂ (740 or 800 ppm). During travel of the buffer through the Teflon tubing and residence of the buffer in the well, a significant amount of equilibration of the [CO₂] with the ambient air should occur⁵⁰. The CO₂ content of the buffers bathing the epidermes during calcium imaging was estimated (see Materials and Methods). [CO₂] of buffer equilibrated with 0 ppm CO₂ was 115 ± 11 ppm, [CO₂] of buffer equilibrated with 740 ppm CO₂ was interpolated to 508 ppm, and [CO₂] of buffer first equilibrated with 800 ppm was 535 ± 23 ppm (± s.e.m., n=3). Based on these measured values, the [CO₂] of buffer first equilibrated with 740 ppm was estimated to be about 508 ppm.

Stomatal Responses to [CO₂] Shifts in the Absence of [Ca²⁺]_{cyt}

Transients. Interestingly, commencement of the stomatal aperture response to a CO₂ shift occurs within 5 minutes (Fig. II-1*B*), whereas a longer period of time would be required to establish a new calcium transient pattern (Fig. II-1 *A* and *D*). This indicates that the calcium elevation pattern changes may not directly function in the early guard cell CO₂ responses (see Discussion). Therefore, to test whether [Ca²⁺]_{cyt} transients function in CO₂ regulation of

stomatal movements, we sought a condition under which these transients are abolished.

Guard cells were loaded with the calcium chelator BAPTA, using an esterified form, BAPTA-AM. Incubation of leaf epidermes with a buffer containing 25 μM BAPTA-AM and no added extracellular calcium caused cessation of $[\text{Ca}^{2+}]_{\text{cyt}}$ transients in 12 of 12 cells in CO_2 -free buffer (Fig. II-2A). In contrast perfusion of cells with a 0.1 mM KCl buffer in which 200 μM EGTA and no Ca^{2+} was added caused cytosolic Ca^{2+} elevations in some cells. This can be attributed to residual micromolar ($> 10 \mu\text{M}$) Ca^{2+} in the utilized media (inductively-coupled plasma spectroscopy data, not shown), the low EGTA concentration and exchangeable Ca^{2+} in the cell wall matrix⁵¹, which together with the hyperpolarized potentials at low $[\text{K}^+]$ would electrochemically cause Ca^{2+} influx even from a submicromolar extracellular free Ca^{2+} pool, unless high (e.g. 10 mM) EGTA concentrations are added (<http://www.nature.com/nature/journal/v411/n6841/extref/4111053aa.html>). After $[\text{Ca}^{2+}]_{\text{cyt}}$ inhibition baseline ratios changed by only -0.015 ± 0.007 ($n = 12$), indicating no dramatic changes in baseline $[\text{Ca}^{2+}]_{\text{cyt}}$, which contrasts with dramatic reduction in baseline $[\text{Ca}^{2+}]_{\text{cyt}}$ induced by nicotinamide⁴⁸. Note that the esterified 25 μM BAPTA-AM (Fig. II-2A) does not chelate Ca^{2+} (see Methods). Thus the combination of BAPTA loading into cells without addition of Ca^{2+} to the external buffer effectively inhibited $[\text{Ca}^{2+}]_{\text{cyt}}$ elevations in guard cells (Fig. II-2A).

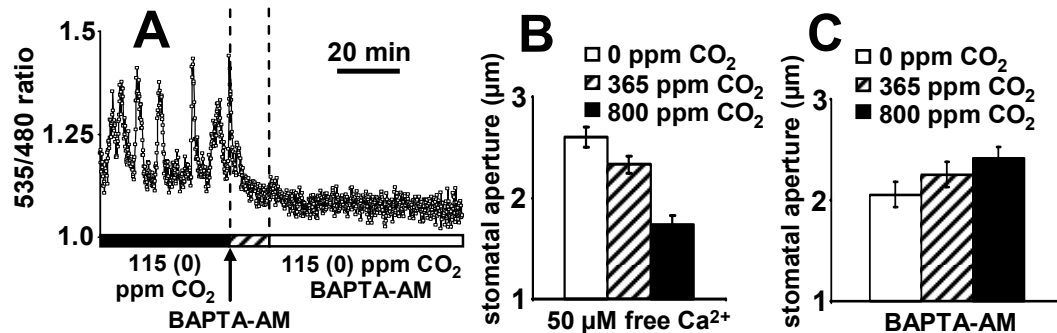


Figure II-2: Loading guard cells with the calcium chelator BAPTA and removing external calcium prevents both $[Ca^{2+}]_{cyt}$ transients in guard cells and CO_2 regulation of stomatal movements. (A) Repetitive $[Ca^{2+}]_{cyt}$ transients recorded in guard cells exposed to low CO_2 solution. Transients were first observed in buffer with 50 μM added Ca^{2+} and low CO_2 . Subsequent incubation with buffer containing 25 μM BAPTA-AM without added calcium led to cessation of repetitive $[Ca^{2+}]_{cyt}$ transients. (B,C) Stomatal apertures following 1 hour incubation in buffers containing 0 ppm CO_2 (white bars), ambient ~ 365 ppm $[CO_2]$ (striped bars), or elevated 800 ppm $[CO_2]$ (black bars) with (B) 50 μM free external calcium or with (C) no added calcium and 25 μM BAPTA-AM ($n = 5$ experiments, 200 stomata per condition in (B), $n = 3$ experiments, 120 stomata per condition in (C)). Values are means \pm s.e.m.).

We then analyzed whether CO_2 -induced stomatal movements are affected when repetitive cytosolic Ca^{2+} transients are abolished. We determined that measurement of robust CO_2 -induced stomatal movement responses in leaf epidermes requires intact epidermal pavement cells surrounding the analyzed stomata. Thus we added a viability stain (fluorescein diacetate) immediately prior to aperture measurements to allow collection of stomatal aperture data exclusively from guard cells surrounded by live pavement cells. In control experiments with 50 μM Ca^{2+} added to the bath solution, stomatal responses to shifts from ambient $[CO_2]$ to either low $[CO_2]$ or

high $[\text{CO}_2]$ showed typical CO_2 -induced stomatal opening and closing responses, respectively (Fig. II-2B; $P = 0.01$ for 0 CO_2 vs. ambient CO_2 , $P < 0.001$ for 800 ppm CO_2 vs. ambient CO_2). However CO_2 -induced stomatal closing and opening did not occur when cells were treated under conditions in which calcium transients were abolished (incubation with BAPTA-AM and absence of added external calcium) (Fig. II-2C; $P > 0.42$ for 0 ppm CO_2 vs. ambient CO_2 , $p 0.28$ for 800 ppm CO_2 vs. ambient CO_2). Thus chelation of internal calcium coupled with an absence of added external calcium both silenced $[\text{Ca}^{2+}]_{\text{cyt}}$ transients (Fig. II-2A) and prevented CO_2 regulation of both CO_2 -regulated stomatal closing and stomatal opening (Fig. II-2C), suggesting that $[\text{Ca}^{2+}]_{\text{cyt}}$ is necessary for the opposing CO_2 -induced guard cell stomatal closing and stomatal opening responses.

Identification and Characterization of a CO_2 -Insensitive Mutant. Strong CO_2 insensitive mutants in stomatal movement responses remain to be identified (see Introduction). To further analyze the significance of CO_2 -regulated $[\text{Ca}^{2+}]_{\text{cyt}}$ transient rate changes for stomatal movements, we analyzed CO_2 signal transduction in stomatal response mutants. Guard cells from the dominant abscisic acid (ABA) insensitive protein phosphatase 2C mutant *abi1-1* showed a reduction in the $[\text{Ca}^{2+}]_{\text{cyt}}$ transient rate upon elevation of CO_2 in 19 of 23 cells and a significantly different average number of transients produced in low and elevated CO_2 , showing a CO_2 response (Fig.

II-3A, $P < 0.001$). Guard cells of the recessive abscisic acid-insensitive *gca2* (*growth controlled by abscisic acid*) mutant have been previously documented to show an aberrant pattern of $[Ca^{2+}]_{cyt}$ transient production compared to wildtype in abscisic acid signal transduction²⁷. Interestingly, when guard cells of the *gca2* mutant were exposed to elevations in $[CO_2]$, no marked change in the $[Ca^{2+}]_{cyt}$ transient rate was observed, whereas parallel wildtype controls (*Ler*) showed typical changes in the transient rate (Fig. II-3A and B). When cells were recorded sequentially in low CO_2 buffer, high CO_2 buffer and then low CO_2 buffer again, only 24% of *gca2* guard cells (7 of 29) reversibly produced more transients in the CO_2 -free buffer than in the high CO_2 buffer. Furthermore, the average rates of $[Ca^{2+}]_{cyt}$ transients in *gca2* guard cells exposed to low and high CO_2 were similar (Fig. II-3A, $P = 0.88$).

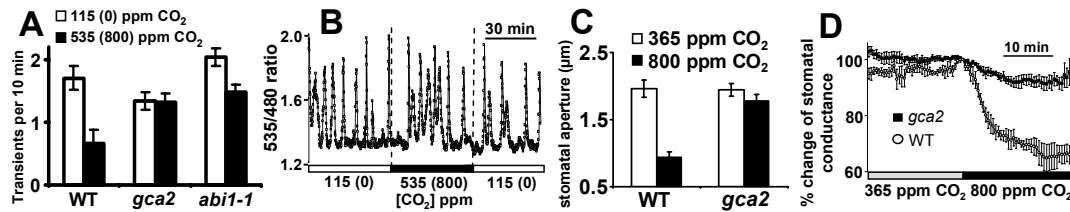


Figure II-3: CO₂ regulation of [Ca²⁺]_{cyt} transients in guard cells and CO₂-induced stomatal closing are impaired in the *gca2* mutant. (A) Automated analysis of [Ca²⁺]_{cyt} transient rates in low CO₂ buffer (white bars) and high CO₂ (black bars) in *gca2* guard cells (n = 29), wild type guard cells (n = 11) recorded in parallel, and *abi1-1* guard cells (n = 23) exposed to low CO₂, then high CO₂, then low CO₂ again. (B) Repetitive [Ca²⁺]_{cyt} transients in a *gca2* guard cell using the protocol described in (A). (C) Stomatal apertures of wildtype and *gca2* following 2 hour incubations in buffers containing ambient (~365) CO₂ (white bars) or elevated (800 ppm) CO₂ (black bars; n = 3 experiments, 120 total stomata per condition). (D) Stomatal conductance changes in intact leaves of whole plants from wildtype (open circles) and *gca2* (closed squares) in response to an increase in [CO₂]. Conductance was normalized to the average conductance at the last 365 ppm data point, averages were 0.0975 ± 0.004 mol m⁻² s⁻¹ in wild type, and 0.126 ± 0.009 mol m⁻² s⁻¹ in *gca2* (n = 4 leaves per genotype). Values in (A), (C), and (D) are means ± s.e.m.

The physiological relevance of the impairment of high CO₂ modulation of the [Ca²⁺]_{cyt} transient rate in *gca2* was investigated by analyzing CO₂-induced stomatal closure responses in leaf epidermis of the *gca2* mutant and wildtype (*Ler*) controls. In contrast to wild type, high CO₂-induced stomatal closure was not observed in *gca2* in stomatal aperture measurements (Fig. II-3C, P < 0.001 for wildtype, P > 0.20 for *gca2*). Next, gas exchange analyses were pursued to determine whether the *gca2* mutant impairs CO₂ responses in intact leaves of growing plants. A small CO₂-induced stomatal closure response was resolved in *gca2* in response to [CO₂] elevation (Fig. II-3D).

However, CO₂-induced reduction in stomatal conductance was dramatically weaker in *gca2* than in wild type leaves (Fig. II-3D, $P < 0.001$). The stomatal density in leaves of *gca2* plants did not differ from wildtype controls (WT 90 ± 19 stomata mm⁻², *gca2* 89 ± 2 stomata mm⁻², \pm s.e.m., $n = 3$, $P = 0.9$). Thus guard cells of the *gca2* mutant showed no statistically significant shifts in the [Ca²⁺]_{cyt} transient rate in response to [CO₂] elevation (Fig. II-3 A and B), and showed strongly attenuated stomatal movements in response to [CO₂] elevation in leaf epidermes and in intact leaves of plants (Fig. II-3 C and D). These data show that *gca2* is a strong elevated CO₂-insensitive mutant and provide genetic evidence that modulation of the [Ca²⁺]_{cyt} transient rate is a component of CO₂ signal transduction in guard cells.

DISCUSSION

Understanding the molecular mechanisms by which CO₂ modulates stomatal apertures is fundamental to understanding the regulation of gas exchange between plants and the atmosphere, and is important for elucidating effects of the combined diurnal changes in leaf [CO₂]¹⁰ and the continuing atmospheric CO₂ elevation on stomatal movements^{3-5,7,8,16}. Our findings build upon an earlier study showing that [Ca²⁺]_{cyt} elevations function in CO₂-induced stomatal movements²² and in addition demonstrate the presence of repetitive [Ca²⁺]_{cyt} transients during guard cell CO₂ signaling. Furthermore, in the present

study we reveal that even at low CO₂ concentrations, that mediate stomatal opening, repetitive [Ca²⁺]_{cyt} transients occur (Figs. II-1 A, D and E, II-2A and II-3B). Furthermore, guard cell [Ca²⁺]_{cyt} imaging experiments for > 90 min show that CO₂ concentration changes modulate the [Ca²⁺]_{cyt} transient pattern in guard cells, as determined by automatic transient detection and wavelet analyses (Fig. II-1 C and D). Moreover both CO₂-induced stomatal closing and CO₂-induced stomatal opening are abolished when [Ca²⁺]_{cyt} transients are experimentally repressed (Fig. II-2). In addition, the *gca2* mutant shows insensitivity to elevated CO₂ in modulation of the [Ca²⁺]_{cyt} transient rate, stomatal closing and stomatal conductance responses in intact leaves showing that *gca2* is a relatively strong high-CO₂ insensitive mutant (Fig. II-3).

Ca²⁺ sensor facilitation model. Our data show that elevated CO₂ causes slow repetitive [Ca²⁺]_{cyt} transients in guard cells, similar to those that function in ABA signaling^{27,28,38}, while low CO₂ causes rapid [Ca²⁺]_{cyt} transients (Figs. II-1 and II-2A). It has been shown that cytosolic calcium transients in guard cells will trigger immediate (Ca²⁺ reactive) stomatal closure^{27,49,52}. Such a stomatal closing response would seem unlikely when the calcium transients are produced in response to a stomatal opening stimulus such as low CO₂. Indeed, the rapid [Ca²⁺]_{cyt} transients induced by low CO₂ in guard cells (Figs. II-1, II-2A, and II-3B) did not cause measurable short term Ca²⁺ reactive stomatal closure responses based on time-resolved stomatal movement

imaging analyses (J. Young, unpublished results). This finding indicates that the stomatal opening signal, low CO₂, produces a signal transduction state or “physiological address”⁵³ in guard cells that does not permit strong Ca²⁺ reactive stomatal closing events to proceed. These results lead us to propose a new model in which, rather than solely causing different patterns of [Ca²⁺]_{cyt} increases, physiological stimuli may also modulate the appropriate calcium sensors (sensor facilitation), affecting when they can respond to [Ca²⁺]_{cyt} transients.

Previous studies showing spontaneous [Ca²⁺]_{cyt} elevations in guard cells and abscisic acid-induced dampening of these [Ca²⁺]_{cyt} transients^{39,48} indicate that ABA-induced stomatal closing may also make use of Ca²⁺ sensor modulation (facilitation) during stomatal closing. Consistent with this model, a previous study demonstrated that [Ca²⁺]_{cyt} activation of guard cell anion channels can be turned off or inactivated by prior incubation conditions of guard cells⁵⁴. Future studies of Ca²⁺ sensor functions and modifications in guard cells could provide a novel approach and valuable insights into the mechanisms by which opposing cellular responses can be mediated by Ca²⁺ in the same cell type.

Interestingly, the present study provides evidence that [CO₂] modulation of the cytosolic Ca²⁺ transient rate itself is not involved in the earliest stomatal movements in response to [CO₂] shifts. Measurable stomatal conductance changes occur more rapidly than the establishment of a new calcium transient

pattern (Figs. II-1 A, B, and D, and II-3D). This suggests the existence of events downstream of initial CO₂ responses that trigger modulation of the calcium spike frequency. One such event could be a change in membrane polarization. Reports have shown that decreases in [CO₂] cause hyperpolarization, while increases in [CO₂] cause depolarization of the guard cell plasma membrane^{11,55-57}. These changes in membrane voltage are associated with ion channel and ion pump activities that mediate stomatal movements. Low CO₂-induced hyperpolarization would activate voltage-gated K⁺ influx channels⁵⁸ and provide the driving force for K⁺ uptake, contributing to stomatal opening⁵⁹. Hyperpolarization would also lead to an increase in calcium transient frequency, probably through the activation of hyperpolarization-activated calcium-permeable channels in the plasma membrane^{29,48,60,61}. Conversely, high CO₂-induced depolarization via CO₂ activation of anion channels^{11,12} would activate voltage-gated K⁺ efflux channels⁵⁸ contributing to ion efflux and stomatal closure⁶².

Based on previous studies, high CO₂-induced depolarization would also cause a decrease in calcium transient frequency^{29,48}. This suppression of calcium transients by depolarization likely contributes to the absence of repetitive calcium transients in response to CO₂ changes in the report of Webb et al., in which depolarizing (50 mM extracellular KCl) conditions were used, allowing identification of high CO₂-induction of a [Ca²⁺]_{cyt} increase²². Under lower more physiological external K⁺ and long-term [Ca²⁺]_{cyt} imaging, we

unexpectedly demonstrate that $[Ca^{2+}]_{cyt}$ elevations also occur at low CO_2 that mediates stomatal opening (Figs. II-1 and II-2A).

The slowing in the $[Ca^{2+}]_{cyt}$ pattern upon depolarization would be predicted to occur after an initial high CO_2 -induced stomatal closing response, as was found in the present study (Figs. II-1 A, B and D, and II-3D).

Facilitation of Ca^{2+} sensors by stomatal closing signals, as proposed above, would cause rapid Ca^{2+} reactive stomatal closure irrespective of the $[Ca^{2+}]_{cyt}$ transient pattern, as previously shown for Ca^{2+} reactive stomatal closure in response to imposed Ca^{2+} transients^{27,49}. The subsequent slowing of the $[Ca^{2+}]_{cyt}$ transient pattern in response to elevated CO_2 (Figs. II-1 A, C and D, and II-3A) could on the other hand contribute to maintaining long term “ Ca^{2+} programmed” stomatal closure²⁷.

High CO_2 insensitivity of *gca2* mutant. In addition to modulating stomatal movements, CO_2 also modulates the density of stomata in leaves^{63,64}. In different Arabidopsis accessions the density of stomata can be up- or down-regulated upon CO_2 elevation⁶⁵. To date one mutant, *hic*, has been isolated that impairs CO_2 regulation of stomatal density⁶⁶. *HIC* encodes a long-chain fatty acid biosynthesis enzyme that does not affect the more rapid regulation of stomatal movements⁶⁶. These findings together with our findings that *gca2* disrupts CO_2 -induced stomatal closing, but does not affect stomatal density provide genetic evidence that CO_2 regulation of stomatal density and CO_2

regulation of stomatal movements underlie distinct signal transduction pathways.

abi1-1 and *abi2-1* have been shown to exhibit a degree of CO₂ insensitivity¹⁸, with the extent of CO₂ sensitivity proposed to depend on plasma membrane polarization^{19,20}. However, apart from the conditional *abi1-1* and *abi2-1* mutants, previously no strong CO₂-insensitive mutant has been described that affects CO₂ regulation of stomatal movements in plants. The *gca2* mutant does not exhibit changes in the [Ca²⁺]_{cyt} transient rate in response to CO₂ changes and has a strongly attenuated stomatal movement response to elevated CO₂ in leaf epidermes and in intact leaves (Fig. II-3). Another ABA insensitive mutant *ost1*, which encodes a protein kinase that is activated during early ABA signal transduction²¹, also did not affect stomatal CO₂ responses²¹, further suggesting that initial ABA and CO₂ signaling networks differ but converge at the level of *gca2* and downstream ion channel regulation^{11,12}.

gca2 has previously been shown to disrupt ROS activation of Ca²⁺-permeable channels (I_{Ca}) in guard cells⁶¹. *gca2* also exhibits an aberrant ABA-induced [Ca²⁺]_{cyt} pattern in guard cells²⁷, which may be due to a hyperpolarized state based on the model derived here. Previous findings indicate *gca2* regulation of the [Ca²⁺]_{cyt} elevation pattern via Ca²⁺ feedback regulation of I_{Ca} channels in ABA signaling^{27,61} and this may be a point of cross talk with CO₂ signal transduction. Stomatal conductance measurements

show that the *gca2* mutant impairs initial high CO₂-induced stomatal closing responses (Fig. II-3D). This result combined with the above findings and the Ca²⁺ sensor facilitation model proposed here, suggest that the *gca2* mutant may affect mechanisms that function close to the facilitation of Ca²⁺ sensors during stomatal movements. Isolation of the *gca2* mutant gene and further molecular characterization of GCA2 functions may thus shed light into the model proposed here that stomatal movement stimuli modulate Ca²⁺ sensors.

In summary, we have found that repetitive [Ca²⁺]_{cyt} transients are observed even during low CO₂-induced stomatal opening. CO₂ concentration changes modulate the [Ca²⁺]_{cyt} transient pattern in guard cells and these occur after initial stomatal movement responses. Furthermore, experimental repression of CO₂-regulated [Ca²⁺]_{cyt} transients abolishes CO₂-induced stomatal opening and closing. The *gca2* mutant causes a strong CO₂ insensitivity. The present findings lead us to propose a new model of cellular calcium signaling in which facilitation and inactivation of calcium sensors by physiological stimuli may provide a basis for mediating distinct responses to cytosolic calcium elevations in the same cell type.

ACKNOWLEDGEMENTS

We thank Roger Tsien and Gethyn Allen for discussions and suggestions and Peter Wagner (Division of Physiology, UCSD) for protocols on CO₂ buffer

measurements. Supported by grants from the National Science Foundation (MCB 0417118) and the National Institutes of Health (R01GM060396) and in part the Department of Energy (DE-FG02-03ER15449) to J.I.S.

REFERENCES CITED

1. Leggett, J., Pepper, W. J. & Swart, R. J. in *Climate Change 1992: The Supplementary Report to the IPCC Scientific Assessment* (ed. Houghton JT, C. B., Varney SK) 69-95 (Cambridge University Press, Cambridge, 1992).
2. Norby, R. J., Wullschleger, S. D., Gunderson, C. A., Johnson, D. W. & Ceulemans, R. Tree responses to rising CO₂ in field experiments: implications for the future forest. *Plant Cell and Environment* **22**, 683-714 (1999).
3. Hungate, B. A., Holland, E. A., Jackson, R. B., Stuart Chapin III, F., Mooney, H. A. et al. The fate of carbon in grasslands under carbon dioxide enrichment. *Nature* **388**, 576-579 (1997).
4. DeLucia, E. H., Hamilton, J. G., Naidu, S. L., Thomas, R. B., Andrews, J. A. et al. Net primary production of a forest ecosystem with experimental CO₂ enrichment. *Science* **284**, 1177-9 (1999).
5. LaDeau, S. L. & Clark, J. S. Rising CO₂ levels and the fecundity of forest trees. *Science* **292**, 95-8 (2001).
6. Ainsworth, E. A. & Long, S. P. What have we learned from 15 years of free-air CO₂ enrichment (FACE)? A meta-analytic review of the responses of photosynthesis, canopy. *New Phytologist* **165**, 351-371 (2005).
7. Medlyn, B. E., Barton, C. V. M., Broadmeadow, M. S. J., Ceulemans, R., De Angelis, P. et al. Stomatal conductance of forest species after

- long-term exposure to elevated CO₂ concentration: a synthesis. *New Phytologist* **149**, 247-264 (2001).
8. Drake, B. G., Gonzalez-Meler, M. A. & Long, S. P. More efficient plants: A consequence of rising atmospheric CO₂? *Annual Review of Plant Physiology and Plant Molecular Biology* **48**, 609-639 (1997).
 9. Bunce, J. A. Carbon dioxide effects on stomatal responses to the environment and water use by crops under field conditions. *Oecologia* **140**, 1-10 (2004).
 10. Hanstein, S., de Beer, D. & Felle, H. H. Miniaturised carbon dioxide sensor designed for measurements within plant leaves. *Sensors and Actuators B: Chemical* **81**, 107-114 (2001).
 11. Brearley, J., Venis, M. A. & Blatt, M. R. The effect of elevated CO₂ concentrations on K⁺ and anion channels of *Vicia faba* L. guard cells. *Planta* **203**, 145-154 (1997).
 12. Raschke, K., Shabahang, M. & Wolf, R. The slow and the quick anion conductance in whole guard cells: their voltage-dependent alternation, and the modulation of their activities by abscisic acid and CO₂. *Planta* **217**, 639-650 (2003).
 13. Hanstein, S. M. & Felle, H. H. CO₂-triggered chloride release from guard cells in intact fava bean leaves. Kinetics of the onset of stomatal closure. *Plant Physiology* **130**, 940-950 (2002).
 14. MacRobbie, E. A. C. Signal transduction and ion channels in guard cells. *Philosophical Transactions of the Royal Society of London Series B-Biological Sciences* **353**, 1475-1488 (1998).
 15. Schroeder, J. I., Allen, G. J., Hugouvieux, V., Kwak, J. M. & Waner, D. Guard cell signal transduction. *Annual Review of Plant Physiology and Plant Molecular Biology* **52**, 627-658 (2001).
 16. Hetherington, A. M. & Woodward, F. I. The role of stomata in sensing and driving environmental change. *Nature* **424**, 901-8 (2003).

17. Assmann, S. M. The cellular basis of guard cell sensing of rising CO₂. *Plant Cell and Environment* **22**, 629-637 (1999).
18. Webb, A. A. R. & Hetherington, A. M. Convergence of the abscisic acid, CO₂, and extracellular calcium signal transduction pathways in stomatal guard cells. *Plant Physiology* **114**, 1557-1560 (1997).
19. Leymarie, J., Lasceve, G. & Vavasseur, A. Interaction of stomatal responses to ABA and CO₂ in *Arabidopsis thaliana*. *Australian Journal of Plant Physiology* **25**, 785-791 (1998).
20. Leymarie, J., Vavasseur, A. & Lasceve, G. CO₂ sensing in stomata of *abi1-1* and *abi2-1* mutants of *Arabidopsis thaliana*. *Plant Physiology and Biochemistry* **36**, 539-543 (1998).
21. Mustilli, A.-C., Merlot, S., Vavasseur, A., Fenzi, F. & Giraudat, J. *Arabidopsis* OST1 protein kinase mediates the regulation of stomatal aperture by abscisic acid and acts upstream of reactive oxygen species production. *Plant Cell* **14**, 3089-3099 (2002).
22. Webb, A. A. R., McAinsh, M. R., Mansfield, T. A. & Hetherington, A. M. Carbon dioxide induces increases in guard cell cytosolic free calcium. *Plant Journal* **9**, 297-304 (1996).
23. Schwartz, A., Ilan, N. & Grantz, D. A. Calcium effects on stomatal movement in *Commelina communis* L - use of EGTA to modulate stomatal response to light, KCl and CO₂. *Plant Physiology* **87**, 583-587 (1988).
24. Schroeder, J. I. & Hagiwara, S. Cytosolic calcium regulates ion channels in the plasma membrane of *Vicia faba* guard cells. *Nature* **338**, 427-430 (1989).
25. McAinsh, M. R., Brownlee, C. & Hetherington, A. M. Abscisic acid-induced elevation of guard cell cytosolic Ca²⁺ precedes stomatal closure. *Nature* **343**, 186-188 (1990).

26. Leckie, C. P., McAinsh, M. R., Allen, G. J., Sanders, D. & Hetherington, A. M. Abscisic acid-induced stomatal closure mediated by cyclic ADP-ribose. *Proceedings of the National Academy of Sciences of the United States of America* **95**, 15837-15842 (1998).
27. Allen, G. J., Chu, S. P., Harrington, C. L., Schumacher, K., Hoffman, T. et al. A defined range of guard cell calcium oscillation parameters encodes stomatal movements. *Nature* **411**, 1053-1057 (2001).
28. Staxen, I. I., Pical, C., Montgomery, L. T., Gray, J. E., Hetherington, A. M. et al. Abscisic acid induces oscillations in guard cell cytosolic free calcium that involve phosphoinositide-specific phospholipase C. *Proc Natl Acad Sci U S A* **96**, 1779-84 (1999).
29. Grabov, A. & Blatt, M. R. Membrane voltage initiates Ca^{2+} waves and potentiates Ca^{2+} increases with abscisic acid in stomatal guard cells. *Proc Natl Acad Sci U S A* **95**, 4778-4783 (1998).
30. Kinoshita, T., Nishimura, M. & Shimazaki, K. Cytosolic Concentration of Ca^{2+} Regulates the Plasma Membrane H^{+} -ATPase in Guard Cells of Fava Bean. *Plant Cell* **7**, 1333-1342 (1995).
31. Irving, H. R., Gehring, C. A. & Parish, R. W. Changes in cytosolic pH and calcium of guard cells precede stomatal movements. *Proc Natl Acad Sci U S A* **89**, 1790-4 (1992).
32. Curvetto, N., Darjania, L. & Delmastro, S. Effect of two cAMP analogs on stomatal opening in *Vicia faba*: Possible relationship with cytosolic calcium concentration. *Plant Physiology and Biochemistry* **32**, 365-72 (1994).
33. Cousson, A. & Vavasseur, A. Putative involvement of cytosolic Ca^{2+} and GTP-binding proteins in cyclic-GMP-mediated induction of stomatal opening by auxin in *Commelina communis* L. *Planta* **206**, 308-14 (1998).

34. Mansfield, T. A., Hetherington, A. M. & Atkinson, C. J. Some Current Aspects of Stomatal Physiology. *Annual Review of Plant Physiology and Plant Molecular Biology* **41**, 55-75 (1990).
35. Gomez, T. M. & Spitzer, N. C. In vivo regulation of axon extension and pathfinding by growth-cone calcium transients. *Nature* **397**, 350-5 (1999).
36. Borodinsky, L. N., Root, C. M., Cronin, J. A., Sann, S. B., Gu, X. et al. Activity-dependent homeostatic specification of transmitter expression in embryonic neurons. *Nature* **429**, 523-30 (2004).
37. Dolmetsch, R. E., Xu, K. & Lewis, R. S. Calcium oscillations increase the efficiency and specificity of gene expression. *Nature* **392**, 933-6 (1998).
38. Allen, G. J., Chu, S. P., Schumacher, K., Shimazaki, C. T., Vafeados, D. et al. Alteration of stimulus-specific guard cell calcium oscillations and stomatal closing in *Arabidopsis det3* mutant. *Science* **289**, 2338-2342 (2000).
39. Allen, G. J., Kwak, J. M., Chu, S. P., Llopis, J., Tsien, R. Y. et al. Cameleon calcium indicator reports cytoplasmic calcium dynamics in *Arabidopsis* guard cells. *Plant Journal* **19**, 735-747 (1999).
40. Kuchitsu, K., Ward, J. M., Allen, G. J., Schelle, I. & Schroeder, J. I. Loading acetoxymethyl ester fluorescent dyes into the cytoplasm of *Arabidopsis* and *Commelina* guard cells. *New Phytologist* **153**, 527-533 (2002).
41. Wagner, P. D., Naumann, P. F. & Laravuso, R. B. Simultaneous Measurement of 8 Foreign Gases in Blood by Gas-Chromatography. *Journal of Applied Physiology* **36**, 600-605 (1974).
42. Lev-Ram, V., Mehta, S. B., Kleinfeld, D. & Tsien, R. Y. Reversing cerebellar long-term depression. *Proc Natl Acad Sci U S A* **100**, 15989-93 (2003).

43. Gorbunova, Y. V. & Spitzer, N. C. Dynamic interactions of cyclic AMP transients and spontaneous Ca^{2+} spikes. *Nature* **418**, 93-6 (2002).
44. Miyawaki, A., Griesbeck, O., Heim, R. & Tsien, R. Y. Dynamic and quantitative Ca^{2+} measurements using improved cameleons. *Proc Natl Acad Sci U S A* **96**, 2135-40 (1999).
45. Kumar, P. & FofoulaGeorgiou, E. Wavelet analysis for geophysical applications. *Reviews of Geophysics* **35**, 385-412 (1997).
46. Allan, A. C., Fricker, M. D., Ward, J. L., Beale, M. H. & Trewavas, A. J. Two transduction pathways mediate rapid effects of abscisic acid in *Commelina* guard cells. *Plant Cell* **6**, 1319-1328 (1994).
47. Kerr, R., Lev-Ram, V., Baird, G., Vincent, P., Tsien, R. Y. et al. Optical imaging of calcium transients in neurons and pharyngeal muscle of *C. elegans*. *Neuron* **26**, 583-94 (2000).
48. Klüsener, B., Young, J. J., Murata, Y., Allen, G. J., Mori, I. C. et al. Convergence of calcium signaling pathways of pathogenic elicitors and abscisic acid in *Arabidopsis* guard cells. *Plant Physiol* **130**, 2152-63 (2002).
49. Li, Y., Wang, G. X., Xin, M., Yang, H. M., Wu, X. J. et al. The parameters of guard cell calcium oscillation encodes stomatal oscillation and closure in *Vicia faba*. *Plant Science* **166**, 415-421 (2004).
50. Thomas, R. The effect of carbon dioxide on the intracellular pH and buffering power of snail neurones. *J Physiol (Lond)* **255**, 715-735 (1976).
51. Grignon, C. & Sentenac, H. pH and Ionic Conditions in the Apoplast. *Annual Review of Plant Physiology and Plant Molecular Biology* **42**, 103-128 (1991).

52. Yang, H. M., Zhang, X. Y., Wang, G. X., Li, Y. & Wei, X. P. Cytosolic calcium oscillation may induce stomatal oscillation in *Vicia faba*. *Plant Science* **165**, 1117-1122 (2003).
53. McAinsh, M. R., Brownlee, C. & Hetherington, A. M. Calcium ions as second messengers in guard cell signal transduction. *Physiologia Plantarum* **100**, 16-29 (1997).
54. Allen, G. J., Murata, Y., Chu, S. P., Nafisi, M. & Schroeder, J. I. Hypersensitivity of abscisic acid-induced cytosolic calcium increases in the Arabidopsis farnesyltransferase mutant era1-2. *Plant Cell* **14**, 1649-1662 (2002).
55. Roelfsema, M. R. G., Hanstein, S., Felle, H. H. & Hedrich, R. CO₂ provides an intermediate link in the red light response of guard cells. *Plant Journal* **32**, 65-75 (2002).
56. Hedrich, R., Neimanis, S., Savchenko, G., Felle, H. H., Kaiser, W. M. et al. Changes in apoplastic pH and membrane potential in leaves in relation to stomatal responses to CO₂, malate, abscisic acid or interruption of water supply. *Planta* **213**, 594-601 (2001).
57. Ishikawa, H., Aizawa, H., Kishira, H., Ogawa, T. & Sakata, M. Light-Induced-Changes of Membrane-Potential in Guard-Cells of *Vicia-Faba*. *Plant and Cell Physiology* **24**, 769-772 (1983).
58. Schroeder, J. I., Raschke, K. & Neher, E. Voltage dependence of K⁺ channels in guard-cell protoplasts. *Proceedings of the National Academy of Sciences of the United States of America* **84**, 4108-4112 (1987).
59. Kwak, J. M., Murata, Y., Baizabal-Aguirre, V. M., Merrill, J., Wang, M. et al. Dominant negative guard cell K⁺ channel mutants reduce inward-rectifying K⁺ currents and light-induced stomatal opening in *Arabidopsis*. *Plant Physiology* **127**, 473-485 (2001).
60. Hamilton, D. W. A., Hills, A., Kohler, B. & Blatt, M. R. Ca²⁺ channels at the plasma membrane of stomatal guard cells are activated by

- hyperpolarization and abscisic acid. *Proceedings of the National Academy of Sciences of the United States of America* **97**, 4967-4972 (2000).
61. Pei, Z. M., Murata, Y., Benning, G., Thomine, S., Klusener, B. et al. Calcium channels activated by hydrogen peroxide mediate abscisic acid signalling in guard cells. *Nature* **406**, 731-734 (2000).
 62. Hosy, E., Vavasseur, A., Mouline, K., Dreyer, I., Gaymard, F. et al. The *Arabidopsis* outward K⁺ channel GORK is involved in regulation of stomatal movements and plant transpiration. *Proceedings of the National Academy of Sciences of the United States of America* **100**, 5549-5554 (2003).
 63. Beerling, D. & Kelly, C. Stomatal density responses of temperate woodland plants over the past seven decades of CO₂ increase: a comparison of Salisbury (1927) with contemporary data. *Am. J. Bot.* **84**, 1572- (1997).
 64. Woodward, F. I. & Kelly, C. K. The Influence of CO₂ Concentration on Stomatal Density. *New Phytologist* **131**, 311-327 (1995).
 65. Woodward, F. I., Lake, J. A. & Quick, W. P. Stomatal development and CO₂: ecological consequences. *New Phytologist* **153**, 477-484 (2002).
 66. Gray, J. E., Holroyd, G. H., van der Lee, F. M., Bahrami, A. R., Sijmons, P. C. et al. The HIC signalling pathway links CO₂ perception to stomatal development. *Nature* **408**, 713-716 (2000).

The text of this section, in full, has been submitted for publication of the material by authors Young, J.J., Mehta, S., Grill, E., and Schroeder, J.I. I generated all data and was the primary writer for this paper.

CHAPTER II

Carbon dioxide signaling in guard cells via calcium response modulation and

CO₂ insensitivity of *gca2* mutant

Section B

Supplementary Data

Stomatal opening in *gca2*. In addition to the stomatal closing responses of *gca2* reported in the main section of Chapter II, stomatal opening responses were also measured using both gas exchange and direct stomatal aperture measurements. These results, although preliminary, suggest that *gca2* does not exhibit a strong impairment in CO₂-induced stomatal opening.

Gas exchange experiments were first performed on plants grown in a growth chamber (16 hour light/8 hour dark cycle at 75 $\mu\text{mol m}^{-2} \text{s}^{-1}$ and 20 °C) and measured at the bench (Fig. II-S1). These experiments showed a weaker stomatal opening response to low CO₂ in *gca2* compared to wildtype though the *gca2* low CO₂ stomatal opening response was stronger than the *gca2* high CO₂ closing response.

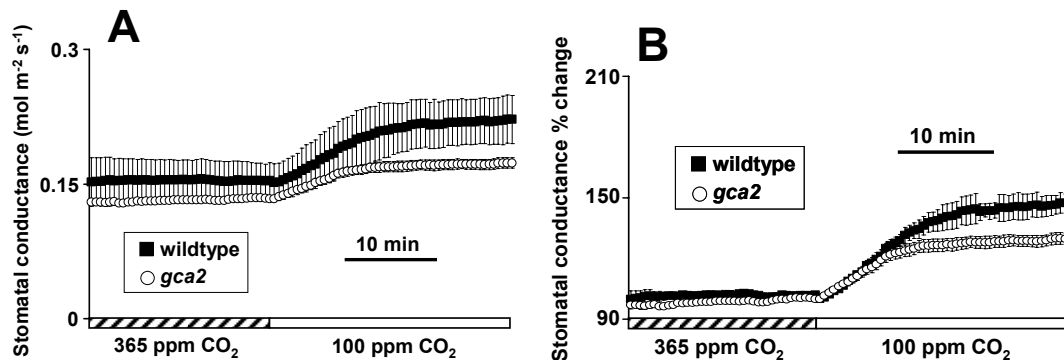


Figure II-S1: Increase in stomatal conductance in response to low CO₂ is slightly impaired in *gca2*. Gas exchange measurements were performed on *gca2* and wildtype (Ler). Plants were grown in a growth chamber and measured at the bench. Results plotted as raw values (A) and as percentage change (B). Values are mean \pm SD. For wildtype, n=3 leaves and for *gca2*, n=6.

Gas exchange experiments were also performed on plants grown and measured in a growth room (16 hour light/8 hour dark cycle at $75 \mu\text{mol m}^{-2} \text{s}^{-1}$ and 26.5°C , Fig. II-S2). In these experiments the low CO_2 stomatal opening response was again stronger than the high CO_2 stomatal closing response in *gca2*. In fact, the percentage of stomatal opening in *gca2* was the same as wildtype, although *gca2* had a lower stomatal conductance in ambient CO_2 . Also, in these experiments *gca2* stomata opened more slowly than did the wildtype.

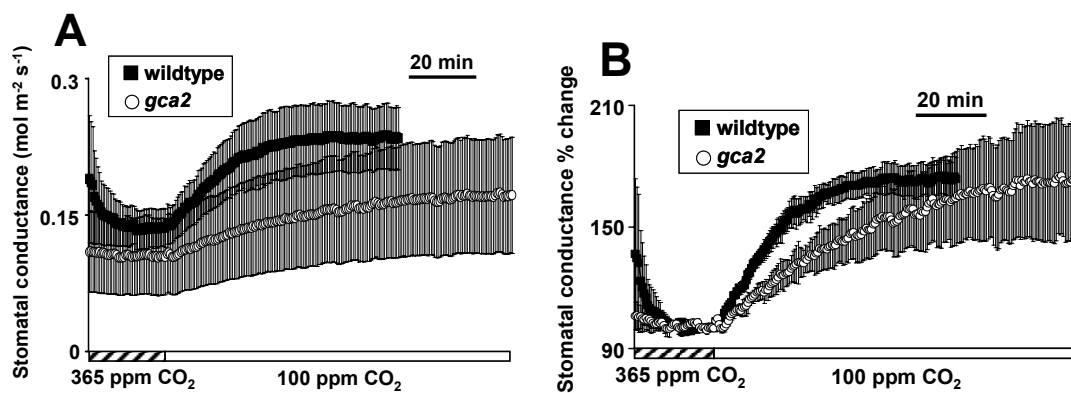


Figure II-S2: Increase in stomatal conductance in response to low CO_2 is slightly impaired in *gca2*. Gas exchange measurements were performed on *gca2* and wildtype (Ler). Plants were grown and measured in a growth room. Results plotted as raw values (A) and as percentage change (B). Values are mean \pm SD. For both genotypes, $n=3$ leaves.

Direct stomatal aperture measurements were also performed in the *gca2* mutant (Fig. II-S3). Like in the gas exchange experiments, a stronger CO_2 -induced stomatal opening response was observed in *gca2* compared to the CO_2 -induced stomatal closing response (Fig. II-3C). While significant

stomatal closure in response to high CO₂ was not resolved ($P > 0.2$, Fig. II-3C), significant stomatal opening in response to low CO₂ was resolved ($P = 0.01$, Fig. II-S3). In the wildtype controls measured in parallel with *gca2*, stomatal opening was not resolved ($P > 0.4$). This is likely a result of variability in these experiments and only 2 of these experiments were successfully performed.

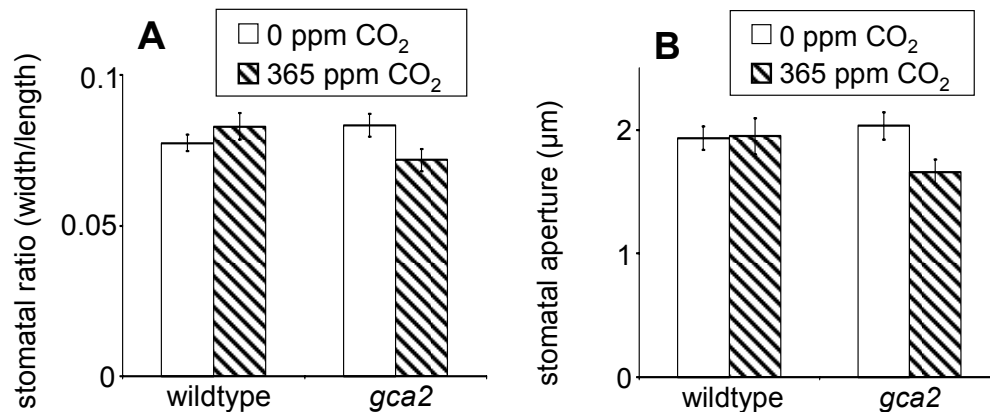


Figure II-S3: *gca2* exhibits stomatal opening in response to low [CO₂]. Stomatal measurements were made on intact epidermal layers in *gca2* and wildtype (Ler) in parallel. Measurements were double blinded; both the genotype and [CO₂] were unknown. Significant stomatal opening was measured in *gca2* ($P = 0.01$). Results are presented as stomatal ratio (width/length, A) and stomatal width only (B), and show mean \pm s.e.m. for $n=2$ experiments for wildtype and $n=3$ experiments for *gca2*, 40 stomata per experiment and per condition.

Both gas exchange and direct stomatal measurement assays with *gca2* suggest that *gca2* exhibits at most a minor impairment in low CO₂-induced stomatal opening. Additional experiments should be performed to confirm and quantify this observation. If this result is confirmed, *GCA2* would likely encode

a stomatal closing signal transducer, perhaps one that responds to calcium. Activated GCA2 may reduce the rate of cytosolic calcium transient production by inducing membrane depolarization, perhaps by activating anion channels (Fig. II-S4). This is suggested by the findings that the *gca2* mutant has faster calcium transients compared to wildtype in the presence of ABA and Ca^{2+} , as these could result from an abnormally hyperpolarized membrane in *gca2*. Based on gas exchange and stomatal aperture measurements, most of the stomatal opening pathway likely remains intact in *gca2*.

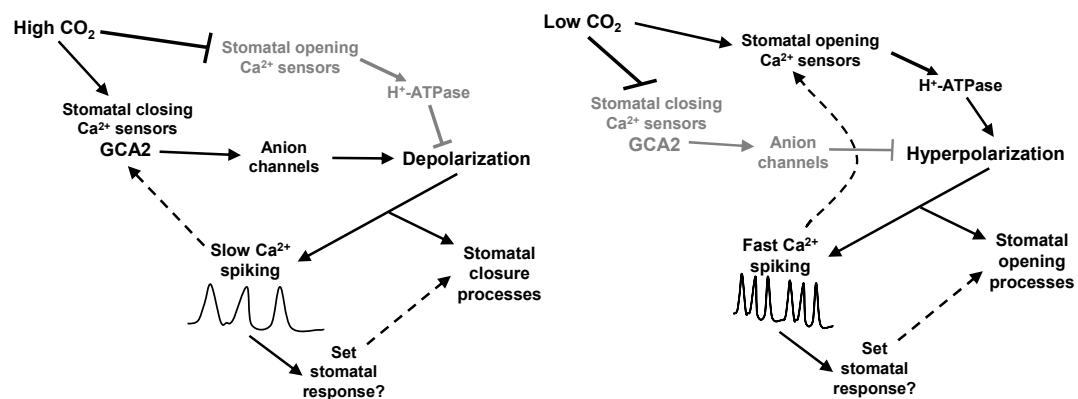


Figure II-S4: Model for CO₂ modulation of calcium transient rate and stomatal movements and apertures. Hypothesized mechanisms by which high CO₂ (left) and low CO₂ (right) can affect calcium transients and stomatal turgor, based on current findings.

Additional calcium transient analyses. The most obvious change in the calcium transient pattern upon changing the [CO₂] was the rate of calcium transients. However, it also appeared that transient widths and amplitudes might be different, and cursory analyses were performed to examine that. Average amplitudes of spikes from 13 cells were calculated and suggested

that spikes in 115 ppm CO₂ might be slightly larger than those in 508 ppm CO₂, although this difference was not significant with 95% confidence (Fig. II-S5A, $P = 0.13$).

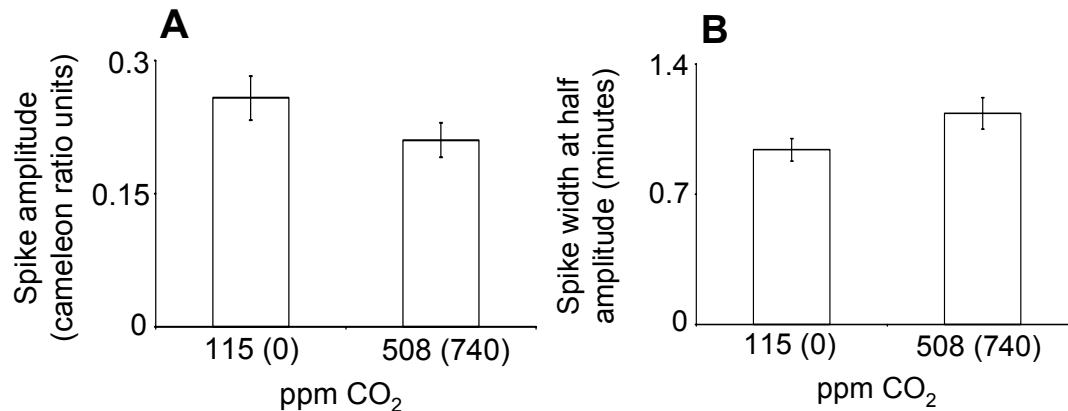


Figure II-S5: Calcium transient amplitudes and widths appear slightly different in low and high CO₂. (A) Average spike amplitudes calculated in low and high CO₂ for 13 of the cells exposed to the series of CO₂ shifts depicted in Figure II-1A (low – high – low CO₂). (B) Average spike widths calculated in low and high CO₂ for 16 of the cells exposed to the series of CO₂ shifts depicted in Figure II-1A. Spike width was measured at the amplitude equal to half the total spike amplitude.

Average width of calcium spikes were also calculated for 16 cells (Fig. II-S5B). The calculated widths suggest that transients in high CO₂ have a slightly longer duration than those in low CO₂ ($P = 0.06$). Thus both the amplitude and width analyses performed suggest that, for transients produced in low and high CO₂, significant differences in the characteristics of the transients themselves likely exist. However, these differences are probably smaller than those in cytosolic calcium transient rates, which differ by approximately 2-fold (Fig. II-1C).

Observation of calcium transients in ambient CO₂. Based on the different rates of calcium transients observed at different [CO₂] (Fig. II-1A and C), and the slow kinetics of the resetting of the calcium transient rate relative to the early stomatal movements, I hypothesized that calcium transient rates might be important for setting the desired stomatal aperture. To test this hypothesis, I performed experiments with ambient CO₂. If the hypothesis is true, one would expect that the rate of calcium transients produced in ambient CO₂ would be intermediate between the rates produced in high and low CO₂. Calcium imaging experiments done in which switches were made between low, ambient and high CO₂ in different orders produced highly variable results. This may be because the cells were not kept in one condition long enough for the new aperture to be fully set (phase lengths ranged from 30 to 45 minutes). Thus when a new [CO₂] was introduced, the calcium transient rate did not change consistently. This effect was likely heightened in these experiments relative to those experiments using only high and low CO₂ (Fig. II-1A), because of the less extreme [CO₂] shifts imposed. If only the initial phase of the experiment is analyzed, reducing the possible artifactual influence of sudden weak shifts in CO₂, the calcium transient patterns were more consistent. Analyzing the periodicities of transients in the first phase of experiments did show an intermediate periodicity in ambient CO₂, with the periods in ambient CO₂ differing significantly from the periods in low CO₂ and high CO₂ (Fig. II-S6, P<0.05).

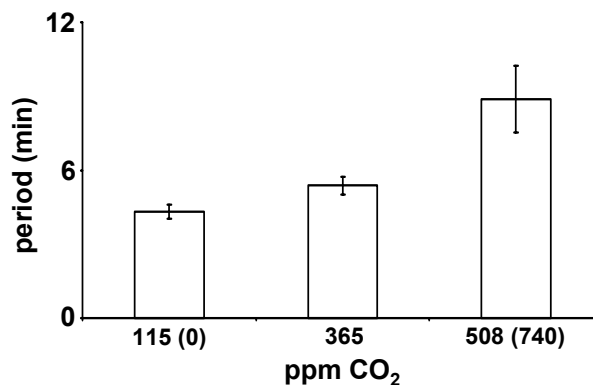


Figure II-S6: Calcium transients produced in ambient (365 ppm) CO₂ have a periodicity in between those produced in low and high CO₂. Although these experiments incorporated multiple shifts between different CO₂ concentrations, only transients observed in the initial phase are analyzed here. Values represent mean periodicity \pm s.e.m. (n = 19 cells for 115 ppm CO₂, 17 cells for 365 ppm CO₂, and 4 cells for 508 ppm CO₂).

Another prediction that derives from the hypothesis that the calcium transient rate dictates the stomatal aperture set point is that, in the absence of stimuli, there should be a steady, consistent transient rate that would maintain the desired stomatal aperture. To test this I wanted to observe calcium transients over a long period of time absent any perturbation to look at the baseline activity of these cells. I recorded from 6 cells for over four hours without intentionally administering any stimuli. A variety of spike patterns were

seen (Fig. II-S7).

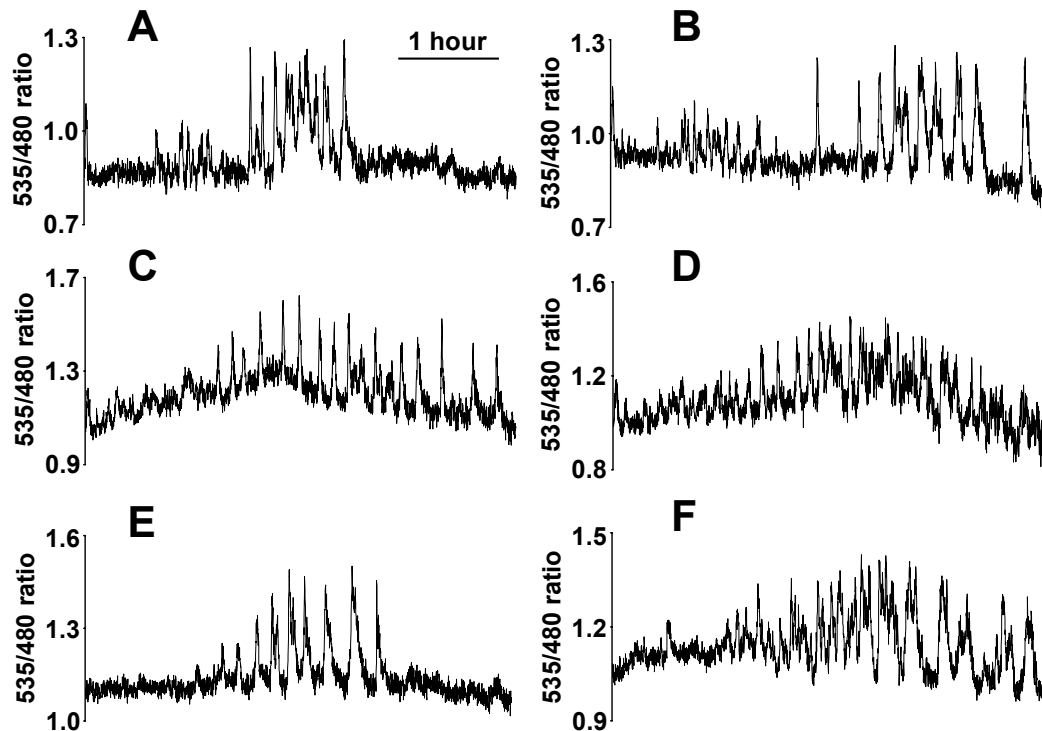


Figure II-S7: Unstimulated guard cells exhibit a variety of calcium patterns. Cytosolic calcium transients recorded in guard cells for over 4 hours without any applied stimulus. Graphs A and B depict data recorded simultaneously from two guard cells that form a stomatal pair, as do graphs C and D and graphs E and F. Time bar applies to all graphs.

These recordings reveal several interesting features of guard cell calcium dynamics. First, the calcium patterns generated vary from cell to cell with calcium transients differing in amplitude, duration, and rate. Second, even in this case where no stimulus is applied, the calcium transients produced in a single cell vary over time with regard to these same parameters. Third, there are extended periods in which no calcium transients are produced. Fourth, guard cells of a stomatal pair exhibit similar, though not exactly synchronized,

behavior, a phenomenon observed in other experiments but made more obvious here due to the lengthy recording.

Thus there does not appear to be a constant, consistent background calcium transient pattern upon which alterations can be imposed and lead to aperture adjustment. Note, however, that although stimuli were not intentionally applied, this does not mean that the environment was rigidly static. Calcium patterns may constantly be adjusting to fine tune the stomatal aperture to the prevailing conditions. Changes in calcium patterns within individual cells over time may have been the result of responses to unintended perturbations. Furthermore, what is observed in these cells can be interpreted as a constant, consistent calcium pattern to a degree, as extended phases with a fairly consistent rate, amplitude, and duration of calcium transients are observed which then abruptly change to a new consistent pattern. The length of these phases, on the order of 1-2 hours, also is in line with the hypothesis that the calcium transient rate may be important in dictating a new set point for stomatal aperture following a change in CO₂ or other conditions. If this were the case, one would expect that the transient pattern would persist long enough to allow stomata to achieve a new steady state aperture, and 1-2 hours is in the right time frame (Fig. II-1B, II-3D, II-S1, II-S2). The observation of phases in which there are no calcium transients runs counter to the simple model that a constant transient rate is required to maintain a certain amount of guard cell turgor. However, it may be that a series of transients constituting a

phase of sufficient duration (e.g. 1 hour) is enough to set the turgor pressure. Following such a phase, the transients could be stopped so long as the conditions do not change, which would call for a new turgor set point. Such a system is suggested by the finding that a series of transients with certain parameters can maintain closure through a long period of time during which transients are not produced¹. Finally, the similar patterns generated by guard cells of a stomatal pair make sense since the turgor changes in guard cells of a stomatal pair are typically also similar. It is interesting to consider how the calcium patterns in guard cells might be coordinated between partnered guard cells. In sum, these observations fit with a model that the calcium transient pattern can underlie regulation of guard cell apertures.

Stomatal responses of *abi1-1* and *abi2-1*. *abi1-1* and *abi2-1* are ABA-insensitive mutants that were previously characterized as having stomata that are either fully insensitive to changes in $[\text{CO}_2]$ ² or partially insensitive to changes in $[\text{CO}_2]$ ^{3,4}, depending upon experimental conditions. In calcium imaging assays, I found that *abi1-1* exhibits an alteration in calcium transient rates in response to $[\text{CO}_2]$ shifts which is significant though smaller than the alteration in wildtype, and contrasts with the ABA-insensitive mutant *gca2* which shows no $[\text{CO}_2]$ -induced alteration in the calcium transient rate (Fig. II-3a). I also performed assays to test the stomatal movement response of *abi1-*

1 under conditions similar to those used in the calcium imaging experiments (Fig. II-S8).

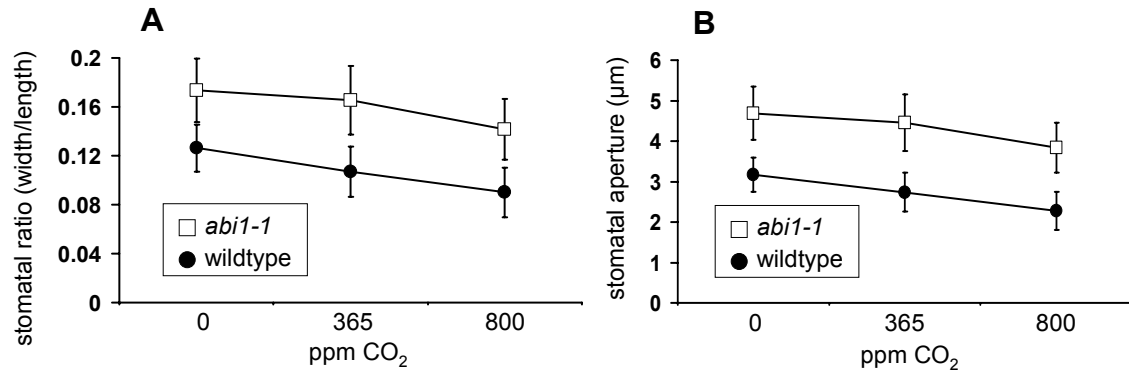


Figure II-S8: *abi1-1* exhibits stomatal closure in response to high [CO₂]. Stomatal measurements were made on intact epidermal layers in *abi1-1* and wildtype (Ler) in parallel. Measurements were double blinded; both the genotype and [CO₂] were unknown. Highly significant opening (difference between values at 365 ppm and 0 ppm CO₂, $p < 0.001$) and closure (difference between values at 365 ppm and 800 ppm CO₂, $p < 0.001$) were measured in wildtype, and highly significant closure (difference between values at 365 ppm and 800 ppm CO₂, $p < 0.001$) was measured in *abi1-1*. Stomatal opening in *abi1-1* (difference between values at 365 ppm and 800 ppm CO₂) was not measured to be significant ($p = 0.16$). Results are presented as stomatal ratio (width/length, A) and stomatal width (B), and show mean \pm s.e.m. for $n = 8$ experiments, 40 stomata per experiment and per condition.

These results showed significant stomatal closure but not significant opening in *abi1-1*. However, significant stomatal opening may be measured if additional experiments are performed, since there is a high degree of variability in the responses. Stomatal opening may also be limited because the *abi1-1* stomata are relatively wide open even at ambient CO₂. Thus further stomatal opening at low CO₂ may be difficult to achieve. Furthermore, the high [Ca²⁺]_{cyt} transient rates in *abi1-1* (Fig. II-3A) correspond, based on our findings, to more open stomata as are observed in *abi1-1*.

Gas exchange experiments were also performed on *abi1-1*. An experimental challenge was encountered, as under conditions normally used for gas exchange experiments with wildtypes or other mutants, the *abi1-1* leaves rapidly wilted which prohibited data collection. Based on additional pilot experiments, future gas exchange measurements performed with *abi1-1* could be successful if different conditions are used: the measured leaf should be kept in high humidity during the experiment and a very low rate of airflow through the leaf chamber should be applied, to reduce wilting.

Gas exchange experiments were also performed on *abi2-1*. The leaves of *abi2-1* did not wilt as easily as those of *abi1-1* and therefore gas exchange data was easier to obtain from *abi2-1*. A few experiments done with *abi2-1* testing both opening in low CO₂ and closing in high CO₂ showed that *abi2-1* has a very robust stomatal response to CO₂ changes (Fig. II-S9).

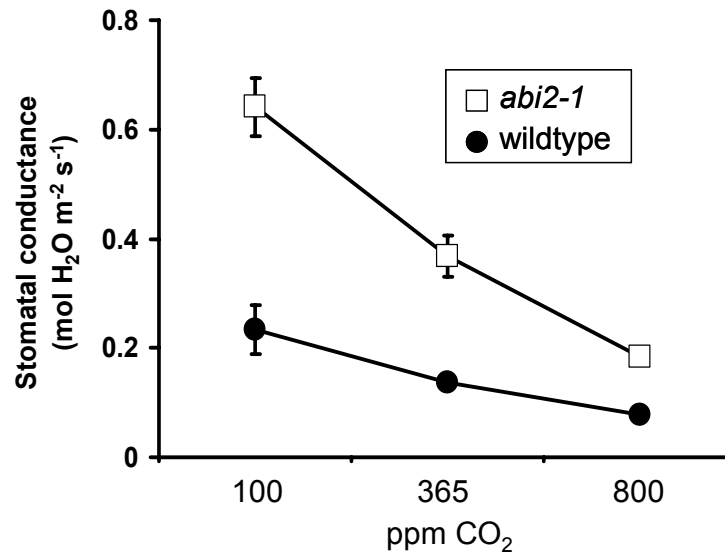


Figure II-S9: *abi2-1* exhibits strong stomatal stomatal movements in response to changes in [CO₂]. Gas exchange measurements were performed on *abi2-1* and wildtype (Ler) leaves. Data points represent mean steady-state values \pm SD. For wildtype, n=3 leaves, error bars are smaller than symbols where not seen. For *abi2-1*, n=2 leaves for the 100 ppm value, 3 leaves for the ambient value, and 1 leaf for the 800 ppm value.

More experiments would need to be performed to quantify the *abi2-1* response to CO₂, but these preliminary experiments clearly show a significant response. Thus preliminary data with *abi1-1* and *abi2-1* suggest that under our experimental conditions, *abi1-1* and *abi2-1* generally exhibit robust stomatal responses to CO₂. This contrasts with earlier results²⁻⁴ which show either completely or partially impaired CO₂ responses in these mutants. As suggested by Leymarie and colleagues⁴, the divergent observations made by different groups probably result from variations in experimental conditions. Importantly, under our conditions in which *abi1-1* and *abi2-1* mutants do not show impaired CO₂ responses, the *gca2* mutant exhibits a strong impairment

in its stomatal CO₂ response in CO₂ modulation of the Ca²⁺ transient rate, stomatal movement assays in intact epidermal layers and stomatal conductance assays using gas exchange in intact leaves (Fig. II-3). This demonstrates that *gca2* has a substantially stronger impairment in CO₂ responses than *abi1-1* and *abi2-1*.

Stomatal responses of additional genotypes. To attempt to elucidate the genetic mechanisms behind stomatal CO₂ responses, I performed gas exchange experiments on several mutants that we hypothesized might have aberrant CO₂ stomatal responses (Fig. II-S10). Three wildtypes (Col.0, Ler, and WS) were also tested. *AE1* encodes an anion exchanger that may play a role in stomatal movements (N. Leonhardt, unpublished). *CPK6* and *CPK3* are calcium-dependent protein kinases that affect ABA signaling mechanisms (I. Mori, unpublished). *MRP5* is an ABC transporter involved in guard cell signaling⁵. *CLC-E* is a putative anion channel. *CA1* and *CA2* are carbonic anhydrase genes that are highly expressed in guard cells. *abi2* and *gca2* are included here for comparison. These preliminary data show that the *gca2* mutant shows the strongest insensitivity to high CO₂. Further experiments would be needed to determine whether some of these mutants show weaker impairments in CO₂ responses.

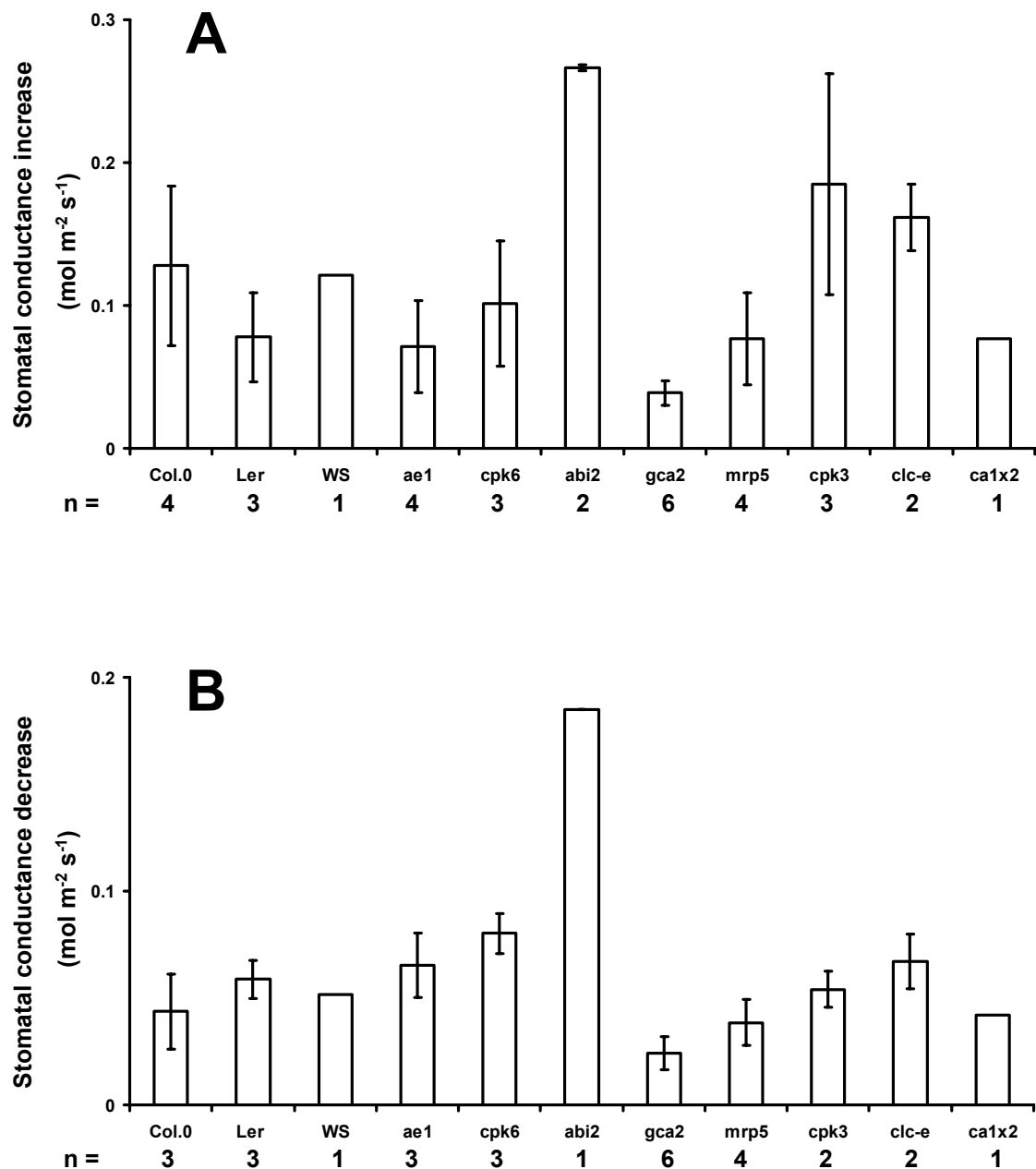


Figure II-S10: CO₂ stomatal conductance responses of various genotypes. Several mutants were tested to look for a mutant with an abnormal CO₂ response. Bars depict extent of stomatal opening upon a shift from ambient to 100 ppm CO₂ (A) or extent of stomatal closing upon a shift from ambient to 800 ppm CO₂ (B). Values are means ± s.e.m. for the number of experiments listed below the bar.

Additional methods for testing requirement of calcium transients for CO₂ stomatal responses. Prior to using BAPTA-AM to silence calcium transients (Fig. II-2), I tried using EGTA and La³⁺ to accomplish the goal of finding a condition in which calcium transients would not occur and then measuring stomatal movements under that condition. Both EGTA and La³⁺ were able to robustly silence calcium transients in calcium imaging experiments. 50 μM La³⁺ shut off Ca²⁺ transients in low CO₂ in 8 of 8 cells. 250 μM EGTA shut off Ca²⁺ transients in low CO₂ in 11 of 12 cells, and shut off Ca²⁺ transients in high CO₂ in 6 of 6 cells. However, in direct stomatal measurement assays, neither EGTA nor La³⁺ consistently affected stomatal movements. In the presence of 50 μM La³⁺, stomata consistently responded to CO₂. In the presence of 5 mM EGTA, CO₂-induced stomatal movements were sometimes inhibited, other times not. I also attempted to apply La³⁺ to intact leaves either through the petiole or by coating the leaf in a solution containing La³⁺ and Silwet as a surfactant and then measure stomatal conductance using the Li-6400 gas exchange machine. Treatments with high concentrations of La³⁺ (1 mM) applied through the petiole caused a large drop in stomatal conductance independent of other stimuli. Application of Silwet to the leaf caused a significant reduction in stomatal responses to CO₂. Applying 0.1 mM La³⁺ through the petiole allowed for observation of conductance responses to CO₂ changes, although some leaf damage was incurred. In these experiments, like in the direct stomatal measurement assays, La³⁺ did not affect stomatal CO₂

responses. These data suggest that directly buffering cytosolic calcium using BAPTA-AM is more effective at shutting off stomatal calcium signaling than applying EGTA or La^{3+} extracellularly. Furthermore, if La^{3+} indeed fails to prevent stomatal responses to CO_2 while BAPTA-AM succeeds, that could allow a basis for refining the contribution of different calcium entry/release pathways to stomatal movements.

REFERENCES CITED

1. Allen, G. J., Chu, S. P., Harrington, C. L., Schumacher, K., Hoffman, T. et al. A defined range of guard cell calcium oscillation parameters encodes stomatal movements. *Nature* **411**, 1053-1057 (2001).
2. Webb, A. A. R. & Hetherington, A. M. Convergence of the abscisic acid, CO_2 , and extracellular calcium signal transduction pathways in stomatal guard cells. *Plant Physiology* **114**, 1557-1560 (1997).
3. Leymarie, J., Lasceve, G. & Vavasseur, A. Interaction of stomatal responses to ABA and CO_2 in *Arabidopsis thaliana*. *Australian Journal of Plant Physiology* **25**, 785-791 (1998).
4. Leymarie, J., Vavasseur, A. & Lasceve, G. CO_2 sensing in stomata of *abi1-1* and *abi2-1* mutants of *Arabidopsis thaliana*. *Plant Physiology and Biochemistry* **36**, 539-543 (1998).
5. Klein, M., Perfus-Barbeoch, L., Frelet, A., Gaedeke, N., Reinhardt, D. et al. The plant multidrug resistance ABC transporter AtMRP5 is involved in guard cell hormonal signalling and water use. *Plant Journal* **33**, 119-129 (2003).

CHAPTER III

Convergence of calcium signaling pathways of pathogenic elicitors and
abscisic acid in *Arabidopsis* guard cells

ABSTRACT

A variety of stimuli, such as abscisic acid (ABA), reactive oxygen species (ROS), and elicitors of plant defense reactions, have been shown to induce stomatal closure. Our study addresses commonalities in the signaling pathways that these stimuli trigger. A recent report showed that both ABA and ROS stimulate a NADPH-dependent, hyperpolarization-activated Ca^{2+} influx current in *Arabidopsis thaliana* guard cells (Pei et al., 2000, Nature 406:731-734). We found that yeast (*Saccharomyces cerevisiae*) elicitor and chitosan, both elicitors of plant defense responses, also activate this current and activation requires cytosolic NAD(P)H. These elicitors also induced elevations in the concentration of free cytosolic calcium ($[\text{Ca}^{2+}]_{\text{cyt}}$) and stomatal closure in guard cells. ABA and ROS elicited $[\text{Ca}^{2+}]_{\text{cyt}}$ oscillations in guard cells only when extracellular Ca^{2+} was present. In a 5 mM KCl extracellular buffer, 45% of guard cells exhibited spontaneous $[\text{Ca}^{2+}]_{\text{cyt}}$ oscillations that differed in their kinetic properties from ABA-induced Ca^{2+} increases. These spontaneous $[\text{Ca}^{2+}]_{\text{cyt}}$ oscillations also required the availability of extracellular Ca^{2+} and depended on the extracellular potassium concentration. Interestingly, when ABA was applied to spontaneously oscillating cells, ABA caused cessation of $[\text{Ca}^{2+}]_{\text{cyt}}$ elevations in 62 of 101 cells, revealing a new mode of ABA signaling. These data show that

fungal elicitors activate a shared branch with ABA in the stress signal transduction pathway in guard cells that activates plasma membrane I_{Ca} channels and support a requirement for extracellular Ca^{2+} for elicitor and ABA signaling, as well as for cellular $[Ca^{2+}]_{cyt}$ oscillation maintenance.

INTRODUCTION

Calcium acts as an intracellular second messenger, coupling extracellular stimuli to intracellular and whole plant responses (Hepler and Wayne, 1985; Sanders et al., 1999). Guard cells have been developed as a model system for dissecting early signal transduction processes in plant cells. Guard cells respond to a great variety of external stimuli including abscisic acid (ABA) (McAinsh et al., 1990; Schroeder and Hagiwara, 1990), auxin (Gehring et al., 1990; 1998), ozone (Clayton et al., 1999), and reactive oxygen species (ROS) (McAinsh et al., 1996; Pei et al., 2000) with an increase in the cytoplasmic free Ca^{2+} concentration and subsequent stomatal movements (for reviews see Blatt, 2000; Schroeder et al., 2001a). Cytosolic Ca^{2+} increases downregulate inward-rectifying K^+ channels and activate anion channels, providing mechanisms for Ca^{2+} -dependent stomatal closure (Schroeder and Hagiwara, 1989). Particularly well analyzed is the Ca^{2+} response of guard cells to the phytohormone ABA (McAinsh et al., 1990; Schroeder and Hagiwara 1990; Blatt and Armstrong, 1993; Schmidt et al., 1995; Leckie et al., 1998;

Allen et al., 1999a; Staxén et al., 1999; MacRobbie, 2000; Hugouvieux et al., 2001; for reviews: Blatt, 2000; Schroeder et al., 2001b).

ABA has been shown to activate a hyperpolarization-dependent Ca^{2+} -permeable current in the plasma membrane, leading to Ca^{2+} influx and an increase in the cytoplasmic free Ca^{2+} concentration (Hamilton et al., 2000; Pei et al., 2000). Furthermore, it has been demonstrated that ABA elevates levels of ROS, and that elevated ROS levels stimulate Ca^{2+} permeable " I_{Ca} " cation currents in the plasma membrane (Pei et al., 2000). I_{Ca} channels have been shown to be permeable to several cations including Mg^{2+} (Pei et al., 2000). The ABA insensitive mutants *gca2*, *abi1-1* and *abi2-1* disrupt I_{Ca} channel activation at distinct points providing genetic evidence for this newly recognized branch in ABA signaling (Pei et al., 2000; Murata et al., 2001).

ROS production in guard cells is induced not only by ABA, but also by the elicitors of plant defense reactions chitosan and oligogalacturonic acid (Lee et al., 1999). These elicitors also promote stomatal closing (Lee et al., 1999). In plant cells other than guard cells, it is known that one of the first responses to elicitors is an elevation in cytosolic Ca^{2+} which lies upstream of NADPH-oxidase activation (Knight et al., 1991; Zimmermann et al., 1997; Mithöfer et al., 1999; Blume et al., 2000). Pathogen-induced Ca^{2+} influx has been reported to occur both before (Schwacke et al., 1992; Blume et al., 2000) and after ROS production (Price et al., 1994; Kawano et al., 2000), indicating that two distinct plasma membrane Ca^{2+} channels may function during

different phases of the response. The similarities between the elicitor-activated and hyperpolarization-induced Ca^{2+} channels in tomato cells (Gelli et al., 1997) and ABA-activated Ca^{2+} channels in guard cells (Hamilton et al., 2000; Pei et al., 2000) suggest that these two stimuli may activate related influx currents.

Ca^{2+} oscillations have been shown to be critical for induction of stomatal closure (Allen, et al., 2000), and are mediated from two general sources, proposed to work in parallel: influx of Ca^{2+} across the plasma membrane (Schroeder and Hagiwara, 1990; Hamilton et al., 2000; MacRobbie, 2000; Pei et al., 2000) and release of Ca^{2+} from internal stores (Leckie et al., 1998; Staxén et al., 1999; MacRobbie, 2000). The concentration of ABA favors either induction of Ca^{2+} influx or Ca^{2+} release mechanisms in *Commelina communis* guard cells (MacRobbie, 2000). At high ABA concentrations ($> 1\mu\text{M}$), Ca^{2+} influx was reported to predominantly contribute to ABA-induced $[\text{Ca}^{2+}]_{\text{cyt}}$ increases, while at low ABA, Ca^{2+} release from internal stores is predominant in *Commelina*. To understand Ca^{2+} -based signal transduction pathways in guard cells, it is therefore necessary to closely analyze the conditions under which Ca^{2+} influx or Ca^{2+} release mechanisms occur. Manganese quenching experiments show that external Ca^{2+} -induced oscillations in cytosolic Ca^{2+} include plasma membrane Ca^{2+} influx (McAinsh et al., 1995). Although extracellular Ca^{2+} is required for ABA-induced changes in stomatal aperture (De Silva et al., 1985; Schwartz, 1985; MacRobbie, 2000;

Webb et al., 2001), and for ABA-induction of a transient $[Ca^{2+}]_{cyt}$ increase in *Vicia* guard cells (Romano et. al., 2000), to date, ABA-induced $[Ca^{2+}]_{cyt}$ oscillations in *Arabidopsis* guard cells have not been analyzed as a function of extracellular Ca^{2+} removal. Here we have analyzed whether intracellular Ca^{2+} release pathways that contribute to Ca^{2+} oscillations are independent of rapid extracellular Ca^{2+} removal.

In the present study we analyze the degree of convergence of stomatal closure pathways induced by different stimuli. We test whether $I_{Ca} Ca^{2+}$ channels represent a shared branch of ABA and elicitor signaling by testing whether these elicitors activate hyperpolarization-induced $I_{Ca} Ca^{2+}$ influx currents. We investigate further the effects of external Ca^{2+} and external $[K^+]$ on $[Ca^{2+}]_{cyt}$ oscillations in multiple stomatal closure signaling pathways. We also reveal a new mode of ABA signaling in which ABA is shown to downregulate spontaneous $[Ca^{2+}]_{cyt}$ oscillations that occur in guard cells (Staxen et. al., 1999; Allen et. al., 1999b).

RESULTS

Elicitors activate NADPH-dependent Ca^{2+} channel currents. It has been shown that chitosan, an elicitor of phytoalexin production in pea (*Pisum sativum*) pods (Hadwiger and Beckman, 1980), induces the production of reactive oxygen species and a reduction of stomatal aperture in guard cells of

tomato and *C. communis* (Lee et al., 1999). We analyzed whether chitosan and yeast (*Saccharomyces cerevisiae*) elicitor, a well-studied elicitor of defense reactions in cell cultures of *Eschscholtzia californica* (Schumacher et al., 1987), could activate plasma membrane Ca^{2+} currents in guard cells similar to the ROS-induced Ca^{2+} currents during ABA signaling. We applied voltage ramps from -18 to -198 mV (following correction for liquid junction potentials). Both chitosan and yeast elicitor activated a hyperpolarization-dependent current in guard cell protoplasts (Fig. III-1). In the absence of elicitors only a small background current with a mean amplitude of -5.7 pA ($n = 17$ protoplasts) at -198 mV was observed. Upon addition of 10 $\mu\text{g/ml}$ yeast elicitor to the bath solution, a hyperpolarization-activated inward current was observed. This current had a mean peak current amplitude of -59.9 pA at -198 mV ($n = 10$ protoplasts). 10 $\mu\text{g/ml}$ chitosan induced a hyperpolarization-activated current with a mean peak amplitude of -119.6 pA ($n = 8$ protoplasts). Average current/voltage relationships from untreated and elicitor treated cells are shown in Figure III-1B. ROS- and ABA-activated I_{Ca} currents have been previously shown to have a “spiky” behaviour (Pei et al., 2000; Murata et al., 2001), which was also observed for elicitor-activated currents (Fig. III-1A) that are activated by hyperpolarization. Figure III-1C shows currents produced by a voltage pulse protocol in the presence of hydrogen peroxide ($n=4$). Note that I_{Ca} currents were not observed in voltage pulse protocols in the absence of hydrogen peroxide (Fig. III-1C, $n=4$).

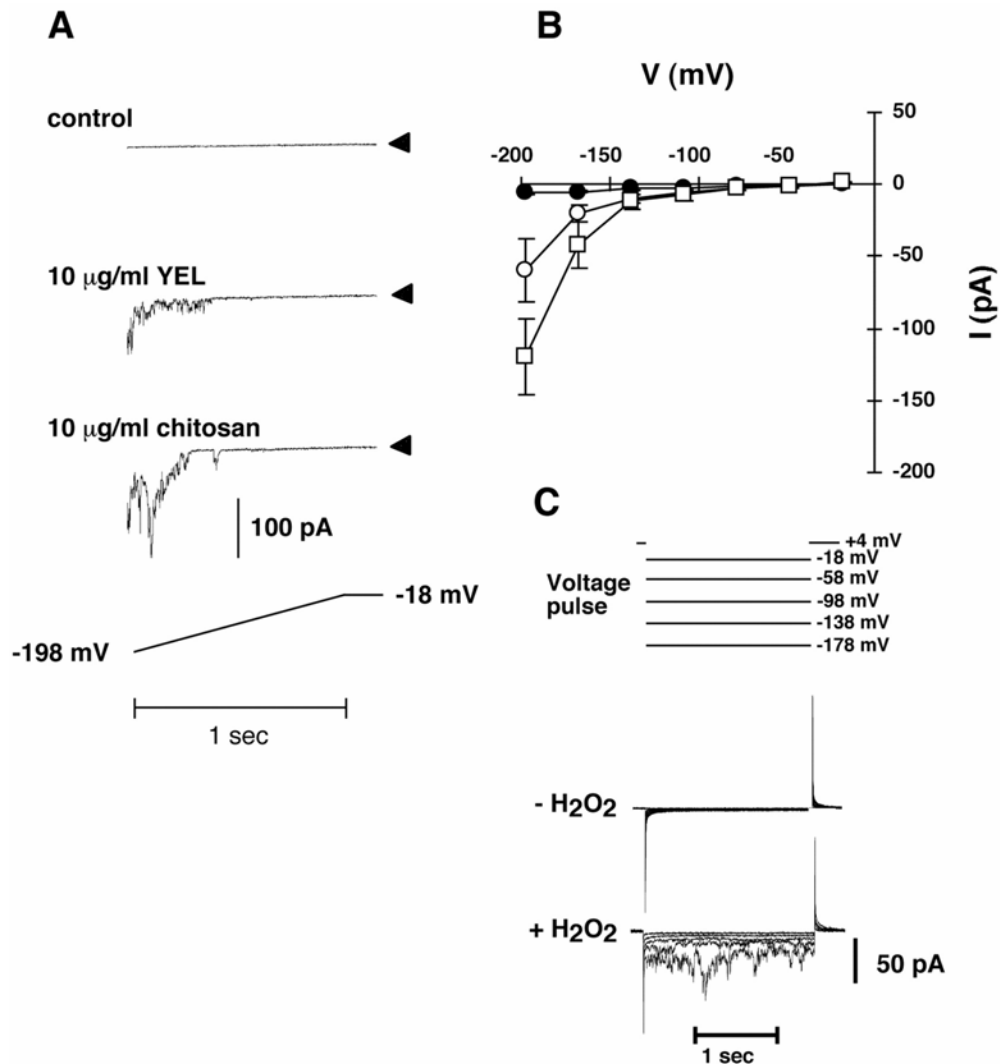


Figure III-1: Elicitor activation of hyperpolarization-dependent currents in *Arabidopsis* guard cells. A, Whole cell currents without or with 10 $\mu\text{g/ml}$ yeast elicitor or chitosan present in the bath solution. Elicitor-activated currents were measured ca. 5 min following elicitor exposure. Voltage ramps (1 second duration) were from -18 to -198 mV (lower panel). The liquid junction potential of -18 mV was corrected for. Arrows on right show zero current levels. Bath solution: 100 mM BaCl_2 , 0.1 mM DTT, 10 mM Mes-Tris, pH 5.6. Pipette solution: 10 mM BaCl_2 , 0.1 mM DTT, 4 mM EGTA, 5 mM NADPH, 10 mM HEPES-Tris, pH 7.1. B, Current/voltage relationship from control and elicitor-treated cells. Experimental conditions are the same as in A. Closed circles: untreated cells ($n = 17$), open circles: yeast elicitor treated cells ($n = 10$), open squares: chitosan treated cells ($n = 8$). C, Currents produced by voltage pulses (top) in the absence (middle) or presence (bottom) of 5 mM H_2O_2 . The liquid junction potential of -18 mV was corrected for.

Interestingly, addition of NADPH to the pipette solution was necessary to activate elicitor- and hyperpolarization-dependent currents. Without NADPH present in the pipette solution, yeast elicitor could not induce hyperpolarization-activated currents (Fig. III-2 A,C; $n = 7$). With NADPH in the pipette yeast elicitor activated the hyperpolarization-activated current (Fig. III-2 B,D; $n = 10$).

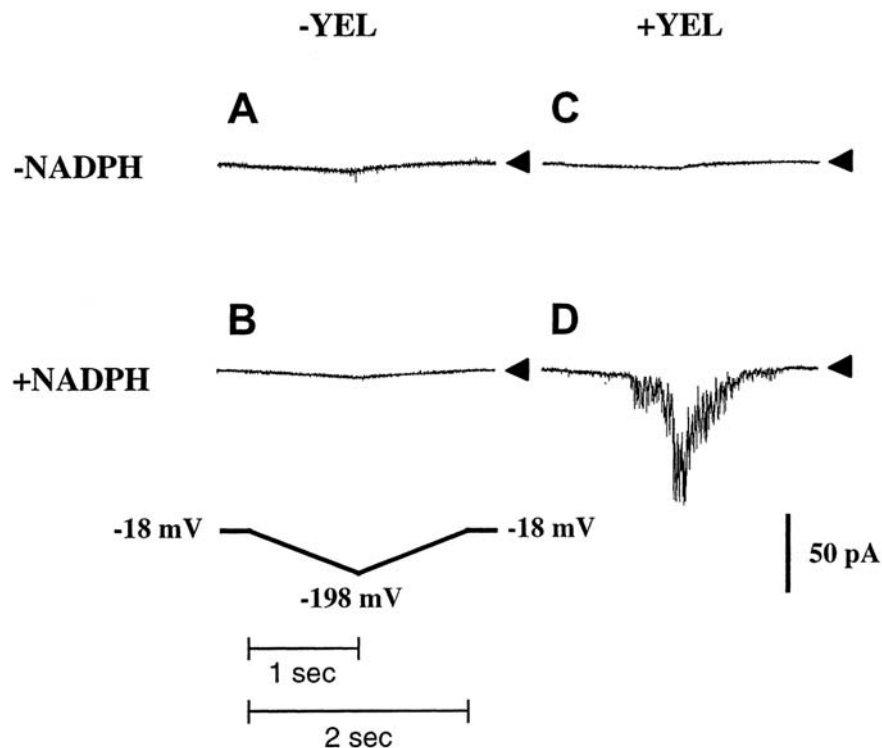


Figure III-2: NADPH-dependence of elicitor-induced hyperpolarization-activated currents. A, Pipette solution: no NADPH; bath solution: no yeast elicitor ($n = 4$). B, Pipette solution: 5 mM NADPH; bath solution: no yeast elicitor ($n = 17$). C, Pipette solution: no NADPH; bath solution: 10 $\mu\text{g/ml}$ yeast elicitor ($n = 7$). D, Pipette solution: 5 mM NADPH; bath solution: 10 $\mu\text{g/ml}$ yeast elicitor ($n = 10$). In all experiments 10 mM BaCl_2 (+ 0.1 mM DTT, 4 mM EGTA, 10 mM HEPES-Tris, pH 7.1) were used as pipette solution and 100 mM BaCl_2 (+ 0.1 mM DTT, 10 mM Mes-Tris, pH 5.6) as bath solution. The applied voltage ramp protocol is shown on lower left. The liquid junction potential of -18 mV was corrected for. Arrows on the right show zero current levels.

Elicitor-induced $[Ca^{2+}]_{cyt}$ elevations require external Ca^{2+} . Both chitosan and yeast elicitor induced repetitive $[Ca^{2+}]_{cyt}$ elevations in guard cells of *A. thaliana* (Fig. III-3A, B). Elicitor concentrations as low as 10 $\mu\text{g/ml}$ were sufficient to induce repetitive $[Ca^{2+}]_{cyt}$ transients in guard cells treated with yeast elicitor ($n = 12$ of 15 cells) or chitosan ($n = 9$ of 9 cells). The relative amplitude and mean duration of yeast elicitor and chitosan-induced $[Ca^{2+}]_{cyt}$ transients is summarized in Table III-I. When yeast elicitor was applied at higher concentrations (50 $\mu\text{g/ml}$), only a single, slowly declining $[Ca^{2+}]_{cyt}$ transient with a relative amplitude of $\Delta\text{ratio}_{585/480} = 0.41 \pm 0.04$ and a mean duration of 22.28 ± 2.67 min (duration at half amplitude of 10.9 ± 1.42 min) was observed (Fig. III-3C, $n = 14$ cells).

Table III-I: Elicitor-induced $[Ca^{2+}]_{cyt}$ transients in guard cells of *A. thaliana*. Data were obtained during the first 30 min after elicitor application. Errors represent standard error of the mean.

Elicitor (10 $\mu\text{g/ml}$)	Rel. Amplitude ($\Delta\text{ratio}_{535/480}$)	Transient Duration ($\Delta t/\text{min}$)	Period (min)	No. of transients	% of cells with transients	Total no. of cells
yeast elicitor	0.45 ± 0.10	2.83 ± 0.76	5.74 ± 1.52	2.58 ± 0.33	80%	15
chitosan	0.66 ± 0.28	2.97 ± 0.32	5.26 ± 0.834	2.44 ± 0.47	100%	9

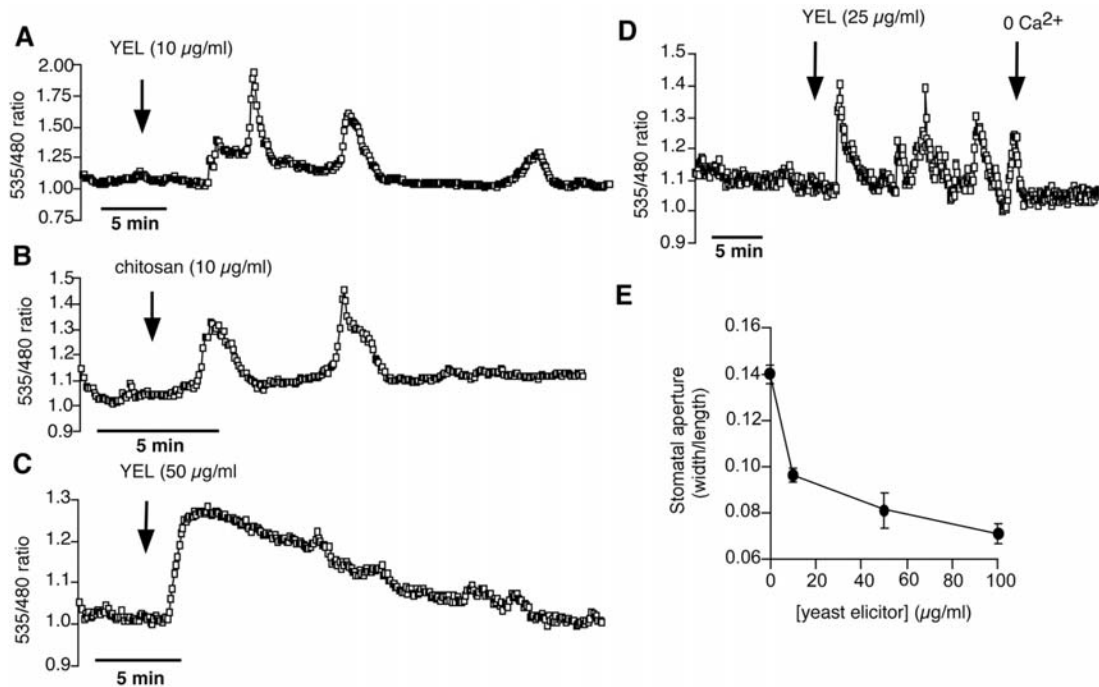


Figure III-3: Elicitor-induced repetitive $[Ca^{2+}]_{cyt}$ transients and stomatal closing. A, Repetitive $[Ca^{2+}]_{cyt}$ transients induced by 10 $\mu\text{g/ml}$ yeast elicitor. B, Repetitive $[Ca^{2+}]_{cyt}$ transients induced by 10 $\mu\text{g/ml}$ chitosan. C, Example of a $[Ca^{2+}]_{cyt}$ transient, induced by 50 $\mu\text{g/ml}$ yeast elicitor. Note that under the imposed conditions only a single $[Ca^{2+}]_{cyt}$ transient with a slow decay time was observed. D, Yeast elicitor-induced $[Ca^{2+}]_{cyt}$ transients require external Ca^{2+} . Epidermal peels were incubated in the standard bath solution (5 mM KCl, 50 μM $CaCl_2$, 10 mM Mes-Tris, pH 6.15). At the indicated timepoint (first arrow) the bath was perfused with a solution containing 25 $\mu\text{g/ml}$ yeast elicitor (5 mM KCl, 50 μM $CaCl_2$, 25 $\mu\text{g/ml}$ yeast elicitor, 10 mM Mes-Tris, pH 6,15). At the second timepoint (second arrow) the bath solution was exchanged with a Ca^{2+} -free solution (5 mM KCl, 250 μM EGTA, 10 mM Mes-Tris, pH 6.15). Immediately after the perfusion with zero Ca^{2+} started, the yeast elicitor-induced $[Ca^{2+}]_{cyt}$ transients ceased. E, Yeast elicitor reduces stomatal aperture. Each data point represents the mean stomatal aperture of 100 analyzed stomata from $n = 4$ replicates. Error bars show standard deviation. Stomatal aperture was measured 2 hours after elicitor application.

Yeast elicitor-induced transient increases in $[Ca^{2+}]_{cyt}$ required the presence of extracellular Ca^{2+} (Fig. III-3D). Elicitor-induced $[Ca^{2+}]_{cyt}$ transients immediately ceased after the bath solution was perfused with a Ca^{2+} -free bath solution (5 mM KCl, 250 μ M EGTA, 10 mM Mes/Tris, pH 6.15) ($n = 12$ cells). Although long-term external Ca^{2+} removal treatment may deplete intracellular calcium levels, it appears unlikely that this depletion is rapid enough to account for the immediate cessation of Ca^{2+} oscillations upon external Ca^{2+} removal. Note also that store operated calcium currents, which are activated by a depletion of intracellular calcium stores, are not activated by extracellular application of EGTA alone (Kwan et. al., 1990; Patterson et. al., 1999). Therefore the cessation of yeast elicitor-induced $[Ca^{2+}]_{cyt}$ elevations by external EGTA (Fig. III-3D) together with elicitor-induced I_{Ca} activation (Figs. III-1 and III-2) demonstrate a requirement of Ca^{2+} influx for this response. We also tested whether yeast elicitor has an effect on stomatal movements in *Arabidopsis* and found a concentration dependent reduction of stomatal aperture using the same concentrations that elicited $[Ca^{2+}]_{cyt}$ transients (Fig. III-3E).

ABA-regulated $[Ca^{2+}]_{cyt}$ elevations. Having shown a requirement of extracellular calcium for elicitor-induced $[Ca^{2+}]_{cyt}$ oscillations, we next tested whether ABA-induced $[Ca^{2+}]_{cyt}$ oscillations share this requirement. As previously shown, ABA (10 μ M) induces repetitive $[Ca^{2+}]_{cyt}$ elevations in cells

($n = 18$ of 40 cells) incubated in a bath solution containing calcium and 10 mM KCl (Fig. III-4A). However, when extracellular Ca^{2+} was buffered to submicromolar concentrations by adding 250 μM EGTA ($n = 12$) or 250 μM BAPTA ($n = 31$) 10 minutes prior to ABA treatment, ABA-induced $[\text{Ca}^{2+}]_{\text{cyt}}$ elevations could not be observed (Fig. III-4B). Readdition of extracellular Ca^{2+} at the end of the experiments led to external Ca^{2+} -induced $[\text{Ca}^{2+}]_{\text{cyt}}$ elevations, showing that these cells were competent to report $[\text{Ca}^{2+}]_{\text{cyt}}$ elevations (Fig. III-4B).

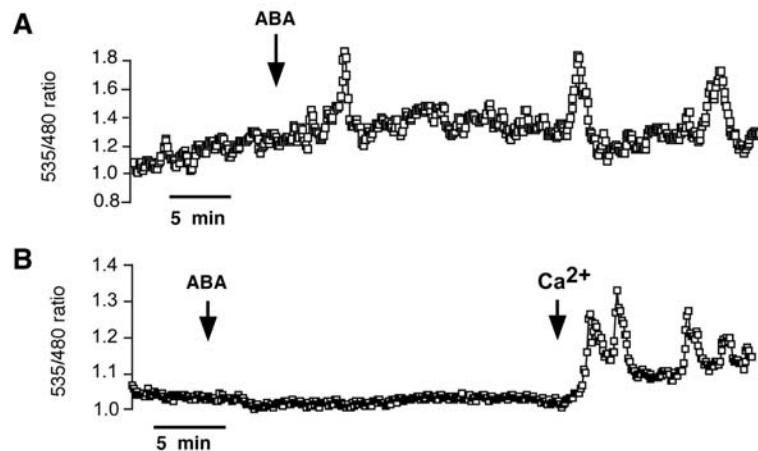


Figure III-4: ABA-induced $[\text{Ca}^{2+}]_{\text{cyt}}$ oscillations in *Arabidopsis* guard cells require extracellular Ca^{2+} . A, Repetitive $[\text{Ca}^{2+}]_{\text{cyt}}$ transients induced by 10 μM ABA. Extracellular solution: 5 mM KCl, 50 μM CaCl_2 , 10 mM Mes/Tris, pH 6.15. B, Guard cells which were incubated in Ca^{2+} -free solutions show no response to 10 μM ABA. Addition of 10 mM external Ca^{2+} at end of experiment caused $[\text{Ca}^{2+}]_{\text{cyt}}$ increases.

With evidence that external calcium is required for ABA-induced $[\text{Ca}^{2+}]_{\text{cyt}}$ oscillations in guard cells, we next examined the role of intracellular Ca^{2+} release pathways on ABA-induced $[\text{Ca}^{2+}]_{\text{cyt}}$ oscillations. We first tested

the pharmacological phospholipase C inhibitor U-73122 and its physiologically inactive analog U-73343 (Staxén et al., 1999), in *Arabidopsis* guard cells. Ten μM ABA was added to the solution bathing epidermal peels. Immediately after ABA-induced $[\text{Ca}^{2+}]_{\text{cyt}}$ transients became visible, the cells were perfused either with 1 μM U-73122 or 1 μM U-73343. In the case of U-73122, a partial inhibition of ABA-induced $[\text{Ca}^{2+}]_{\text{cyt}}$ transients was observed (Fig. III-5A, $n = 6$ cells). Perfusion of guard cells with the inactive analogue U-73343 (1 μM) did not inhibit ABA-induced transients (Fig. III-5B, $n = 10$ cells). In further experiments, epidermal peels were preincubated 30 min in 1 μM U-73122 or U-73343 before ABA (10 μM) was added to the bath solution. In the preincubation experiments with U-73122, no ABA-induced $[\text{Ca}^{2+}]_{\text{cyt}}$ increases were elicited (Fig. III-5C, $n = 6$ cells). Guard cells which were preincubated with U-73343 still responded to ABA (Fig. III-5D, $n = 15$ cells).

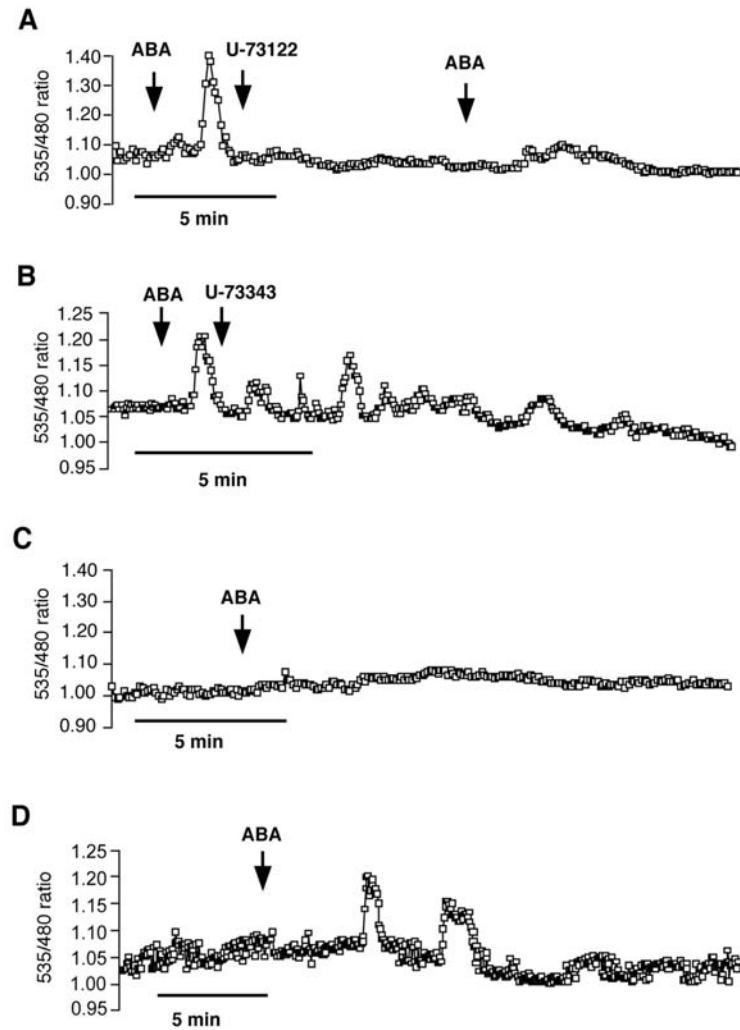


Figure III-5: The PLC inhibitor U-73122 has a negative effect on ABA-induced $[Ca^{2+}]_{cyt}$ oscillations. A, Perfusion with 1 μM U-73122 partially inhibited ABA (10 μM) induced $[Ca^{2+}]_{cyt}$ elevations in guard cells. Sequence of ABA and U-73122 perfusion: Timepoint 1 (first arrow): 10 μM ABA (+ standard bath solution); timepoint 2 (second arrow): 1 μM U-73122 (+ standard bath solution and 10 μM ABA), timepoint 3 (third arrow): 10 μM ABA (+ standard bath solution, without U-73122). B, Perfusion with 1 μM U-73343, an inactive analog of U-73122 has no effect on ABA-induced Ca^{2+} transients. C, After a 30 min preincubation of guard cells in 1 μM U-73122, ABA (10 μM) did not activate $[Ca^{2+}]_{cyt}$ transients in Arabidopsis guard cells. D, A 30 min preincubation of guard cells in 1 μM U-73343 did not inhibit ABA (10 μM)-induced Ca^{2+} transients in guard cells.

Studies have suggested that cyclic ADP ribose is a Ca^{2+} releasing second messenger in ABA signal transduction (Allen et. al., 1995; Wu et. al., 1997; Leckie et. al., 1998). We therefore analyzed the effects of nicotinamide on cameleon expressing guard cells. Nicotinamide blocks cyclic ADP ribose (cADPR) synthesis and has been used to analyze putative roles of cADPR in guard cells and tomato subepidermal cells (Wu et al., 1997; Leckie et al., 1998; Jacob et al., 1999; Macrobbie, 2000). Interestingly, nicotinamide consistently caused a rapid reduction in the cameleon fluorescence ratio of guard cells (Fig. III-6; $n = 44$ of 50 cells) suggesting that nicotinamide has a relatively drastic effect on $[\text{Ca}^{2+}]_{\text{cyt}}$ in *Arabidopsis* guard cells. Levels of basal $[\text{Ca}^{2+}]_{\text{cyt}}$ dropped upon nicotinamide application in both cells that were not treated with ABA (Fig. III-6A; $n = 36$) and ABA-treated cells (Fig. III-6B; $n = 8$). ABA-induced oscillations were inhibited by nicotinamide. This effect of nicotinamide was not due to any influence of nicotinamide on the cameleon protein, as *in vitro* experiments with recombinant yellow cameleon 2.1 protein showed that nicotinamide did not itself alter the fluorescence of cameleon, nor did it alter cameleon fluorescence ratio changes induced by calcium (data not shown). Nicotinamide treated cells were still able to respond to 10 mM external Ca^{2+} with an increase in $[\text{Ca}^{2+}]_{\text{cyt}}$, indicating that these cells were still responsive to external stimuli (Fig. III-6C). Our studies with PLC and cADPR inhibitors show that blocking these two calcium release pathways leads to distinct alterations in calcium homeostasis and signaling.

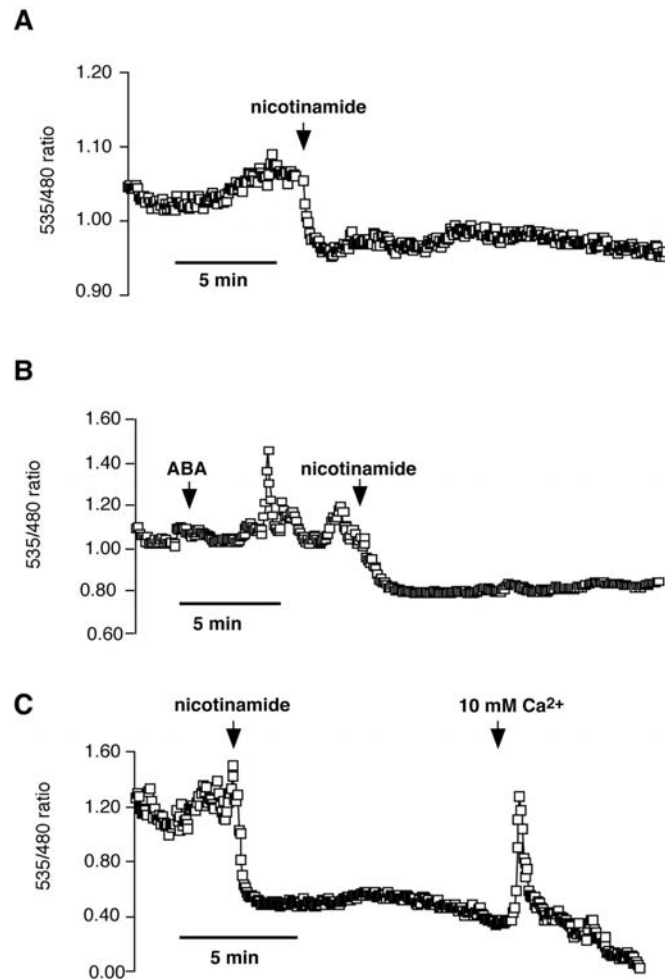


Figure III-6: Nicotinamide causes a drop in $[Ca^{2+}]_{cyt}$ in *Arabidopsis* guard cells. A, 50 mM nicotinamide reduced the baseline $[Ca^{2+}]_{cyt}$ level in untreated guard cells. B, 50 mM nicotinamide reduced the baseline $[Ca^{2+}]_{cyt}$ level and inhibited ABA-induced $[Ca^{2+}]_{cyt}$ oscillations. C, Nicotinamide (50 mM) treated cells are still responsive to the addition of 10 mM external calcium ($n = 7$ of 10 cells).

ROS-induced $[Ca^{2+}]_{cyt}$ elevations. Recent work suggests that reactive oxygen species (ROS) participate in the induction of $[Ca^{2+}]_{cyt}$ elevations by ABA in *Arabidopsis* guard cells, and ROS have been shown to trigger $[Ca^{2+}]_{cyt}$ elevations (McAinsh et al., 1996; Pei et al., 2000). To further investigate

whether the $[Ca^{2+}]_{cyt}$ elevations induced by these two stimuli are indeed part of a shared pathway, we investigated whether ROS-induced $[Ca^{2+}]_{cyt}$ elevations are more prevalent at hyperpolarized membrane potentials, as has been previously shown for ABA-induced $[Ca^{2+}]_{cyt}$ elevations (Grabov and Blatt, 1998). We tested this by recording ROS-induced $[Ca^{2+}]_{cyt}$ elevations in bath solutions with different concentrations of K^+ . A lower extracellular K^+ concentration leads to a more hyperpolarized membrane (Saftner and Raschke 1981; Clint and Blatt 1989; Grabov and Blatt, 1998). In 5 mM KCl, extracellular application of 100 μ M H_2O_2 induced a $[Ca^{2+}]_{cyt}$ transient in all 12 cells tested (Fig. III-7A), either consisting of one ($n = 9$ of 12 cells) or two transients ($n = 3$ of 12 cells). These transients had a mean duration of 3.18 ± 0.31 min, similar to that reported previously (Pei et al., 2000), and a mean relative peak $[Ca^{2+}]_{cyt}$ increase of ($\Delta ratio_{535/480}$) 0.49 ± 0.06 ($n = 12$). In solutions containing 100 mM KCl, H_2O_2 induced $[Ca^{2+}]_{cyt}$ transients in only 12 of 29 (41%) cells (Fig. III-7B); in all cases only a single $[Ca^{2+}]_{cyt}$ transient was observed, and these transients showed smaller $[Ca^{2+}]_{cyt}$ increases (mean $\Delta ratio_{535/480}$ of $0.18 \pm .02$) than those induced in 5 mM KCl. As reported previously (McAinsh et al., 1996; Pei et al., 2000), guard cells that were incubated in Ca^{2+} -free solutions showed no $[Ca^{2+}]_{cyt}$ elevation in response to H_2O_2 . Thus, ROS-induced $[Ca^{2+}]_{cyt}$ elevations and ABA-induced $[Ca^{2+}]_{cyt}$ elevations show enhanced activity at lower external K^+ concentrations, and both require external Ca^{2+} (Fig. III-4B).

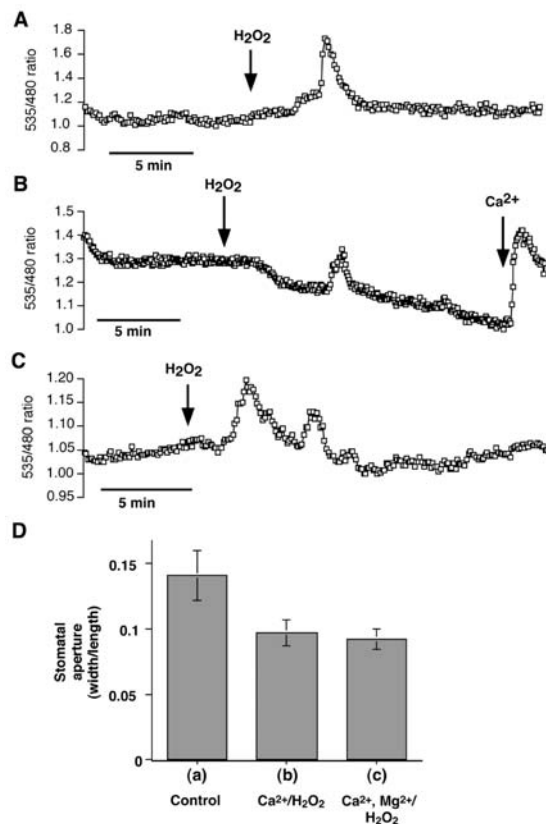


Figure III-7: Hydrogen peroxide-induced $[Ca^{2+}]_{cyt}$ elevations in guard cells of *A. thaliana* are dependent on the extracellular K^+ concentration and are not blocked by external Mg^{2+} . A, A $[Ca^{2+}]_{cyt}$ transient measured in a guard cell in response to 100 μM H_2O_2 . Extracellular solution: 5 mM KCl, 50 μM $CaCl_2$, 10 mM Mes/Tris, pH 6.15. B, 100 μM H_2O_2 induced $[Ca^{2+}]_{cyt}$ elevations in 12 of 29 cells in high extracellular potassium (100 mM KCl, 50 μM $CaCl_2$, 10 mM Mes/Tris, pH 6.15). C, 500 μM Mg^{2+} did not block H_2O_2 -induced Ca^{2+} elevations with 50 μM $CaCl_2$ in the bath. Extracellular solution: 500 μM $MgCl_2$, 50 μM $CaCl_2$, 5 mM KCl, 10 mM Mes/Tris, pH 6.15. D, Hydrogen peroxide-induced stomatal closure is not affected by magnesium. Each data point represents the mean stomatal aperture of 50 analyzed stomata from $n = 6$ replicates. Error bars show standard error of mean (relative to $n=6$). Stomatal aperture was measured 2 hours after application of: a) 0.2 mM $CaCl_2$ (Control), b) 0.2 mM $CaCl_2$, 0.2 mM H_2O_2 or c) 0.2 mM $CaCl_2$, 2 mM $MgCl_2$, 0.2 mM H_2O_2 . In all experiments 0.1 mM EGTA was added to the bath solution to buffer external $[Ca^{2+}]$ close to 0.1 mM (Pei et al., 2000). Hydrogen peroxide did not induce stomatal closure in the absence of this buffering, perhaps because external Ca^{2+} , including locally-released cell wall Ca^{2+} , was too high which can in itself cause partial stomatal closing (McAinsh et al., 1995; Allen et al., 1999a).

Previous experiments showed that ROS-activated I_{Ca} channels in guard cells are non-selective cation channels with a permeability to Mg^{2+} , suggesting that Mg^{2+} might compete with Ca^{2+} for passage through the channel (Pei et al., 2000). To test whether external Mg^{2+} can compete with Ca^{2+} signaling, we monitored ROS-induced $[Ca^{2+}]_{cyt}$ transients in the presence of an extracellular Mg^{2+} concentration (500 μ M) ten-fold higher than that of Ca^{2+} (50 μ M). These conditions had no influence on the induction of $[Ca^{2+}]_{cyt}$ transients by H_2O_2 (Fig. III-7C; $n = 13$ cells). We also performed stomatal closing assays to analyze whether hydrogen peroxide-induced stomatal closure is affected by magnesium. Replacement of 0.2 mM $CaCl_2$ in the bath solution by 2 mM $MgCl_2 + 0.2$ mM $CaCl_2$ had no influence on H_2O_2 -induced stomatal closure (Fig 7D). Exposing guard cells to 10 mM $MgCl_2$ did not cause $[Ca^{2+}]_{cyt}$ oscillations ($n=4$, data not shown), in contrast to the external Ca^{2+} response (Fig. III-4B). These data show that external Mg^{2+} cannot replace Ca^{2+} in inducing Ca^{2+} oscillations. Similarly, in the absence of external Ca^{2+} , shifts in the extracellular KCl concentration from 0.1 mM to 100 mM caused no changes in cameleon fluorescence ratios (Allen et al., 2001, supplemental web data, <http://www.nature.com/nature/journal/v411/n6841/extref/4111053aa.html>). These data further support that oscillations in cameleon ratios were not due to oscillations in cytosolic Cl^- concentrations.

Spontaneous $[Ca^{2+}]_{cyt}$ oscillations require external calcium. There is now quite compelling evidence that $[Ca^{2+}]_{cyt}$ elevations are an important component of guard cell signal transduction for multiple stimuli, such as ABA, Ca^{2+} and ROS. Interestingly, guard cells also frequently show spontaneously arising $[Ca^{2+}]_{cyt}$ oscillations, i.e. oscillations which are not induced by the extracellular application of such stimuli (Fig. III-8, Allen et al., 1999b; Staxén et al., 1999; Allen et al., 2001). We examined whether these spontaneous oscillations share properties with induced $[Ca^{2+}]_{cyt}$ oscillations by testing their dependence on extracellular K^+ and Ca^{2+} . As occurred with ABA- and ROS-induced oscillations, lower extracellular potassium concentrations led to increases in the occurrence of spontaneous $[Ca^{2+}]_{cyt}$ oscillations (Table III-II). Guard cells which were incubated in 5 mM KCl showed spontaneous $[Ca^{2+}]_{cyt}$ transients in approximately 45% of the 33 cells analyzed in this study. Note that the percentage of cells showing spontaneous $[Ca^{2+}]_{cyt}$ oscillations varies in different preparations, but they are commonly observed in guard cells (Grabov and Blatt, 1998; Allen et al., 1999b; Staxén et al., 1999). Cells which showed spontaneous $[Ca^{2+}]_{cyt}$ transients ($n = 15$ of 33 cells) exhibited an average of 2.07 ± 0.29 transients in 5 mM KCl (30 min recording interval; Table III-II, Fig. III-8A). In 0.1 mM KCl, the percentage of guard cells exhibiting spontaneous $[Ca^{2+}]_{cyt}$ transients was increased to 88% ($n = 42$ of 48 cells), and the average number of transients per cell was increased to 3.71 ± 0.25 (Table III-II, Fig. III-8B). Spontaneous $[Ca^{2+}]_{cyt}$ oscillation periods were shorter than those reported

for ABA-induced $[Ca^{2+}]_{cyt}$ oscillation periods (Table III-II; Allen et al., 2001). In solutions containing 100 mM KCl, spontaneous $[Ca^{2+}]_{cyt}$ oscillations were not observed (Fig. III-8C). Interestingly however, these same cells still produced transient $[Ca^{2+}]_{cyt}$ elevations when exposed to high extracellular Ca^{2+} (10 mM) (Fig. III-8C).

Table III-II: Spontaneous $[Ca^{2+}]_{cyt}$ transients in guard cells of *A. thaliana*. Summarized is the dependence of spontaneous $[Ca^{2+}]_{cyt}$ transients on the external K^+ concentration. Data were obtained during the first 30 min of each experiment. Errors represent standard error of the mean.

[KCl] (mM)	Rel. peak increase $[Ca^{2+}]_{cyt}$ ($\Delta ratio_{535/480}$)	Transient Duration ($\Delta t/min$)	Period (min)	No. of transients	% of cells with transients	Total no. of cells
0.1	0.25 ± 0.02	1.47 ± 0.13	5.91 ± 0.71	3.71 ± 0.25	88%	48
5	0.23 ± 0.03	2.68 ± 0.32	6.75 ± 1.43	2.07 ± 0.29	45%	33
100	0	0	0	0	0%	10

Upon removal of extracellular Ca^{2+} , as with ABA-induced $[Ca^{2+}]_{cyt}$ oscillations, spontaneous $[Ca^{2+}]_{cyt}$ oscillations rapidly ceased to occur (Fig. III-8D, $n = 19$ cells). A guard cell displaying spontaneous $[Ca^{2+}]_{cyt}$ transients under continuous perfusion with the standard bath solution (containing 5 mM KCl) was perfused with an EGTA-containing solution at timepoint 1. The $[Ca^{2+}]_{cyt}$ oscillations immediately ceased following the perfusion with zero Ca^{2+} . At timepoint 2, the cell was perfused again with the standard bath

solution containing 50 μM CaCl_2 , which induced a rapid recovery of $[\text{Ca}^{2+}]_{\text{cyt}}$ oscillations.

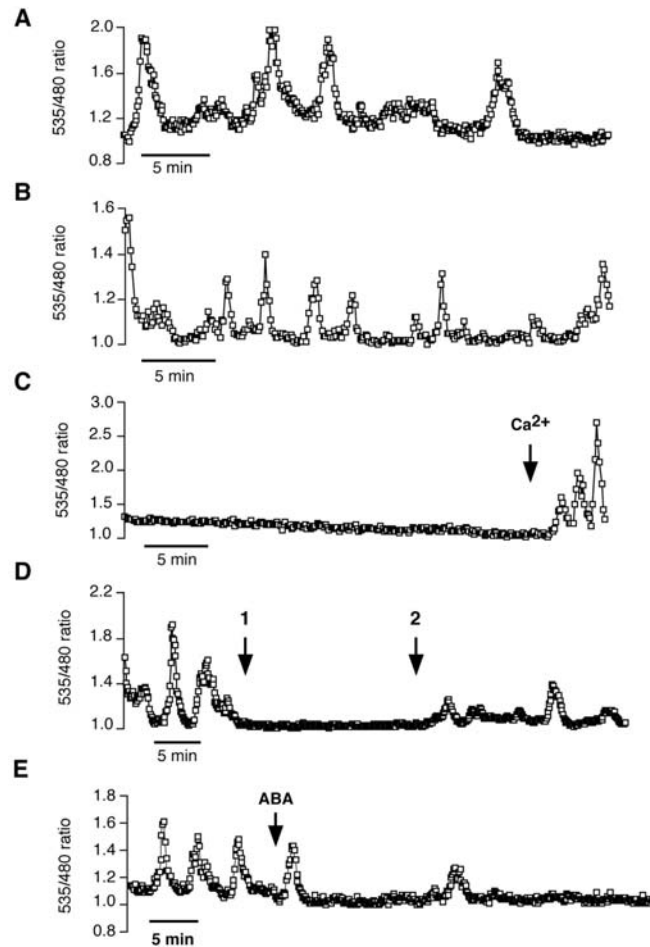


Figure III-8: Spontaneous $[Ca^{2+}]_{cyt}$ oscillations in guard cells of *A. thaliana* are dependent on the Ca^{2+} and K^+ concentration of the bath solution. A, Spontaneous $[Ca^{2+}]_{cyt}$ oscillations in a 5 mM KCl-solution (+50 μ M $CaCl_2$, 10 mM Mes/Tris, pH 6.15). B, The frequency of spontaneous $[Ca^{2+}]_{cyt}$ transients is increased in solutions containing low K^+ concentrations (0.1 mM KCl, 50 μ M $CaCl_2$, 10 mM Mes/Tris, pH 6.15, see also Table I). C, Guard cells showed no spontaneous $[Ca^{2+}]_{cyt}$ transients in high potassium solutions (100 mM KCl, 50 μ M $CaCl_2$). Note that 10 mM external Ca^{2+} triggered Ca^{2+} transients in guard cells, incubated in the same high potassium solutions. D, Perfusion with a Ca^{2+} -free solution (perfusion start at timepoint 1) inhibited spontaneous $[Ca^{2+}]_{cyt}$ transients. When cells were reperfused with a 50 μ M Ca^{2+} -containing standard bath solution (timepoint 2), a recovery of spontaneous $[Ca^{2+}]_{cyt}$ transients was observed ($n = 19$ cells). E, Spontaneous $[Ca^{2+}]_{cyt}$ oscillations were suppressed in 62 of 101 of guard cells (61%) by the application of 5 μ M ABA. ABA was applied at the time indicated by the arrow.

In Ca^{2+} imaging experiments to date, ABA was added to cells that showed no spontaneous Ca^{2+} oscillations (e.g. McAinsh et al., 1990; Schroeder and Hagiwara, 1990; Gilroy et al., 1991; Allan et al., 1994; Staxén et al., 1999; Allen et al., 1999b; Allen et al., 2001). Here we analyzed the effect of ABA on spontaneously oscillating guard cells. The spontaneous Ca^{2+} oscillation period (Table II) was shorter than that of ABA-induced Ca^{2+} oscillations (Allen et al., 2001). Interestingly, in cells that were showing spontaneous $[\text{Ca}^{2+}]_{\text{cyt}}$ oscillations at the beginning of the experiment, ABA, in a substantial number of experiments, lead to a rapid cessation of $[\text{Ca}^{2+}]_{\text{cyt}}$ oscillation activity. Complete spontaneous oscillation suppression occurred within 10-15 min following ABA application via the continuous perfusion stream and occurred in $n = 62$ of 101 spontaneously oscillating cells treated with ABA (61%; Fig. III-8E). In the remaining cells ABA did not cause cessation of spontaneous $[\text{Ca}^{2+}]_{\text{cyt}}$ oscillations. In a few of the cells ($n = 14$) where ABA suppressed spontaneous $[\text{Ca}^{2+}]_{\text{cyt}}$ oscillations, oscillations re-activated following a 30-40 min quiescent period. The ability of ABA to abolish spontaneous $[\text{Ca}^{2+}]_{\text{cyt}}$ oscillations is a novel finding and may be associated with a retuning of signal transduction components for ABA signaling and/or ABA-induced depolarization.

DISCUSSION

Elicitor-induced $[Ca^{2+}]_{cyt}$ oscillations. In tomato (Gelli et al., 1997) and parsley (Zimmermann et al., 1997), two distinct types of plant defense elicitor-activated Ca^{2+} influx currents have been described. The elicitor-induced currents in tomato cells activate at hyperpolarizing membrane potentials similar to those found here (Gelli et al., 1997), and show similarities to the ABA, ROS and hyperpolarization activated Ca^{2+} currents (I_{Ca}) of *Arabidopsis* guard cells (Pei et al., 2000), whereas in parsley cells elicitors activate very large conductance channels (>250 ps) at more depolarized potentials (Zimmerman et al., 1997). We attempted to establish whether I_{Ca} can be activated by elicitors in *Arabidopsis* guard cells. We used two different elicitors of plant defense reactions in our studies. Chitosan, which has previously been shown to cause the production of reactive oxygen species and stomatal closing in tomato and *Commelina* guard cells (Lee et al., 1999) and yeast elicitor, an elicitor with broad activity (induction of benzophenanthridine alkaloids, generation of reactive oxygen species, induction of intracellular pH shifts) in many diverse plant species (Blechert et al., 1995; Roos et al., 1998). We demonstrate that both chitosan and yeast elicitor activate a hyperpolarization-dependent current in guard cells, which resembles I_{Ca} in its voltage dependence. Furthermore, cytosolic NAD(P)H was necessary to activate this current (Fig. III-2), which correlates with recent findings on a

NAD(P)H requirement for ABA activation of I_{Ca} (Murata et al., 2001). Therefore the chitosan- and yeast elicitor-induced production of reactive oxygen species in guard cells (Lee et al., 1999) may occur via modulation of NAD(P)H-dependent mechanisms, as has been demonstrated in plant defense responses (Keller et al., 1998). The ROS thus produced could activate I_{Ca} , leading to the observed elicitor-induced increases in $[Ca^{2+}]_{cyt}$.

The presented findings support the previously proposed model that ROS activation of I_{Ca} channels is part of a shared branch or “cassette” of stress signaling pathways (Pei et al., 2000; Schroeder et al., 2001b) and suggests that NAD(P)H-dependent activation of I_{Ca} channels represents a cross talk mechanism between ABA and defense signaling. For both elicitor signaling and ABA signaling, the specific reactive oxygen intermediate(s) that mediates signal transduction remains to be determined and could include H_2O_2 , O_2^- , 1O_2 , and OH^- , among others. In addition, production of the reactive oxygen molecule NO has recently been shown to be induced by ABA in guard cells (Neill et al., 2002). The *abi1-1* and *abi2-1* protein phosphatase 2Cs (PP2C) have been shown to impair ABA signaling in guard cells upstream of I_{Ca} activation (Murata et al., 2001). Recent findings show that H_2O_2 inhibits the PP2C activities of both ABI1 (Meinhard and Grill, 2001) and ABI2 (Meinhard et al., 2002), which in turn could contribute to I_{Ca} activation.

Yeast elicitor evoked stomatal closing in guard cells in a concentration dependent manner. Ca^{2+} imaging experiments demonstrated that both elicitors

induce transient elevations in the cytoplasmic Ca^{2+} concentration of guard cells. The elicitor concentrations which induced $[\text{Ca}^{2+}]_{\text{cyt}}$ transients (10 $\mu\text{g/ml}$) were sufficient to trigger stomatal closing responses. Yeast elicitor-induced $[\text{Ca}^{2+}]_{\text{cyt}}$ increases required the availability of extracellular Ca^{2+} ions. This indicates that an initial Ca^{2+} influx is necessary for the observed $[\text{Ca}^{2+}]_{\text{cyt}}$ increases. This observation is in accordance with studies showing that extracellular Ca^{2+} is necessary for the induction of plant defense responses against pathogens (Yang et al., 1997; Scheel, 1998; Blume et al., 2000).

Influx and internal release of Ca^{2+} in guard cell signaling. Although other studies have recently addressed the requirement of extracellular Ca^{2+} for guard cell Ca^{2+} increases (Romano et al., 2000; MacRobbie, 2000), the contribution of external Ca^{2+} to $[\text{Ca}^{2+}]_{\text{cyt}}$ oscillations, which have been shown to be an important part of Ca^{2+} signaling in guard cells (Allen, et. al., 2000), has not yet been determined. The abundance of Ca^{2+} release mechanisms in guard cells could lead to the hypothesis that ABA-induced Ca^{2+} elevations in *Arabidopsis* guard cells can occur after external Ca^{2+} removal. Here we show that $[\text{Ca}^{2+}]_{\text{cyt}}$ oscillations do not occur in the absence of extracellular Ca^{2+} . This was shown for oscillations induced by ABA and plant defense elicitors, as well as for spontaneously arising $[\text{Ca}^{2+}]_{\text{cyt}}$ oscillations. This is consistent with previous work that showed that the earliest increases in $[\text{Ca}^{2+}]_{\text{cyt}}$ in response to ABA $[\text{Ca}^{2+}]_{\text{cyt}}$ elevations can occur near the plasma membrane (McAinsh et

al., 1992) as well as with a recent tracer flux study showing that extracellular Ca^{2+} contributes to ABA-induced K^+ (Rb^+) efflux at $>1 \mu\text{M}$ ABA in *Commelina communis* guard cells (MacRobbie, 2000).

Although the presence of external Ca^{2+} was a prerequisite for the induction of cytoplasmic Ca^{2+} transients under our experimental conditions, these data do not contradict the importance of internal Ca^{2+} release mechanisms. Experiments in *Commelina* with U-73122, an inhibitor of plant phospholipase C (Staxén et al., 1999), showed that ABA-induced cytoplasmic Ca^{2+} transients were suppressed in guard cells which were preincubated in $1 \mu\text{M}$ U-73122. Experiments on *Arabidopsis* guard cells correlate with these results (Fig. III-5, A and C). These findings suggest that inositol 1,4,5 trisphosphate (IP_3) triggered Ca^{2+} release mechanisms may contribute to ABA-induced $[\text{Ca}^{2+}]_{\text{cyt}}$ increases in *Arabidopsis*. Present simplified models consider parallel functioning of Ca^{2+} influx and PLC-dependent Ca^{2+} release mechanisms. Interestingly, however, our results, as well as the requirement of calcium for plant PLC activity (Kopka et al., 1998; Hernández-Sotomayor et al., 1999) suggest that PLC activation and Ca^{2+} influx may be interdependent. Genetic analyses will be important to test this proposed linkage in activation of Ca^{2+} influx and PLC-dependent pathways.

Experiments using the cADPR blocker nicotinamide showed a rapid reduction in basal calcium levels in 88% of guard cells (Fig. III-6 A-C). Detailed microinjection studies strongly support a role for cADPR in ABA signaling (Wu

et al., 1997; Leckie et al., 1998). The results presented here show a difference in the actions of cADPR and PLC inhibitors. The reduction in basal $[Ca^{2+}]_{cyt}$ levels by nicotinamide may contribute to the additive effects of nicotinamide and U-73122 on inhibition of ABA-induced stomatal closing and Rb^+ efflux (Jacob et al., 1999; MacRobbie 2000). The present findings are consistent with models suggesting that cADPR functions in parallel with other Ca^{2+} -dependent pathways (Jacob et al., 1999; MacRobbie 2000). In the present study nicotinamide also reduced ABA-induced $[Ca^{2+}]_{cyt}$ elevations, which correlates with models including cADPR as a second messenger in ABA signaling (Wu et al., 1997; Leckie et al., 1998). It is also possible that nicotinamide reduces overall $[Ca^{2+}]_{cyt}$ levels, thus increasing the threshold required for ABA-induced $[Ca^{2+}]_{cyt}$ elevations to proceed. Genetic alteration and inducible silencing of individual mechanisms and Ca^{2+} imaging will be important for dissecting the underlying differential contributions of Ca^{2+} release mechanisms to Ca^{2+} signaling. Additionally, the effect of nicotinamide suggests that cADPR may play a role in cytosolic calcium homeostasis.

ABA inhibition of spontaneous oscillations. Surprisingly, we show that ABA causes cessation of spontaneously occurring $[Ca^{2+}]_{cyt}$ oscillations in the majority of guard cells ($n = 62$ of 101). These data reveal a new, previously not investigated mode of ABA action. A recent study has shown that a “window” of cytosolic $[Ca^{2+}]_{cyt}$ oscillation parameters encodes steady-state stomatal closing

in *Arabidopsis* (Allen et al., 2001). Interestingly, the periods of spontaneous $[Ca^{2+}]_{cyt}$ oscillations found here (6 min; Table II), based on the data of Allen et al., (2001) would correspond to little or no stomatal closure. (Note, however, that we expect that the range of $[Ca^{2+}]_{cyt}$ oscillation parameters that mediate stomatal movements are dynamic and exhibit a dependence on environmental and cellular conditions.) The data presented here indicate that ABA may repress $[Ca^{2+}]_{cyt}$ oscillations not associated with ABA signaling in order for ABA responses to proceed. ABA-induced depolarization is predicted to cause cessation of spontaneous $[Ca^{2+}]_{cyt}$ elevations (Grabov and Blatt, 1998). This hypothesis is supported by our data indicating that high external K^+ , which causes depolarization (Grabov and Blatt, 1998), also mitigate ROS-induced $[Ca^{2+}]_{cyt}$ elevations (Fig. III-8C), thus depolarization may contribute to the ABA inhibition of spontaneous Ca^{2+} elevations revealed here.

Effect of $[K^+]_{ext}$ on $[Ca^{2+}]_{cyt}$ oscillations. We show that the percentage of cells that show either spontaneous or ROS-induced $[Ca^{2+}]_{cyt}$ elevations is reduced at elevated extracellular potassium concentrations. Earlier work in *Vicia faba* demonstrated that the membrane potential of guard cells exhibits a near-Nernstian dependence on $[K^+]_{ext}$, i.e. the lower the $[K^+]_{ext}$, the more hyperpolarized the plasma membrane (Saftner and Raschke, 1981; Clint and Blatt, 1989). Furthermore, the non-selective nature of an ABA-activated Ca^{2+} influx current in *Vicia faba* guard cells, results in reversal potentials that are

more negative (e.g. -10 mV) than a Ca^{2+} selective channel would show (e.g. $> +60$ mV) (Schroeder and Hagiwara, 1990). Consistent with these findings, 50 mM KCl produced a low probability of ABA-induced Ca^{2+} elevations in previous studies (Gilroy et al., 1991; Allan et al., 1994). Thus these data suggest that $[\text{Ca}^{2+}]_{\text{cyt}}$ elevations are favoured by hyperpolarized membranes. This is in agreement with other studies in *Vicia* guard cells that show that $[\text{Ca}^{2+}]_{\text{cyt}}$ elevations accompany membrane hyperpolarization (Grabov and Blatt, 1998) and low external K^+ concentrations (Gilroy et al., 1991; Allen et al., 2000).

Conversely, we found that $[\text{Ca}^{2+}]_{\text{cyt}}$ elevations induced by high extracellular calcium did not appear affected by $[\text{K}^+]_{\text{ext}}$ (end of trace in Fig. III-8C). Previous research has shown that Ca^{2+} influx mediates the initial phase of $[\text{Ca}^{2+}]_{\text{cyt}}$ transients induced by external Ca^{2+} (McAinsh et al., 1995). Even in 100 mM KCl, a large rise in $[\text{Ca}^{2+}]_{\text{cyt}}$ was always seen immediately following extracellular application of 10 mM CaCl_2 (Fig. III-8C). This suggests that a hyperpolarization-independent mechanism for generation of $[\text{Ca}^{2+}]_{\text{cyt}}$ elevations is acting under these conditions or that 10 mM Ca^{2+} shifts the reversal potential of plasma membrane Ca^{2+} channels sufficiently positive to allow Ca^{2+} influx as would be expected for non-selective Ca^{2+} permeable channels found in *Vicia* guard cells (Schroeder and Hagiwara, 1990). Note that more than one plasma membrane Ca^{2+} channel is likely to contribute to cytosolic Ca^{2+} elevations in guard cells (Hamilton et al., 2000), assuming that

the open probability of hyperpolarization-activated Ca^{2+} channels is not altered by physiological factors and ion gradients.

CONCLUSIONS

The present study demonstrates that elicitors activate plasma membrane I_{Ca} channels in an NADPH-dependent manner providing strong evidence for a shared signaling cassette of early ABA and elicitor signaling in guard cells. Furthermore, removal of extracellular Ca^{2+} causes rapid cessation of elicitor- and ABA-induced as well as spontaneous cytosolic $[\text{Ca}^{2+}]_{\text{cyt}}$ oscillations in guard cells, suggesting a requirement of Ca^{2+} influx for operation of the guard cell Ca^{2+} signaling system. Detailed analyses of spontaneous Ca^{2+} oscillations in guard cells show that these differ from typical ABA-induced Ca^{2+} elevations and indeed that ABA can inhibit spontaneous oscillations. Additionally, data suggest that Ca^{2+} influx and phospholipase C are interdependent rather than simply acting in parallel in mediating ABA-induced cytosolic Ca^{2+} elevations, whereas the pharmacological cADPR inhibitor nicotinamide has a unique effect of lowering baseline cytosolic Ca^{2+} levels in *Arabidopsis* guard cells.

MATERIALS AND METHODS

Plant material and growth. Plants of *Arabidopsis thaliana* (ecotype Landsberg erecta) stably expressing yellow cameleon 2.1 under the control of the constitutive 35 S promoter (Allen et al., 1999b) were used in our experiments to measure $[Ca^{2+}]_{\text{cyt}}$ levels in guard cells. *Arabidopsis thaliana* seedlings were grown at 20⁰C in a controlled environment growth chamber (Conviron model E 15; Controlled Environments, Asheville, North Carolina, USA) under a 16 h light/8 h dark cycle with a photon fluency rate of 75 $\mu\text{mol m}^{-2} \text{sec}^{-1}$. Pots were watered every 2 – 3 days with deionized water and plants were misted with deionized water daily to keep the humidity close to 70%.

Stomatal movement analyses. Stomatal movement analyses were performed as described previously (Pei et al., 1997, Allen et al., 1999a). Rosette leaves from 4 - 6 week old plants were detached and floated for 2h in opening solution in the light (photon fluency rate of 75 $\mu\text{mol m}^{-2} \text{sec}^{-1}$). Depending on the type of experiment, we used two different opening solutions. Opening solution I (5 mM KCl, 50 $\mu\text{M CaCl}_2$, 10 mM Mes-Tris, pH 6.15) was used to study the effect of elicitors on stomatal aperture, opening solution II (10 mM KCl, 0.1 mM EGTA, 10 mM Mes-KOH, pH 6.15) to analyse the effect of hydrogen peroxide. After 2h, yeast elicitor or chitosan was added to opening solution I. In the case of the H₂O₂ experiments the following solutions were added to opening solution II as indicated: a) (Control) 0.2 mM CaCl₂, b) 0.2 mM CaCl₂, 0.2 mM H₂O₂ or c) 0.2 mM CaCl₂, 2 mM MgCl₂, 0.2 mM H₂O₂ (free

external Ca^{2+} was about 0.1 mM). After a further incubation period, the leaves were blended in a Waring Blender, the resulting epidermal fragments were filtered out with a 30 μm nylon mesh, and guard cell aperture ratios were measured as described (Pei, et. al., 1997).

Elicitor preparation. Chitosan was purchased from Calbiochem, prepared as previously described (Walker-Simmons et al., 1984), then dissolved in stomatal opening solution I. Yeast elicitor was prepared according to the method of Schumacher et al. (1987). Briefly, 1 kg of commercial baker's yeast (*Saccharomyces cerevisiae*) was dissolved in 1.5 l of sodium citrate buffer (20 mM, pH 7.0) and autoclaved at 121⁰C and 1.1 bar for 60 min. The autoclaved suspension was centrifuged at 10,000 x g for 20 min. The resulting supernatant was mixed with 1 volume of ethanol and stirred gently overnight. The resulting precipitate was then centrifuged at 10,000 x g for 20 min. The supernatant of this centrifugation step was subjected to another ethanol precipitation overnight. The elicitor precipitate was lyophilized and stored at -20⁰C until use.

[Ca²⁺]_{cyt} imaging experiments. Epidermal strips of *Arabidopsis* leaves were mounted on coverslips with medical adhesive (Hollister Inc., Libertyville, Illinois, USA) and incubated in a solution containing 5 mM KCl, 50 μM CaCl_2 , and 10 mM Mes/Tris, pH 6.15. To promote stomatal opening, the strip was

illuminated for 2 h (photon fluency rate of $125 \mu\text{mol m}^{-2} \text{sec}^{-1}$) at 22°C before measurements started. YC 2.1 $[\text{Ca}^{2+}]_{\text{cyt}}$ imaging experiments were performed as described previously (Allen et al., 1999b; 2000). The present imaging system differed from the one described by Allen et al. (1999) and was outfitted with a 440 ± 10 nm filter with a 455 DCLP dichroic mirror for excitation and interchanging 485 ± 20 and 535 ± 15 filters for emission. Note that in the present and also recent studies (Allen et al., 2000; Allen et al., 2001; Hugouvieux et al., 2001) *Arabidopsis* lines were used that show higher cameleon expression levels than the initially reported studies (Allen et al., 1999b) and that these lines allowed imaging at a reduced excitation intensity which did not excite measurable chloroplast fluorescence. A slow baseline drift due to YFP bleaching was linearly subtracted. The lowest ratio value in each individual experiment was defined as ratio 1. Transient duration was defined as the time interval between the start and end of a transient unless otherwise noted; period was defined as the time between two peaks of consecutive transients. Results are reported as average \pm standard error of the mean.

In vitro cameleon assay. Fluorescence emission profiles of purified YC 2.1 protein were measured using a fluorimeter. Measurement was made in buffer (100 mM KCl, 10 mM MOPS, pH 7.2) with or without 50 mM nicotinamide and with either nominally zero calcium (100 μM EDTA) or 4 mM CaCl_2 .

Electrophysiology. Whole-cell voltage-clamp experiments on *Arabidopsis* guard cells were performed by using an Axopatch 200 amplifier (Axon Instruments) as described (Pei et al., 1997). Liquid junction potentials were corrected. For data analysis AXOGRAPH 3.5 was used. Standard solutions contained 100 mM BaCl₂, 0.1 mM DTT, 10 mM Mes-Tris, pH 5.6 in the bath and 10 mM BaCl₂, 0.1 mM DTT, 4 mM EGTA, 0 or 5 mM NADPH, 10 mM HEPES-Tris, pH 7.1 in the pipette. Exchange of initial bath solution with bath solution containing 10 µg/ml elicitor or chitosan was achieved by pipetting. Bath and pipette osmolalities were adjusted to 485 and 500 mmol kg⁻¹, respectively, using D-sorbitol.

ACKNOWLEDGMENTS

We thank Stephen Adams and Roger Tsien for support with *in vitro* measurements on recombinant cameleon and discussions.

REFERENCES CITED

Allan AC, Fricker MD, Ward JL, Beale MH, and Trewavas AJ (1994) Two transduction pathways mediate the rapid effects of abscisic acid in *Commelina* guard cells. *Plant Cell* 6: 1319-1328

Allen GJ, Muir SR and Sanders D (1995) Release of Ca²⁺ from individual plant vacuoles by both InsP3 and cyclic ADP-ribose. *Science* 268: 735-737

- Allen GJ, Kuchitsu K, Chu SP, Murata Y, and Schroeder JI (1999a) *Arabidopsis* *abi1-1* and *abi2-1* phosphatase mutations reduce abscisic acid-induced cyt oplasmic calcium rises in guard cells. *Plant Cell* 19: 1785-1798
- Allen GJ, Kwak JM, Chu SP, Llopis J, Tsien RY, Harper JF and Schroeder JI (1999b) Cameleon calcium indicator reports cyt oplasmic calcium dynamics in *Arabidopsis* guard cells. *Plant J.* 19: 735-747
- Allen GJ, Chu SP, Schumacher K, Shimazaki CT, Vafeados D, Kemper A, Hawke SD, Tallman G, Tsien RY, Harper JF, Chory J and Schroeder JI (2000) Alteration of stimulus-specific guard cell calcium oscillations and stomatal closing in *Arabidopsis* *det3* mutant. *Science* 289: 2338-2342
- Allen GJ, Chu SP, Harrington CL, Schumacher K, Hoffman T, Tang YY, Grill E, and Schroeder JI (2001) A defined range of guard cell calcium oscillation parameters encodes stomatal movements. *Nature* 411: 1053-1057
- Blatt MR and Armstrong F (1993) K^+ channels of stomatal guard cells – abscisic acid-evoked control of the outward rectifier mediated by cyt oplasmic pH. *Planta* 191: 330-341
- Blatt MR (2000) Ca^{2+} signaling and control of guard-cell volume in stomatal movements. *Curr. Opin. Plant Biol.* 3: 196-204
- Blechert S, Brodschelm W, Hölder S, Kammerer L, Kutchan TM, Müller MJ, Xia ZQ and Zenk MH (1995) The octadecanoic pathway: Signal molecules for the regulation of secondary pathways. *Proc. Natl. Acad. Sci.* 92: 4099-4105
- Blume B, Nürnberger T, Nass N and Scheel D (2000) Receptor-mediated increase in cyt oplasmic free calcium required for activation of pathogen defense in parsley. *Plant Cell* 12: 1425-1440
- Clayton H, Knight MR, Knight H, McAinsh MR and Hetherington AM (1999) Dissection of the ozone-induced calcium signature. *Plant J.* 17: 575-579
- Clint GM and Blatt MR (1989) Mechanisms of fusicoccin action: evidence for concerted modulations of secondary K^+ transport in a higher plant cell. *Planta* 178: 495-508
- De Silva DLR, Hetherington AM and Mansfield TA (1985) Synergism between calcium ions and abscisic acid in preventing stomatal opening. *New Phytol.* 100: 473-482

Gehring CA, Irving HR and Parish RW (1990) Effects of auxin and abscisic acid on intracellular pH and free Ca^{2+} . Proc. Natl. Acad. Sci. 87: 9645-9649

Gehring CA, McConchie RM, Venis MA and Parish RW (1998) Auxin-binding-protein antibodies and peptides influence stomatal opening and alter cytoplasmic pH. Planta 205: 581-586

Gelli A, Higgins VJ and Blumwald E (1997) Activation of plant plasma membrane Ca^{2+} -permeable channels by race-specific fungal elicitors. Plant Physiol. 113: 269-279

Gilroy S, Fricker MD, Read ND and Trewavas AJ (1991) Role of calcium in signal transduction of *Commelina* guard cells. Plant Cell 3: 333-344

Grabov A and Blatt MR (1998) Membrane voltage initiates Ca^{2+} waves and potentiates Ca^{2+} increases with abscisic acid in stomatal guard cells. Proc. Natl. Acad. Sci. 95: 4778-4783

Hadwiger LA and Beckman JM (1980) Chitosan as a component of pea-Fusarium solani interactions. Plant Physiol. 66: 205-211

Hamilton DW, Hills A, Köhler B and Blatt MR (2000) Ca^{2+} channels at the plasma membrane of stomatal guard cells are activated by hyperpolarization and abscisic acid. Proc. Natl. Acad. Sci. 97: 4967-4972

Hepler PK and Wayne RO (1985) Calcium and plant development. Annu. Rev. Plant Phys. 36: 397-439

Hernández-Sotomayor SMT, Santos-Briones CDL, Muñoz-Sánchez JA, and Loyola-Vargas VM (1999) Kinetic analysis of phospholipase C from *Catharanthus roseus* transformed roots using different assays. Plant Physiol. 120: 1075-1082

Hugouvieux V, Kwak JM, and Schroeder JIS (2001) An mRNA cap binding protein, ABH1, modulates early abscisic acid signal transduction in *Arabidopsis*. Cell 106: 477-487

Jacob T, Ritchie S, Assmann SM, and Gilroy S (1999) Abscisic acid signal transduction in guard cells is mediated by phospholipase D activity. Proc. Natl. Acad. Sci. 96: 12192-12197

Kawano T and Muto S (2000) Mechanism of peroxidase actions for salicylic acid-induced generation of active oxygen species and an increase in cytosolic calcium in tobacco cell suspension. J. of Exp. Bot. 51: 685-693

Keller T, Damude HG, Werner D, Doerner P, Dixon RA and Lamb C (1998) A plant homolog of the neutrophil NADPH oxidase gp91phox subunit gene encodes a plasma membrane protein with Ca^{2+} binding motifs. *Plant Cell* 10: 255-266

Knight MR, Campbell AK, Smith SM and Trewavas AJ (1991) Transgenic plant aequorin reports the effects of touch and cold-shock and elicitors on Ca^{2+} cytoplasmic calcium. *Nature* 352: 524-526

Kopka J, Pical C, Hetherington AM and Müller-Röber B (1998) Ca^{2+} /phospholipid-binding (C_2) domain in multiple plant proteins: novel components of the calcium-sensing apparatus. *Plant Mol. Biol.* 36: 627-637

Kwan CY, Takemura H, Obie JF, Thastrup O and Putney JW (1990) Effects of MeCh, thapsigargin and La^{3+} on plasmalemmal and intracellular Ca^{2+} transport in lacrimal acinar cells. *Am. J. Physiol.* 258: C1006-C1015

Leckie CP, McAinsh MR, Allen GJ, Sanders D and Hetherington AM (1998) Abscisic acid-induced stomatal closure mediated by cyclic ADP-ribose. *Proc. Natl. Acad. Sci.* 95: 15837-15842

Lee S, Choi H, Suh S, Doo IS, Oh KY, Choi EJ, Schroeder Taylor AT, Low PS and Lee Y (1999) Oligogalacturonic acid and chitosan reduce stomatal aperture by inducing the evolution of reactive oxygen species from guard cells of tomato and *Commelina communis*. *Plant Physiol.* 121: 147-152

MacRobbie, EAC (2000) ABA activates multiple Ca^{2+} fluxes in stomatal guard cells, triggering vacuolar K^+ (Rb^+) release. *Proc. Natl. Acad. Sci.* 97: 12361-12368

McAinsh MR, Brownlee C and Hetherington AM (1990) Abscisic acid-induced elevation of guard cell cytosolic Ca^{2+} precedes stomatal closure. *Nature* 343: 186-188

McAinsh MR, Brownlee C and Hetherington AM (1992) Visualizing changes in cytosolic-free Ca^{2+} during the response of stomatal guard cells to abscisic acid. *Plant Cell* 4: 1113-1122

McAinsh MR, Webb AAR, Taylor JE and Hetherington AM (1995) Stimulus-induced oscillations in guard cell cytosolic free calcium. *Plant Cell* 7: 1207-1219

McAinsh MR, Brownlee C and Hetherington AM (1996) Changes in stomatal behavior and guard cell cytosolic free calcium in response to oxidative stress. *Plant Physiol* 111: 1031-1042

Meinhard M and Grill E (2001) Hydrogen peroxide is a regulator of ABI1, a protein phosphatase 2C from *Arabidopsis*. *Febs Lett.* 508: 443-446

Meinhard M, Rodriguez PL and Grill E (2002) The sensitivity of ABI2 to hydrogen peroxide links the abscisic acid-response regulator to redox signaling. *Planta* 214: 775-782

Mithöfer A, Ebel J, Bhagwat AA, Boller T and Neuhaus-Url G (1999) Transgenic aequorin monitors cytosolic calcium transients in soybean cells challenged with β -glucan or chitin elicitors. *Planta* 207: 566-574

Murata Y, Pei ZM, Mori IC and Schroeder JI (2001) ABA activation of plasma membrane Ca^{2+} channels in guard cells requires NAD(P)H and is differentially disrupted upstream and downstream of reactive oxygen species production in the *abi1-1* and *abi1-2* PP2C mutants. *Plant Cell* 13: 2513-2523

Neill SJ, Desikan R, Clarke A and Hancock JT (2002) Nitric oxide is a novel component of abscisic acid signaling in stomatal guard cells. *Plant Physiol.* 128: 13-16

Patterson RL, van Rossum DB and Gill DL (1999) Store-Operated Ca^{2+} entry: evidence for a secretion-like coupling model. *Cell* 98: 487-499

Pei ZM, Kuchitsu K, Ward JM, Schwarz M and Schroeder JI (1997) Differential abscisic acid regulation of guard cell slow anion channels in *Arabidopsis* wild-type and *abi1* and *abi2* mutants. *Plant Cell* 9: 409-423

Pei ZM, Murata Y, Benning G, Thomine S, Klüsener B, Allen GJ, Grill E and Schroeder JI (2000) Calcium channels activated by hydrogen peroxide mediate abscisic acid signaling in guard cells. *Nature* 406: 731-734

Price AH, Taylor A, Ripley SJ, Griffiths A, Trewavas AJ and Knight MR (1994) Oxidative signals in tobacco increase cytosolic calcium. *Plant Cell* 6: 1301-1310

Romano LA, Jacob T, Gilroy, S and Assmann SM (2000) Increases in cytosolic Ca^{2+} are not required for abscisic acid-inhibition of inward K^{+} currents in guard cells of *Vicia faba* L. *Planta* 211: 209-217

Roos W, Evers S, Hieke M, Tschöpe M and Schumann B (1998) Shifts of intracellular pH distribution as a part of the signal mechanism leading to the elicitation of benzophenanthridine alkaloids. *Plant Physiol* 118: 349-364

Saftner RA and Raschke K (1981) Electrical potentials in stomatal complexes. *Plant Physiol* 67: 1124-1132

Sanders D, Brownlee C and Harper JF (1999) Communicating with calcium. *Plant Cell* 11: 691-706

Scheel D (1998) Resistance response physiology and signal transduction. *Curr. Opin. Plant Biol.* 1: 305-310

Schmidt C, Schelle I, Liao YJ and Schroeder JI (1995) Strong regulation of slow anion channels and abscisic acid signaling in guard cells by phosphorylation and dephosphorylation events. *Proc. Natl. Acad. Sci.* 92: 9535-9539

Schroeder JI and Hagiwara S (1989) Cytosolic calcium regulates ion channels in the plasma membrane of *Vicia faba* guard cells. *Nature* 338: 427-430

Schroeder JI and Hagiwara S (1990) Repetitive increases in cytosolic Ca^{2+} of guard cells by abscisic acid activation of non-selective Ca^{2+} -permeable channels. *Proc. Natl. Acad. Sci.* 87: 9305-9309

Schroeder JI, Allen GJ, Hugouvieux V, Kwak JM and Waner D (2001a) Guard cell signal transduction. *Ann. Rev. Plant Physiol. Plant Mol. Biol.* 52: 627-658

Schroeder JI, Kwak JM and Allen GJ (2001b) Guard cell abscisic acid signaling and engineering drought hardiness in plants. *Nature* 410: 327-330

Schumacher HM, Gundlach H, Fiedler F and Zenk MH (1987) Elicitation of benzophenanthridine alkaloid synthesis in *Eschscholtzia* cell cultures. *Plant Cell Reports* 6: 410-413

Schwacke R and Hager H (1992) Fungal elicitors induce a transient release of active oxygen species from cultured spruce cells that is dependent on Ca^{2+} and protein kinase activity. *Planta* 187: 136-141

Schwartz A (1985) Role of calcium and EGTA on stomatal movements in *Commelina communis*. *Plant Physiol* 79: 1003-1005

Staxén I, Pical C, Montgomery LT, Gray JE, Hetherington AM and McAinsh MR (1999) Abscisic acid induces oscillations in guard-cell cytosolic free

calcium that involve phosphoinositide-specific phospholipase C. *Proc. Natl. Acad. Sci.* 96: 1779-1784

Walker-Simmons M, Jin D, West CA, Hadwiger L and Ryan CA (1984) Comparison of proteinase inhibitor-inducing activities and phytoalexin elicitor activities of a pure fungal endopolygalacturonase, pectic fragments, and chitosans. *Plant Physiol.* 76: 833-836

Webb AAR, Larman MG, Montgomery LT, Taylor JE and Hetherington AM (2001) The role of calcium in ABA-induced gene expression and stomatal movements. *Plant J.* 26: 351-362

Wu Y, Kuzma J, Maréchal E, Graeff R, Lee HC, Foster R, and Chua N-H (1997) Abscisic acid signaling through cyclic ADP-ribose in plants. *Science* 278: 2126-2130

Yang Y, Shah J and Klessig DF (1997) Signal perception and transduction in plant defense responses. *Genes Dev.* 11: 1621-1639

Zimmermann S, Nürnberger T, Frachisse JM, Wirtz W, Guern J, Hedrich R and Scheel D (1997) Receptor mediated activation of a plant Ca^{2+} -permeable ion channel involved in pathogen defense. *Proc. Natl. Acad. Sci.* 94: 2751-2755

The text of this chapter, in full, is a reprint of the material as it appears in Plant Physiology, Klüsener, B., Young, J.J., Murata, Y., Allen, G.J., Mori, I.C., Hugouvieux, V., and Schroeder, J.I. (2002). I generated the data for Figures 7A-C, Fig. 8 A-D and some of the data for 8E, and Table II, and was the primary writer for this paper.

CHAPTER IV

Arabidopsis HT1 kinase controls stomatal pore aperture in response to
atmospheric CO₂

Section A

Manuscript

ABSTRACT

Plants regulate water loss and CO₂ uptake by modulating the aperture size of stomatal pores located in leaf epidermes. Stomata are surrounded by two guard cells which are able to sense a multitude of environmental signals and integrate this information¹. While much progress has been made in our understanding of the molecular mechanisms underlying stomatal responses to stimuli such as light and water stress, it has remained obscure how guard cells respond to and sense CO₂²⁻⁴. With a leaf thermal imaging CO₂ screen we report the isolation of two allelic *Arabidopsis* mutants (high temperature 1; *ht1-1* and *ht1-2*) altered in their ability to control stomatal movements in response to CO₂. The strong allele, *ht1-2* exhibits a dramatically impaired and inverse CO₂ response but functional responses to light and abscisic acid, suggesting a specific role for *HT1* in stomatal CO₂ signaling. *HT1* encodes a protein kinase expressed mainly in guard cells. Phosphorylation assays demonstrate that the activity of the HT1 protein carrying the *ht1-1* or *ht1-2* mutation is greatly impaired or abolished, respectively. Furthermore, dominant negative HT1kw transgenic plants which lack HT1 kinase activity show a disrupted CO₂ response underlining the importance of the HT1 kinase for CO₂ signaling.

RESULTS

To study the molecular processes involved in the control of stomatal movements in response to [CO₂], we have screened for mutants with altered CO₂ responses based on thermal imaging of plants. Plantlets derived from an ethyl methanesulfonate (EMS) mutagenized population in the *Arabidopsis* ecotype Columbia (Col-0) were grown for 3 weeks in a growth chamber, and were then subjected to low [CO₂] (100 ppm) for at least one hour before analysis by thermography (see Supplementary Methods for details). Low [CO₂] causes stomatal opening and thus measurable leaf cooling in wild-type (WT) plants (Fig. IV-1). By screening approximately 40,000 M₂ plants, two mutant lines, *ht1-1* and *ht1-2* (*high leaf temperature1*) were isolated that exhibited higher leaf temperature than the other plants under low [CO₂] (Fig. IV-1). WT plants showed significant leaf temperature changes in response to changes from ambient [CO₂] (350 ppm) to low (100 ppm) or doubled CO₂ (700 ppm) concentrations (Fig. IV-1 a-c). The ability to respond to CO₂-concentration changes was reduced (*ht1-1*; Fig. IV-1 e-g,) or absent (*ht1-2*; Fig. IV-1 i-k) in the *ht1* mutants. Representative time-courses of changing leaf temperatures in the WT and the mutants are available as a Supplementary Figure (Fig. IV-S1).

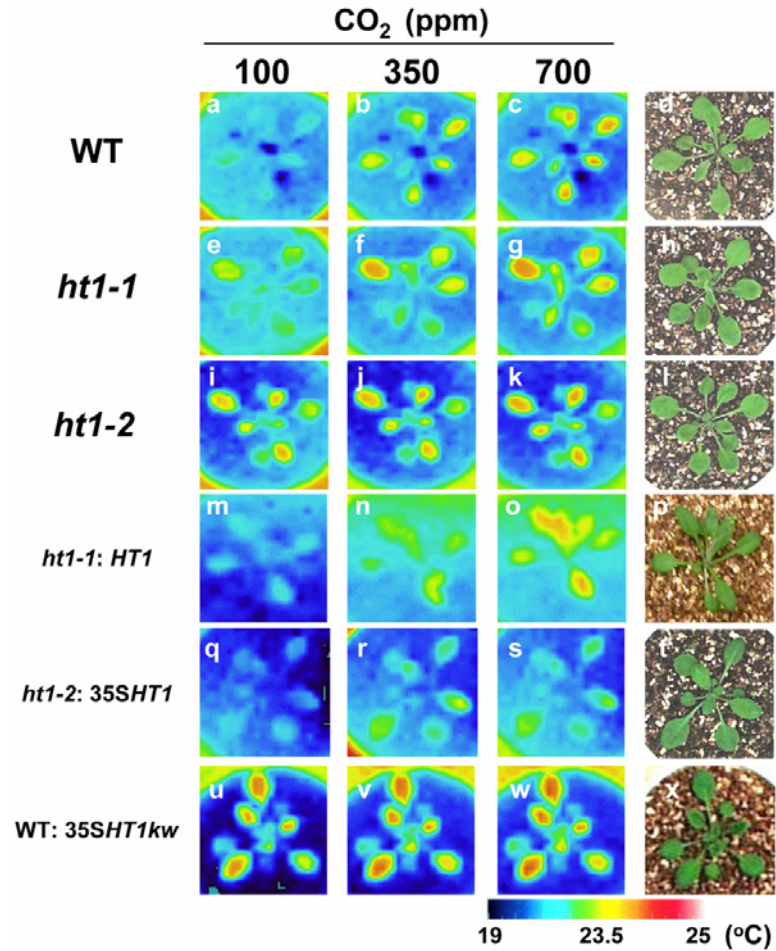


Figure IV-1: Changes in leaf temperature of WT, *ht1* mutants and transgenic plants in response to [CO₂] changes. Three-week old plants (images on the right) were subjected to low (100 ppm), normal (350 ppm) and high (700 ppm) [CO₂]. Thermal images of WT (a-c), *ht1-1* (e-f) and *ht1-2* (i-k) seedlings. m-p, *ht1-1* mutant plant harbouring a transgene with the *HT1* genomic sequence. q-t, *ht1-2* mutant plant harbouring a transgene with the *HT1* cDNA. u-x, transgenic plants overexpressing a dominant-negative *HT1* (*HT1kw*) isoform in the WT background.

The stomatal density of 3-week-old leaves is similar in WT and *ht1* plants (125 ± 15.8 , 124 ± 14.3 and 122 ± 10.2 stomata/mm² in WT, *ht1-1* and *ht1-2*, respectively; means \pm SD; n=18 leaves). Stomatal size, the growth rate, and the morphology of vegetative and floral organs were identical for the three

genotypes (data not shown). The dependence of stomatal aperture on $[\text{CO}_2]$ in the WT and the *ht1* mutants (Fig. IV-2e) paralleled that of leaf temperature (Figs 1 and S1). As active leaf cooling is caused by transpiration through stomata⁵, our results indicated that the higher leaf temperature of *ht1* was due to a reduction of stomatal aperture rather than to a reduced stomatal density, and that changes in leaf temperature in response to $[\text{CO}_2]$ were caused by changes of stomatal aperture.

We investigated the response of stomatal conductance of *ht1* and WT control plants to changes in the air CO_2 content (Fig. IV-2a, b). In intact leaves, increases in $[\text{CO}_2]$ from 365 ppm to 800 ppm induced a pronounced decrease in stomatal conductance in the WT, a slight decrease in *ht1-1*, and, intriguingly, a small increase in *ht1-2*. Raising $[\text{CO}_2]$ to 2000 ppm induced a further reduction in stomatal conductance in the WT, no significant response in *ht1-1*, and a further increase in *ht1-2* (Fig. IV-2a). Absolute levels of stomatal conductance in the three genotypes in 2000 ppm CO_2 were similar, indicating that stomata were already closed at low CO_2 in the *ht1* mutants. Stomatal movement analyses confirmed this hypothesis (Fig. IV-2e).

Decreasing $[\text{CO}_2]$ from 365 to 100 ppm induced a large increase in stomatal conductance in the WT, a smaller one in *ht1-1*, and a slight decrease in *ht1-2* (Fig. IV-2b). An additional drop to 0 ppm induced a further small increase in the WT, a substantially larger increase in *ht1-1*, and an additional small decrease in *ht1-2* (Fig. IV-2b).

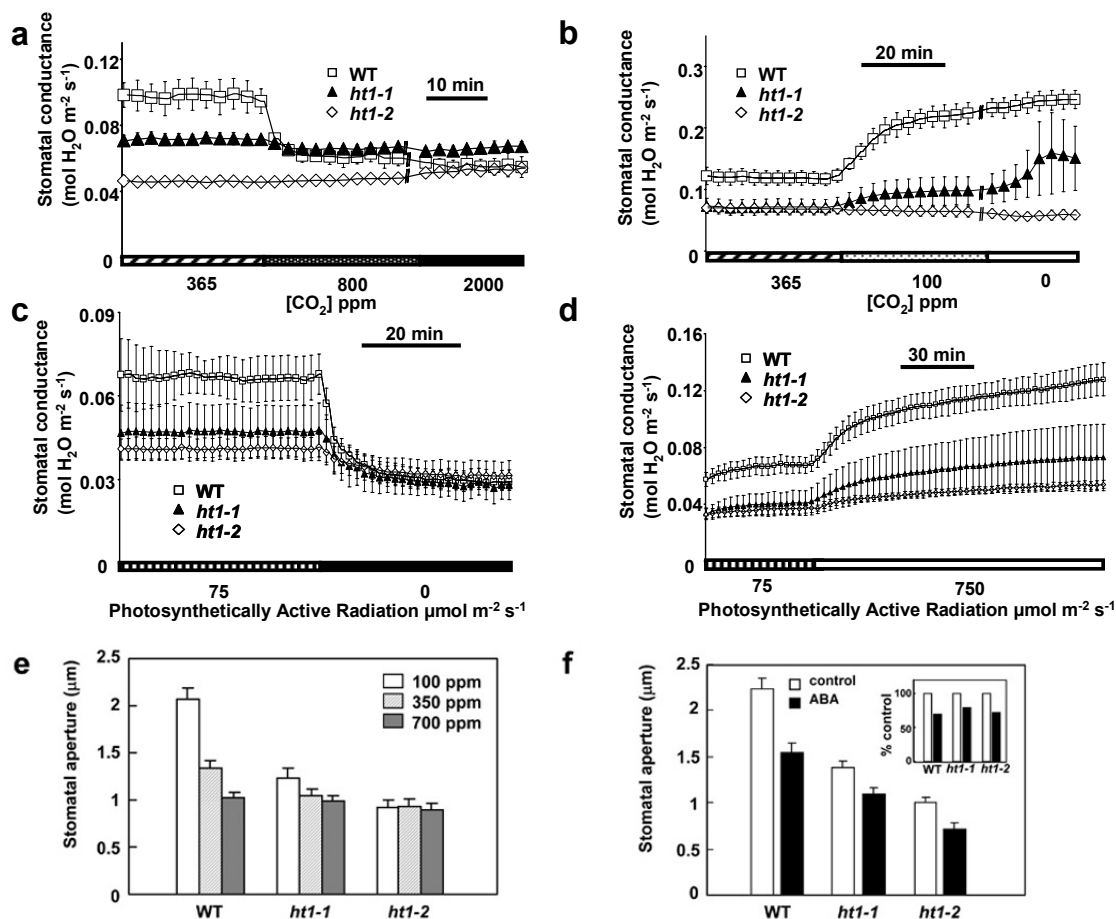


Figure IV-2: *ht1* mutations impair CO₂ inducible changes in stomatal responses. Time courses of stomatal conductance in response to changes in [CO₂] (a, b) and to changes in light intensities (c, d) in *ht1* mutant and WT leaves. The [CO₂] (a, b) or light fluence rates (μmol m⁻² s⁻¹) (c, d) are indicated at the bottom of the figures. Data represent the mean ± SEM of 3 leaves from 5-6 week old plants. e, CO₂ response of stomatal aperture in *ht* mutants. Three-week-old plants were incubated at the indicated [CO₂] (100 ppm, white bars; 350 ppm, hatched bars; 700 ppm, closed bars). Abaxial epidermal peels of the plants were taken from the sixth or seventh leaf and were used immediately for aperture determination. Data represent means ± SEM (n = 60) of 3 independent experiments. f, Comparison of ABA-induced stomatal closing in WT and the *ht1* mutants. Detached leaves were incubated with 0.5 μM ABA (closed bars) or without ABA (open bars) and the stomatal apertures were measured as described previously²¹ with minor modifications. Data presented are the means of 63 stomatal apertures ± SEM. Inset, ABA-induced stomatal closure normalized to stomatal apertures without added ABA in the three lines.

The responses of *ht1* mutants to light and dark exposures with [CO₂] held at ambient levels were analyzed to determine whether the mutant alleles are insensitive to light changes. Darkness caused drops in stomatal conductance down to similar levels in the three lines, although the downward step was largest in the WT due to the greatly different conductance levels before the stimulus (Fig. IV-2c). Increasing light intensity resulted in a large increase of stomatal conductance in the WT, a smaller one in *ht1-1*, and a still smaller increase in *ht1-2* (Fig. IV-2d).

In summary, *ht1-1* stomatal conductance did not change in response to increases in [CO₂] above ambient levels (Fig. IV-2a), and the sensitivity of *ht1-1* to drops in [CO₂] was shifted to lower CO₂ concentrations relative to the WT (Fig. IV-2b). The inverse responses seen in the *ht1-2* mutant (Fig. IV-2a, b) may be the result of the intact activity of a counter-balancing regulator of the normal CO₂-induced stomatal response in the absence of the HT1 regulator.

In contrast to the CO₂ responses, *ht1* mutants did respond to changes in light intensity, qualitatively in the same direction as WT responses (Fig. IV-2c, d). In this case, *ht1-2* did not show any inverse response to light compared to WT responses. One reason for the reduced light response in *ht1* mutants (Fig. IV-2c, d) might be that stomatal opening by light is induced to some extent by a decrease in CO₂ through photosynthesis^{6, 7}. Furthermore, a degree of cross talk among stomatal movement signals is expected, as all

signals regulate downstream ion transport processes^{2, 8}. Thus, *HT1* mediates a mainly CO₂-dependent reaction and does not have a purely structural or a general physiological function that would play similar roles in all stomatal movement responses.

This interpretation was further supported by the finding that the stomata of *ht1* mutants respond to abscisic acid (ABA), a phytohormone that triggers stomatal closure, to the same extent as those of the WT (Fig. IV-2f). Stomatal apertures of *ht1-1* and *ht1-2* plants were generally smaller than WT apertures at ambient CO₂ (Fig 2e, f), which correlates with the increased leaf temperatures of the *ht1* mutants (Fig. IV-1). Normalization to non-ABA control stomatal apertures showed that there was no significant difference in stomatal closing responses to ABA among WT and the *ht1* mutants (Fig. IV-2f, inset; Generalized Linear Models, family=quasi and link=log, P>0.3, n=376). Furthermore, both *ht1-1* and *ht1-2* seeds germinated at similar rates as WT seeds on substrates containing from 0 to 1 μM ABA (Fig. IV-S2). We conclude that *ht1* mutants are normal with respect to their ABA responses.

The *HT1* locus was mapped to a location between two Cereon SNP markers, CER451254 and CER460537, on chromosome 1 (Fig. IV-3a). Sequencing of this 46kb region revealed that a putative kinase gene, At1g62400, harbored a point mutation at nucleotide 796 in *ht1-1* that resulted in the exchange of Arg-211 for Lys (Fig. IV-3b). In the *ht1-2* mutant allele, a single base pair substitution was detected at the donor splice site of the first

intron at nucleotide 448 (Fig. IV-3b). This resulted in an in-frame 42-bp deletion at positions 406–447 corresponding to deletion of 14 amino acid residues, Val-136 to Gln-149.

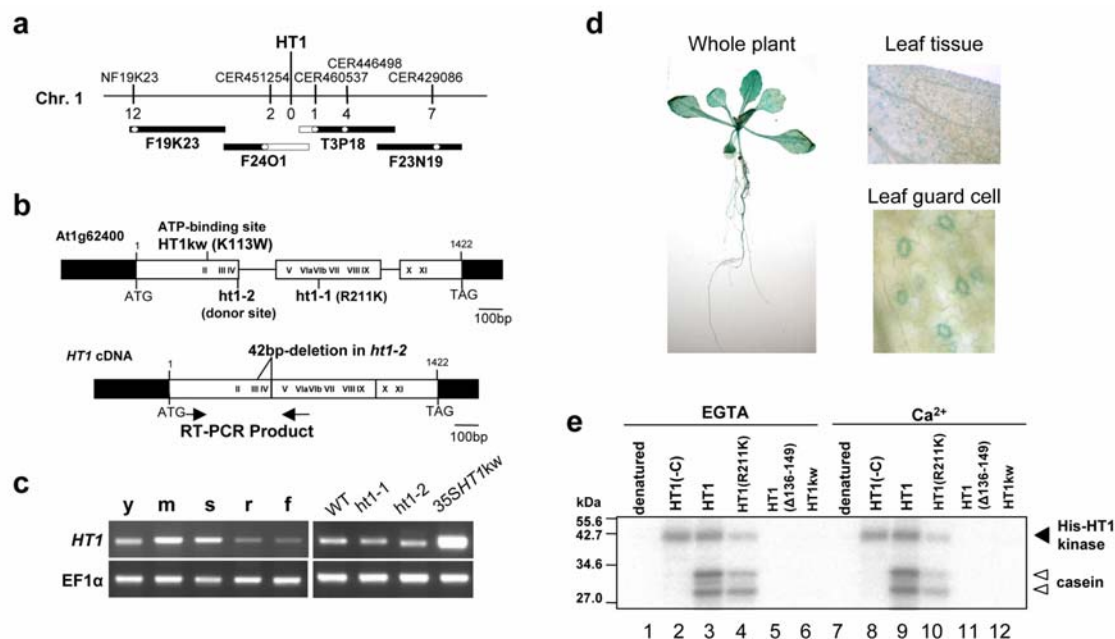


Figure IV-3: HT1 is a protein kinase expressed in guard cells. a, Map-based cloning of the HT1 gene. Genetic mapping of 1074 chromosomes localized HT1 (white rectangle) to the 46-kb region between the markers CER451254 on BAC F24O1 and CER460537 on BAC T3P18. b, Structure of the HT1 gene. HT1 consists of 3 exons (open boxes); Black boxes highlight the 5' and 3' UTR, respectively. Conserved subdomains of the protein kinase family are indicated by roman numerals. *ht1-1* and *ht1-2* indicate the mutation sites. In subdomain II there is an invariant lysine (K113). Arrows indicate regions used in RT-PCR (Fig. IV-3c). c, RT-PCR analysis of HT1 mRNA. Expression in young leaf (y) from the 10-day-old WT seedlings, mature leaf (m) and roots (r) from 3-week-old, stems (s) and flowers (f) from 4-week-old WT plants (left) is shown. Expression in aerial parts of 3-week-old WT, mutants (*ht1-1*, *ht1-2*) and transgenic (35SHT1kw) plants (right). The EF1 α gene was used as an internal standard for cDNA amounts. d, HT1 expression pattern of HT1-promoter-GUS (pHT1::GUS) transgenic plants. e, Phosphorylation activity of HT1 and the indicated mutant proteins *in vitro* (see text). Assays were performed in the presence (Ca²⁺; right 6 lanes) or absence (EGTA; left 6 lanes) of CaCl₂. Closed arrowhead indicates signals from autoradiograms of autophosphorylated proteins. Open arrowheads indicate phosphorylation of casein.

We transformed *ht1* plants with a 4.4–kb genomic fragment including At1g62400 (*ht1: HT1*) (see Supplementary Methods for details). Six independent homozygous *ht1: HT1* lines showed low leaf temperature under low [CO₂], and a dependence of leaf temperature on [CO₂] which resembled that of WT plants, showing *ht1* complementation (Fig. IV-1, m-o; *ht1-1: HT1*). The *ht1-2* mutant was also complemented by the genomic *ht1:HT1* vector (data not shown). These data suggested that At1g62400 corresponded to *HT1*. A similar result was obtained in the plants of *ht1-2: 35SHT1* lines, in which the *HT1* cDNA was expressed under the control of the CaMV 35S promoter (Fig. IV-1, q-s; *ht1-2: 35SHT1*; *ht1-1: 35SHT1* showed similar results, data not shown) (see Supplementary Methods for details).

Using RT-PCR analysis, the *HT1* mRNA was detected in leaves, stems, roots and flowers (Fig. IV-3c, left). *HT1* mRNA was generally of low abundance and was usually not detected in Northern blots in these samples. Characterization of transgenic plants harboring a transcriptional fusion of the β -glucuronidase (GUS) reporter gene and the *HT1* promoter (pHT1::GUS) further indicated that *HT1* expression occurred in the whole plant (Fig. IV-3d left). In leaves, the expression of *HT1* was mostly confined to guard cells (Fig. IV-3d right). In agreement with this observation, the expression of *HT1* was highest in mature leaves which have more abundant stomata (Fig. IV-3c, left).

Furthermore, microarray analyses show that the *HT1* gene (At1g62400) is preferentially expressed in guard cells compared to mesophyll cells⁹.

RT-PCR experiments showed that the PCR product (primers, see Fig. IV-3b) in *ht1-2* was smaller than that in the WT, most probably due to the 42 bp deletion (Fig. IV-3c, right). Little difference in *HT1* mRNA abundance between WT, *ht1-1* and *ht1-2* was observed in mature leaves (Fig. IV-3c, right). CO₂ treatment had also no detectable effect on the level of *HT1* mRNA (data not shown). Thus, the *ht1* mutations described seem to affect HT1 function rather than the abundance of HT1.

The *HT1* complementary DNA was cloned by RT-PCR using total RNA prepared from 3-week old plants. The first in-frame ATG codon of the transcript initiated an ORF encoding a 390 amino acid protein with a predicted molecular mass of 44 kDa (Fig. IV-3b). The putative HT1 protein has all of the conserved features of the catalytic domains of protein kinases except for subdomain I¹⁰ (Fig. IV-3b). To determine whether the HT1 protein and its mutants possess phosphorylation activity we expressed each one as a His-tagged construct in *E. coli* and performed *in vitro* kinase assays. The recombinant HT1 protein (His-HT1) proved capable of autophosphorylation (Fig. IV-3e, lanes 2, 8) and casein phosphorylation (Fig. IV-3e, lanes 3, 9) when incubated with [γ -³²P]ATP. Site-directed mutagenesis of *ht1-1* (His-HT1(R211K)), which converted the conserved active-site residue Arg 211 into Lys, caused reduction in the phosphorylation activity (Fig. IV-3e, lanes 4, 10).

No significant levels of kinase activity were detected for the analogous His-construct of *ht1-2*, which contains a 14 amino acid deletion corresponding to a part of the kinase subdomains IV and IV (His-HT1(Δ 136-149); Fig. IV-3e, lanes 5, 11). Thus, the kinase activities of the WT HT1 and its two mutants corresponded nicely to the phenotypes observed in whole plants. The kinase activities of HT1 and HT1(R211K) were Ca^{2+} -independent (Fig. IV-3e, lanes 2-4 and 8-10), and the proteins phosphorylated not only casein but also myelin basic protein (MBP; data not shown).

Lys-113 of HT1 corresponds to a highly conserved residue in subdomain II (Fig. IV-3b) that is required for activity in most protein kinases¹⁰. To verify that the phosphorylation signal was due to HT1 phosphorylation, Lys-113 was changed to Trp by means of site-directed mutagenesis¹¹. The mutant protein (HT1kw) exhibited no kinase activity (Fig. IV-3, lanes 6, 12), resembling denatured HT1 (Fig. IV-3, lanes 1, 7). To ensure that the CO_2 response in stomata depended on HT1 kinase activity, experiments were carried out using a transgenic line overexpressing this inactive HT1 isoform controlled by the CaMV35S promoter in WT background (Fig. IV-1, u-x; WT: 35SHT1kw, Fig. IV-3c right) (see Supplementary Methods for details). The transgenic line showed higher leaf temperature at low $[\text{CO}_2]$ (Fig. IV-1u), and the sensitivity to CO_2 was suppressed (Fig. IV-1, u-w). These CO_2 responses were similar to those observed in *ht1-2* plants (Fig. IV-1, i-k). Therefore, the

data demonstrate that HT1 protein kinase activity is required for normal stomatal responses to CO₂.

HT1 is the first functionally and molecularly defined gene involved in a specific CO₂ signalling pathway that mediates stomatal movements. Leaf temperature, stomatal response and gas exchange analyses of the *ht1* mutants show that *ht1* stomatal apertures are more closed at ambient CO₂ and that *ht1* kinase mutant stomata show less stomatal opening at low CO₂ concentrations. These data suggest that *ht1* mutation causes a CO₂ hypersensitive stomatal closing response, that impairs low CO₂-induced stomatal opening (Figs. IV-1, IV-2a, b and IV-2e). In contrast, light stimulation continues to cause stomatal opening (Fig. IV-2c, d). Biochemical and electrophysiological studies have provided insights concerning the functions of important factors in CO₂ signaling, including cytosolic Ca²⁺, K⁺ and anion - channels^{8,12-18}. The identification of the HT1 protein kinase as a key molecular regulator in stomatal CO₂ sensing will help to unravel the CO₂ signal transduction network that controls stomatal movements.

METHODS

Plant material. All *Arabidopsis* lines used in this study were derived from the Columbia (Col-0) background. EMS-mutagenised Col M₂ seeds were purchased from Lehle Seeds (Round Rock, TX, USA).

Gas exchange. Recordings of stomatal conductance were made with a Li-Cor 6400 Portable Photosynthesis system (LI-COR Inc., NE). Unless otherwise noted, leaves were kept at constant humidity of 14 mmol H₂O mol⁻¹, constant temperature at 26.5 °C and constant light of 75 μmol m⁻² s⁻¹ or constant [CO₂] of 365 ppm.

RT-PCR analysis. Total RNA extraction was performed, and single-stranded cDNA synthesized from total RNA was used as RT-PCR templates according to the method described by Sugimoto *et al.*¹⁹. We used 1 μl of the RT reaction as a template in 10 μl PCR-reactions. PCR was run for 27 cycles of 30 s at 94 °C, 30 s at 55 °C, and 1 min at 72 °C. The RT-PCR primers for *HT1* and its mutants were 5'-GGAATCTTGGTCGATGATCC-3' and 5'-CAATGGTGGTCTTTCGTTCTT-3'. The amplified DNA fragments covered base-pairs 161 to 921 of *HT1*. As an internal standard for cDNA, a 700-bp fragment of the EF1α cDNA was amplified as described²⁰.

Analysis of GUS activity. A pHT1::GUS construct was obtained by amplifying 2kb of the *HT1* promoter region from genomic DNA using the oligonucleotides 5'-cttctctaagctttcgatgcaaacca-3' and 5'-ccatatgtctggttatggttca-3'; the product was then inserted into the pGEM-T Easy Vector. A HindIV-PmeI fragment including the *HT1* promoter sequences was cloned into the HindIV and SmaI

sites of the pBI101. GUS activity was assayed on 2 week-old seedlings grown on MS plates after over night incubation with 5-bromo-4-chloro-3-indolyl-D-glucuronide as a substrate. All sequences amplified by PCR were confirmed by sequencing.

Preparation of recombinant proteins. An NdeI site was introduced in front of the ATG start codon of HT1 and ht1 mutants by PCR using each cDNA as a template. HT1kw was produced by site-directed mutagenesis and the polymerase chain reaction as described¹¹. The constructs were then ligated in-frame into the pET-28a (+) vector (Novagen), and were confirmed by DNA sequencing. BL21(DE3) cells transformed with pET-28a (+) constructs were induced with 1mM IPTG for 16 h at 25 °C. His-tagged proteins were purified on nickel columns (Amersham Biosciences). Purified His-tagged proteins were recognized specifically by Anti-His-probe antibodies (Toyobo) in an immunoblot analysis (data not shown).

***In vitro* phosphorylation assay.** An autophosphorylation assay was performed by incubating purified recombinant proteins (1 µg) in reaction buffer (25 mM Tris, pH 7.5, 10 mM MgCl₂ and 1 mM CaCl₂ or EGTA) in the presence of 0.6 µCi [γ -³²P]ATP at 30 °C for 15 min. The reaction was stopped by the addition of SDS loading buffer, and kinase activities were detected by autoradiography after proteins had been resolved on a 12 % SDS-

polyacrylamide gel. Phosphorylation activities of HT1 and its mutants were determined in 10 μ l of the kinase reaction buffer using 0.15 μ g casein as a substrate under the same conditions.

ACKNOWLEDGEMENTS

We thank Y. Machida and K. Harada, K. M. Kawano, E. Kasuya and all of the members of our laboratory for technical assistance and discussion. We also thank the Arabidopsis Biological Resource Center, Cereon Genomics, for access to polymorphism information. This research was supported by the Ministry of Agriculture, Forestry and Fisheries of Japan and the Japan Society of the Promotion of Science (K.I.), and by National Science Foundation and National Institutes of Health grants (J.I.S.).

REFERENCES CITED

1. Willmer, C. M. & Fricker, M. D. *Stomata*, 2nd edn. London, UK: Chapman & Hall (1996).
2. MacRobbie, E. A. C. Signal transduction and ion channels in guard cells. *Phil. Trans. R. Soc. Lond. B.* 353, 1475-1488 (1998).
3. Schroeder, J. I., Kwak, J. M. & Allen, G. J. Guard cell abscisic acid signalling and engineering drought hardiness in plants. *Nature* 410, 327-330 (2001).
4. Hetherington, A. M. & Woodward, F. I. The role of stomata in sensing and driving environmental change. *Nature* 424, 901-908 (2003).

5. Merlot, S. *et al.* Use of infrared thermal imaging to isolate Arabidopsis mutants defective in stomatal regulation. *Plant J.* 30, 601-609 (2002).
6. Olsen R. L., Pratt R. B., Gump P., Kemper A. & Tallman G. Red light activates a chloroplast-dependent ion uptake mechanism for stomatal opening under reduced CO₂ concentrations in *Vicia* spp. *New Phytol.* 153, 497-508 (2002).
7. Roelfsema, M. R., Hanstein, S., Felle, H. H. & Hedrich, R. CO₂ provides an intermediate link in the red light response of guard cells. *Plant J.* 32, 65-75 (2002).
8. Schroeder, J. I., Allen, G. J., Hugouvieux, V., Kwak, J. M. & Waner, D. Guard cell signal transduction. *Annu. Rev. Plant Physiol. Plant Mol. Biol.* 52, 627-658 (2001).
9. Leonhardt, N. *et al.* Microarray expression analyses of Arabidopsis guard cells and isolation of a recessive abscisic acid hypersensitive protein phosphatase 2C mutant. *Plant Cell* 16, 596-615 (2004).
10. Hanks S. K., Quinn A. M. & Hunter T. The protein kinase family: Conserved features and deduced phylogeny of the catalytic domains. *Science* 241, 42-52 (1988).
11. Soyano, T., Nishihama, R., Morikiyo, K., Ishikawa, M. & Machida, Y. NQK1/NtMEK1 is a MAPKK that acts in the NPK1 MAPKKK-mediated MAPK cascade and is required for plant cytokinesis. *Genes Dev.* 17, 1055-1067 (2003).
12. Webb, A. A. R., McAinsh M. R., Mansfield T. A. & Hetherington A. M. Carbon dioxide induces increases in guard cell cytosolic free calcium. *Plant J.* 9, 297-304 (1996).
13. Schwartz, A., Ilan, N. & Grantz, D. A. Calcium effects on stomatal movement in *Commelina communis* L. – use of EGTA to modulate stomatal response to light, KCl and CO₂. *Plant Physiol.* 87, 583-587 (1988).
14. Brearley J., Venis M. A. & Blatt M. R. The effect of elevated CO₂ concentrations on K⁺ and anion channels of *Vicia faba* L. guard cells. *Planta* 203, 145-154 (1997).
15. Assmann S. M. The cellular basis of guard cell sensing of rising CO₂. *Plant Cell Environ.* 22, 629-637 (1999).

16. Hanstein, S. M. & Felle, H. H. CO₂-triggered chloride release from guard cells in intact fava bean leaves. Kinetics of the onset of stomatal closure. *Plant Physiol.* 130, 940-950 (2002).
17. Raschke K., Shabahang M. & Wolf R. The slow and the quick anion conductance in whole guard cells: their voltage-dependent alternation, and the modulation of their activities by abscisic acid and CO₂. *Planta* 217, 639-650 (2003).
18. Vavasseur, A. & Raghavendra, A. S. Guard cell metabolism and CO₂ sensing. *New Phytol.* 165, 665-682 (2005).
19. Sugimoto, H. *et al.* The *virescent-2* mutation inhibits translation of plastid transcripts for the plastid genetic system at an early stage of chloroplast differentiation. *Plant Cell Physiol.* 45, 985-996 (2004).
20. Mustilli A.-C., Merlot S., Vavasseur A., Fenzi F. & Giraudat J. Arabidopsis OST1 protein kinase mediates the regulation of stomatal aperture by abscisic acid and acts upstream of reactive oxygen species production. *Plant Cell* 14, 3089-3099 (2002).
21. Pei, Z. M., Kuchitsu, K., Ward, J. M., Schwarz, M. & Schroeder, J. I. Differential abscisic acid regulation of guard cell slow anion channels in Arabidopsis wild-type and *abi1* and *abi2* mutants. *Plant Cell* 9, 409-423 (1997).

CHAPTER IV

Arabidopsis HT1 kinase controls stomatal pore aperture in response to
atmospheric CO₂

Section B

Supplementary Data and Methods

SUPPLEMENTARY DATA

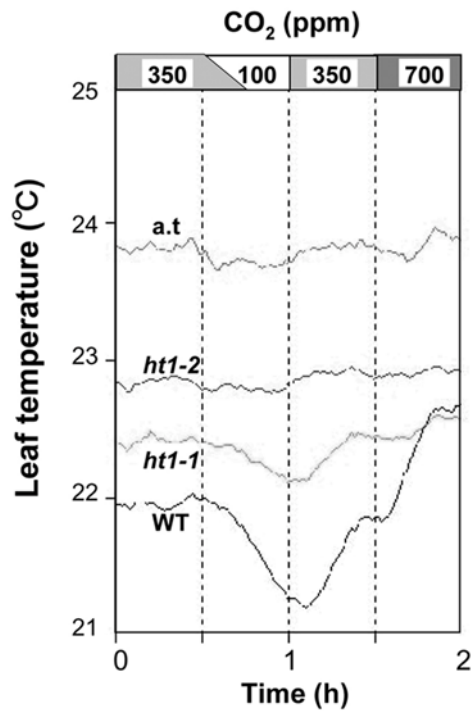


Figure IV-S1: CO₂ response of leaf temperature measured by a thermistor. The leaf temperature at the abaxial surface was monitored using a micro-thermistor probe (P2L-64, Technol Seven, Japan) held in place with a fly trapping paste (Nisso shoji, Co., LTD. Japan). The sensitivity of the thermistor was 0.01 °C, and measurements were taken at 1 min intervals. Air temperature (a. t.) in close proximity to the plants was measured concurrently using an additional thermistor probe.

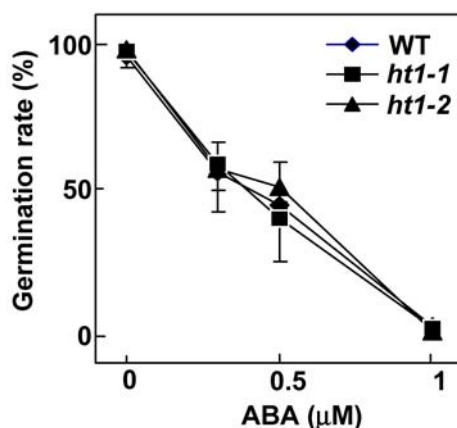


Figure IV-S2: Effect of ABA on *ht1* seed germination. Seeds were plated on a medium supplemented with the indicated concentrations of ABA, and incubated for 4 days at 22 °C under constant light. The number of germinated seeds was expressed as the percentage of the total number of seeds plated. Data represent the mean \pm SD of 3 independent experiments (60 seeds were plated per data point).

SUPPLEMENTARY METHODS

Mutant screen. M₂ seeds were grown on half strength MS medium supplemented with 1% (w/v) sucrose and 0.5% gellan gum at pH 5.7 for 18 days in a growth chamber (22 °C, 70 % RH, with constant light of 230 $\mu\text{mol m}^{-2} \text{s}^{-1}$). The plants were then transplanted into pots with vermiculite moistened with nutrients. After 3 days, the pots were incubated under constant light (43 $\mu\text{mol m}^{-2} \text{s}^{-1}$) in a growth cabinet (23 °C, 43 % RH) that was equipped with an automatic CO₂ control unit (FR-SP, Koito Co., Japan). The plants were subjected to low CO₂ condition (100 ppm) for at least one hour before thermal images were obtained using a thermography apparatus (TVS-8000MkII, Nippon Avionics, Co. LTD., Japan) that includes an infrared camera equipped

with a 18.2 ° (H)×13.6 ° (V) lens. The camera is equipped with a cooled 160 (H) x 120 (V) InSb array detector responsive to short infrared waves (3.6-4.6 μm band). The specified temperature resolution was 0.025 °C at room temperature. Leaf emissivity was set to 1 since an absolute measurement of leaf temperature was not required. The camera was mounted vertically at approximately 1 m above the leaf canopy for observations and was connected to a color monitor to facilitate observation of individual plants. Images were fed into a personal computer. Individual plants with a higher leaf temperature than the WT were selected using an infrared image. These candidate mutants were grown to maturity and their phenotypes were retested in the next (M_3) generation.

Transgenic plants. Transgenic *Arabidopsis* plants were generated by *Agrobacterium tumefaciens*-mediated transformation. For functional complementation of the *ht1* mutants, the *HT1* genomic region (nucleotides 54586 to 58950 of BAC F24O1) containing *At1g62400* was amplified by PCR from genomic DNA using the oligonucleotides 5'-cttctctaagctttcgatgcaaacca-3' and 5'- gatgtattgcaagagctgatcaattgggtcatgagacgac-3' and was then inserted into the pGEM-T Easy Vector (Promega). A Sall-MunI fragment including the *HT1* genomic sequences was cloned into the Sall-EcoRI site of the T-DNA vector pBI101. The *HT1* cDNA was obtained using the SMART RACE PCR kit (Clontech, CA) according to the manufacturer's instructions. The full-length

cDNA was then amplified using Pfu DNA polymerase (Stratagene) with the oligonucleotides 5'-taccgggatttgtttccttctctgtttctgc-3' and 5'-tagagctctcaataagtatcattatatacatcac-3'; the amplified DNA was inserted into SmaI-SacI site of the T-DNA vector pBI121. A 35SHT1kw construct was created by introduction of the HT1kw fragment (see Method) into PshAI-BamHI of the *HT1* cDNA followed by cloning into pBI121 as described above.

The text of Chapter IV, in full, has been submitted for publication of the material by authors Hashimoto, M., Negi, J., Young, J., Schroeder, J.I., and Iba, K. I generated the data for Figure IV-2 A-D.

CHAPTER V

Discussion

The work presented in this thesis contains some interesting observations regarding CO₂ signaling in guard cells. From these observations arise both hypotheses about the signaling mechanisms involved, and new questions. In this discussion I first present attempts made to further elucidate guard cell CO₂ signaling that failed to produce meaningful data. I close the discussion with a model summarizing my hypotheses regarding the workings of this signaling system.

Calcium imaging in intact leaves. It would be highly advantageous to be able to perform calcium imaging in intact leaves rather than in intact epidermal layers. Such a condition would be a more accurate representation of the conditions the guard cells face normally, with regards to parameters that strongly impinge on guard cell behavior such as ion concentrations, CO₂ concentrations, and the effects of surrounding cells. My experimental results suggest that the intact epidermal layer preparation used is inferior to an intact leaf preparation in terms of robustness of stomatal responses and the degree to which the experimental situation represents natural behavior. Robust stomatal aperture movements have not been observed during calcium imaging or protocols similar to calcium imaging, in contrast to the consistent changes in

stomatal conductance measured in intact leaves using gas exchange measurements. Furthermore, a wide variety of apoplastic factors have been shown to affect Ca^{2+} transient behavior (e.g. ABA, Ca^{2+} , K^+ , ROS) or are likely to because they are known to regulate guard cell turgor (e.g. H^+ , Cl^- , NO_3^- , sucrose, malate). Apoplastic concentrations of these factors are largely regulated by metabolism of other cell types in the leaf, transport through the leaf, and transpiration through stomatal pores, which do not occur normally in intact epidermal layers. Thus the Ca^{2+} transient behavior seen in intact epidermal layers, both in a null condition and in response to shifts in $[\text{CO}_2]$, may differ in important ways from that in an intact leaf. As a result, I had hoped to develop a method to image calcium in guard cells in an intact leaf, ideally one still attached to a plant. I describe those efforts here.

Inverted compound microscope

I first attempted to visualize calcium levels in guard cells using an inverted compound epifluorescence scope. The calcium was monitored using plants transformed with yellow cameleon 2.1 under the constitutive 35S promoter. Calcium imaging failed in this situation because there was a lot of contaminating fluorescence from other cells, mostly from mesophyll cells lying interior to the guard cells. Recently, progress has been made on this project by others in the lab. Yingzhen Yang has generated plants expressing yellow cameleon 3.6 (which has a higher signal to noise ratio than yellow cameleon

2.1) under a guard cell-specific promoter. Alex Costa is currently imaging intact leaves from these plants on the inverted compound epifluorescence scope and has succeeded in observing calcium transients.

Two photon confocal microscope

Using 35S-yellow cameleon 2.1 plants, I also tried a two photon confocal imaging system which restricts fluorophore excitation to a narrowly defined region in the z dimension, which could solve the problem of contaminating fluorescence from cells lying interior to the guard cells. This work was done with Hiroyuki Hakozaki in the National Center for Microscopy and Imaging Research, run by Mark Ellisman. Changes in cameleon ratios in response to changes in calcium had previously been successfully imaged using a two photon confocal system in HeLa cells by Mark Ellisman's group¹.

Before trying to visualize calcium changes in the intact leaf, we tried to evaluate the suitability of two photon imaging for cameleon in guard cells by using intact epidermal layers – the preparation that has been used extensively in my calcium imaging experiments. Unfortunately, even in this tried and true preparation, no cameleon ratio changes could be resolved. We tried bathing cells in 10 mM extracellular calcium, which induces large amplitude repetitive calcium transients, but no change in baseline was observed. We also tried bathing the cells in 20 mM calcium while permeabilizing the membrane with ionomycin. This should cause a large increase in intracellular calcium and

hence the cameleon ratio. This expectation was confirmed by imaging on a compound epifluorescence scope. However, in the two photon confocal system, again there was no change in the baseline.

The shortcoming of the two photon approach probably was that the signal was too weak. Throughout the experiments, the guard cell cameleon fluorescence was dim, and we had to overcome the low fluorescence by using long exposure times, averaging frames, and using laser wavelengths that would increase the excitation of cyan fluorescent protein (CFP) but also decrease the amount of fluorescence resonance energy transfer relative to the amount of direct excitation of the yellow fluorescent protein (YFP), thus decreasing signal to noise. To further test the confocal system's suitability for our experiments, Paul Steinbach from Roger Tsien's lab visualized purified yellow cameleon 2.1 protein droplets using the two photon confocal system. Again, the fluorescence was quite low given the nature of the sample, although ratio differences were seen with purified cameleon protein in high and low calcium conditions. In summary, I believe the two photon confocal system failed mainly because the cameleon images were not bright enough and the tuning of the lasers and optical system appeared not to be optimized for cameleon imaging.

Simultaneous Ca²⁺ imaging and stomatal aperture monitoring. One of the difficulties in interpreting the role of calcium transients in stomatal movements

is that with our current protocols, the two phenomena are observed independent of each other and both exhibit a high degree of variability from cell to cell. For this reason, it could be quite revealing to observe calcium transients and stomatal movements at the same time in the same cells. Such an assay could more precisely link different calcium transient patterns with specific stomatal behaviors, as well as provide more information on the kinetics of stomatal responses relative to the timing of calcium spikes.

Once a protocol was developed which could resolve stomatal movements in response to CO₂ in intact epidermal layers (Figs. II-2B and C and II-3C), attempts to image calcium transients and record stomatal apertures were made, but unfortunately did not succeed. The protocol involved doing a normal calcium imaging experiment during which brightfield images, which capture stomatal apertures, are periodically taken. Cameleon expression was used as an indicator of viability, to ensure that both guard cells and the pavement cells surrounding them remained alive during the course of the experiment. While calcium transients were observed during these experiments, stomatal movement responses to CO₂ were not. I thought that one likely reason might be the strong, periodic blue light stimulation used to excite CFP that necessarily accompanies cameleon-based calcium imaging. However, a few experiments were also tried on the microscope stage with constant white light illumination (mimicking conditions during stomatal movement assays) and without calcium imaging (and thus no high-intensity

blue light stimulation), and stomatal movements still did not occur. There must be something about the conditions present when an intact epidermal layer is incubated on the microscope stage that are less conducive for stomatal movements than is the case when that same epidermal layer is incubated in a growth chamber with an air stream of a defined $[\text{CO}_2]$, as is done for stomatal movement assays (Figs. II-2B and C and II-3C). Achievement of this important goal merits further effort. One approach being pursued is to experiment with the blue light insensitive mutants *npq1* and the *phot1 phot2* double mutant.

Stomatal response to imposed Ca^{2+} transients during low CO_2 exposure.

An experiment was designed to test our hypothesis that low CO_2 inactivates Ca^{2+} sensors that would normally stimulate stomatal closure. Previous reports have shown that calcium transients imposed by alternately perfusing hyperpolarizing, high calcium buffer and depolarizing, low calcium buffer over intact epidermal layers trigger rapid “ Ca^{2+} reactive” stomatal closure responses²⁻⁴. I aimed to test whether these stomatal closure responses to imposed calcium transients would still occur in the presence of low CO_2 , or indeed whether calcium transients with the correct parameters could, in the presence of low CO_2 , cause stomatal opening. Preliminary results showed that stomatal closure does still occur in the presence of low CO_2 , but more experiments have to be done to conclude this. One complication is that, as mentioned earlier, stomatal movements in response to CO_2 changes have not

yet been resolved when CO₂ changes are administered to intact epidermal layers on the microscope stage. As long as CO₂ responses in this situation are suspect, results from the experiment described here cannot be highly valued. Another complication is that these imposed calcium transients are produced by alternately depolarizing and hyperpolarizing the membrane. Because we hypothesize that membrane polarization plays a central role in stomatal movements in response to CO₂, these polarization changes might have a strong impact on stomatal behavior in this assay. Thus it would be better if calcium transients could be imposed without also imposing membrane voltage changes, perhaps by using caged calcium.

A role for calcium in early stomatal movements. Although it is unlikely that calcium transient rate modulation would play a role in early CO₂-induced stomatal movements, that is not to suggest that early stomatal movements do not involve calcium at all. Indeed the total prevention of stomatal movements by BAPTA-AM (Fig. II-2C) suggest that calcium probably does play a role in early stomatal movements. Alternatively, early stomatal movements may occur even in the presence of BAPTA-AM, but not be maintained if the calcium transients are only important for sustaining the response. One way to distinguish between these two possibilities would be to measure stomata at early time points following a shift in [CO₂] in the presence of BAPTA-AM and

see if the stomata have a quick response to CO₂ that is eventually reversed, or if there is never a response.

Calcium transient patterns in *ht1* mutants. Because the *ht1* mutants have a strong impairment in CO₂ stomatal responses, it would be very interesting to test whether the calcium signaling in these mutants is also aberrant. I observed calcium transients in *ht1-1* and the wildtype genetic background of *ht1-1*, Col.0, while imposing shifts in [CO₂] (Fig. V-1)

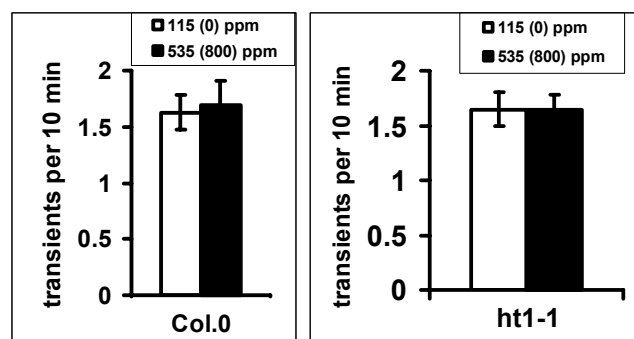


Figure V-1: Calcium transient rates are not altered by [CO₂] in the wildtype Col.0 and *ht1-1*. Calcium transient rates were calculated using automated spikecounter analysis from Col.0 (n = 27) and *ht1-1* (n = 23) guard cells exposed first to 115 ppm CO₂, then 535 ppm CO₂, then 115 ppm CO₂ again, similar to Fig. II-1A. Values are means ± s.e.m.

Neither the *ht1-1* nor the wildtype Col.0 exhibited a change in calcium transient rate upon a shift in CO₂ (P > 0.75). It is quite surprising that the wildtype did not produce a calcium pattern change given that our evidence suggests a role for calcium transient rate changes in stomatal movements (Chapter II), and that the Col.0 wildtype stomata respond to changes in [CO₂]

(Figs. II-S10, IV-1 and IV-2). However, subsequent work failed to resolve stomatal movements in response to CO₂ and external calcium in our intact epidermal layer preparation (M. Israelsson, unpublished). It appears that this tissue preparation may not be suitable for resolving normal CO₂ or calcium responses in Col.0. It would be useful to try other tissue preparations, and/or to obtain *ht1* mutant(s) in a different background (Ler, or *phot1 phot2*, to remove possible contributions of blue light signaling).

CO₂ stomatal signaling model. Based on the observations presented in this dissertation, as well as earlier findings, I propose a model for how calcium transients may function in CO₂ stomatal signaling (Fig. V-2). Central features of this model are the existence of two separate processes that direct stomatal aperture changes, and the role of calcium transient rate modulation in stomatal regulation.

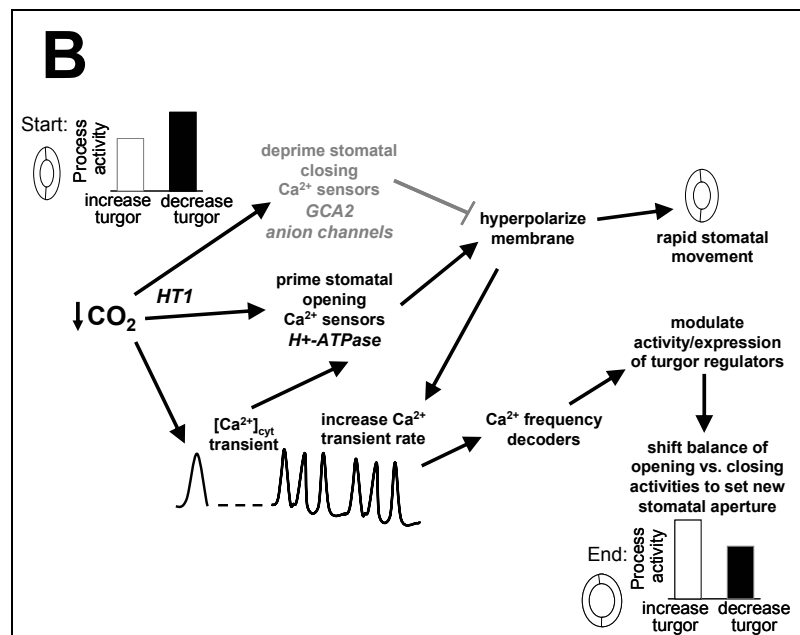
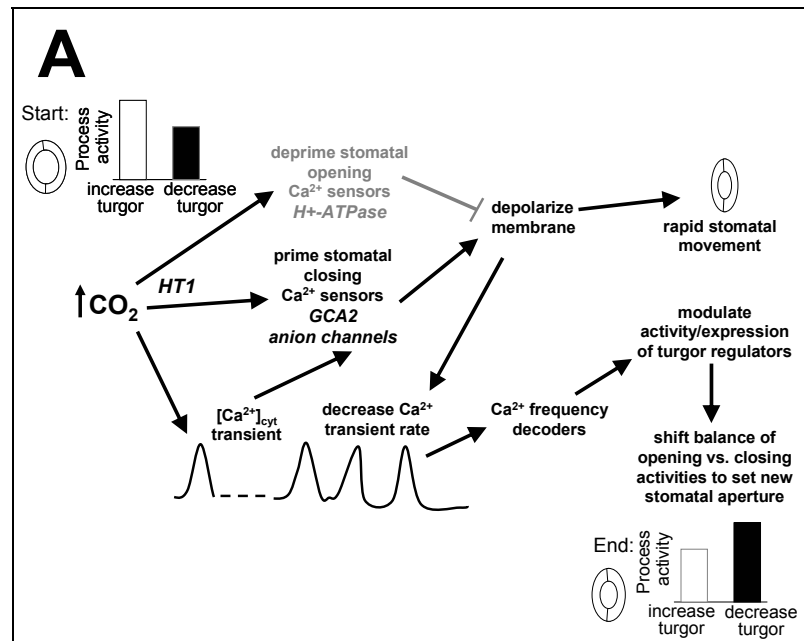


Figure V-2: Models for the role of calcium transients in CO₂ stomatal regulation. The models depict hypothesized series of events that could mediate stomatal responses to CO₂. The opposing responses to stomatal closing (A) and stomatal opening (B) are shown.

Our data show that CO₂ quickly triggers stomatal movements. Gas exchange measurements reveal that responses to CO₂ shifts occur within a minute. Thus there is likely a short pathway between detection of a [CO₂] change and an early stomatal response, which may include modulation of activity of channels/transporters and adjustment of membrane voltage (see Discussion of Chapter II). An early stomatal movement may be triggered by a calcium transient, but is too rapid to involve a change in the calcium transient rate.

The role of the calcium transient pattern may be to set the desired absolute stomatal aperture. Several observations support this hypothesis. ABA and external calcium also produce different rates of calcium transients depending on the concentration of the stimulus^{5,6}. For ABA, external calcium, and CO₂, higher concentrations cause both a slower rate of calcium transients and more closed stomata, making the calcium transient rate a good candidate for a cellular information source which can be translated into a stomatal aperture.

There is also strong evidence from a previous study for the existence of two distinct calcium transient-directed stomatal movement processes, one rapid and directed by individual calcium transients (termed “Ca²⁺ reactive”), another longer-lasting and directed by calcium transient patterns (termed “Ca²⁺ programmed”). This illuminating study further showed that different

calcium transient rates result in different steady-state apertures following the cessation of transients, supporting the idea that the transient rate sets a new aperture.

Additionally, two phases of stomatal movement are typically seen in response to CO₂. In most gas exchange experiments monitoring responses to CO₂ shifts, there is first a rapid change in stomatal conductance and then a slower conductance response (Fig. II-1B and 3D). These two kinetically distinct stomatal movement phases could represent the two separate processes hypothesized here: an early, calcium transient rate-independent response and a later, calcium transient rate-dependent response.

How could the calcium transient rate set the stomatal aperture?

Evidence is emerging that many calcium-regulated signaling proteins are sensitive to calcium transient rates. These include such well-known calcium detectors as calmodulin⁷, CaM kinase II⁸, and protein kinase C⁹. Stomatal set point would result from the balance of activities that serve to increase or decrease guard cell turgor pressure. Based on the correlation between slower calcium transients and stomatal closure, slow calcium transients would preferentially activate calcium decoders that trigger decreased guard cell turgor, while fast calcium transients would preferentially activate calcium decoders that trigger increased guard cell turgor. These calcium pattern transducers would modulate the relative activities and quantities of turgor regulators such as channels, transporters, and carbohydrate metabolizing

enzymes, to set guard cell turgor at a specific level. The level of activity of the calcium detectors and/or their targets may persist long after the calcium transients have ceased. Detection of a stimulus would change the calcium transient rate, which would dictate a new turgor set point.

Due to the complete absence of positive stomatal movements in response to CO₂ in the *ht1-2* mutant (Fig. IV-2 A ,B and E), the *HT1* gene likely plays a critical role in this early short pathway. Furthermore, the finding that the *HT1* gene contributes more significantly to CO₂-induced stomatal movements than to light- or ABA-induced stomatal movements (Fig. IV-2) suggests that *HT1* lies close to CO₂ perception, at an early point in the pathway upstream of significant convergence with other stomatal signaling pathways.

Conversely, *GCA2* appears to lie downstream of convergence of stomatal signaling pathways, since stomata of the *gca2* mutant are also insensitive to ABA and external calcium. This fits with the idea that ABA and external calcium also regulate stomatal apertures via a modulation of the calcium transient rate in a similar way to CO₂. *GCA2* appears to play a role in directing calcium transient rate modulation in response to these stimuli (Figs. II-3B and 3C, ²). Based on a weaker impairment of *gca2* stomata in stomatal opening (Figs. II-S1, S2, and S3), *GCA2* likely directs stomatal closing responses.

There is still much to be learned about the inner workings of this interesting signaling pathway. New information obtained via calcium imaging of stomata in intact leaves, simultaneous observation of calcium transients and stomatal movements, and further elucidation of the roles of *HT1*, *GCA2*, and other genes in this signaling pathway could greatly enhance our understanding of CO₂ stomatal signaling.

REFERENCES CITED

1. Fan, G. Y., Fujisaki, H., Miyawaki, A., Tsay, R. K., Tsien, R. Y. et al. Video-rate scanning two-photon excitation fluorescence microscopy and ratio imaging with cameleons. *Biophysical Journal* **76**, 2412-2420 (1999).
2. Allen, G. J., Chu, S. P., Harrington, C. L., Schumacher, K., Hoffman, T. et al. A defined range of guard cell calcium oscillation parameters encodes stomatal movements. *Nature* **411**, 1053-1057 (2001).
3. Li, Y., Wang, G. X., Xin, M., Yang, H. M., Wu, X. J. et al. The parameters of guard cell calcium oscillation encodes stomatal oscillation and closure in *Vicia faba*. *Plant Science* **166**, 415-421 (2004).
4. Yang, H. M., Zhang, X. Y., Wang, G. X., Li, Y. & Wei, X. P. Cytosolic calcium oscillation may induce stomatal oscillation in *Vicia faba*. *Plant Science* **165**, 1117-1122 (2003).
5. Mcainsh, M. R., Webb, A. A. R., Taylor, J. E. & Hetherington, A. M. Stimulus-Induced Oscillations in Guard-Cell Cytosolic-Free Calcium. *Plant Cell* **7**, 1207-1219 (1995).
6. Staxen, I. I., Pical, C., Montgomery, L. T., Gray, J. E., Hetherington, A. M. et al. Abscisic acid induces oscillations in guard cell cytosolic free

calcium that involve phosphoinositide-specific phospholipase C. *Proc Natl Acad Sci U S A* **96**, 1779-84 (1999).

7. Craske, H., Takeo, T., Gerasimenko, O., Vaillant, C., Torok, K. et al. Hormone-induced secretory and nuclear translocation of calmodulin: Oscillations of calmodulin concentration with the nucleus as an integrator. *Proceedings of the National Academy of Sciences of the United States of America* **96**, 4426-4431 (1999).
8. De Koninck, P. & Schulman, H. Sensitivity of CaM kinase II to the frequency of Ca²⁺ oscillations. *Science* **279**, 227-230 (1998).
9. Violin, J. D., Zhang, J., Tsien, R. Y. & Newton, A. C. A genetically encoded fluorescent reporter reveals oscillatory phosphorylation by protein kinase C. *Journal of Cell Biology* **161**, 899-909 (2003).

APPENDIX A
Methods Development

In the course of my thesis research, I developed or optimized several techniques for data acquisition or analysis. I describe significant technical advances in this chapter.

Measurement of CO₂ Concentrations in Buffer. In calcium imaging experiments testing the effect of [CO₂] on guard cell calcium dynamics, [CO₂] concentrations are applied by bubbling buffer with air of a defined [CO₂] and then perfusing that buffer via a peristaltic pump and flexible tubing to the sample chamber. There is a period of 90 seconds during which the buffer travels through the flexible tubing en route to the sample. Because this tubing is permeable to CO₂, during this transit period the buffered [CO₂] will partially equilibrate with the [CO₂] in the air. Therefore the [CO₂] in the buffer that is actually applied to the sample will not be the same as the [CO₂] of the air initially bubbled into the buffer. For this reason I measured the [CO₂] of the buffer after travel through the perfusion system.

The Li-6400 Portable Photosynthesis System, equipped with infrared gas analyzers, is very good at measuring low concentrations of CO₂ in air, but cannot directly measure the [CO₂] in solution. Therefore to measure the CO₂ content in my buffers I used a technique that allows for calculation of [CO₂] in buffer by measuring the [CO₂] in air equilibrated with the buffer. This technique was introduced to me by Dr. Peter Wagner, Chief of Division of Physiology at UCSD¹, and is detailed here.

Buffer that had been bubbled for at least 2 hours with either 0 ppm [CO₂] or 800 ppm [CO₂] was perfused with the peristaltic pump through the tubing into a small well with the same dimensions as the recording chamber (1.22 cm², 200 µl capacity) formed from a coverslip adhered to a glass slide with a drilled hole, mimicking the situation encountered during calcium imaging. After pooling in the well for about 3-5 seconds, the buffer was drawn into an air-tight glass syringe fitted with a stopcock. Perfusion rate was 85 seconds per ml. 3-5 ml buffer was collected in this way, which took about 5-8 minutes. A volume of CO₂-free air was then introduced into the syringe, and equilibrated with the buffer by vigorous shaking for 5 minutes on a tabletop shaker or by hand. Following equilibration, the gas was transferred to another glass syringe, then evacuated into the Li-6400 via the match chamber where it was read by the “reference” infrared gas analyzer.

The original concentration of CO₂ in the buffer following perfusion was calculated using a mass balance. This mass balance states that the mass of CO₂ present in the original buffer must equal the mass of CO₂ present in both the buffer and the gas following equilibration. This equation can be expressed as follows:

$$P_0 \times S \times V_L = P_1 \times S \times V_L + P_1 / (P_B - P_{H_2O}) \times V_G$$

where P_0 is the original concentration of CO_2 in the buffer, P_1 is the equilibrated (measured) concentration of CO_2 , V_G is the volume of gas, V_L is the volume of liquid, P_B is the barometric pressure, $P_{\text{H}_2\text{O}}$ is the saturated vapor pressure of water at room temperature, and S is the solubility of CO_2 in the buffer under the prevailing conditions. This equation can be solved for P_0 and rewritten as follows:

$$P_0 = P_1 \times \{1.0 + (V_G/V_L)/[(P_B - P_{\text{H}_2\text{O}}) \times S]\}$$

The value of S for CO_2 will depend on many factors including solute concentrations and pH, so it was determined empirically by repeating the equilibration and measurement procedures 2 more times on the same buffer sample. In other words, after measurement of the equilibrated $[\text{CO}_2]$ as described above, the same buffer was then equilibrated with a new volume of gas, and the $[\text{CO}_2]$ of that gas measured, after which the process was repeated a third time. The same mass balance equation was used, this time on the second iteration of the equilibration procedure.

$$P_1 \times S \times V_{L1} = P_2 \times S \times V_{L2} + P_2/(P_B - P_{\text{H}_2\text{O}}) \times V_G$$

Here P_1 and P_2 are the concentrations of CO_2 in the buffer following the first equilibration and the second equilibration, respectively, V_{L1} is the volume of

liquid for the first equilibration, V_{L2} is the volume of liquid for the second. V_G here is the volume of gas for the second equilibration. Note that the second equilibration must be used to calculate the solubility because two measured equilibrated CO_2 concentrations are required (in this case, P_1 and P_2). Solving the mass balance for S yields the following equation:

$$S = [1/(P_B - P_{\text{H}_2\text{O}}) \times V_G] / [(P_1/P_2) \times V_{L1} - V_{L2}]$$

From the second equilibration, a solubility value can be calculated, and if this process is repeated a third time, a second solubility value can be calculated. The accuracy of the solubility values can then be judged from the amount of variation between the two calculated values for S .

When I performed these measurements on my buffers, the buffers bubbled with high CO_2 (800 ppm) produced a consistent solubility value. 5 solubility measurements using 3 different samples yielded a solubility coefficient of 2.35 ± 0.04 (error is s.e.m.). Solubility coefficients calculated from measurements on buffers bubbled with low CO_2 (0 ppm) were more variable (2.97 ± 0.29 , 12 measurements from 6 samples, error is s.e.m.). The average value measured in low CO_2 was also substantially higher than the value measured in high CO_2 . I attribute the higher variability in the low CO_2 measurements and the higher average value to a stronger influence of contamination at the very low concentrations of CO_2 present in those

experiments. Therefore I felt that the value obtained from high CO₂ experiments was more accurate, and I used the solubility value of 2.35 to calculate the CO₂ concentrations in the buffers following perfusion. These values were 115 ppm ± 11 ppm for buffer bubbled with 0 ppm CO₂ and 535 ppm ± 27 ppm for buffer bubbled with 800 ppm CO₂ (error is s.e.m. for n=3).

Gas Exchange. I initiated the use of the Li-6400 Portable Photosynthesis System in the laboratory. Using the Li-6400, stomatal conductance values can be derived from measurements of transpiration rates. Experiments performed revealed some important strategies for obtaining optimal gas exchange data.

The first strategy is to generate healthy plants with large leaves. A large leaf is needed to reach the Li-6400's recording chamber, and to fill the chamber as much as possible, which will increase the signal to noise ratio. This requires that the plants be grown in good conditions until a fairly advanced age (5-7 weeks). Another important strategy is to have the growth conditions and recording conditions as similar as possible. A good way to achieve this is to record the plants in the same place that they are grown. Most of my experiments were done in a large growth room, where recordings can easily be made, but growth conditions are suboptimal. If healthy plants cannot be grown in a growth room (this could be the case if the pathogen load in the growth rooms is too high, or when working with a unhealthy and/or small mutant), then plants can be grown in a growth chamber and recorded on the

bench top. In extreme cases where leaves cannot be grown large enough under normal conditions, short day growing conditions could be used (e.g. 8 hours light/16 hours dark), which results in larger leaves. During the recording, it is optimal to keep all conditions as fixed as possible, except for the test variable. Thus, ideally, humidity, $[\text{CO}_2]$, light, and temperature should all be controlled; each of these parameters can be controlled automatically by the machine.

CO_2 Stomatal Movement Response Assays. Although gas exchange worked well for measuring stomatal movements in response to changes in $[\text{CO}_2]$, I wanted to develop robust CO_2 stomatal movement assays in tissue preparations that were similar to those used in calcium imaging assays, to better connect observed cytosolic calcium behavior with stomatal behavior. Thus, I measured stomatal apertures in intact epidermal layers using a microscope following incubations in different CO_2 concentrations.

I discovered that, in the intact epidermal preparation, robust stomatal responses to CO_2 require live pavement cells surrounding the guard cells. In areas where the pavement cells are dead, guard cell apertures are open wider than in areas where the pavement cells are alive, and appear less responsive to high CO_2 as a closing stimulus. To distinguish live pavement cells and live guard cells from dead cells, I used fluorescein diacetate (FDA, Sigma, F-7378), a dye which is retained and metabolized to a fluorescent molecule in

living but not dead cells. FDA was added to achieve a final concentration of 0.0007% (w/v) 2 minutes prior to measurement.

Analysis of Calcium Transients. Analyses of calcium transient rates became central to my research. Scanning a cameleon ratio data trace by eye and subjectively choosing areas of the trace that appear to represent calcium transients will not result in a reproducible analysis and renders the results vulnerable to experimenter bias. For this reason I sought to develop a more objective approach. Three main strategies were attempted, one of which was deemed to be the most appropriate. All three strategies are described in this chapter.

Fast Fourier Transformation. Fast Fourier Transformations (FFT) convert a time-varying signal into a function generated from the summation of a series of sinusoidal waves of varying periodicities and amplitudes. The larger the amplitude of a wave, the stronger that periodicity is represented in the original data. Transformation of a trace of calcium signaling data by FFT will return information about the periodicity of transients without the experimenter having to decide where the transients are located within the trace. Because the FFT reports the strength of the frequency components that it detects, one could use those strength determinations as a basis for separating the signal from the noise.

Several problems became apparent as I experimented with the technique and used it with my data. The main problem with analyzing calcium transients with FFT is that the strength of frequency components is not only a function of the signal to noise ratio, but also of how regular the periodicity of the transients is. Thus obvious transients that clearly represent signal but that occur with an irregular frequency could generate frequency components of a similar or lower strength (spectral density) as noise that has a relatively more regular periodicity. Since the calcium transients likely include complex stochastic events, this is a significant problem.

I performed FFT on several different experimental series using the FFT-NLLS analysis software package developed by Marty Straume, mathematician at the NSF Center for Biological Timing at the University of Virginia²⁻⁴. This software program accepts a time series and returns the major frequency components detected in the data along with the Relative Amplitude Error (RAE) for each frequency component. This value reflects both the strength (amplitude) of the frequency component in the signal and the error associated with that value. An RAE of zero would denote a perfect frequency component (with no associated error), while an RAE of one indicates a no-confidence frequency component (the error is equal to the amplitude). I analyzed the FFT results returned by FFT-NLLS in a few different ways.

One analysis involved plotting the FFT data as histograms (Figure A-1). For the histograms, each CO₂ treatment phase of each cell was transformed

separately, and only the frequency component with the lowest RAE was included in the histogram. In rare cases, there were two frequency components of similarly low RAE, in those cases both frequency components were included. Since the RAE is inversely proportional to the strength of the rhythmic component, and since RAE varies between 0 and 1, the estimate of frequency component strength I used was $1 - \text{RAE}$ rounded to the nearest tenth. These significant frequency components were separated into bins on the x-axis based on the periodicity of the sinusoidal waves detected. The amplitude on the y-axis equals the sum of all frequency component strength (1-RAE) values from all cells for that bin. For example, if, in the first low CO₂ phase, there were two cells that had frequency components in the 4-5 minute range with a strength of 4 (meaning an RAE of 6) and one cell that had a strength of 3 (meaning an RAE of 7) then the y value for the 4-5 minute bin would be $4 + 4 + 3 = 11$.

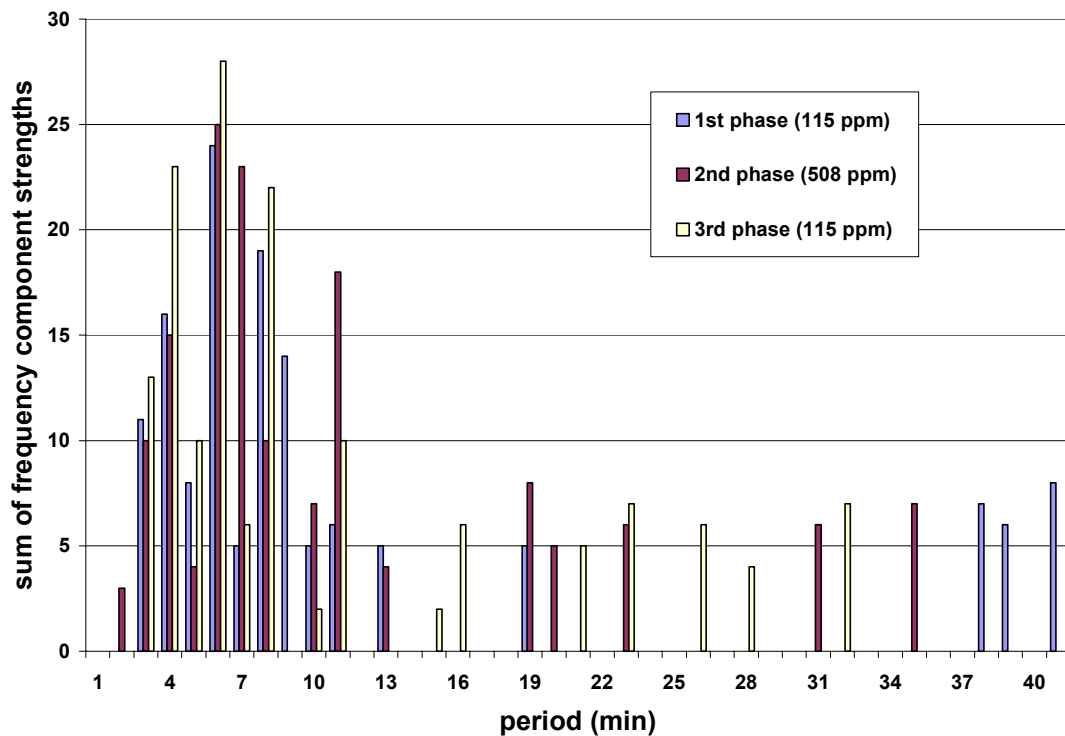


Figure A-1: Fast Fourier Transformation of calcium imaging data represented as a weighted histogram. The highest ranking frequency components returned by FFT for each phase of CO₂ treatment were separated into bins on the x-axis, plotted in terms of periodicity. The amplitude on the y-axis equals the sum of all frequency component strength values from all cells for that bin. (6 cells are represented in this graph).

The histograms revealed a distribution which peaked at 6 minutes and showed small values for periods longer than 15 minutes. There are some outlying data points at periods longer than 15 minutes, but these periodicities are atypical and may represent low-frequency noise, at least in some cases. It is difficult to see a difference in the distribution of periodicities between the low and high CO₂ conditions. A weighted average of the FFT results was also generated based on the experimental data that generated the histogram. This

weighted analysis did not show as large a difference between transient periodicities in low and high CO₂ as was calculated for transients detected by eye (Figure A-2).

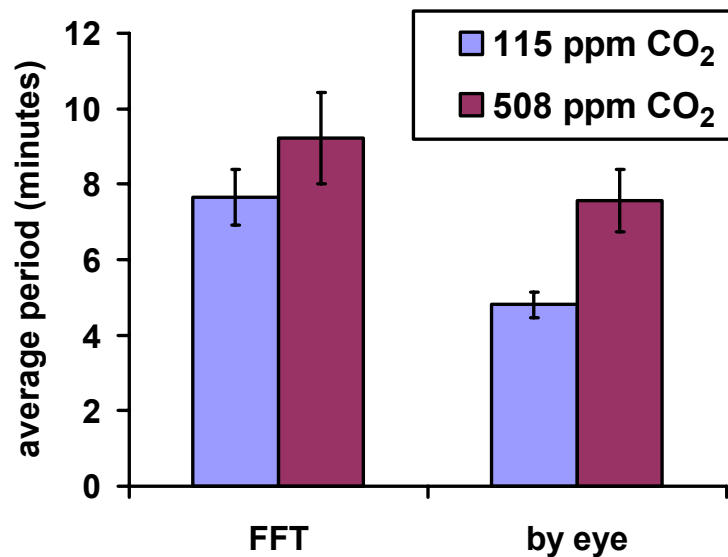


Figure A-2: Average period of major FFT spectral components in calcium imaging data. A weighted average of strongly represented FFT functions in calcium imaging data recorded in different CO₂ concentrations is compared with average periods of transients detected by eye in the same data set (12 cells are represented). Waveforms with periodicities greater than 15 minutes were excluded from this analysis.

I also plotted data as a scatter plot. Figure A-3 shows a scatter plot of the same data displayed as a histogram in Figure A-2. In these scatter plots, in contrast to the histograms, all of the frequency components returned by the FFT program are plotted (except those with an RAE > 1), not only those with the highest strength.

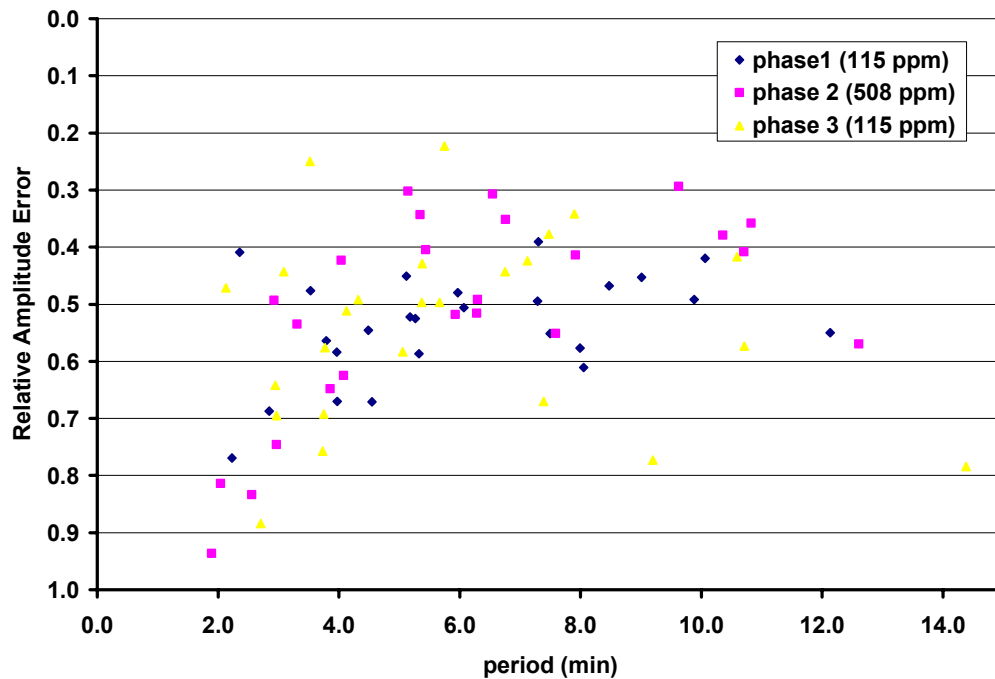


Figure A-3: Fast Fourier Transformation of calcium imaging data represented as a scatter plot. All frequency components returned by the FFT for each phase of CO₂ treatment were plotted according to their periodicity and their Relative Amplitude Error. This data represents the results from 6 cells.

As with the histogram, the trend toward longer periodicities in phases with higher [CO₂] suggested by subjective analyses was difficult to see. The FFT approach was abandoned after discussion with my Ph.D. thesis committee because Ca²⁺ transients are poorly described by sinusoidal wave forms, and because large data sets would be required to quantify significant differences in transient frequencies given the slow rate of calcium transients in guard cells.

Wavelet Transformation. Wavelet transformation is very similar to Fast Fourier Transformation. The main difference is that wavelets report information about the strength of periodic signals in the data at different times within the data trace⁵. This is accomplished by choosing a function and then calculating a goodness of fit of the data trace for the function at each time point at a range of function widths. I performed wavelet transformations on individual data traces using the Morlet wavelet function (Figure A-4).

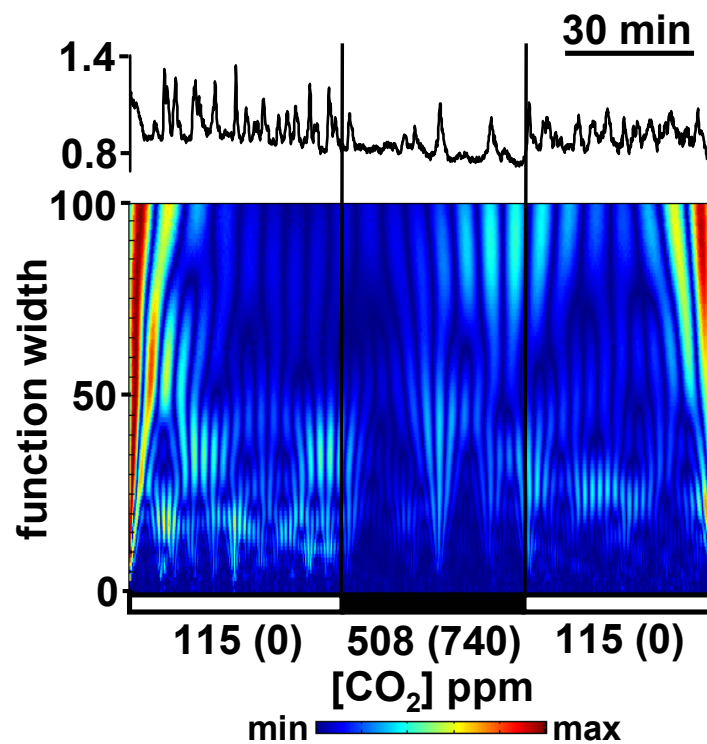


Figure A-4: Wavelet transformation of calcium imaging data. Data from a single guard cell exposed to low and high $[\text{CO}_2]$. Top: Raw data trace of cameleon ratios. Bottom: Wavelet transformation of the raw data. Color scale depicts goodness of fit of the function at that coordinate. Artifactual edge effects of the wavelet analysis are apparent at the left and right borders.

Individual wavelet graphs often suggested higher frequencies and more transients in low CO₂ treatments than in high CO₂ treatments, mirroring the trend apparent by eye. The main drawbacks with the wavelets are that it is not straightforward to evaluate the data quantitatively, particularly if the main effect of CO₂ is to shift or modulate the cytosolic Ca²⁺ pattern, rather than cause consistent Ca²⁺ transient frequencies at each [CO₂], and that it is not straightforward to relate wavelet results directly to transient parameters.

Spikecounter Program for Spike Detection. After discussion with my thesis committee, I analyzed whether an automated technique for detecting calcium transients would be the most appropriate approach. Transient detection would allow for the most straightforward and flexible analyses and most accurately reflect what appeared to be the important characteristics of the data. Samar Mehta, a Neurosciences graduate student in David Kleinfeld's lab in the Department of Physics, and I developed a software program in the Matlab programming environment that accepts calcium imaging data and marks regions of the data trace where a calcium transient is detected, usually without any decisions being made by the experimenter. This is the technique I settled on as my analysis method of choice for calcium imaging data.

The program first calculates the first derivative of the data. This step helps to separate the signal from the noise, because the first derivative highlights two features that are consistently true of our calcium transients and

less true of the noise. First, that there is a large change in amplitude in a short amount of time (i.e. the slope changes quickly), and second, that the signal rises to a peak and then falls back. Next each point in the first derivative trace is fit to a function that roughly approximates the characteristic shape of transients in the first derivative trace. This simple function is called a Haar wavelet (Figure A-5).

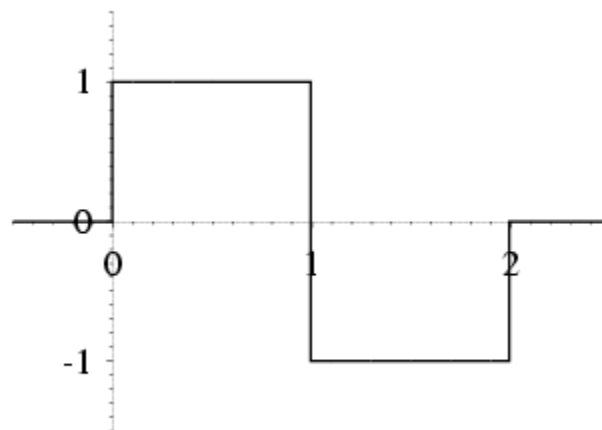


Figure A-5: Haar wavelet function. The Haar wavelet, which approximates the shape transients produce in a first derivative graph, is used for matched filtering in the spikecounter program.

This is a process called “matched filtering” and is accomplished using a wavelet transformation, although only one function width is used. The wavelet coefficients, which reflect the quality of the fit at each point, then constitute the final matrix. The program then counts a transient every time the signal exceeds a threshold (the “detect” threshold), provided it also dips below a “reset” threshold (to prevent against small scale features from being counted as transients). The key feature of this data treatment is that the same

thresholds (detect threshold of 0.15, reset threshold of -0.1) and function width settings (width of 186 seconds) work well for most data traces, only failing when the signal to noise ratio is uncharacteristically low. Thus when the same settings can be used for all experiments this succeeds in removing any user bias and allows a consistent, repeatable basis for spike determination. Using spikecounter, calcium transient rates were calculated by dividing the number of spikes detected by the program in each phase of an experiment, by the total amount of time represented in that phase.

Note that, because spikes in low and high CO₂ likely have slightly different average widths (see Chapter II, Supplementary Data), data sets were analyzed with different function widths. Significantly more spikes were consistently detected in low CO₂ than in high CO₂ using a range of spike widths that detected what appeared by eye to be mostly reasonable spikes. This shows that the optimal function width for low CO₂ and high CO₂ transients is not radically different. Visual inspection of spikes detected using the 186 second function width appeared to result in the most accurate spike detection at both CO₂ concentrations.

REFERENCES CITED

1. Wagner, P. D., Naumann, P. F. & Laravuso, R. B. Simultaneous Measurement of 8 Foreign Gases in Blood by Gas-Chromatography. *Journal of Applied Physiology* **36**, 600-605 (1974).

2. Plautz, J. D., Straume, M., Stanewsky, R., Jamison, C. F., Brandes, C. et al. Quantitative analysis of *Drosophila* period gene transcription in living animals. *Journal of Biological Rhythms* **12**, 204-217 (1997).
3. Straume, M., Frasier-Cadoret, S. & Johnson, M. in *Topics in Fluorescence Spectroscopy, Volume 2: Principles* (ed. Lakowicz, J.) 177-240 (Plenum, New York, 1991).
4. Johnson, M. & Frasier, S. Nonlinear least squares analysis. *Methods Enzymol* **117**, 301-342 (1985).
5. Burke Hubbard, B. *The world according to wavelets* (A K Peters, Ltd., Natick, 1996).

APPENDIX B

Phosphatidylinositol 3- and 4-phosphate are required for normal stomatal movements

ABSTRACT

Phosphatidylinositol (PI) metabolism plays a central role in signaling pathways in both animals and higher plants. Stomatal guard cells have been reported to contain PI 3-phosphate (PI3P) and PI 4-phosphate (PI4P), the products of PI 3-kinase (PI3K) and PI 4-kinase (PI4K) activities. In this study, we tested the roles of PI3P and PI4P in stomatal movements. Both wortmannin (WM) and LY294002 inhibited PI3K and PI4K activities in guard cells and promoted stomatal opening induced by white light or the circadian clock. WM and LY294002 also inhibited stomatal closing induced by abscisic acid (ABA). Furthermore, overexpression in guard cells of GFP:EBD (green fluorescent protein:endosome binding domain of human EEA1) or GFP:FAPP1PH (PI-four-P adaptor protein-1 pleckstrin homology domain), which bind to PI3P and PI4P, respectively, increased stomatal apertures under darkness and white light and partially inhibited stomatal closing induced by ABA. The reduction in ABA-induced stomatal closing with reduced levels of PI monophosphate seemed to be attributable, at least in part, to impaired Ca^{2+} signaling, because WM and LY294002 inhibited ABA-induced cytosolic Ca^{2+} increases in guard cells. These results suggest that PI3P and PI4P play an important role in the modulation of stomatal

closing and that reductions in the levels of functional PI3P and PI4P enhance stomatal opening.

INTRODUCTION

Guard cells surrounding stomata control both the influx of CO₂ required for photosynthesis and water loss from plants through transpiration to the atmosphere. The size of the stomata is regulated through volume changes of guard cells under the concerted influence of light, temperature, CO₂, and phytohormones. Previous experiments have shown that guard cell signaling is mediated by numerous factors, including Ca²⁺, pH, reactive oxygen species (ROS), protein kinases and phosphatases, the cytoskeleton, ion channels, and phosphoinositides (Assmann and Shimazaki, 1999; Hwang et al., 2000; Schroeder et al., 2001).

Phosphoinositides are a family of inositol-containing phospholipids found in all eukaryotic cells. It has been established that these lipids play many important roles throughout plant life (Drøbak et al., 1999; Stevenson et al., 2000). Phosphatidylinositol (PI) kinases catalyze the addition of phosphates to specific positions on the inositol ring of PI. The PI kinases include PI 3-kinase (PI3K) and PI 4-kinase (PI4K), which synthesize PI 3-phosphate (PI3P) and PI 4-phosphate (PI4P). PI 5-kinase has not yet been found, and PI 5-phosphate is likely to be produced from the degradation of PI 4,5-bisphosphate (PI45P₂)

(Hinchliffe et al., 1998). In animals, several distinct PI3K isoforms are involved in the regulation of diverse cellular processes, including vesicle trafficking, proliferation, cytoskeletal organization, Glc transport, and cell volume recovery (Rameh and Cantley, 1999). However, in plants, only one PI3K type, which is a PI-specific PI3K related to yeast Vps34p, has been found. The plant PI3K has been suggested to be involved in root nodule development, plant growth and development, vesicle trafficking from Golgi to vacuoles, and regulation of the transcriptional process (Hong and Verma, 1994; Welters et al., 1994; Bunney et al., 2000; Kim et al., 2001).

PI4K catalyzes the production of PI4P, the only known precursor of PI45P₂, which can be cleaved into inositol 1,4,5-trisphosphate (IP₃) and diacylglycerol by phospholipase C; therefore, it represents a critical point of regulation of PI-dependent pathways. In mammalian and yeast cells, PI4Ks also are important for membrane biogenesis and vesicle trafficking from the ER to the Golgi and the plasma membrane (Roth, 1999). In plant cells, two PI4K genes have been cloned (Stevenson et al., 2000). Although previous studies have succeeded in localizing the enzyme activities of these PI4Ks to the plasma membrane, nucleus, cytosol, and cytoskeleton (Drøbak et al., 1999), their functions remain poorly understood.

PI3P and PI4P exist in guard cells of *Commelina communis*, in which they are suggested to be involved in guard cell signaling (Parmar and Brearley, 1993, 1995). Phosphoinositide metabolism has been shown to play

important roles in abscisic acid (ABA)–induced cytosolic calcium concentration ($[Ca^{2+}]_{cyt}$) changes and stomatal closing (Gilroy et al., 1990; Staxén et al., 1999). In addition, endogenous PI monophosphate (PIP) levels in guard cells change rapidly in response to treatment with ABA (Lee et al., 1996). However, the specific role of PIP in guard cells has not been studied previously. In this study, we present evidence that supports the involvement of PI3P and PI4P of guard cells in stomatal movements and ABA-induced Ca^{2+} signaling.

RESULTS

Wortmannin and LY294002 promote stomatal opening induced by white light or by the circadian clock in the dark and inhibit stomatal closing induced by ABA. To investigate whether PI3P and PI4P in guard cells are involved in stomatal movements, we treated guard cells of *Vicia faba* leaves with wortmannin (WM) or LY294002, inhibitors of PI3K and PI4K. These inhibitors were used in the micromolar range because micromolar concentrations of these inhibitors have been reported previously to inhibit the activity of PI kinases in plant cells (Matsuoka et al., 1995; Xue et al., 1999; Kim et al., 2001). In the presence of 1 or 10 μ M WM, stomatal opening movements induced by the circadian clock under darkness or white light were enhanced greatly ($P < 0.001$; Fig. B-1A). WM at 1 μ M increased stomatal opening induced by the circadian clock in the dark to 214% compared with the control

and to 140% in the light compared with the control. WM at 10 μM enhanced stomatal opening further (an increase of 279 and 178% compared with the control under darkness and white light, respectively). LY294002, a PI kinase inhibitor structurally distinct from WM, also enhanced stomatal opening under darkness and white light at 100 μM ($P < 0.001$).

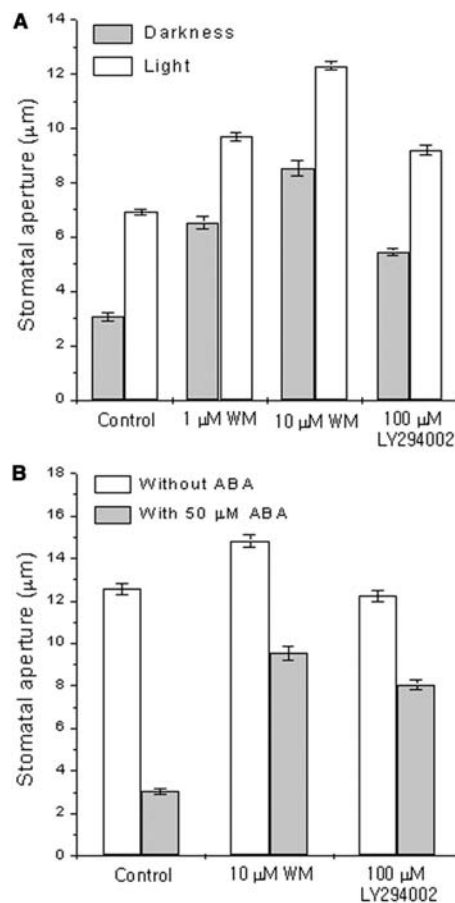


Figure B-1. Effects of WM and LY294002 on stomatal movements in *Vicia*. (A) Effects on stomatal opening. Epidermal fragments were incubated with WM, LY294002, or 0.2% DMSO (as a solvent control) for 3 h under darkness or white light beginning at h 3 to 4 of the usual photoperiod. (B) Effects on stomatal closing. Fully opened stomata were pretreated with WM, LY294002, or 0.2% DMSO (as a solvent control) for 30 min and treated with 50 μM ABA for 1 h. Final apertures (average \pm SE) from 120 measurements from three independent experiments are presented.

We also tested the effects of these inhibitors on ABA-induced stomatal closing. In the absence of the inhibitors, stomatal apertures after 1 h of treatment with 50 μ M ABA were 24% of control without ABA (Fig. B-1B). In the presence of the inhibitor WM at 10 μ M or LY294002 at 100 μ M, stomatal apertures remained at 64 and 66% of controls without ABA, respectively ($P < 0.001$; Fig. B-1B). Similar results were obtained from another plant species; in *C. communis* guard cells, stomatal opening induced by white light or the circadian clock was enhanced, and stomatal closing induced by ABA was inhibited (data not shown). These findings suggest an important role for PI3P and PI4P in guard cells for stomatal movements.

WM and LY294002 commonly inhibit both PI3K and PI4K activities in guard cells. To determine whether these inhibitors reduce the enzyme activities of PI3K and PI4K in guard cells, we prepared protein extracts from guard cell-enriched epidermis pretreated with the inhibitors and then assayed the kinase activities in these extracts. PI3K and PI4K activities were detected in the membrane fraction but not in the cytosolic fraction of proteins extracted from guard cell-enriched samples in an in vitro assay with γ -³²P-ATP (Fig. B-2). This is in contrast to findings in other plant cells, in which PI kinase activity has been detected in both soluble and membrane fractions as well as in the cytoskeleton and nucleus (Hong and Verma, 1994; Munnik et al., 1998). The level of radiolabeling of PI4P was approximately 9- to 10-fold higher than that

of PI3P, indicating that PI4K activity dominates PI3K activity. Treatment with WM or LY294002 inhibited both PI3K and PI4K activities. Compared with the control, WM reduced PI4K activity to $41\% \pm 15\%$ at $1 \mu\text{M}$, to $16\% \pm 3\%$ at $10 \mu\text{M}$, and almost abolished all activity at $30 \mu\text{M}$ (to $8\% \pm 3\%$). WM also inhibited PI3K activity almost completely at $1 \mu\text{M}$ (to $9\% \pm 7\%$). LY294002 ($100 \mu\text{M}$) inhibited the activities of PI3K (to $35\% \pm 14\%$) and PI4K (to $64\% \pm 13\%$) compared with the controls.

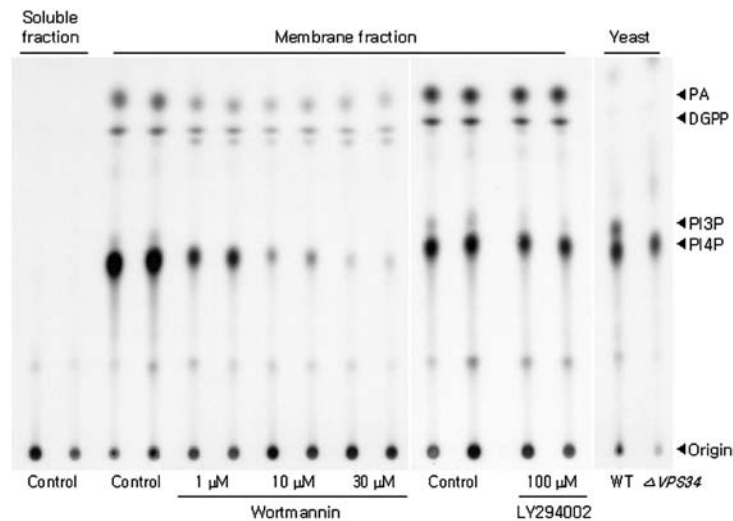


Figure B-2: Effects of WM and LY294002 on the activities of PI3K and PI4K in guard cells of *Vicia*. Epidermal fragments were illuminated for 3 h in 10 mM KCl and 10 mM Mes-KOH buffer, pH 6.1, with or without inhibitors. Proteins were extracted from guard cell-enriched epidermal tissues, separated into membrane and soluble fractions as described in Methods, and incubated with $\gamma\text{-}^{32}\text{P}\text{-ATP}$ and PI for 15 min. The lipid products were extracted and separated on a *trans*-1,2-diaminocyclohexane-*N,N,N',N'*-tetraacetic acid-treated thin layer chromatography plate with a borate-based separation system. Proteins prepared from wild-type (WT) and mutant ΔVPS34 (defective in PI3K) yeast also were assayed for kinase activities to help identify the PI3P and PI4P bands. A representative from two independent experiments with similar results is shown. DGPP, diacylglycerolpyrophosphate; PA, phosphatidic acid.

WM has been reported to inhibit not only PI kinases but also other related lipid kinases (Vanhaesebroeck et al., 2001). If PI kinase inhibitors inhibit PI4P 5-kinase (PI4P5K) as well, then they may act by reducing the level of PI45P₂, which could decrease the ABA-induced release of IP₃, an important second messenger in guard cells (Gilroy et al., 1990; Lee et al., 1996; Staxén et al., 1999). Thus, the possibility that PI kinase inhibitors also might inhibit PI4P5K was tested using guard cell-enriched samples. The PI bisphosphate band appeared only when exogenous PI4P was present in the in vitro kinase assay (Fig. B-3). Because PI4P 3-kinase has never been reported in plant cells, we suggest that the band corresponds to the PI4P5K product, PI45P₂. WM at 1, 10, and 30 μ M reduced PI4P5K activity in guard cells to 58, 38, and 20%, respectively. However, LY294002 at 100 μ M did not inhibit PI4P5K activity significantly (to 92% \pm 5% of control; $P > 0.05$, $n = 3$). Interestingly, under experimental conditions in which only endogenous but no exogenous PI was present in the assay, LY294002 specifically inhibited PI3K activity (to 65% \pm 4% of control; $P < 0.05$, $n = 3$) but not PI4K activity (to 92% \pm 11% of control; $P > 0.05$, $n = 3$). The specificity of LY294002 for PI kinases supports the notion that the inhibitory effects of this inhibitor are attributable mainly to reduced PIP levels rather than to reduced PI45P₂ levels.

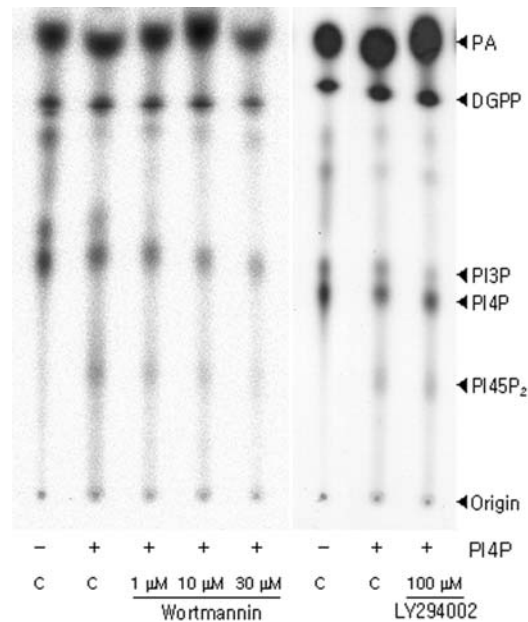


Figure B-3: Effects of WM and LY294002 on PI4P5K activity in guard cells of *Vicia*. All experimental procedures were as described in Fig. B-2 except that the membrane fraction of the guard cell preparation was incubated for 30 min with γ -³²P-ATP in the presence or absence of PI4P. In control samples without any exogenous lipid substrate, no PI45P₂ band was detected. In all samples, some endogenous lipids from the membrane fraction were phosphorylated. C, control; DGPP, diacylglycerolpyrophosphate; PA, phosphatidic acid.

Overexpression of the PI3P binding endosome binding domain construct

***GFP:EBD* increases stomatal apertures under darkness and white light**

and inhibits stomatal closing induced by ABA. WM and LY294002

interfered with the activity of both PI3K and PI4K; therefore, it was difficult to

determine which PIP contributed to stomatal movements. To answer this

question, we overexpressed in guard cells GFP:EBD (green fluorescent

protein:endosome binding domain of human EEA1) (Fig. B-4A , construct a),

which binds specifically to PI3P (Kim et al., 2001). Fig. B-4C shows a

fluorescence image of a guard cell expressing GFP:EBD. GFP:EBD, which

has been reported to localize to membranous structures (Gillooly et al., 2000; Kim et al., 2001), appeared to localize at, or close to, vesicles and tonoplast membranes in guard cells (Fig. B-4C). We compared the apertures of half-stoma bordered by transformed guard cells (At) expressing GFP:EBD with those of nontransformed neighbor guard cells (An) (Fig. B-4B).

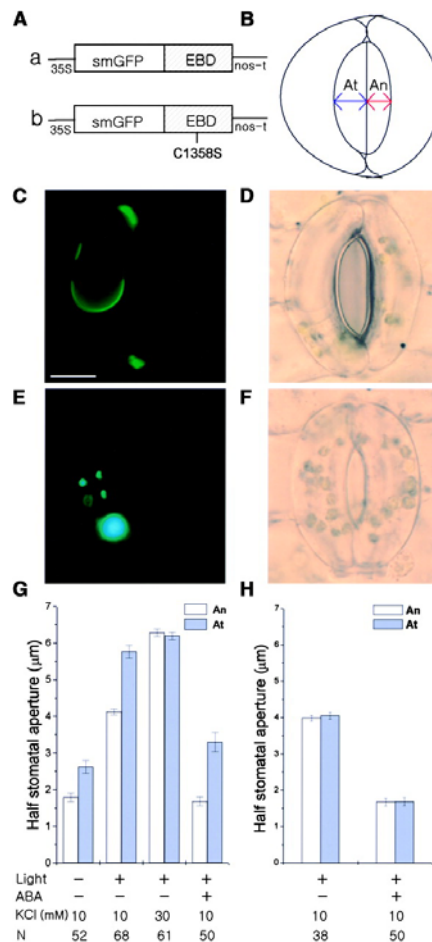


Figure B-4: Effects of overexpressed GFP:EBD on stomatal movements in *Vicia*. (A) Diagram of the constructs *GFP:EBD* (a) and *GFP:EBDC1358S* (b). (B) Cartoon of the method of measurement of half-stomatal apertures bordered by transformed (At) or nontransformed (An) guard cells. (C) and (D) A guard cell expressing *GFP:EBD* treated with 50 μM ABA for 1 h. (C) Fluorescence image. Bar = 10 μm. (D) Corresponding bright-field image. (E) and (F) A guard cell expressing *GFP:EBDC1358S* treated with 50 μM ABA for 1 h. (E) Fluorescence image. (F) Corresponding bright-field image. The guard cells at right in (D) and (F) were not transformed. The fluorescence images shown in (C) and (E) were taken at the same exposure time. The intense fluorescence of accumulated *GFP:EBDC1358S* looks bluish in (E). (G) and (H) Half-stomatal apertures of *GFP:EBD*-transformed (G) or *GFP:EBDC1358S*-transformed (H) guard cells and nontransformed guard cells under darkness after white light-induced stomatal opening for 3 h and 50 μM ABA-induced stomatal closing for 1 h. Results shown are from three independent experiments (average ± SE). N, number of cells observed.

Overexpressed GFP:EBD increased stomatal apertures under darkness and white light (Fig. B-4G; $P < 0.001$) and inhibited stomatal closing in response to 50 μM ABA (Figs. B-4D and 4G; $P < 0.001$). In the darkness, At was $2.6 \pm 0.18 \mu\text{m}$, whereas An was $1.8 \pm 0.12 \mu\text{m}$. After 3 h of illumination with white light, At was $5.8 \pm 0.18 \mu\text{m}$, whereas An was $4.1 \pm 0.08 \mu\text{m}$. To determine the effects of the overexpressed GFP:EBD on stomatal closing, At and An stomata were induced to open to the same extent, using 30 mM KCl and increasing temperature to 29°C. Subsequent treatment with 50 μM ABA for 1 h reduced An to $1.7 \pm 0.12 \mu\text{m}$, whereas At remained open at $3.3 \pm 0.26 \mu\text{m}$. As a control for the expression of GFP:EBD, we expressed GFP:EBDC1358S (Fig. B-4A, construct b), which does not bind to PI3P (Kim et al., 2001). GFP:EBDC1358S showed a spotty pattern of expression in the cytosol of guard cells (Fig. B-4E), which was similar to that found in Arabidopsis cells (Kim et al., 2001), and it did not alter stomatal movements (Figs. B-4F and 4H). These results provide evidence of an important role for PI3P in stomatal movements.

Overexpression of the PI4P binding construct *GFP:FAPP1PH* increases stomatal apertures under darkness and white light and inhibits stomatal closing induced by ABA. To investigate a possible role for PI4P in stomatal movements, we overexpressed in guard cells GFP:FAPP1PH (PI-four-

phosphate adaptor protein-1 pleckstrin homology domain). Dowler et al. (2000) reported previously that FAPP1PH fused to glutathione S-transferase binds specifically to PI4P in vitro. The fusion protein GFP:FAPP1PH (Fig. B-5A) used in our study specifically bound to PI4P in vitro (Fig. B-5C) and was localized mainly to membrane regions in Arabidopsis mesophyll cell protoplasts (Figs. B-5E and 5G). However, a mutant form, GFP:FAPP1PH[K7E, R18A] (Fig. B-5B), did not bind to PI4P in vitro (Fig. B-5D) and was distributed mainly in the cytosol of Arabidopsis mesophyll cell protoplasts (Figs. B-5F and 5G).

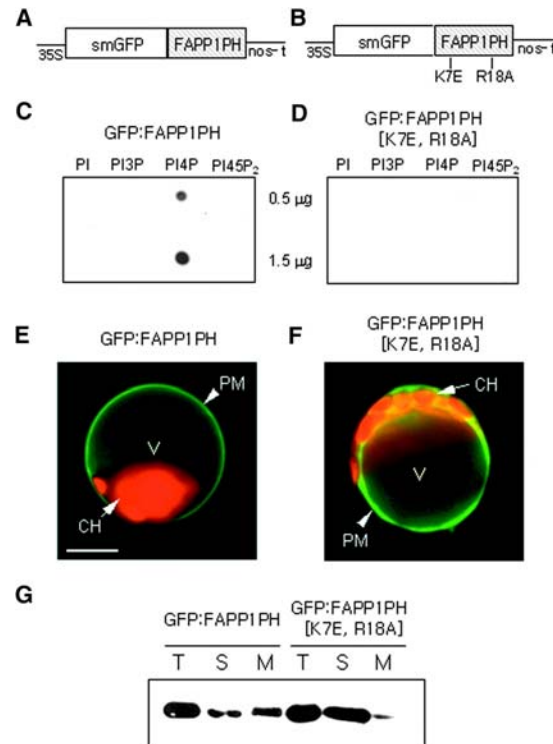


Figure B-5: PI4P-specific binding of GFP:FAPP1PH and Its localization at the plasma membrane in Arabidopsis mesophyll cell protoplasts. (A) and (B) Diagram of the constructs *GFP:FAPP1PH* (A) and *GFP:FAPP1PH*[K7E, R18A] (B). (C) and (D) Phosphoinositide binding properties of GFP:FAPP1PH (C) and GFP:FAPP1PH[K7E, R18A] (D). The phosphoinositide binding affinity of His-tagged GFP:FAPP1PH and GFP:FAPP1PH[K7E, R18A] was assessed by fat-protein gel blot analysis. The binding of GFP:FAPP1PH and GFP:FAPP1PH[K7E, R18A] was detected using a monoclonal anti-His antibody. (E) and (F) In vivo targeting of GFP:FAPP1PH (E) and GFP:FAPP1PH[K7E, R18A] (F). Protoplasts were transformed with *GFP:FAPP1PH* and *GFP:FAPP1PH*[K7E, R18A] and examined at 12 to 36 h after transformation. The images show representative protoplasts at 17 h after transformation. The region where red chloroplasts and cytosolic GFP:FAPP1PH[K7E, R18A] overlap appears yellow in (F). CH, chloroplasts; PM, plasma membrane; V, central vacuole. Bar = 20 μm. (G) Protein gel blot analysis of the localization of GFP:FAPP1PH and GFP:FAPP1PH[K7E, R18A]. Whole cell extracts (T) obtained from the transformed protoplasts were separated into soluble (S) and membrane (M) fractions by ultracentrifugation at 100,000g for 1 h. The membrane fraction was resuspended in the original volume. Proteins in equal volume (30 μL) of each fraction were separated by SDS-PAGE and probed by protein gel blot analysis using monoclonal anti-GFP antibody.

Fig. B-6A shows a fluorescence image of a guard cell expressing GFP:FAPP1PH. GFP:FAPP1PH appeared to localize to or near the plasma membrane and nucleus in guard cells (Fig. B-6A), as has been found for other eukaryotic cells (Payraastre et al., 1992; Balla, 1998; Bunney et al., 2000). We compared apertures of half-stoma bordered by transformed guard cells (At) expressing GFP:FAPP1PH with those of their nontransformed neighbor guard cells (An). As observed for PI3P binding of GFP:EBD, overexpressed GFP:FAPP1PH increased stomatal apertures under darkness and white light (Fig. B-6E; $P < 0.001$) and inhibited stomatal closing in response to 50 μM ABA (Figs. B-6B and 6E; $P < 0.001$). In the darkness, At was $2.0 \pm 0.15 \mu\text{m}$, whereas An was $1.2 \pm 0.12 \mu\text{m}$. After 3 h of illumination with white light, At was $5.2 \pm 0.22 \mu\text{m}$, whereas An was $3.9 \pm 0.16 \mu\text{m}$. To determine the effects of the overexpressed GFP:FAPP1PH on stomatal closing, At and An stomata were induced to open to the same extent, using 30 mM KCl and increasing temperature to 29°C. Subsequent treatment with 50 μM ABA for 1 h reduced An to $1.8 \pm 0.11 \mu\text{m}$, whereas At remained open at $3.1 \pm 0.18 \mu\text{m}$. As a control for the expression of GFP:FAPP1PH, we expressed GFP:FAPP1PH[K7E, R18A], which does not bind to PI4P. GFP:FAPP1PH[K7E, R18A] appeared to localize mainly in the cytosol of guard cells (Fig. B-6C), as found in *Arabidopsis* mesophyll cell protoplasts (Fig. B-5F), and some also appeared as spots and did not alter stomatal movements (Figs. B-6D and 6F). These results suggest that PI4P plays an important role in stomatal movements.

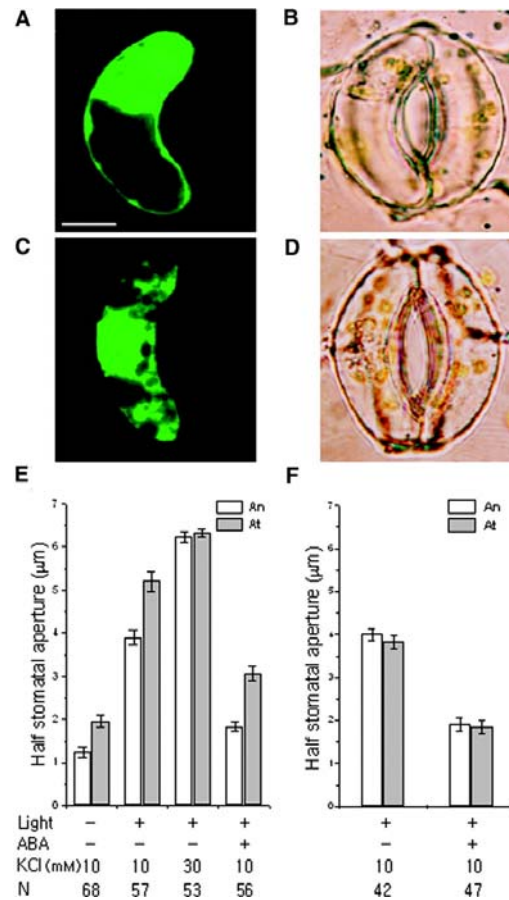


Figure B-6: Effects of overexpressed GFP:FAPP1PH on stomatal movements in *Vicia*. (A) and (B) A guard cell expressing GFP:FAPP1PH treated with 50 μ M ABA for 1 h. (A) Fluorescence image. Bar = 10 μ m. (B) Corresponding bright-field image. (C) and (D) A guard cell expressing GFP:FAPP1PH[K7E, R18A] treated with 50 μ M ABA for 1 h. (C) Fluorescence image. (D) Corresponding bright-field image. The guard cells at right in (B) and (D) were not transformed. (E) and (F) Half-stomatal apertures of *GFP:FAPP1PH*-transformed (E) or *GFP:FAPP1PH*[K7E, R18A]-transformed (F) (At) and nontransformed (An) guard cells under darkness after white light-induced stomatal opening for 3 h and 50 μ M ABA-induced stomatal closing for 1 h. Results shown are from three independent experiments (average \pm SE). N, number of cells observed.

The effect of the PI4P binding construct on stomatal opening is not mediated through reductions in the level of PI45P₂ or IP₃. Because PI4P is

a precursor of PI45P₂, it is possible that the PI4P binding construct inhibits PI45P₂ synthesis and subsequent stimulus-dependent IP₃ release in guard cells. If this is the case, then the PI45P₂ binding construct should show the same effect as the PI4P binding construct. However, the expression of *GFP:PLCδ1PH* (phospholipase Cδ1 pleckstrin homology domain), a PI45P₂ and IP₃ binding construct (Stauffer et al., 1998; Hirose et al., 1999; Kost et al., 1999), in guard cells inhibited white light–induced stomatal opening (Figs. B-7C and 7F), an effect that was opposite to that of the PI4P binding construct *GFP:FAPP1PH* (Fig. B-6). The effect of *GFP:PLCδ1PH* on stomatal opening also was opposite to those of WM and LY294002 (Fig. B-1A). ABA-induced closing of stomata bordered by guard cells expressing *GFP:PLCδ1PH* was similar to that of guard cells expressing *GFP:EBD* or *GFP:FAPP1PH* (Figs. B-4, 6, and 7). Therefore, the PI4P binding construct may reduce ABA-induced stomatal closing, at least in part, by reducing the level of PI45P₂. The expression of GFP alone did not have any effect on stomatal movement.

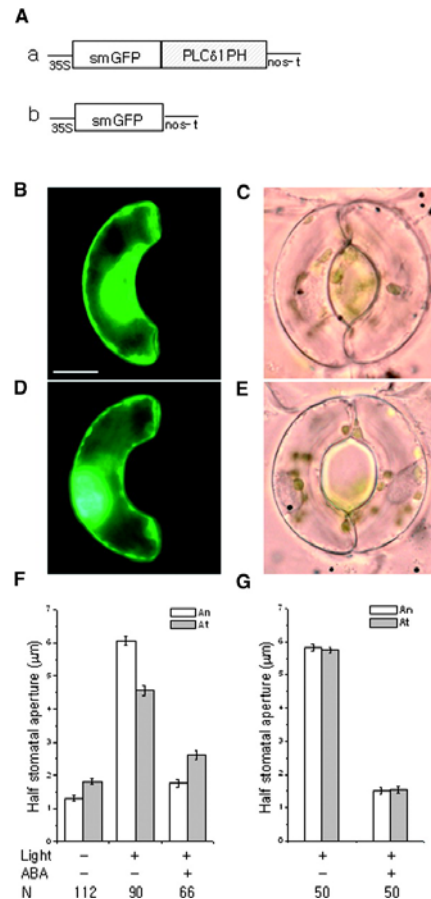


Figure B-7: Effects of overexpressed GFP:PLC δ 1PH on stomatal movements in *Vicia*. (A) Diagram of the constructs *GFP:PLC δ 1PH* (a) and *GFP* (b). (B) and (C) A guard cell expressing GFP:PLC δ 1PH irradiated with white light for 3 h. (B) Fluorescence image. Bar = 10 μ m. (C) Corresponding bright-field image. (D) and (E) A guard cell expressing GFP irradiated with white light for 3 h. (D) Fluorescence image. (E) Corresponding bright-field image. The guard cells at right in (C) and (E) were not transformed. (F) and (G) Half-stomatal apertures of *GFP:PLC δ 1PH*-transformed (F) or *GFP*-transformed (G) guard cells and nontransformed guard cells under darkness after white light-induced stomatal opening for 3 h and 50 μ M ABA-induced stomatal closing for 1 h. The guard cells were incubated in 10 mM KCl and 10 mM Mes-KOH buffer, pH 6.1, at 29°C throughout the experiment. Results shown are from three independent experiments (average \pm SE). N, number of cells observed.

WM and LY294002 inhibit ABA-induced cytosolic Ca²⁺ increases in guard cells. To elucidate the possible mechanisms by which PI3P and PI4P

participate in stomatal movements, we determined if these lipids are involved in ABA-induced Ca^{2+} signaling, an important mediator in stomatal movements (Assmann and Shimazaki, 1999; Schroeder et al., 2001). We measured changes in $[\text{Ca}^{2+}]_{\text{cyt}}$ induced by ABA in the presence or absence of inhibitors (WM or LY294002) in Arabidopsis guard cells expressing yellow cameleon 2.1 as a Ca^{2+} indicator (Allen et al., 1999). WM (10 μM) reduced the probability of ABA-induced $[\text{Ca}^{2+}]_{\text{cyt}}$ increases (Figs. B-8A and 8B; $\chi^2 = 3.34$, $P < 0.05$) as well as the stomatal closing induced by ABA (Fig. B-8C; $P < 0.001$, $n = 120$). In the control group, ABA (50 μM) induced two or more Ca^{2+} transient increases in 59% of guard cells ($n = 17$ of 29), a single transient $[\text{Ca}^{2+}]_{\text{cyt}}$ increase in 17% of guard cells ($n = 5$ of 29), and no response in $[\text{Ca}^{2+}]_{\text{cyt}}$ in 24% of guard cells ($n = 7$ of 29). However, in WM-treated guard cells, the percentage of cells showing two or more ABA-induced Ca^{2+} transient increases declined to 24% ($n = 6$ of 25). Guard cells showing a single transient increase or no change of $[\text{Ca}^{2+}]_{\text{cyt}}$ were 28 and 48%, respectively ($n = 7$ of 25 and $n = 12$ of 25; Fig. B-8B). In addition, WM decreased the average peak of $[\text{Ca}^{2+}]_{\text{cyt}}$ changes even in those guard cells showing Ca^{2+} increases ($P < 0.005$). The average peak $[\text{Ca}^{2+}]_{\text{cyt}}$ change was 211 nM in WM-treated cells and 488 nM in control cells. LY294002 (100 μM) had the same effects on ABA-induced $[\text{Ca}^{2+}]_{\text{cyt}}$ increases (Figs. B-8D and 8E) and stomatal closing (Fig. B-8F; $P < 0.001$, $n = 120$).

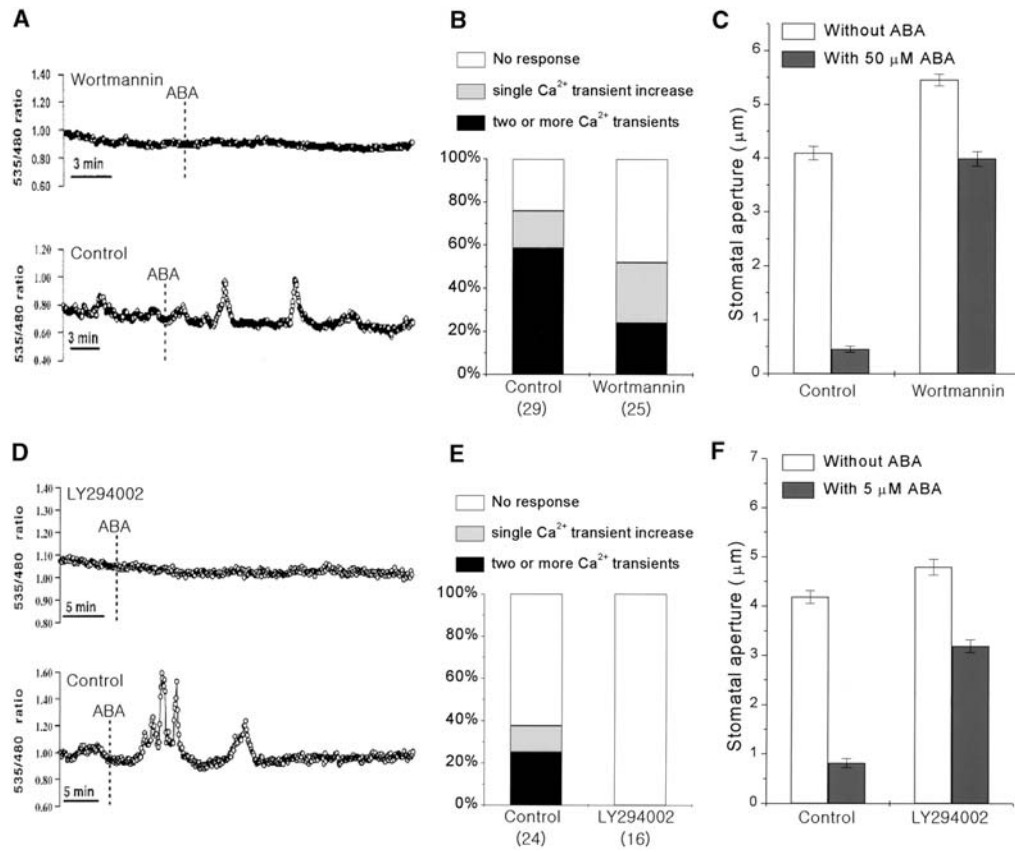


Figure B-8: Effects of WM and LY294002 on the ABA-induced Ca²⁺ increases in guard cells and stomatal closing in Arabidopsis. (A) and (D) ABA-induced cytosolic Ca²⁺ changes in the presence or absence of the inhibitors 10 μM WM (A) and 100 μM LY294002 (D). Vertical lines indicate the time when cells were treated with 50 μM ABA (for the WM assay) or 5 μM ABA (for the LY294002 assay). (B) and (E) Percentage of guard cells showing different types of ABA-induced Ca²⁺ responses in the presence of WM and 50 μM ABA (B) or LY294002 and 5 μM ABA (E). Numbers in parentheses indicate the total numbers of cells analyzed. (C) and (F) Effects of 10 μM WM (C) and 100 μM LY294002 (F) on ABA-induced closing in Arabidopsis stomata. Results shown are from 120 measurements from three independent experiments (average ± SE).

Calcium imaging experiments were performed at 5 μM ABA in

LY294002 to analyze inhibitor effects at a lower ABA concentration. In control cells, ABA (5 μM) induced two or more Ca²⁺ transient increases in 25% of

guard cells ($n = 6$ of 24), a single transient $[Ca^{2+}]_{cyt}$ increase in 12.5% of guard cells ($n = 3$ of 24), and no response in $[Ca^{2+}]_{cyt}$ in 62.5% of guard cells ($n = 15$ of 24). By contrast, none of the LY294002-treated guard cells displayed changes in $[Ca^{2+}]_{cyt}$ in response to ABA ($\chi^2 = 7.74$, $P < 0.005$, $n = 16$). These results suggest that PI3P and/or PI4P are important for ABA-induced Ca^{2+} signaling.

DISCUSSION

To determine whether PI3P and PI4P are important for stomatal movements, we used several different methods, including kinase inhibitor tests, biochemical assays, biolistic transformation of guard cells with chimeric genes encoding GFP-tagged phosphoinositide-specific binding proteins, and calcium imaging. The results consistently showed that PI3P and PI4P in guard cells are involved in normal stomatal movements. Furthermore, the results suggested that these lipids are essential for normal Ca^{2+} signaling induced by ABA.

In the kinase inhibitor test, WM and LY294002 enhanced circadian clock- or white light-induced stomatal opening and inhibited ABA-induced stomatal closing (Figs. B-1A and 1B). Biochemical assays showed that WM inhibited PI3K, PI4K and PI4P5K, whereas LY294002 inhibited PI3K and PI4K but not PI4P5K, in protein extracts from guard cell-enriched epidermal

samples (Figs. B-2 and 3). The specificity of LY294002 for PI kinases is consistent with the notion that alterations in stomatal movement by these inhibitors are caused by the depletion of PI3P and PI4P. We further tested this hypothesis using GFP:EBD and GFP:FAPP1PH, which bind specifically to PI3P and PI4P, respectively. These constructs, when introduced into guard cells by the biolistic bombardment technique, had effects similar to those of WM and LY294002: they increased stomatal apertures under darkness and white light and partially inhibited ABA-induced stomatal closing (Figs. B-4G and 6E). These results support the notion that both PI3P and PI4P are necessary for normal stomatal movements. Overexpression of the lipid binding proteins in guard cells might have blocked the function of target lipids by competing with endogenous lipid binding proteins.

The fusion protein GFP:EBD has been used previously to study trafficking of PI3P in Arabidopsis protoplasts (Kim et al., 2001), and the results showed trafficking of PI3P from the *trans*-Golgi network to the lumen of the central vacuole. The EBD protein consists of a FYVE domain (PI3P binding domain) and a Rab5 binding domain; therefore, it is possible that other mechanisms, such as depletion of a Rab5 homolog by EBD, contributed to the altered responses of stomata bordered by EBD-expressing guard cells. To eliminate this possibility, we used an EBD that has a point mutation at the zinc binding motif of the FYVE domain. The overexpressed EBDC1358S, unlike normal EBD, failed to alter stomatal responses (Fig. B-4H), suggesting that the

effects of EBD on stomatal movements result from the specific binding of PI3P to the FYVE domain of EBD.

GFP:FAPP1PH bound specifically to PI4P (Fig. B-5C), as shown previously for glutathione S-transferase:FAPP1PH (Dowler et al., 2000), was localized at or near the plasma membrane and nucleus of guard cells (Fig. B-6A), and increased stomatal apertures (Fig. B-6E). In contrast, GFP:FAPP1PH mutated at two amino acids in a region of high interspecies homology (Fig. B-5B), showed decreased affinity to PI4P (Fig. B-5D), was localized mainly to the cytosol of guard cells (Fig. B-6C), and had no effects on stomatal apertures (Fig. B-6F). These results suggest that the binding of PI4P by GFP:FAPP1PH has an effect on stomatal movements.

GFP:PLC δ 1PH, which binds specifically to PI45P₂ and its metabolite IP₃, has been used widely to visualize PI45P₂ (Stauffer et al., 1998). Introduction of *GFP:PLC δ 1PH* into guard cells inhibited white light-induced stomatal opening (Figs. B-7C and 7F), an effect that was opposite to that of the PI4P binding construct *GFP:FAPP1PH* (Figs. B-6 and 7). This result suggests that the effect of the PI4P binding construct on stomatal opening is not attributable to a reduction in the PI45P₂ or IP₃ level but to interference with the normal function of PI4P. Therefore, we suggest that PI4P plays a role in stomatal opening movement as part of a PI45P₂- and IP₃-independent pathway in guard cells.

The effect of GFP:PLC δ 1PH on stomatal opening also was opposite to that of WM (Figs. B-1A and 7). Therefore, the effects of WM on stomatal opening are not likely to be attributable to an inhibition of PI4P5K activity but to its inhibitory effect on PI kinase activity. This conclusion is supported further by the fact that the effect of WM was similar to the effects of the two PIP binding constructs, GFP:EBD and GFP:FAPP1PH (Figs. B-1, 4, and 6). The effect of GFP:PLC δ 1PH on ABA-induced stomatal closing was similar to the effects of PIP binding proteins (Figs. B-4, 6, and 7). Therefore, the effect of PI4P binding protein may be mediated at least partly by reductions in the PI45P₂ level, which could reduce ABA-induced IP₃ release and consequently inhibit ABA signaling in guard cells.

The level of a signal mediator for stomatal closing may increase in response to physiological stimuli that induce stomatal closure. For example, IP₃ levels in guard cells increase transiently in response to ABA (Lee et al., 1996), and activities of PI kinases in plant cells have been suggested to increase in response to hyperosmotic stress (Monks et al., 2001). Previously, we showed that the PIP level in guard cell protoplasts fluctuates considerably during ABA treatment (Lee et al., 1996), reaching 140% of the control at 3 and 10 min after ABA treatment, whereas the levels of structural lipids, such as phosphatidylcholine, phosphatidylethanolamine, and phosphatidylglycerol, remain stable. This observation supports a role for PIP in ABA signaling. The possibility that PI kinase activity in guard cells changes in response to ABA

was tested by the in vitro PI kinase assay using protein extracts from guard cell-enriched epidermal samples. Although our assay of the enzyme activities seemed reliable, as indicated by the measurable decreases in enzyme activities in the presence of WM and LY294002 (Fig. B-2), we did not detect any consistent changes in PI kinase activity after ABA treatment. The changes in the enzyme activities were variable and remained within $\pm 40\%$ of control at 3, 5, and 30 min after ABA treatment (data not shown).

It is possible that the activity of PI3K and PI4K may not be changed by closing signals such as ABA, and the roles of their lipid products may be to prime guard cells for subsequent stimulation—for example, by controlling important signal transducers (Tsukazaki et al., 1998). Alternatively, changes in the kinase activities may depend on particular conditions in the membrane, which we were unable to simulate in our in vitro experiments. Regardless of any signal-dependent changes in PI kinase activity, basal levels of kinase activity probably always are present in these cells, and the lipid products of these kinases probably always are undergoing rapid turnover, because inhibitors of PI kinases increased stomatal apertures under all conditions tested, including darkness, light, and ABA treatment (Fig. B-1 and our unpublished results).

Therefore, how do PI3P and PI4P participate in stomatal movements? Oscillations in $[Ca^{2+}]_{\text{cyt}}$ have critical roles in stomatal movements (Allen et al., 1999, 2001), and phosphoinositide metabolism plays important roles in ABA-

induced $[Ca^{2+}]_{cyt}$ changes and stomatal closing (Gilroy et al., 1990; Staxén et al., 1999). Therefore, we studied the effects of WM or LY294002 on $[Ca^{2+}]_{cyt}$ changes induced by ABA using Arabidopsis guard cells expressing yellow cameleon 2.1 as a Ca^{2+} indicator (Allen et al., 1999). We were able to confirm the previously reported effects of ABA on $[Ca^{2+}]_{cyt}$ in control guard cells (Fig. B-8). The patterns of ABA-induced $[Ca^{2+}]_{cyt}$ responses included two or more transient increases, single transient increases, or no perceivable changes. In guard cells pretreated with WM or LY294002, $[Ca^{2+}]_{cyt}$ increases were reduced substantially compared with those in the control cells, suggesting that ABA-induced $[Ca^{2+}]_{cyt}$ signaling is disrupted, although not abolished entirely. These results suggest important functions for PI3P and/or PI4P in Ca^{2+} signaling in guard cells.

Because PI3K has been reported to activate ROS formation in platelets (Bae et al., 2000), PI3K in guard cells also may activate ROS formation, which in turn may activate plasma membrane Ca^{2+} channels (Pei et al., 2000). Recent studies have shown that fungal elicitors and ABA cause ROS production in guard cells and that ROS induce stomatal closing (Lee et al., 1999; Pei et al., 2000), suggesting a critical role for ROS in the mediation of stomatal closing.

WM or LY294002 increased stomatal apertures during opening as well as closing movements. Ca^{2+} acts as a negative regulator of stomatal opening (Schwartz, 1985); thus, if WM or LY294002 decreases $[Ca^{2+}]_{cyt}$, they can

reduce the negative effect of Ca^{2+} on stomatal opening and increase stomatal apertures. Guard cells commonly oscillate between two ranges of membrane voltages, one close to the K^+ equilibrium voltage and the other far negative of the K^+ equilibrium voltage, and hyperpolarized membrane potential induces Ca^{2+} influx (Hamilton et al., 2000). The inhibitors may have blocked Ca^{2+} influx during the hyperpolarization phase of the normal oscillations in membrane voltage, thereby increasing stomatal apertures under all conditions.

The evidence for a role of PI3P or PI4P in Ca^{2+} signaling is compelling. However, it does not exclude additional modes of action of these lipids in guard cells. PIP has been reported to be involved in endocytosis in yeast and mammalian cells (Li et al., 1995; Wurmser and Emr, 1998; Audhya et al., 2000). Vesicle trafficking, including endocytosis, has been suggested to be important for stomatal movements (Blatt, 2000; Kubitscheck et al., 2000). Therefore, the reduction of functional PIP by GFP-tagged proteins may have inhibited endocytosis during stomatal movements. Clearly, further investigation is required to fully reveal the mechanisms by which PI3P and PI4P function in stomatal movements.

In conclusion, we have presented evidence that both PI3P and PI4P in guard cells are involved in normal stomatal movements and that their mechanism of action involves the mediation of $[\text{Ca}^{2+}]_{\text{cyt}}$ increases in response to a closing stimulus. These phosphoinositides also may regulate diverse cellular processes, including signal transduction and vesicle trafficking in guard

cells. The results presented here demonstrate roles for PIP in guard cells and suggest that these plant lipids may be as versatile in their functions as those found in nonplant systems.

MATERIALS AND METHODS

Plant materials. Seeds of *Vicia faba* and *Arabidopsis thaliana* (ecotype Landsberg *erecta*) were planted in a vermiculite-humus soil mixture and fertilized with HYPONeX solution (1 g/L; Hyponex Corp., Marysville, OH). *Vicia* plants were grown in a greenhouse at $22 \pm 2^\circ\text{C}$ with light/dark cycles of 16/8 h. *Arabidopsis* plants (wild type for measurements of stomatal aperture and transgenic plants expressing yellow cameleon 2.1 for calcium imaging) were grown in a growth chamber at $20 \pm 2^\circ\text{C}$ with light/dark cycles of 16/8 h. Fully differentiated young leaves from 3- to 4-week-old plants were used.

Chemicals. Wortmannin (WM; 10 mM) and LY294002 (50 or 100 mM) stock solutions were prepared in 100% DMSO. Both chemicals were purchased from Sigma (St. Louis, MO).

Fluorescent gene constructs of lipid binding proteins. Four constructs were used in this study. To generate the chimeric fusion construct *GFP:EBD*, the endosome binding domain (EBD) encoding the C-terminal fragment of

human EEA1 (amino acid residues 1257 to 1411) was ligated in frame to the C terminus of the soluble modified green fluorescent protein (*smGFP*) coding region lacking the terminator codon. The *FYVEC1358S* mutant also was fused to *smGFP*, resulting in construct *GFP:EBDC1358S* (Kim et al., 2001).

Mouse FAPP1 cDNA (Dowler et al., 2000) corresponding to the pleckstrin homology (PH) domain was amplified by PCR from a cDNA library using two specific primers (5'-CTCGAGATGGAG-GGGGTTCTGTACAAG-3' and 5'-TCACGCTTTGGAGCTCCCAAG-GGC-3'). The PCR product was subcloned into pBluescript KS+ (Stratagene) and then ligated to the C terminus of the GFP coding region lacking the termination codon. The two mutations, K7E and R18A, were introduced into *FAPP1PH* using two sequential PCR amplifications and two sets of primers (R18A, 5'-CAGAACAACCA-TGCAGGCTGCCAACC-3' and 5'-GGTTGGCAGCCTGCATGGTTT-GTTCTG-3'; K7E, 5'-CTCGAGATGGAGGGGTTCTGTACGAGTGG-ACCAAC-3' and 5'-TCACGCTTTGGAGCTCCCAAGGGC-3'). The resulting *FAPP1PH*[K7E, R18A] construct was ligated to the C terminus of the GFP coding region lacking the termination codon. *GFP:PLC δ 1PH* was constructed according to the method described previously (Kost et al., 1999). All chimeric *GFP* fusion constructs were placed under the control of the 35S promoter in a pUC vector for overexpression in guard cells.

Biochemical assay of phosphatidylinositol and phosphatidylinositol monophosphate kinases from guard cells. The abaxial epidermis of *Vicia* leaves was peeled from 15 fully expanded leaves for each sample. The epidermal peels were collected in ice-cold 10 mM KCl and 10 mM Mes-KOH, pH 6.1, and blended in a Waring blender (7010) for 30 s at 18,000 rpm to remove epidermal and mesophyll cells. After this step, only guard cells remained viable (data not shown) (Fukuda et al., 1998). They were washed and collected on a 220- μ m nylon mesh. The prepared epidermal samples were homogenized in liquid N₂ using a mortar and pestle and extracted with buffer (50 mM HEPES-KOH, pH 7.4, 5 mM MgCl₂, 1 mM EDTA, 10 mM DTT, 1 mM 2-mercaptoethanol, 0.7 μ g/mL pepstatin A, 5 μ g/mL aprotinin, 20 μ g/mL leupeptin, and 0.5 mM phenylmethylsulfonyl fluoride). In several experiments, the samples were ground at 4°C for 5 min in the buffer. The homogenate then was centrifuged at 10,000g for 5 min at 4°C. The resulting supernatant was further centrifuged at 100,000g for 1 h at 4°C for separation of the membrane and soluble fractions. Protein was quantified using the Bio-Rad protein assay kit with BSA as a standard, and the same amount of protein was used for all samples in the same experiment.

The phosphatidylinositol (PI) and PI monophosphate (PIP) kinase assay mixture contained 50 mM HEPES-KOH, pH 7.4, 5 mM MgCl₂, 10 mM DTT, 4 to 10 μ g of protein extracts from guard cell-enriched epidermal samples, and 20 to 100 μ M ATP in a total volume of 50 μ L. The reaction was started by adding

10 µg of PI or PI 4-phosphate (Sigma) and 10 µCi of γ -³²P-ATP (Amersham), left at room temperature for 10 to 30 min, and then stopped by the addition of 100 µL of 1 M HCl. For extraction of lipids, 200 µL of chloroform:methanol (1:1, v/v) was added to the sample and vortexed for 20 s. Phase separation was facilitated by centrifugation at 5000 rpm for 2 min in a tabletop centrifuge. The upper phase was removed, and the lower chloroform phase was washed once more with clear upper phase. The washed chloroform phase was dried under a stream of nitrogen gas and redissolved in 30 µL of chloroform. The labeled PI phosphates then were spotted onto *trans*-1,2-diaminocyclohexane-*N,N,N',N'*-tetraacetic acid–treated silica gel 60 thin layer chromatography (TLC) plates (Merck) and separated with a borate buffer system (Walsh et al., 1991). The plates were autoradiographed or quantified using a phosphorimager (FLA-2000R). Yeast wild-type SEY6210 and the *VPS34* deletion mutant PHY102 (SEY6210 *Vps34*Δ1::TRP1) (Stack et al., 1993), kindly provided by S.D. Emr (University of California, San Diego), were used as references for the identification of PI 3-phosphate and PI 4-phosphate bands on TLC plates. To help in the identification of phosphatidic acid, PI 4-phosphate, and PI 4,5-bisphosphate bands, cold phospholipid standards were run in different lanes of the same TLC plate and were visualized by spraying the plate with 1.3% molybdenum oxide in 4.2 M sulfuric acid (Sigma).

Measurements of the stomatal aperture. Fully expanded leaves from 3- to 4-week-old *Vicia* were excised, and epidermal pieces were peeled from the abaxial surface. The epidermal peels were blended in a Waring blender (see above), washed, and collected on a 220- μm nylon mesh. To test the effects of WM and LY294002 on stomatal openings, epidermal fragments were floated on 10 mM KCl and 10 mM Mes-KOH buffer, pH 6.1, with or without added chemicals under darkness or white light ($0.2 \text{ mmol}\cdot\text{m}^{-2}\cdot\text{s}^{-1}$) at 25°C for 3 h beginning at h 3 or 4 of the usual photoperiod. Apertures were measured. For the assay of stomatal closing induced by abscisic acid (ABA), epidermal fragments were exposed to white light ($0.2 \text{ mmol}\cdot\text{m}^{-2}\cdot\text{s}^{-1}$) for 3 h in 30 mM KCl and 10 mM Mes-KOH, pH 6.1. To close the stomata, the epidermis was transferred to 10 mM KCl and 10 mM Mes-KOH, pH 6.1, preincubated for 30 min with or without added chemicals, and treated with $50 \mu\text{M}$ [\pm]-*cis,trans*-ABA for 1 h. Stomatal apertures then were measured using an eyepiece micrometer.

For measurements of stomatal apertures in biolistically transformed leaves, bombarded leaf fragments were floated on the same buffer used above. After stomatal opening or closing, abaxial epidermal pieces were peeled, and each half of the stomatal apertures, bordered by transformed guard cells, and their untransformed neighbors were measured with a fluorescence microscope.

For stomatal closing experiments in *Arabidopsis*, fully expanded leaves were floated on 10 mM KCl and 10 mM Mes-KOH buffer, pH 6.1, under white light ($0.2 \text{ mmol}\cdot\text{m}^{-2}\cdot\text{s}^{-1}$) for 3 h. The inhibitors were added to the medium at 30 min before ABA treatment in closing buffers. The closing buffer for WM experiments contained 10 mM Mes-Tris, pH 6.15, 2 mM KCl, and 200 μM CaCl_2 ; for LY294002 experiments, the closing buffer contained 10 mM Mes-Tris, pH 6.15, 5 mM KCl, and 50 μM CaCl_2 . One hour after the onset of ABA treatment, epidermal pieces were peeled from the abaxial surface, and stomatal apertures were measured using an eyepiece micrometer.

Biolistic gene bombardment into *Vicia* guard cells. Biolistic bombardment of guard cells with fluorescent gene constructs was performed as described previously (Marc et al., 1999) with minor modifications to facilitate gene expression in guard cells. In brief, 2.5 μg of plasmid DNA was mixed with 0.5 mg of 1.0- μm gold particles (Bio-Rad) in a 50- μL aqueous solution. The gold-DNA suspension was dispersed with moderate vortexing and sonication in the presence of 1.25 M CaCl_2 and 17 mM spermidine and kept at room temperature for 5 min. The DNA-coated gold particles then were collected by brief centrifugation, washed, resuspended in ethanol, and spread onto plastic carrier discs for biolistic transformation (Particle Delivery System-1000/He; Bio-Rad). Young leaves (4.5 to 6 cm long) of *Vicia* were excised from 3- to 4-week-old plants and placed with their lower side up onto moist filter paper in

60-mm plastic Petri dishes. The dishes were inserted into the firing chamber, the vacuum was pumped to 27 inches of Hg, and the DNA-coated gold particles were fired into the leaves from a distance of 60 mm at a helium pressure of 1350 p.s.i. Bombarded leaves then were placed onto a humid Petri dish and kept in the dark at room temperature. Within 24 to 84 h, epidermal peels were taken from the bombarded leaves, and transformed guard cells were observed with an Axioskop 2 fluorescence microscope (Carl Zeiss, Jena, Germany).

Protoplast transformation and protein gel blot analysis. For transient expression of GFP:FAPP1PH and GFP:FAPP1PH[K7E, R18A], Arabidopsis mesophyll cell protoplasts were isolated from seedlings grown in a greenhouse. Plasmids were introduced into 300 μ L of protoplast suspension (5×10^6 /mL) by polyethylene glycol-mediated transformation (Jin et al., 2001). Expression of constructs was monitored using a Zeiss Axioplan fluorescence microscope. To obtain whole cell extracts, protoplasts were harvested 17 h after transformation by centrifugation at 50g for 5 min and resuspended in 200 μ L of 50 mM Hepes buffer, pH 7.5, containing 0.1 M NaCl, 2 mM EDTA, 2 mM 2-mercaptoethanol, and 1 mM phenylmethylsulfonyl fluoride. Protoplasts were lysed by sonication and clarified by a brief centrifugation at 5000g. The whole cell extracts were fractionated into soluble and membrane fractions by ultracentrifugation at 100,000g for 1 h. The pellet was resuspended in an

original volume of Hepes buffer. These fractions were probed for the presence of GFP:FAPP1PH and GFP:FAPP1PH[K7E, R18A] by protein gel blot analysis using a monoclonal anti-GFP antibody (Clontech, Palo Alto, CA).

Phospholipid binding assay. To prepare recombinant GFP:FAPP1PH and GFP:FAPP1PH[K7E, R18A] proteins, DNA fragments encoding GFP:FAPP1PH and GFP:FAPP1PH[K7E, R18A] were subcloned into a pRSET-A expression vector (Invitrogen, Carlsbad, CA). The constructs were introduced into BL21 (DE3)LysS, and expression was induced by 0.1 mM isopropylthio- β -galactoside for 2 h. His-tagged GFP:FAPP1PH and GFP:FAPP1PH[K7E, R18A] proteins were purified using a nickel-nitrilotriacetic acid agarose affinity column according to the manufacturer's instructions (Invitrogen). To assess the phosphoinositide binding properties of GFP:FAPP1PH and GFP:FAPP1PH[K7E, R18A], a lipid binding assay was performed by fat-protein gel blot analysis (Dowler et al., 2000). Briefly, 0.5 and 1.5 μ g of phospholipids dissolved in chloroform were spotted onto a nitrocellulose membrane (NitroBind; Micron Separations, Westborough, MA) and allowed to dry at room temperature. The membrane was blocked with 1.5% (w/v) fatty acid-free BSA in TBST (20 mM Tris-HCl, pH 7.5, 150 mM NaCl, and 0.1% [v/v] Tween 20) for 1 h. The membrane was incubated for 12 h at 4°C with gentle stirring in the same solution containing 0.5 μ g/mL affinity-purified GFP:FAPP1PH and GFP:FAPP1PH[K7E, R18A]. After washing three

times with TBST, the blot was incubated with a monoclonal anti-His antibody (Qiagen, Valencia, CA) for 1 h and then washed again with TBST three times. An anti-mouse IgG antibody conjugated with horseradish peroxidase was used as the secondary antibody. Binding of proteins to phospholipids was detected with the enhanced chemiluminescence detection system (Amersham).

Imaging of cytosolic calcium concentration in intact guard cells of

Arabidopsis. Experimental procedures for epidermal strip preparation and fluorescence ratio measurements were performed essentially as described by Allen et al. (1999, 2001) with a minor modification. In brief, rosette leaves of *Arabidopsis* (ecotype Landsberg *erecta*) expressing p35S–yellow cameleon 2.1–BAR were mounted onto a glass cover slip that had been coated with medical adhesive (Hollister Inc., Libertyville, IL). Then the adaxial surface of leaves was removed with a razor blade, and the remaining abaxial epidermis was incubated immediately in a small Petri dish containing a bathing medium (for WM experiments, 10 mM Mes-Tris, pH 6.15, 2 mM KCl, and 200 μ M CaCl₂; for LY294002 experiments, 10 mM Mes-Tris, pH 6.15, 5 mM KCl, and 50 μ M CaCl₂). To open the stomates, the Petri dish was illuminated for 2 h (120 μ mol·m⁻²·s⁻¹) before fluorescence ratio measurements. DMSO, WM, or LY294002 was added to the solution at 30 min before measurements were taken. [\pm]-*cis,trans*-ABA (5 or 50 μ M) was added by perfusion at 5 to 10 min after fluorescence measurements began. Ca²⁺ transient increases were

counted when cytosolic calcium concentration ratio change was > 0.1 unit above the baseline and distinguishable from the background.

Upon request, all novel materials described in this article will be made available in a timely manner for noncommercial research purposes. No restrictions or conditions will be placed on the use of any materials described in this article that would limit their use for noncommercial research purposes.

ACKNOWLEDGEMENTS

We thank S.D. Emr for yeast strains and B. Drøbak and S. Lee for providing protocols for the PI kinase assay. We also thank Myungki Min for performing the fat-protein gel blot experiment. This research was supported by the Crop Functional Genomics Center of Korea (Grant CG1-1-15) and the Pohang University of Science and Technology Basic Science Research Institute research fund awarded to Y.L. and in part by National Science Foundation Grant MCB 0077791 (to J.I.S.). J.M.K. was supported by a fellowship from the Human Frontier Science Program Organization. This work also was supported in part by a grant from the National Creative Research Initiatives program of the Ministry of Science and Technology (Korea) to I.H.

REFERENCES CITED

Allen, G.J., Chu, S.P., Harrington, C.L., Schumacher, K., Hoffmann, T., Tang, Y.Y., Grill, E., and Schroeder, J.I. (2001). A defined range of guard cell calcium oscillation parameters encodes stomatal movements. *Nature* 411, 1053–1057.

Allen, G.J., Kwak, J.M., Chu, S.P., Llopis, J., Tsien, R.Y., Harper, J.F., and Schroeder, J.I. (1999). Cameleon calcium indicator reports cytoplasmic calcium dynamics in *Arabidopsis* guard cells. *Plant J.* 19, 735–747.

Assmann, S.M., and Shimazaki, K. (1999). The multisensory guard cell: Stomatal responses to blue light and abscisic acid. *Plant Physiol.* 119, 809–816.

Audhya, A., Foti, M., and Emr, S.D. (2000). Distinct roles for the yeast phosphatidylinositol 4-kinases, Stt4p and Pik1p, in secretion, cell growth, and organelle membrane dynamics. *Mol. Biol. Cell* 11, 2673–2689.

Bae, Y.S., Sung, J.Y., Kim, O.S., Kim, Y.J., Hur, K.C., Kazlauskas, A., and Rhee, S.G. (2000). Platelet-derived growth factor-induced H₂O₂ production requires the activation of phosphatidylinositol 3-kinase. *J. Biol. Chem.* 275, 10527–10531.

Balla, T. (1998). Phosphatidylinositol 4-kinases. *Biochim. Biophys. Acta* 1436, 69–85.

Blatt, M.R. (2000). Ca²⁺ signalling and control of guard-cell volume in stomatal movements. *Curr. Opin. Plant Biol.* 3, 196–204.

Bunney, T.D., Watkins, P.A., Beven, A.F., Shaw, P.J., Hernandez, L.E., Lomonosoff, G.P., Shanks, M., Peart, J., and Drøbak, B.K. (2000). Association of phosphatidylinositol 3-kinase with nuclear transcription sites in higher plants. *Plant Cell* 12, 1679–1688.

Dowler, S., Currie, R.A., Campbell, D.G., Deak, M., Kular, G., Downes, C.P., and Alessi, D.R. (2000). Identification of pleckstrin-homology-domain-containing proteins with novel phosphoinositide-binding specificities. *Biochem. J.* 351, 19–31.

Drøbak, B.K., Dewey, R.E., and Boss, W.F. (1999). Phosphoinositide kinases and the synthesis of polyphosphoinositides in higher plant cells. *Int. Rev. Cytol.* 189, 95–130.

Fukuda, M., Hasezawa, S., Asai, N., Nakajima, N., and Kondo, N. (1998). Dynamic organization of microtubules in guard cells of *Vicia faba* L. with diurnal cycle. *Plant Cell Physiol.* 39, 80–86.

Gillooly, D.J., Morrow, I.C., Lindsay, M., Gould, R., Bryant, N.J., Gaullier, J.M., Parton, R.G., and Stenmark, H. (2000). Localization of phosphatidylinositol 3-phosphate in yeast and mammalian cells. *EMBO J.* 19, 4577–4588.

Gilroy, S., Read, N.D., and Trewavas, A.J. (1990). Elevation of cytoplasmic calcium by caged calcium or caged inositol trisphosphate initiates stomatal closure. *Nature* 346, 769–771.

Hamilton, D.W., Hills, A., Kohler, B., and Blatt, M.R. (2000). Ca^{2+} channels at the plasma membrane of stomatal guard cells are activated by hyperpolarization and abscisic acid. *Proc. Natl. Acad. Sci. USA* 97, 4967–4972.

Hinchliffe, K.A., Ciruela, A., and Irvine, R.F. (1998). PIPkins1, their substrates and their products: New functions for old enzymes. *Biochim. Biophys. Acta* 1436, 87–104.

Hirose, K., Kadowaki, S., Tanabe, M., Takeshima, H., and Iino, M. (1999). Spatiotemporal dynamics of inositol 1,4,5-trisphosphate that underlies complex Ca^{2+} mobilization patterns. *Science* 284, 1527–1530.

Hong, Z., and Verma, D.P.S. (1994). A phosphatidylinositol 3-kinase is induced during soybean nodule organogenesis and is associated with membrane proliferation. *Proc. Natl. Acad. Sci. USA* 91, 9617–9621.

Hwang, J.U., Eun, S.O., and Lee, Y. (2000). Structure and function of actin filaments in mature guard cells. In *Actin: A Dynamic Framework for Multiple Plant Cell Functions*, C.J. Staiger, F. Baluska, D. Volkmann, and P.W. Barlow, eds (Dordrecht, The Netherlands: Kluwer Academic Publishers), pp. 427–436.

Jin, J.B., Kim, Y.A., Kim, S.J., Lee, S.H., Kim, D.H., Cheong, G.W., and Hwang, I.H. (2001). A new dynamin-like protein, ADL6, is involved in trafficking from the *trans*-Golgi network to the central vacuole in Arabidopsis. *Plant Cell* 13, 1511–1526.

Kim, D.H., Eu, Y.J., Yoo, C.M., Kim, Y.W., Pih, K.T., Jin, J.B., Kim, S.J., Stenmark, H., and Hwang, I.H. (2001). Trafficking of phosphatidylinositol 3-phosphate from the *trans*-Golgi network to the lumen of the central vacuole in plant cells. *Plant Cell* 13, 287–301.

Kost, B., Lemichez, E., Spielhofer, P., Hong, Y., Tolias, K., Carpenter, C., and Chua, N.H. (1999). Rac homologues and compartmentalized phosphatidylinositol 4,5-bisphosphate act in a common pathway to regulate polar pollen tube growth. *J. Cell Biol.* 145, 317–330.

Kubitscheck, U., Homann, U., and Thiel, G. (2000). Osmotically-evoked shrinking of guard cell protoplasts causes retrieval of plasma membrane into the cytoplasm. *Planta* 210, 423–431.

Lee, S., Choi, H., Suh, S., Doo, I.S., Oh, K.Y., Choi, E.J., Taylor, A.T.S., Low, P.S., and Lee, Y. (1999). Oligogalacturonic acid and chitosan reduce stomatal aperture by inducing the evolution of reactive oxygen species from guard cells of tomato and *Commelina communis*. *Plant Physiol.* 121, 147–152.

Lee, Y.S., Choi, Y.B., Suh, S., Lee, J., Assmann, S.M., Joe, C.O., Kelleher, J.F., and Crain, R.C. (1996). Abscisic acid-induced phosphoinositide turnover in guard-cell protoplasts of *Vicia faba*. *Plant Physiol.* 110, 987–996.

Li, G., D'Souza-Schorey, C., Barbieri, M.A., Roberts, R.L., Klippel, A., Williams, L.T., and Stahl, P.D. (1995). Evidence for phosphatidylinositol 3-kinase as a regulator of endocytosis via activation of Rab5. *Proc. Natl. Acad. Sci. USA* 92, 10207–10211.

Marc, J., Granger, C.L., Brincat, J., Fisher, D.D., Kao, T., McCubbin, A.G., and Cyr, R.J. (1999). A GFP-MAP4 reporter gene for visualizing cortical microtubule rearrangements in living epidermal cells. *Plant Cell* 10, 1927–1940.

Matsuoka, K., Bassham, D.C., Raikhel, N.V., and Nakamura, K. (1995). Different sensitivity to wortmannin of two vacuolar sorting signals indicates the presence of distinct sorting machineries in tobacco cells. *J. Cell Biol.* 130, 1307–1318.

Monks, D.E., Aghoram, K., Courtney, P.D., DeWald, D.B., and Dewey, R.E. (2001). Hyperosmotic stress induces the rapid phosphorylation of a soybean phosphatidylinositol transfer protein homolog through activation of the protein kinases SPK1 and SPK2. *Plant Cell* 13, 1205–1219.

Munnik, T., Irvine, R.F., and Musgrave, A. (1998). Phospholipid signalling in plants. *Biochim. Biophys. Acta* 1389, 222–272.

Parmar, P.N., and Brearley, C.A. (1993). Identification of 3-phosphorylated and 4-phosphorylated phosphoinositides and inositol phosphates in stomatal guard cells. *Plant J.* 4, 255–263.

Parmar, P.N., and Brearley, C.A. (1995). Metabolism of 3-phosphorylated and 4-phosphorylated phosphatidylinositols in stomatal guard cells of *Commelina communis* L. *Plant J.* 8, 425–433.

Payrastre, B., Nievers, M., Boonstra, J., Breton, M., Verkleij, A.J., and Van Bergen en Henegouwen, P.M. (1992). A differential location of

phosphoinositide kinases, diacylglycerol kinase, and phospholipase C in the nuclear matrix. *J. Biol. Chem.* 267, 5078–5084.

Pei, Z.M., Murata, Y., Benning, G., Thomine, S., Klusener, B., Allen, G.J., Grill, E., and Schroeder, J.I. (2000). Calcium channels activated by hydrogen peroxide mediate abscisic acid signalling in guard cells. *Nature* 406, 731–734.

Rameh, L.E., and Cantley, L.C. (1999). The role of phosphoinositide 3-kinase lipid products in cell function. *J. Biol. Chem.* 274, 8347–8350.

Roth, M.G. (1999). Lipid regulators of membrane traffic through the Golgi complex. *Trends Cell Biol.* 9, 174–179.

Schroeder, J.I., Kwak, J.M., and Allen, G.J. (2001). Guard cell abscisic acid signalling and engineering drought hardiness in plants. *Nature* 410, 327–330.

Schwartz, A. (1985). Role of Ca^{2+} and EGTA on stomatal movements in epidermal peels of *Commelina communis* L. *Plant Physiol.* 79, 1003–1005.

Stack, J.H., Herman, P.K., Schu, P.V., and Emr, S.D. (1993). A membrane-associated complex containing the Vps15 protein kinase and the Vps34 PI 3-kinase is essential for protein sorting to the yeast lysosome-like vacuole. *EMBO J.* 12, 2195–2204.

Stauffer, T.P., Ahn, S., and Meyer, T. (1998). Receptor-induced transient reduction in plasma membrane PtdIns(4,5)P₂ concentration monitored in living cells. *Curr. Biol.* 8, 343–346.

Staxén, I., Pical, C., Montgomery, L.T., Gray, J.E., Hetherington, A.M., and McAinsh, M.R. (1999). Abscisic acid induces oscillations in guard-cell cytosolic free calcium that involve phosphoinositide-specific phospholipase C. *Proc. Natl. Acad. Sci. USA* 96, 1779–1784.

Stevenson, J.M., Perera, I.Y., Heilmann, I., Persson, S., and Boss, W.F. (2000). Inositol signaling and plant growth. *Trends Plant Sci.* 5, 252–258.

Tsukazaki, T., Chiang, T.A., Davison, A.F., Attisano, L., and Wrana, J.L. (1998). SARA, a FYVE domain protein that recruits Smad2 to the TGF β receptor. *Cell* 95, 779–791.

Vanhaesebroeck, B., Leever, S.J., Ahmadi, K., Timms, J., Katso, R., Driscoll, P.C., Woscholski, R., Parker, P.J., and Waterfield, M.D. (2001). Synthesis and function of 3-phosphorylated inositol lipids. *Annu. Rev. Biochem.* 70, 535–602.

Walsh, J.P., Caldwell, K.K., and Majerus, P.W. (1991). Formation of phosphatidylinositol 3-phosphate by isomerization from phosphatidylinositol 4-phosphate. *Proc. Natl. Acad. Sci. USA* 88, 9184–9187.

Welters, P., Takegawa, K., Emr, S.D., and Chrispeels, M.J. (1994). AtVPS34, a phosphatidylinositol 3-kinase of *Arabidopsis thaliana*, is an essential protein with homology to a calcium-dependent lipid binding domain. *Proc. Natl. Acad. Sci. USA* 91, 11398–11402.

Wurmser, A.E., and Emr, S.D. (1998). Phosphoinositide signaling and turnover: PtdIns(3)P, a regulator of membrane traffic, is transported to the vacuole and degraded by a process that requires luminal vacuolar hydrolase activities. *EMBO J.* 17, 4930–4942.

Xue, H.W., Pical, C., Brearley, C., Elge, S., and Muller-Rober, B. (1999). A plant 126-kDa phosphatidylinositol 4-kinase with a novel repeat structure: Cloning and functional expression in baculovirus-infected insect cells. *J. Biol. Chem.* 274, 5738–5745.

The text of this section, in full, is a reprint of the material as it appears in *The Plant Cell*, Jung, J.-Y., Kim, Y.-W., Kwak, J.M., Hwang, J.-U., Young, J., Schroeder, J.I., Hwang, I., and Lee, Y. (2002). I generated some of the data for Fig. B-8.

APPENDIX C

Localization, Ion Channel Regulation, and Genetic Interactions during Abscisic

Acid Signaling of the Nuclear mRNA Cap-Binding Protein, ABH1

ABSTRACT

Abscisic acid (ABA) regulates developmental processes and abiotic stress responses in plants. We recently characterized a new Arabidopsis mutant, *abh1*, which shows ABA-hypersensitive regulation of seed germination, stomatal closing, and cytosolic calcium increases in guard cells (V. Hugouvieux, J.M. Kwak, J.I. Schroeder [2001] Cell 106: 477-487). *ABH1* encodes the large subunit of a dimeric Arabidopsis mRNA cap-binding complex and in expression profiling experiments was shown to affect mRNA levels of a subset of genes. Here, we show that the dimeric ABH1 and AtCBP20 subunits are ubiquitously expressed. Whole-plant growth phenotypes of *abh1* are described and properties of ABH1 in guard cells are further analyzed. Complemented *abh1* lines expressing a green fluorescent protein-ABH1 fusion protein demonstrate that ABH1 mainly localizes in guard cell nuclei. Stomatal apertures were smaller in *abh1* compared with wild type (WT) when plants were grown at 40% humidity, and similar at 95% humidity. Correlated with stomatal apertures from plants grown at 40% humidity, slow anion channel currents were enhanced and inward potassium channel currents were decreased in *abh1* guard cells compared with WT. Gas exchange measurements showed similar primary humidity responses in *abh1* and WT, which together with results from *abh1/abi1-1* double-mutant

analyses suggest that *abh1* shows enhanced sensitivity to endogenous ABA. Double-mutant analyses of the ABA-hypersensitive signaling mutants, *era1-2* and *abh1*, showed complex genetic interactions, suggesting that ABH1 and ERA1 do not modulate the same negative regulator in ABA signaling. Mutations in the RNA-binding protein *sad1* showed hypersensitive ABA-induced stomatal closing, whereas *hyl1* did not affect this response. These data provide evidence for the model that the mRNA-processing proteins ABH1 and SAD1 function as negative regulators in guard cell ABA signaling.

INTRODUCTION

The plant hormone abscisic acid (ABA) controls several physiologically important stress and developmental responses throughout the life cycle of plants. During seed development, ABA triggers the acquisition of nutritive reserves, desiccation tolerance, maturation, and dormancy (Marcotte et al., 1992; Koornneef et al., 1998; Finkelstein et al., 2002). Later, during vegetative growth, ABA is the internal signal that enables plant adaptive responses to adverse environmental conditions such as drought, salt, and cold stresses (Marcotte et al., 1992; Koornneef et al., 1998; Leung and Giraudat, 1998).

In response to drought, ABA is synthesized and induces closure of stomatal pores, located on the leaf surface, to limit water loss by transpiration.

Stomatal pores are surrounded by pairs of guard cells whose turgor regulates stomatal pore apertures. ABA induces stomatal closure via efflux of K^+ and anions from guard cells and removal of organic osmolytes (MacRobbie, 1998; Schroeder et al., 2001). Ion channel-mediated efflux of anions and K^+ and stomatal closure are controlled by ABA-induced cytosolic calcium ($[Ca^{2+}]_{cyt}$) increases (Schroeder and Hagiwara, 1989; McAinsh et al., 1990; MacRobbie, 1998).

An increasing number of genetic mutations that contribute to ABA signaling in guard cells have been characterized recently. These genes include two type 2C protein phosphatases, *abi1-1* and *abi2-1* (Leung et al., 1994, 1997; Meyer et al., 1994), a farnesyl transferase β -subunit, *ERA1* (Cutler et al., 1996; Pei et al., 1998), an ABA-activated protein kinase mutant (*aapk*; Li et al., 2000), a GTP-binding protein α -subunit, *GPA1* (Wang et al., 2001), dominant mutations in a GTPase protein, *Atrac1-1* (Lemichez et al., 2001), and an mRNA cap-binding protein, *ABH1* (Hugouvieux et al., 2001). Genes that affect ABA responses at the transcriptional level in seed germination and development have also been identified encoding three transcriptional regulators, *ABI3* (Giraudat et al., 1992), *ABI4* (Finkelstein et al., 1998), and *ABI5* (Finkelstein and Lynch, 2000). Two RNA-binding proteins, a double-stranded RNA-binding protein, HYL1 (Lu and Fedoroff, 2000), and a protein similar to an Sm-like snRNP protein, SAD1 (Xiong et al., 2001a) were recently described to affect ABA regulation of seed germination. The *sad1*

mutation also caused enhanced ABA-induced expression of marker genes, but is drought hypersensitive (Xiong et al., 2001a). The *fry1* mutant shows a superinduction of ABA- and stress-responsive genes and revealed the involvement of an inositol polyphosphate 1-phosphatase in ABA signaling (Xiong et al., 2001b).

We recently characterized the *abh1* mutation (Hugouvieux et al., 2001) that points to a link between mRNA metabolism and ABA signaling. *ABH1* encodes a homolog to yeast (*Saccharomyces cerevisiae*) and human (*Homo sapiens*) *CBP80* genes and functions as the large subunit of an Arabidopsis mRNA cap-binding complex (CBC). No other *ABH1* homologs are present in the Arabidopsis genome. Disruption of *ABH1* results in ABA-hypersensitive regulation of seed germination, ABA-hypersensitive stomatal closing, reduced wilting during drought, and, interestingly, ABA-hypersensitive $[Ca^{2+}]_{cyt}$ increases in guard cells, demonstrating amplification of early ABA signaling mechanisms (Hugouvieux et al., 2001). In yeast and mammals, CBC is involved in mRNA metabolism (Lewis and Izaurralde, 1997). DNA microarray experiments comparing the level of expression of genes in wild type (WT) and *abh1* showed that a limited number of genes in *abh1* are down-regulated, some of which may correspond to negative regulators of ABA signaling in guard cells. The recent isolation of three recessive ABA-hypersensitive mutants, *abh1*, *hyl1*, and *sad1*, which all encode RNA-associated proteins,

gives rise to a new model by which RNA processing modulates and/or participates in ABA signal transduction.

To better understand ABH1 functions in plants, in the present work we characterize the pattern of *ABH1* gene expression and associated whole-plant growth phenotypes of *abh1*. We also analyze ABH1 protein localization in guard cells and genetic interactions between ABH1 and the early ABA signaling components *abi1-1* and ERA1 during stomatal regulation. In addition, we further characterize stomatal responses of *abh1*, *sad1*, and *hyl1* which show differential effects on ABA-induced stomatal closing in *hyl1* compared with *abh1* and *sad1*. Responses in *sad1* strengthen the hypothesis that RNA processing contributes to ABA signal transduction in guard cells.

RESULTS

***ABH1* expression is ubiquitous.** *ABH1* was shown to be expressed in guard cells (Hugouvieux et al., 2001). Northern-blot analyses were performed on poly(A⁺) RNA extracted from WT roots, leaves, flowers, and stems to analyze *ABH1* gene expression in various organs. As shown in Figure C-1, *ABH1* transcript was present in all tissues analyzed, with high expression in flowers. The *AtCBP20* gene encodes the small subunit of the CBC and is required for in vitro binding of ABH1 to the 7-methyl guanosine cap structure of mRNA

(Hugouvieux et al., 2001). *AtCBP20* showed the same expression pattern as *ABH1* (Fig. C-1).

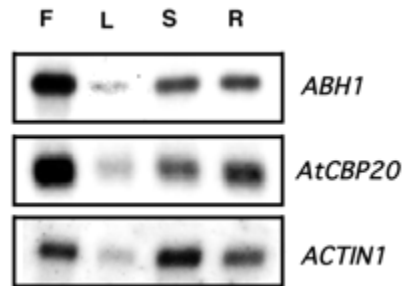


Figure C-1: Expression level of the CBC subunits, *ABH1* and *AtCBP20*, is ubiquitous. Northern-blot analyses were performed on approximately 2 μ g of poly(A⁺) RNA (extracted from flowers [F], stems [S], leaves [L], and roots [R]) in WT Arabidopsis. *ABH1* or *AtCBP20* cDNAs were used as probes. *Actin1* probe was used as a loading control.

WT transgenic seedlings expressing the β -glucuronidase (GUS) reporter gene under the control of the *ABH1* promoter (genomic sequence containing 1.2 kb from the 5' end of the *ABH1* start site; Hugouvieux et al., 2001) were used to further analyze in which tissues the *ABH1* promoter was active. As expected, GUS activity was detected in roots and hypocotyls (Fig. C-2A), cotyledons (Fig. C-2B), and leaves (Fig. C-2C). GUS activity was not detected in root or apical meristems (data not shown). The *ABH1* promoter was highly active in vascular tissues (hypocotyls, roots, cotyledons, and leaves; Fig. C-2, A-C). *ABH1* expression was also observed in the vascular tissues of petals (data not shown). In 2-d-old seedlings, GUS activity was often first visually detectable in the hypocotyl (Fig. C-2E); however, this restricted expression pattern disappeared in 8-d-old seedlings, suggesting a

developmental control of *ABH1* expression. The *ABH1* promoter was active in guard cells (Fig. C-2D; Hugouvieux et al., 2001). The same patterns of expression were observed in three independent homozygous lines.

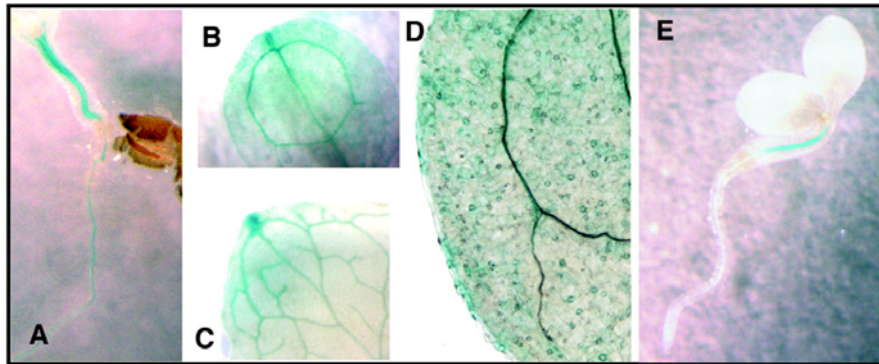


Figure C-2: Analysis of GUS activity in WT plants transformed with the GUS reporter gene under the control of the *ABH1* promoter. A through E, GUS activity in the hypocotyl and root of an 8-d old seedling (A), a cotyledon of an 8-d old seedling (B), a mature leaf (C), guard cells (D), and the hypocotyl of 2-d-old seedling (E).

ABA Treatment Does Not Change *ABH1* Transcript Level. *ABH1* is a negative regulator of ABA signaling (Hugouvieux et al., 2001). We further investigated whether ABA treatment induces changes in the *ABH1* transcript level. As shown in Figure C-3, treatment of WT leaves with 100 μ M ABA for 4 h did not change *ABH1* transcript levels (Fig. C-3; $n = 2$ experiments). In control experiments, the transcript level of ABA-inducible genes was increased in WT plants, including *COR47* (Fig. C-3), *RAB18*, *ABI1*, and *ABI2* (data not shown). Treatments with lower concentrations of ABA (0.1, 1, and 10 μ M) were also performed and again showed no ABA regulation of *ABH1* at the transcript

level. The lack of ABA regulation of *ABH1* mRNA levels was also observed after drought treatment (data not shown). As positive controls, under drought conditions, induction of the drought-induced gene, *COR47*, was observed (data not shown).

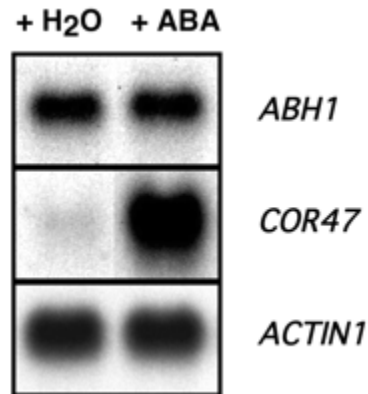


Figure C-3: *ABH1* expression level is not regulated by ABA. WT leaves from five individual plants were sprayed with 100 μ M ABA or water in parallel control experiments. Four hours later, poly(A⁺) RNA was extracted and 2 μ g was used in northern-blot analyses using *ABH1* cDNA and the *COR47* genomic fragment as a probe. *Actin1* probe was used as a loading control. Similar results were obtained in two replicates, and in the WT ecotype Wassilewskija (data not shown).

Growth and Developmental Phenotypes of *abh1*. Considering the expression pattern of the *ABH1* gene in vegetative tissues (Figs. 1 and 2), several morphological and growth characteristics of *abh1* and WT plants were analyzed. *abh1* plants showed a slightly serrated leaf phenotype (Fig. C-4, top left) that is complemented in *abh1* plants expressing the WT copy of the *ABH1* gene (Fig. C-4, lower right). Interestingly, this leaf phenotype was also observed in homozygous *abh1/era1-2* and *abh1/abi1-1* double mutants, which

were indistinguishable from the *abh1* mutant in leaf morphology (data not shown).

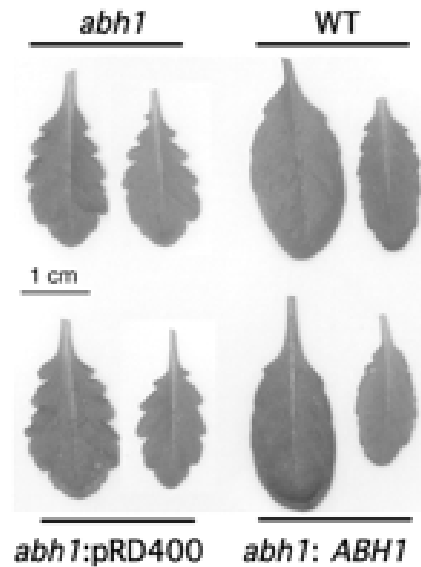


Figure C-4: *abh1* plants show a serrated leaf phenotype that is complemented by the *ABH1* gene. Two rosette leaves of each plant are shown after 7 weeks of growth. *abh1* lines complemented with the *ABH1* promoter and gene (*abh1:ABH1*) were generated as described (Hugouvieux et al., 2001). *abh1* lines transformed with the vector control pRD400 only (*abh1:pDR400*) were used as controls.

After exposure of seeds to 4°C for 4 d, 6-month-old *abh1* and WT seeds germinated at the same rate in the absence of exogenous ABA (Hugouvieux et al., 2001). Under these conditions, *abh1* plants were smaller than WT after 3 weeks of growth (Fig. C-5A) and showed a delay in bolting and flowering time after 6 weeks (Fig. C-5B). However, *abh1* and WT appeared very similar at maturity (Fig. C-5C). An approximately 5- to 10-d delay was observed in flowering of *abh1* plants compared with WT. This delay

varied among plants showing slightly different genetic penetrance among individual plants. The same number of leaves (between eight and 10) was observed in *abh1* and WT plants when they started bolting, suggesting that *abh1* growth is slowed compared with WT and that *abh1* is not a late-flowering mutant that shows an increased leaf number when flowering. To further investigate whether *abh1* growth was slower compared with WT, we followed the shoot and the main root's development in *abh1* and WT seedlings grown in petri dishes. As shown in Figure C-5D, the appearance and development of the first two leaves were delayed in *abh1* compared with WT after 6 and 9 d of growth. Root length was slightly decreased in *abh1* compared with WT after 11 d of growth, although root length was similar after 2 d in both WT and *abh1* (Fig. C-5E). These data suggested that *abh1* growth is delayed compared with WT. Morphological characteristics of *abh1* and WT plants were further analyzed and compared at maturity. As summarized in Table C-I, the only significant difference observed between *abh1* and WT was in the length of the main stem, which was decreased in *abh1* by approximately 15% to 20%. No significant differences were observed in the number of seeds per plant, the number of petals per flower, or the number of secondary and lateral branches. These data showed that the *abh1* mutation does not significantly affect important developmental processes during growth and further reaffirms the relative dearth of pleiotropic effects of the *abh1* mutation.

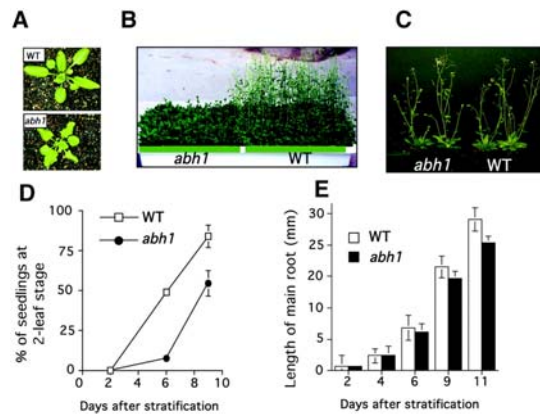


Figure C-5: *abh1* growth is slower compared with WT. A, *abh1* and WT rosettes are shown after 3 weeks of growth. For the same age, *abh1* rosettes are smaller and show a smaller number of leaves. B, WT and *abh1* plants are shown after 6 weeks of growth. The delay in flowering is about 5 to 10 d in *abh1*. C, When *abh1* and WT growth was synchronized, WT and *abh1* plants showed similar whole-plant phenotypes (see also Table I). D, Development of the first two leaves in *abh1* and WT seedlings grown in petri dishes. Data represent the mean of five experiments \pm SE ($n = 30$ seedlings per line for each experiment). E, Root elongation after 2, 6, 9, and 11 d in *abh1* and WT. The Figure C-shows a representative experiment \pm SD ($n = 60$). D and E, Error bars are smaller than symbols when not visible. The slower growth in *abh1* was complemented by the *ABH1* gene (data not shown). A, B, D, and E, WT and *abh1* plants were grown in parallel in a growth chamber after stratification for 4 d at 4°C from seeds between 3 to 6 months old.

Table C-I. Morphological characteristics of *abh1* and WT. More than 20 *abh1* and WT plants were grown in parallel in each experiment (Exp) after their growth was synchronized (see "Materials and Methods"). Plants used for measurements were selected randomly. Measurements were performed after 9 weeks, except for the petals, which were counted when flowers had opened (6-8 weeks). SEs of the mean are shown.

Property	WT	<i>abh1</i>
Length of the main stem (cm) ^a	Exp 1: 34.03 ± 1.18 Exp 2: 26.65 ± 0.79	29.5 ± 1.49 ^e 21.07 ± 0.7 ^e
No. of lateral branches ^a	Exp 1: 2.6 ± 0.22 Exp 2: 1.8 ± 0.29	2.9 ± 0.18 2 ± 0.39
No. of secondary stems ^a	Exp 1: 4.28 ± 0.42 Exp 2: 4.85 ± 0.4	4.14 ± 0.34 4.42 ± 0.429
Length of the siliques ^b	1.45 ± 0.017	1.41 ± 0.01
No. of seeds/siliques ^b	40.75 ± 1.84	41.87 ± 2.16
Weight of seeds/plants (mg) ^c	68 ± 0.007	70 ± 0.006
No. of petals per flower ^d	4.009 ± 0.09	4.049 ± 0.21

^a *n* = 7 and 10 in Exp 1 and 2, respectively. ^b *n* = 30. ^c *n* = 10. ^d *n* = 100. ^e Significant difference from WT.

ABH1 Is Mainly Localized in the Nucleus. We showed that ABH1, together with AtCBP20, binds the 7-methyl guanosine cap structure of mRNA in vitro, and that its disruption leads to abnormal transcript accumulation of a limited number of genes in planta (Hugouvieux et al., 2001), which suggests that ABH1 has a role in mRNA processing. To obtain further insights into ABH1 function in guard cells, we analyzed where the protein was localized.

To investigate the subcellular localization of the ABH1 protein, ABH1 and green fluorescent protein (GFP) coding sequences were fused in frame to produce both N- and C-terminal fusions. *abh1* mutant plants expressing the N-terminal fusion protein, GFP-ABH1, showed complementation of the *abh1* mutant based on seed germination assays with ABA and on suppression of the serrated leaf phenotype (data not shown), illustrating that GFP-ABH1 was functional. The C-terminal fusion protein, ABH1-GFP, showed no complementation of the *abh1* mutant based on ABA-dependent seed germination analyses and on the persistence of the serrated leaf phenotype (data not shown). These data suggest that the C-terminal domain of ABH1 is important for ABH1 function. Thus, further analyses were performed on the functional GFP-ABH1 lines. The subcellular localization of GFP-ABH1 was analyzed in guard cells and epidermal cells (Fig. C-6, A-I). Untransformed WT plants, as expected, showed no GFP fluorescence (Fig. C-6, A and E). The GFP-ABH1 fusion protein was mainly found in nuclei in both WT and *abh1* plants and a slight GFP activity was detected in the cytosol (Fig. C-6, G-I). The same pattern of expression was observed using the C-terminal fusion (data not shown). In control experiments, in which WT plants expressed the GFP protein fused to the GUS protein, the GFP-GUS fusion protein was detected in the cytosol (Fig. C-6F). The nuclear localization of GFP-ABH1 and complementation of *abh1* by this fusion protein support the proposed function of ABH1 as a subunit of a nuclear RNA CBC.

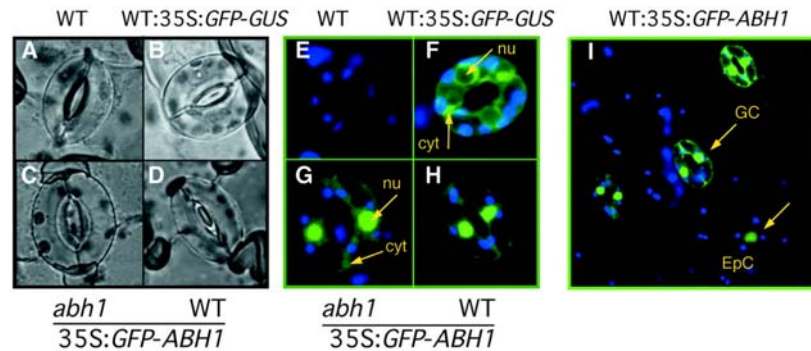


Figure C-6: GFP-ABH1 fusion protein is localized mainly in nuclei in WT and *abh1*. A through D, Bright-field images of guard cells used to study GFP fluorescence in E through H. Blue and green colors show chloroplast (emission 488 nm) and GFP (emission 522 nm) fluorescence, respectively. F, WT control transformed with GFP fused to the GUS protein (pCAMBIA1303; GenBank accession no. AF23299) shows that GFP-GUS is not localized in nuclei (nu), but rather in the cytosol (cyt). G, *abh1*-complemented lines with 35S:*GFP-ABH1* construct show GFP fluorescence mainly in nuclei. H and I, Epidermal strips from WT transformed with the 35S:*GFP-ABH1* construct show GFP fluorescence mainly in the nuclei in guard cells (GC) and epidermal cells (EpC). The same pattern of expression was observed in three independent lines.

Anion and Potassium Channel Activity in *abh1*. To better understand the function of ABH1 in guard cell signaling, we further investigated guard cell phenotypes in *abh1* plants. When stomatal apertures were measured in leaves harvested directly from plants grown under low humidity (40%), stomatal apertures of *abh1* were smaller than those of WT plants (Fig. C-7A). WT stomatal apertures were restored in three homozygous *abh1* lines transformed with the *ABH1* gene (Fig. C-7A). In contrast, for plants exposed to 95% humidity (overnight treatment), stomatal apertures in *abh1* and WT were similar (*abh1* stomatal aperture width/length, 0.17 ± 0.04 ; WT stomatal

aperture width/length, 0.16 ± 0.02 ; $n = 3$ experiments \pm SD). The smaller stomatal apertures observed in *abh1* plants exposed to 40% humidity possibly resulted either from hypersensitivity to endogenous ABA or because *abh1* showed an altered response to low humidity.

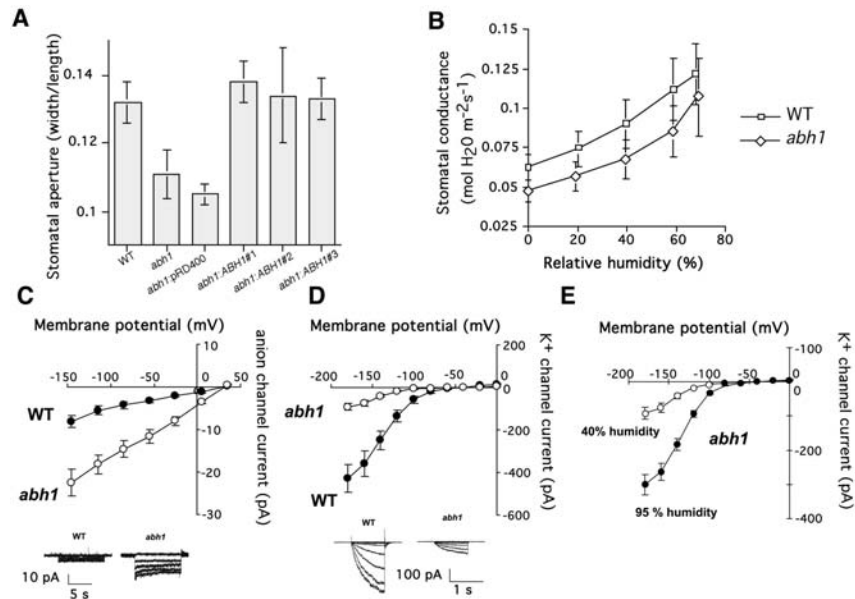


Figure C-7: Stomatal aperture and guard cell anion and K^+ in channel activity are modified in *abh1*. A, Stomatal apertures in *abh1* are smaller than in WT in plants grown at 40% humidity. Leaves were directly harvested from plants grown in a 40% humidity growth chamber and stomatal apertures were measured without any pre-incubation in opening solution. Three independent *abh1* lines complemented with the *ABH1* locus (*abh1:ABH1* nos. 1, 2, and 3) show stomatal apertures similar to WT. *abh1* control plants transformed with vector only (*abh1:pRD400*) show *abh1* stomatal apertures. The data represent the mean \pm SD of three independent experiments. B, Relative changes in leaf gas exchange in response to different humidity levels are similar in *abh1* and WT. Stomatal conductance of WT and *abh1* at several humidities was measured in intact leaves using a Li-6400 infrared gas analyzer (LI-COR, Inc., Lincoln, NE). Stomata were acclimated first to a high humidity ($\geq 80\%$ RH), then the humidity was sequentially dropped and new steady-state conductances determined at each humidity level. New steady states were achieved within 5 to 15 min after the humidity step. Data represent the mean \pm SE of three independent experiments. C and D, Whole-cell current voltage relationships recorded in WT and *abh1* guard cells isolated from 40% humidity-grown plants showed a constitutive activation of slow anion channel currents and a decreased inward-rectifying K^+ (K^+ in) channel activity in *abh1* compared with WT (WT, $n = 26$ [C]; $n = 13$ [D]) and (*abh1*: $n = 35$ [C]; $n = 14$ [D]). Inserts show examples of ion current recordings. E, Whole-cell current voltage relationships recorded in *abh1* guard cells isolated from either 40% humidity-grown plants ($n = 14$ cells) or after 72 h of high humidity (95%) treatment ($n = 17$ cells). Anion and K^+ currents were recorded from 4- to 6-week-old plants as described in "Materials and Methods."

To distinguish between these two possibilities, we investigated the humidity response of *abh1* plants by comparing stomatal conductances of WT and *abh1* at various humidities using an infrared gas analyzer (Fig. C-7B). Gas exchange in *abh1* plants at 40% humidity was slightly reduced compared with WT (Fig. C-7B), consistent with stomatal aperture measurements (Fig. C-7A). Stomata of *abh1* closed upon introduction of lower humidity, as did WT stomata (Fig. C-7B). The rapid response in gas exchange experiments to step changes in humidity was previously shown to be independent of ABA signaling in Arabidopsis (Assmann et al., 2000). Indistinguishable gas exchange responses to step changes in humidity in *abh1* and WT (Fig. C-7B) suggest that *abh1* does not directly modulate the rapid primary humidity response. We also observed that stomatal apertures of *abi1-1* were generally larger than those of WT plants (Landsberg *erecta* [Ler] background) when no ABA was added, including plants grown at 40% humidity (described later), and *abi1-1* does not affect the stomatal response to humidity (Assmann et al., 2000). These findings are consistent with the hypothesis that reduced stomatal apertures in *abh1* at low humidity are because of signaling mediated by endogenous ABA.

ABA induces cytosolic Ca^{2+} increases, which in turn activate slow anion channels and inhibit K^+_{in} channels in guard cells (Schroeder and Hagiwara, 1989; McAinsh et al., 1990). The activities of guard cell slow anion channels and K^+_{in} channels were investigated in *abh1* and WT grown at 40% humidity,

which causes reduced stomatal apertures in *abh1* (Fig. C-7A). Patch clamp experiments performed on guard cell protoplasts from plants grown under low humidity showed that in *abh1* guard cells, anion currents were consistently larger than those in the WT guard cells (Fig. C-7C; $P < 0.001$). Furthermore, anion currents ($n = 6$) showed reduction to WT magnitudes in a complemented line ($P = 0.15$; data not shown). Control experiments were performed on the ABA-hypersensitive mutant, *era1-2*. In *era1-2*, no constitutive activation of guard cell anion channels was observed in the absence of exogenous ABA ($n = 8$, data not shown), confirming previous findings (Pei et al., 1998). These data show a difference in slow anion channel regulation in the absence of exogenous ABA in *abh1* (Fig. C-7C) and *era1*, indicating different functions of these two negative regulators of ABA signaling.

K^+_{in} channel currents were substantially smaller in *abh1* guard cells than in WT guard cells from plants grown at 40% humidity without addition of exogenous ABA (Fig. C-7D; $P < 0.001$). K^+_{in} currents ($n = 6$) showed recovery of WT magnitudes in a complemented line ($P = 0.74$). Furthermore, when plants were exposed to high (95%) humidity for 3 d, K^+_{in} channel current magnitudes in *abh1* guard cells were significantly larger ($n = 17$) than those in *abh1* guard cells from 40% humidity-grown plants ($n = 14$) ($P < 0.001$ at -180 mV; Fig. C-7E). K^+_{in} channel currents in *abh1* guard cells grown at 95% showed recovery, but remained slightly smaller than the current magnitudes of WT grown at 40% humidity (Fig. C-7, D and E). Anion channel and K^+_{in}

channel activities recorded in *abh1* guard cells isolated from plants grown at 40% humidity (Fig. C-7, C and D) correlated with the reduced stomatal apertures and reduced gas exchange found in *abh1* leaves (Fig. C-7A).

ABA Induction of Stomatal Closure in *abh1/abi1-1* and *abh1/era1-2*

Double Mutants. To further investigate genetic interactions of *abh1* with previously characterized early ABA signaling mutants, stomatal responses in homozygous *abh1/era1-2* and *abh1/abi1-1* double mutants were analyzed. In the *abh1/era1-2* double mutant, stomatal closure in response to ABA was similar to the response in *abh1* alone when plants were treated overnight at high humidity (Fig. C-8A). However, stomatal apertures of plants grown at 40% humidity were similar in *abh1/era1-2* and *era1-2* and similar to WT (Fig. C-8B).

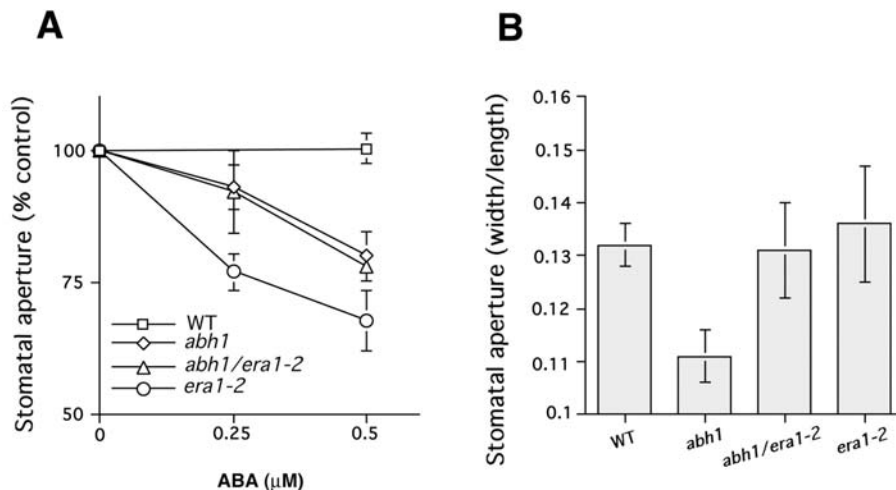


Figure C-8: Stomatal aperture phenotypes in the presence and absence of ABA in the *abh1/era1-2* double mutant. A, ABA-induced stomatal closure in the *abh1/era1-2* double mutant is similar to *abh1*. Plants were kept overnight in high (95%) humidity and then leaves were pre-incubated for 2 h in opening solution, under light. ABA was then added and stomatal apertures measured after 2 more hours. Stomatal aperture is expressed relative to the mean of stomatal aperture measured with no ABA for each line. Stomatal aperture ratio (width/length) with no ABA were 0.17 ± 0.016 , 0.175 ± 0.015 , 0.23 ± 0.029 , and 0.21 ± 0.016 for WT, *abh1*, *era1-2*, and *abh1/era1-2*, respectively. B, Stomatal apertures in *abh1/era1-2* plants grown at 40% humidity show similar opening to *era1-2* and WT. Leaves were directly harvested from plants grown in a 40% humidity growth chamber about 6 h after onset of the 16-h day/night period and stomatal apertures were measured without any pre-incubation in stomatal opening solution. Data in A and B represent the mean \pm SE of three independent experiments with a minimum of 20 stomatal apertures measured per experiment and condition.

The complex interaction of *abh1* and *era1-2* was also observed for non-guard cell phenotypes. For example, the increased number of petals described in *era1-2* (Ziegelhoffer et al., 2000) compared with WT was also observed in the *abh1/era1-2* double mutant (data not shown), whereas the *abh1* serrated leaf phenotype (Fig. C-4A) was unchanged in *abh1/era1-2* compared with *abh1*. However, the delay in growth of *abh1/era1-2* was increased compared

with both *abh1* and *era1-2*, suggesting additive effects in this response (data not shown). The ability to produce siliques and seeds was strongly reduced in *abh1/era1-2* (data not shown). All these data stress the complexity by which *abh1* and *era1-2* interact in planta, suggesting that they may target distinct processes in the ABA signaling network that have differential relative importance in different tissues and depending on conditions. Furthermore, *era1* is known to have pleiotropic phenotypes because it is the only farnesyl transferase β -subunit gene in Arabidopsis; therefore, many *era1* phenotypes would be expected not to show an interaction with *abh1*. ERA1-associated mechanisms that are considered not to be linked to ABA signaling include the Wiggum flower development phenotype and farnesylation of the AP1 transcription factor (Yalovsky et al., 2000; Ziegelhoffer et al., 2000).

Stomatal apertures in response to ABA were also investigated in the *abh1/abi1-1* double mutant. As shown in Figure C-9A, 1 μ M ABA did not cause significant stomatal closure in the *abh1/abi1-1* double mutant, but induced stomatal closing in the WT. At 10 μ M ABA, however, stomata closed in the *abh1/abi1-1* double mutants, whereas they remained widely opened in *abi1-1*. These data showed that ABA-induced stomatal closing in the *abh1/abi1-1* double mutant is more ABA sensitive than in the *abi1-1* background. These data correlate with an intermediate ABA sensitivity of the *abh1/abi1-1* double mutant in seed germination that lies between the *abh1* and *abi1-1* sensitivities (Hugouvieux et al., 2001).

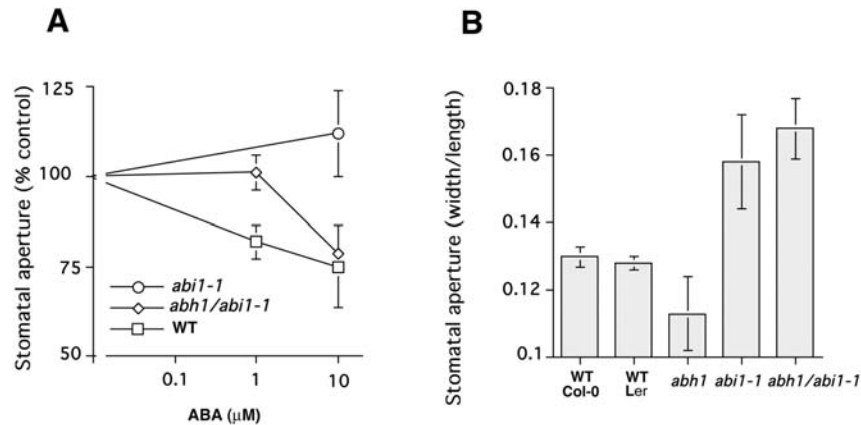


Figure C-9: Stomatal aperture phenotypes in the presence or absence of ABA in the *abh1/abi1-1* double mutant. A, ABA-induced stomatal closure in *abh1/abi1-1* double mutant shows an intermediate response relative to *abi1-1* and WT. Leaves were pre-incubated for 2 h in stomatal opening solution, under light, and then ABA was added and stomatal apertures measured after 2 more h. Stomatal aperture is expressed relative to the mean of stomatal apertures measured with no ABA for each line. Stomatal aperture ratio (width/length) with no ABA were 0.187 ± 0.016 , 0.194 ± 0.011 , and 0.157 ± 0.015 for WT, *abh1/abi1-1*, and *abi1-1*, respectively. B, Stomatal apertures in *abh1/abi1-1* plants grown at 40% humidity are as wide as *abi1-1*. Leaves were directly harvested from plants grown in a 40% humidity growth chamber and stomatal apertures were measured without any pre-incubation in stomatal opening solution. A and B, Data represent the mean \pm SD of three independent experiments.

However, because *abh1* and *abi1-1* mutants are in the Columbia and Ler backgrounds, respectively, we have also isolated a control line that carries the *abi1-1* mutation in an *ERECTA* WT background, from F₂ seeds resulting from *abh1/abi1-1* crosses. The control line and its progeny showed a strong insensitivity to 10 μM ABA (stomatal aperture after ABA treatment was $93\% \pm 7\%$ of the maximal stomatal aperture measured with no ABA). Transgenic expression of *abi1-1* in tobacco (*Nicotiana benthamiano*) confers strong insensitivity to ABA (Armstrong et al., 1995), confirming that the

dominant *abi1-1* mutant protein functions in many backgrounds. The *abh1* mutation partially suppresses this dominant *abi1-1* phenotype.

Stomatal apertures of *abi1-1* plants, measured directly from plants grown at 40% humidity, were generally larger than those of WT plants (*Ler* background; Fig. C-9B). Under the same conditions, stomatal apertures in the *abh1/abi1-1* double mutant were similar to *abi1-1* (Fig. C-9B). These findings are also consistent with the hypothesis that reduced stomatal apertures in *abh1* at low humidity are because of a response to low levels of endogenous ABA as the *abi1-1* mutation causes ABA insensitivity to low ABA concentrations in the *abi1-1/abh1* double mutant (Fig. C-9A).

ABA-Hypersensitive Stomatal Closure in *sad1*. Mutations in three RNA-binding proteins have been described recently that show ABA hypersensitivity (Lu and Fedoroff, 2000; Hugouvieux et al., 2001; Xiong et al., 2001a). In addition to the mRNA cap binding protein ABH1 (Hugouvieux et al., 2001), these genes include a double-stranded RNA-binding protein, HYL1 (Lu and Fedoroff, 2000) and a protein with similarity to an Sm-like snRNP protein, SAD1 (Xiong et al., 2001a). We investigated whether the *sad1* and *hyl1* mutations affect stomatal movements. ABA-induced stomatal closure in the *sad1* mutant showed a reproducible ABA hypersensitivity compared with the WT ecotype C24 (Fig. C-10). In contrast, in the *hyl1* mutant, ABA-induced stomatal closure was similar to the WT ecotype Nossen in two independent

lines of investigation (N. Fedoroff, personal communication; $n = 3$ independent experiments; data not shown).

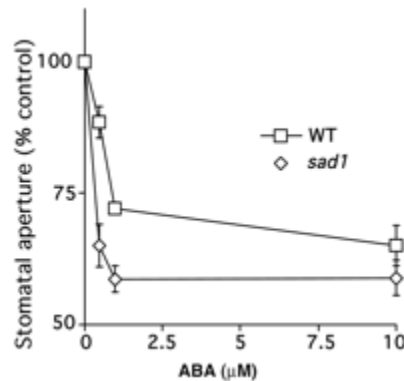


Figure C-10: ABA-hypersensitive stomatal closing in the *sad1* mutant. Plants were kept overnight in high (95%) humidity and then leaves were pre-incubated for 2 h in opening solution, under light. ABA was then added and stomatal apertures measured after 2 more h in *sad1* and WT C24 ecotype. Stomatal apertures are expressed relative to the mean stomatal apertures measured without ABA addition for each line. Stomatal aperture ratios (width/length) without ABA addition were 0.158 ± 0.01 and 0.145 ± 0.006 for WT and *sad1*, respectively. Data represent the mean \pm SE of three independent experiments. Error bars are smaller than symbols when not visible.

DISCUSSION

In a previous report, we described the isolation and characterization of a new recessive ABA-hypersensitive Arabidopsis mutant, *abh1*. *abh1* shows ABA hypersensitivity in seed germination, stomatal closure, and ABA-induced guard cell calcium increases (Hugouvieux et al., 2001). ABH1 was shown to function in vitro as a subunit of a dimeric mRNA CBC and *ABH1* gene expression is necessary for the correct expression level of a subset of genes

in the Arabidopsis genome (Hugouvieux et al., 2001). The isolation of *abh1* points to a link between mRNA metabolism and correct ABA signaling.

To better understand ABH1 function at the whole-plant level and in guard cells, we further investigated *ABH1* gene expression and regulation, ABH1 protein localization, and we further characterized *abh1* mutant phenotypes, *sad1* and *hyl1* phenotypes in guard cells, and genetic interactions between *ABH1* and two well-described early ABA signaling components, *ERA1* and *abi1-1*.

ABH1 Expression Pattern and Nuclear Localization. The *ABH1* gene is expressed in all tissues tested (Figs. 1 and 2). However, our data further show that the *ABH1* expression level varies between tissues and also appears to depend on the developmental stage. Further research will be needed to determine whether different expression levels affect ABH1 functions in these tissues or at these developmental stages. It is intriguing to note that the *abh1* mutation has no visible impact on flower morphology even though *ABH1* mRNA levels are high (Fig. C-1). Thus, it is possible that some ABH1 functions may be conditional and/or that this expression pattern is related to the *abh1* phenotype in seeds.

ABH1 expression does not appear to be affected by external ABA application (Fig. C-3), nor by drought stress. Similar results were observed in the case of the *SAD1* gene (Xiong et al., 2001a). In humans, CBC activity is

increased in response to growth factors (Wilson et al., 1999). It has been proposed that this increased CBC activity may be because of posttranslational modification of the ABH1 homolog, CBP80; for example, by phosphorylation (Wilson and Cerione, 2000), although direct evidence has not been yet reported. The CBC is also known to interact with several proteins from the spliceosome complex and translation machinery (Fortes et al., 2000; Ishigaki et al., 2001; McKendrick et al., 2001). The x-ray crystal structure of a human CBC was recently determined and suggested that CBP80 could behave as a platform protein for nuclear cap-related RNA-processing proteins (Mazza et al., 2001). Thus, it is tempting to speculate that in response to ABA, ABH1 activity may be regulated by posttranslational modifications and/or interaction with new regulators. Note that *sad1* does not interact in yeast two-hybrid experiments with either ABH1 or AtCBP20 (Xiong et al., 2001a). However, a larger complex that includes these proteins cannot be excluded.

Using protein database motif searches, no clear nuclear localization signal can be detected in the ABH1 protein sequence, in contrast to the human and yeast homologs (data not shown). The *abh1* mutant was complemented by an N-terminal GFP-ABH1 fusion protein, which was predominantly localized to the nucleus (Fig. C-6). In contrast, a C-terminal ABH1-GFP fusion did not complement *abh1*. The ABH1 protein has a C-terminal extension compared with yeast and animal CBP80 that could be related to specific unknown properties of ABH1 (Hugouvieux et al., 2001).

The nuclear localization correlates with the function of ABH1 as a subunit of a nuclear CBC as described in yeast and mammals (Lewis and Izaurrealde, 1997). We also observed a slight GFP fluorescence in the cytosol (Fig. C-6). Although the steady-state level of CBC is mainly nuclear, it is well established that CBC moves into the cytosol during mRNA export in yeast, insects, and vertebrates and is later recycled back into the nucleus (Goerlich et al., 1996; Visa et al., 1996; Shent et al., 2000).

Whole-Plant and Stomatal Responses of *abh1*. Although *ABH1* is expressed in several plant tissues, *abh1* plants showed only a slightly slowed growth, a serrated leaf phenotype, and a slightly smaller stem length at maturity compared with WT (Figs. 4 and 5; Table I). No other clearly visible phenotypes were detected at the morphological level. Similarly, the yeast mutant disrupted in *CBP80* shows a growth delay compared with WT, depending on the carbon source used (Uemura and Jigami, 1992).

In the present study, we characterized further *abh1* phenotypes in guard cells. *abh1* stomatal pore apertures were significantly reduced compared with WT when plants were grown in a growth chamber at 40% humidity (Fig. C-7A). Reduced stomatal apertures correlated with both a constitutive activation of slow anion channels and a reduction in K^+ _{in} channel activity in *abh1* guard cells (Fig. C-7, B, C, and E). The stomatal phenotype of *abh1* plants grown at 40% humidity correlates with ion channel activities, even

though ion channel activities were measured after protoplastation (see "Materials and Methods"). These data suggest that the modulation of ion channel activities in *abh1* revealed here may be because of longer term regulatory mechanisms such as posttranslational modification and/or potential alteration of expression levels of ABA transducers (Hugouvieux et al., 2001).

Slow anion channels are activated by cytosolic Ca^{2+} elevations and ABA (Schroeder and Hagiwara, 1989; Grabov et al., 1997; Pei et al., 1997; Allen et al., 1999) and K^+ channels are down-regulated by cytosolic Ca^{2+} elevations and by ABA (Schroeder and Hagiwara, 1989; Blatt and Armstrong, 1993). ABA content in *abh1* and WT plants are similar in sufficiently watered plants, and ABA content increased to the same extent in both WT and *abh1* after desiccation (Hugouvieux et al., 2001). The primary responses of *abh1* and WT stomates to rapid humidity changes were similar (Fig. C-7B). Therefore, we propose that reduced stomatal apertures observed in *abh1* at 40% humidity are because of a response to endogenous ABA. This model is supported by the finding that *abh1/abi1-1* double mutants do not show reduced stomatal apertures at 40% humidity (Fig. C-9B) and that *abi1-1* does not function in humidity signaling (Assmann et al., 2000).

The *abh1/era1-2* double mutant shows an additive ABA-hypersensitive phenotype in seed germination assays (Hugouvieux et al., 2001). Interestingly, ABA-induced stomatal closure in the *abh1/era1-2* double mutant does not show additive effects of the two mutants (Fig. C-8). Under the imposed

conditions, the *abh1/era1-2* double mutant showed an ABA hypersensitivity similar to *abh1*. However, when stomatal apertures were measured in plants grown at 40% humidity, stomatal apertures of the double mutant were similar to those in *era1-2* stomatal apertures (Fig. C-8B). These data suggest complex interactions of the *abh1* and *era1-2* mutants, indicating that they affect different components or branches in ABA signaling that change their relative contribution to ABA signal transduction depending on conditions. In the *abh1/abi1-1* double mutant, however, ABA sensitivity was decreased compared with the *abi1-1* mutant (Fig. C-9B), which correlated with seed germination assays in response to ABA (Hugouvieux et al., 2001), suggesting a less complex interaction of *abi1-1* and ABH1, which may be explained by the dominant nature of the *abi1-1* mutant.

Distinct ABA Responses in Guard Cells of *sad1* and *abh1* Compared with *hyl1*. The Sm-like snRNP protein, SAD1, was suggested to function in mRNA processing in ABA signaling and homeostasis (Xiong et al., 2001a). The independent isolation of *abh1* and *sad1* by two different screens strengthens the recent hypothesis that mRNA-processing proteins function as negative regulators in ABA signaling. Furthermore, the recessive double-stranded RNA-binding protein mutant *hyl1* also shows ABA hypersensitivity (Lu and Fedoroff, 2000). In the present study, we analyzed stomatal responses of *sad1* and *hyl1*. Although *sad1* showed ABA hypersensitivity in stomatal movement responses

(Fig. C-10), *hyl1* did not (data not shown; N. Fedoroff, personal communication). These data suggest that *hyl1* may modulate ABA signaling via a mechanism independent of *abh1* and *sad1*. These results are consistent with the finding that HYL1 binds double-stranded RNA, which appears to be mechanistically different from the proposed SAD1 function and ABH1 cap-binding activity. Furthermore, the *hyl1* mutation also modulates the sensitivity to auxin and cytokinin (Lu and Fedoroff, 2000), showing a clear difference from *abh1* and *sad1* (Hugouvieux et al., 2001; Xiong et al., 2001a).

Although both *sad1* and *abh1* show hypersensitivity to exogenous ABA (Fig. C-10; Hugouvieux et al., 2001), there are distinct differences in the two mutants. The *sad1* mutation results in reduced ABA levels in drought-stressed plants because of a feedback mechanism from ABA signaling to ABA biosynthesis (Xiong et al., 2001a). Consistent with these findings, detached *sad1* rosettes showed an enhanced transpiration rate compared with WT (Xiong et al., 2001a). In contrast, the *abh1* mutation does not affect endogenous ABA levels and *abh1* causes reduced transpiration (Hugouvieux et al., 2001) and reduced stomatal apertures. Despite these differences, it is conceivable that ABH1 and SAD1 participate in a complex RNA-processing network that modulates ABA signaling, in such a manner that the two mutants have clearly distinguishable effects but some similarities in their phenotypes, which include ABA hypersensitivity in seed germination (Hugouvieux et al., 2001; Xiong et al., 2001) and in stomatal closing (Fig. C-10).

In conclusion, we show that *ABH1* is widely expressed in plants and that ABH1 shows preferentially nuclear localization. The negative regulators of ABA signaling, ABH1 and the farnesyl transferase β -subunit ERA1, show complex genetic interactions and differential effects indicating that these two genes act at different locations in the ABA signal network. Findings that both *abh1* and *sad1* show similar sensitivity to exogenous ABA, whereas the *hyl1* mutant did not affect stomatal apertures in response to ABA, further strengthen the hypothesis that RNA processing modulates early ABA signaling.

MATERIALS AND METHODS

Plant Growth and Culture Conditions. *abh1*, other Arabidopsis mutants, and the corresponding WT ecotypes were grown side by side in growth chambers: 40% humidity, 16-h-light/8-h-dark cycle, temperature 20°C, and photon fluency rate of 75 $\mu\text{mol m}^{-2} \text{s}^{-1}$. Unless otherwise stated, WT plants are from the Columbia ecotype. When required, the growth of *abh1* and WT plants was synchronized by sowing *abh1* plants 1 week earlier than WT. To test the sensitivity of seeds to ABA, in the case of *abh1* lines complemented with the N-terminal GFP-ABH1 fusion, seeds were plated on minimal medium (0.25 \times Murashige and Skoog medium) containing 0.3 μM ABA. After 4 d at 4°C, seeds were transferred to 28°C and continuous light and germination was scored after 5 more d. Seeds used for comparative studies were from plants

grown and harvested in parallel. For seedling growth assays, 6-month-old *abh1* and WT seeds were germinated on Murashige and Skoog plates. Germination was scored after 2 d to make sure that all the seedlings were at the two-cotyledon stages and the root length was estimated using a micrometer under a dissecting microscope. Seeds that showed a delay in germination were removed from the plates in both WT and *abh1*. After 2, 6, 9, and 11 d of growth, root length was measured and the development of the shoot was studied by analyzing the appearance and development of new leaves under the microscope.

GFP-ABH1 Fusion Constructs and Plant Transformation. To generate N- and C-terminal fusion proteins between ABH1 and GFP proteins, the full-length *ABH1* cDNA was amplified using *Pfu* DNA polymerase (Stratagene, La Jolla, CA). Primers used for PCR included specific restriction sites at both ends, to allow the cloning of *ABH1* and *GFP* in frame in the vector GFP-JFH1 (kindly provided by Dr. Jeff Harper, The Scripps Research Institute, La Jolla, CA). PCR-amplified constructs were confirmed by sequencing (Retrogen, San Diego). *Agrobacterium tumefaciens* strain C58 was used to generate transgenic *Arabidopsis* plants using the floral dip technique (Clough and Bent, 1998).

Confocal Microscopy. The subcellular localization of ABH1 fused to GFP was assessed by scanning confocal laser microscopy in epidermal strips prepared as described (Allen et al., 1999). Epidermal strips were mounted between two cover slips on an Axiovert 35M microscope (Zeiss, Jena, Germany) coupled to an MCr-1000 scanning laser confocal system (Bio-Rad Laboratories, Hercules, CA). Argon laser light (488-nm wavelength, 30% power) was used to excite GFP and emission light was measured at 522 nm. Transmission images were collected in parallel. Autofluorescence was monitored at 488 nm.

GUS Staining. GUS activity was assayed on either seedlings grown on Murashige and Skoog plates or soil, after 24 h of incubation in a solution containing 2 mM 5-bromo-4-chloro-3-indolyl--D-glucuronide, 0.1 M Na₂HPO₄ (pH 7.2), 0.1% (w/v) K⁺ ferrocyanide, 0.1% (w/v) ferricyanide, and 0.1% (v/v) Triton. Experiments were performed on three independent WT:ABH1-GUS lines. WT control plants showed no GUS activity (data not shown).

RNA-Blot Analyses. Total RNA was extracted from flowers, leaves, stems, and roots of 5- to 6-week-old WT plants using Trizol reagent (Life Technologies/Gibco-BRL, Rockville, MD). Poly(A⁺) RNA was further purified using the μ MACS mRNA Isolation Kit (Miltenyi Biotec, Auburn, CA) according to the manufacturer's instructions. To examine whether ABA regulates *ABH1*

gene expression, total RNA and poly(A⁺) RNA were extracted from rosette leaves of WT plants sprayed with 100 μ M ABA, 4 h before extraction. Several complementary experiments were carried out using 1, 10, and 100 μ M ABA for different application times. Total and poly(A⁺) RNA were separated in a 1.2% (w/v) denaturing agarose gel, and then transferred onto a Hybond N⁺ membrane (Amersham, Buckinghamshire, UK). The blots were hybridized with ³²P-labeled *ABH1* cDNA and/or a *Cor47* genomic fragment amplified by PCR using the forward and reverse primers, 5'GAT CGA AAT GGT TGA TAA GAG ATC3' and 5'CAC ACT CTC CGA CAC TGG TAC C3', respectively.

Stomatal Movement Analyses. Stomatal aperture measurements were performed as described (Pei et al., 1997; Allen et al., 2000). Stomata from 5- to 6-week-old plants were opened by exposing excised leaves for 2 h to white light (intensity: 125 μ mol m⁻² s⁻¹), floating in a stomatal opening solution containing 5 mM KCl, 10 μ M CaCl₂, and 10 mM MES (pH 6.15), in the growth chamber at 20°C. Stomatal apertures were measured 2 h after ABA was added (Pei et al., 1997). When experiments were performed with *abh1*, *era1-2*, *sad1*, and *abh1/era1-2* double mutants, plants were subjected to an overnight high (95%) humidity treatment before incubation of the leaves in stomatal opening solution. Control experiments were performed in parallel with no ABA added. Leaves were then blended for 30 s and epidermal peels collected as described (Allen et al., 1999). Stomatal apertures were measured (pore

width/length) by focusing on the focal plane of guard cells in epidermal strips (Ichida et al., 1997).

Stomatal Conductance. Stomatal responses to humidity were determined by measuring transpiration rates using a Li-6400 infrared gas analyzer (LI-COR, Inc.). Chamber temperature and carbon dioxide concentration were maintained at 23°C and 400 $\mu\text{L L}^{-1}$, respectively. Constant illumination of 500 $\mu\text{mol quanta m}^{-2}\text{s}^{-1}$ photosynthetically active radiation was provided by a red and blue LED light source.

Electrophysiology. Anion and K^+ currents were recorded from guard cell protoplasts of 4- to 6-week-old plants (Ichida et al., 1997; Pei et al., 1997) grown either at 40% humidity or after 72 h of high-humidity treatment (95%). The solutions used in patch clamp experiments were composed of 150 mM CsCl, 2 mM MgCl_2 , 6.7 mM EGTA, 3.35 mM CaCl_2 , and 10 mM HEPES-Tris, pH 7.1, in the pipette medium and of 30 mM CsCl, 2 mM MgCl_2 , 1 mM CaCl_2 , and 10 mM MES-Tris, pH 5.6, in the bath medium, for anion channel activity measurement (Pei et al., 1997). For K^+ current measurements, the pipette solution was composed of 30 mM KCl, 70 mM-Glu, 2 mM MgCl_2 , 6.7 mM EGTA, 3.35 mM CaCl_2 , 5 mM ATP, and 10 mM HEPES-Tris, pH 7.1. The bath solution contained 30 mM KCl, 40 mM CaCl_2 , 2 mM MgCl_2 , and 10 mM MES-Tris, pH 5.5 (Pei et al., 1997). For all solutions, osmolarity was adjusted to

485 mmol kg⁻¹ for bath solutions and 500 mmol kg⁻¹ for pipette solutions by addition of D-sorbitol.

ACKNOWLEDGEMENTS

We thank Gethyn Allen for advice on confocal microscopy and members of the laboratory for discussions, and David Waner, Christine Salomon, and Jorieth Jose for assistance. We thank Drs. Nina Fedoroff and Jian-Kang Zhu for providing *hyl1* and *sad1* mutants and for discussion.

REFERENCES CITED

Allen GJ, Chu SP, Schumacher K, Shimazaki CT, Vafeados D, Kemper A, Hawke SD, Tallman G, Tsien RY, Harper JF, et al (2000) Alteration of stimulus-specific guard cell calcium oscillations and stomatal closing in *Arabidopsis det3* mutant. *Science* 289: 2338-2342

Allen GJ, Kuchitsu K, Chu SP, Murata Y, Schroeder JI (1999) *Arabidopsis abi1-1* and *abi2-1* phosphatase mutations reduce abscisic acid-induced cytoplasmic calcium rises in guard cells. *Plant Cell* 11: 1785-1798

Armstrong F, Leung J, Grabov A, Brearley J, Giraudat J, Blatt MR (1995) Sensitivity to abscisic acid of guard-cell K⁺ channels is suppressed by *abi1-1*, a mutant *Arabidopsis* gene encoding a putative protein phosphatase. *Proc Natl Acad Sci USA* 92: 9520-9524

Assmann SM, Snyder JA, Lee Y-RJ (2000) ABA-deficient (*aba1*) and ABA-insensitive (*abi1-1*, *abi2-1*) mutants of *Arabidopsis* have a wild-type stomatal response to humidity. *Plant Cell Environ* 23: 387-395

Blatt MR, Armstrong F (1993) Potassium channels of stomatal guard cells: abscisic acid-evoked control of the outward rectifier mediated by cytoplasmic pH. *Planta* 191: 330-341

- Clough SJ, Bent AF (1998) Floral dip: a simplified method for *Agrobacterium*-mediated transformation of *Arabidopsis thaliana*. *Plant J* 16: 735-743
- Cutler S, Ghassemian M, Bonetta D, Cooney S, McCourt P (1996) A protein farnesyl transferase involved in abscisic acid signal transduction in *Arabidopsis*. *Science* 273: 1239-1241
- Finkelstein RR, Gampala SS, Rock CD (2002) Abscisic acid signaling in seeds and seedlings. *Plant Cell Suppl* 14: S15-45
- Finkelstein RR, Lynch TJ (2000) The *Arabidopsis* abscisic acid response gene *ABI5* encodes a basic leucine zipper transcription factor. *Plant Cell* 12: 599-609
- Finkelstein RR, Wang ML, Lynch TJ, Rao S, Goodman HM (1998) The *Arabidopsis* abscisic acid response locus *ABI4* encodes an APETALA 2 domain protein. *Plant Cell* 10: 1043-1054
- Fortes P, Inada T, Preiss T, Hentze MW, Mattaj IW, Sachs AB (2000) The yeast nuclear cap binding complex can interact with translation factor eIF4G and mediate translation initiation. *Mol Cell* 6: 191-196
- Giraudat J, Hauge BM, Valon C, Smalle J, Parcy F, Goodman HM (1992) Isolation of the *Arabidopsis* *ABI3* gene by positional cloning. *Plant Cell* 4: 1251-1261
- Görlich D, Kraft R, Kostka S, Vogel F, Hartmann E, Laskey RA, Mattaj IW, Izaurralde E (1996) Importin provides a link between nuclear protein import and UsnRNA export. *Cell* 87: 21-32
- Grabov A, Leung J, Giraudat J, Blatt MR (1997) Alteration of anion channel kinetics in wild-type and *abi1-1* transgenic *Nicotiana benthamiana* guard cells by abscisic acid. *Plant J* 12: 203-213
- Hugouvieux V, Kwak JM, Schroeder JI (2001) An mRNA cap binding protein, ABH1, modulates early abscisic acid signal transduction in *Arabidopsis*. *Cell* 106: 477-487
- Ichida AM, Pei Z-M, Baizabal-Aguirre VM, Turner KJ, Schroeder JI (1997) Expression of a Cs⁺-resistant guard cell K⁺ channel confers CS⁺-resistant, light-induced stomatal opening in transgenic *Arabidopsis*. *Plant Cell* 9: 1843-1857
- Ishigaki Y, Li X, Serin G, Maquat LE (2001) Evidence for a pioneer round of mRNA translation: mRNAs subject to nonsense-mediated decay in mammalian cells are bound by CBP80 and CBP20. *Cell* 106: 607-617

- Koornneef M, Leon-Kloosterziel KM, Schwartz SH, Zeevaart JAD (1998) The genetic and molecular dissection of abscisic acid biosynthesis and signal transduction in *Arabidopsis*. *Plant Physiol Biochem* 36: 83-89
- Lemichez E, Wu Y, Sanchez JP, Mettouchi A, Mathur J, Chua NH (2001) Inactivation of AtRac1 by abscisic acid is essential for stomatal closure. *Genes Dev* 15: 1808-1816
- Leung J, Bouvier-Durand M, Morris PC, Guerrier D, Cheddor F, Giraudat J (1994) *Arabidopsis* ABA response gene *ABI1*: features of a calcium-modulated protein phosphatase. *Science* 264: 1448-1452
- Leung J, Giraudat J (1998) Abscisic acid signal transduction. *Annu Rev Plant Physiol Plant Mol Biol* 49: 199-222
- Leung J, Merlot S, Giraudat J (1997) The *Arabidopsis* abscisic acid-insensitive2 (*ABI2*) and *ABI1* genes encode homologous protein phosphatases 2C involved in abscisic acid signal transduction. *Plant Cell* 9: 759-771
- Lewis JD, Izaurralde E (1997) The role of the cap structure in RNA processing and nuclear export. *Euro J Biochem* 247: 461-469
- Li J, Wang X-Q, Watson MB, Assmann SM (2000) Regulation of abscisic acid-induced stomatal closure and anion channels by guard cell AAPK kinase. *Science* 287: 300-303
- Lu C, Fedoroff N (2000) A mutation in the *Arabidopsis* *HYL1* gene encoding a dsRNA binding protein affects responses to abscisic acid, auxin, and cytokinin. *Plant Cell* 12: 2351-2366
- MacRobbie EAC (1998) Signal transduction and ion channels in guard cells. *Philos Trans R Soc London* 353: 1475-1488
- Marcotte WR, Guiltinan MJ, Quatrano RS (1992) ABA-regulated gene expression: *cis*-acting sequences and *trans*-acting factors. *Biochem Soc Trans* 20: 93-97
- Mazza C, Ohno M, Segref A, Mattaj JW, Cusack S (2001) Crystal structure of the human nuclear cap binding complex. *Mol Cell* 8: 383-396
- McAinsh MR, Brownlee C, Hetherington AM (1990) Abscisic acid-induced elevation of guard cell cytosolic calcium precedes stomatal closure. *Nature* 343: 186-188

- McKendrick L, Thompson E, Ferreira J, Morley SJ, Lewis JD (2001) Interaction of eukaryotic translation initiation factor 4G with the nuclear cap-binding complex provides a link between nuclear and cytoplasmic functions of the m⁷ guanosine cap. *Mol Cell Biol* 21: 3632-3641
- Meyer K, Leube MP, Grill E (1994) A protein phosphatase 2C involved in ABA signal transduction in *Arabidopsis thaliana*. *Science* 264: 1452-1455
- Pei Z-M, Ghassemian M, Kwak CM, McCourt P, Schroeder JI (1998) Role of farnesyltransferase in ABA regulation of guard cell anion channels and plant water loss. *Science* 282: 287-290
- Pei Z-M, Kuchitsu K, Ward JM, Schwarz M, Schroeder JI (1997) Differential abscisic acid regulation of guard cell slow anion channels in *Arabidopsis* wild-type and *abi1* and *abi2* mutants. *Plant Cell* 9: 409-423
- Schroeder JI, Allen GJ, Hugouvieux V, Kwak JM, Waner D (2001) Guard cell signal transduction. *Annu Rev Plant Physiol Plant Mol Biol* 52: 627-658
- Schroeder JI, Hagiwara S (1989) Cytosolic calcium regulates ion channels in the plasma membrane of *Vicia faba* guard cells. *Nature* 338: 427-430
- Shent EC, Stage-Zimmermann T, Chui P, Silver PA (2000) The yeast mRNA-binding protein Npl3p interacts with the cap-binding complex. *J Biol Chem* 275: 23718-23724
- Uemura H, Jigami Y (1992) GCR3 encodes an acidic protein that is required for expression of glycolytic genes in *Saccharomyces cerevisiae*. *J Bacteriol* 174: 5526-5532
- Visa N, Izaurralde E, Ferreira J, Daneholt B, Mattaj IW (1996) A nuclear cap-binding complex binds Balbiani ring pre-mRNA cotranscriptionally and accompanies the ribonucleoprotein particle during nuclear export. *J Cell Biol* 133: 5-14
- Wang XQ, Ullah H, Jones AM, Assmann SM (2001) G protein regulation of ion channels and abscisic acid signaling in *Arabidopsis* guard cells. *Science* 292: 2070-2072
- Wilson KF, Cerione RA (2000) Signal transduction and post-transcriptional gene expression. *Biol Chem* 381: 357-365
- Wilson KF, Fortes P, Singh US, Ohno M, Mattaj IW, Cerione RA (1999) The nuclear cap-binding complex is a novel target of growth factor receptor-coupled signal transduction. *J Biol Chem* 274: 4166-4173

Xiong L, Gong Z, Rock CD, Subramanian S, Guo Y, Xu W, Galbraith D, Zhu JK (2001a) Modulation of abscisic acid signal transduction and biosynthesis by an Sm-like protein in *Arabidopsis*. *Dev Cell* 1: 771-781

Xiong L, Lee B-h, Ishitani M, Lee H, Zhang C, Zhu J-K (2001b) *FIERY1* encoding an inositol polyphosphate 1-phosphatase is a negative regulator of abscisic acid and stress signaling in *Arabidopsis*. *Genes Dev* 15: 1971-1984

Yalovsky S, Rodriguez-Concepcion M, Bracha K, Toledo-Ortiz G, Gruissem W (2000) Prenylation of the floral transcription factor APETALA1 modulates its function. *Plant Cell* 12: 1257-1266

Ziegelhoffer EC, Medrano LJ, Meyerowitz EM (2000) Cloning of the *Arabidopsis* WIGGUM gene identifies a role for farnesylation in meristem development. *Proc Natl Acad Sci USA* 97: 7633-7638

The text of this section is a reprint of the material as it appears in Plant Physiology, Hugouvieux, V., Murata, Y., Young, J.J., Kwak, J.M., Mackesy, D.Z., and Schroeder, J.I. (2002). I generated the data for Fig. C-7B.

APPENDIX D

The Nitrate Transporter AtNRT1.1 (CHL1) Functions in Stomatal Opening and Contributes to Drought Susceptibility in Arabidopsis

ABSTRACT

The movement of guard cells in stomatal complexes controls water loss and CO₂ uptake in plants. Examination of the dual-affinity nitrate transporter gene *AtNRT1.1* (*CHL1*) revealed that it is expressed and functions in *Arabidopsis* guard cells. *CHL1* promoter- β -glucuronidase and *CHL1* promoter-green fluorescent protein constructs showed strong expression in guard cells, and immunolocalization experiments with anti-CHL1 antibody confirmed these results. To assess *CHL1* function, *chl1* mutant plants grown in the presence of nitrate were examined. Compared with wild-type plants, *chl1* mutants had reduced stomatal opening and reduced transpiration rates in the light or when deprived of CO₂ in the dark. These effects result in enhanced drought tolerance in *chl1* mutants. At the cellular level, *chl1* mutants showed reduced nitrate accumulation in guard cells during stomatal opening and failed to show nitrate-induced depolarization of guard cells. In wild-type guard cells, nitrate induced depolarization, and nitrate concentrations increased threefold during stomatal opening. These results identify an anion transporter that functions in stomatal opening and demonstrate that *CHL1* supports stomatal function in the presence of nitrate.

INTRODUCTION

Stomata act as ports that regulate the uptake of CO₂ for photosynthesis and the evaporation of water for transpiration in plants. Gas exchange through stomatal pores in the leaves of plants is regulated by the turgor-driven expansion and contraction of guard cells in response to environmental and internal signals, including light, humidity, CO₂, phytohormones, calcium, and reactive oxygen species (reviewed by Blatt, 2000; Assmann and Wang, 2001; Dietrich et al., 2001; Schroeder et al., 2001; Roelfsema and Hedrich, 2002). Changes in guard cell turgor are driven by fluxes of K⁺ and Cl⁻ and, depending on the growth conditions and the time of day, the accumulation or loss of malate and Suc (reviewed by Talbott and Zeiger, 1998; Blatt, 2000; Assmann and Wang, 2001; Dietrich et al., 2001; Schroeder et al., 2001). For example, light-induced stomatal opening involves activation of the plasma membrane H⁺-ATPase, which results in the hyperpolarization of the plasma membrane and the opening of inward-rectifying K⁺ channels. The influx of K⁺ is accompanied by an influx of Cl⁻ and an accumulation of malate.

The search for ion channel/transporter genes involved in stomatal movement has led to the identification of multiple K channel genes that are expressed and function in guard cells (Dietrich et al., 2001; Kwak et al., 2001; Pilot et al., 2001; Schroeder et al., 2001; Szyroki et al., 2001). It is thought that

multiple K channels, and not just one, are essential for stomatal opening (Dietrich et al., 2001; Szyroki et al., 2001). No anion channel/transporter gene responsible for stomatal opening has been identified to date. Cl⁻ influx during stomatal opening has been proposed to occur via H⁺/Cl⁻ symport, but no electrophysiological data or molecular analyses to support this model have been reported (Assmann and Wang, 2001; Dietrich et al., 2001). Stomatal closing involves the efflux of potassium via outward K channels and of anions via two types of anion channels: slow or S-type and rapid or R-type (guard cell anion channel [GCAC]) channels (Schroeder and Keller, 1992; Dietrich and Hedrich, 1994). The S-type channels may be composed of or be regulated by ATP binding cassette proteins (Leonhardt et al., 1997, 1999, 2001). One ATP binding cassette transporter, AtMRP5, has been shown to be required for glibenclamide (a modulator of K-ATP and cystic fibrosis transmembrane conductance regulator chloride channels)–induced opening of stomates and thus may serve as a channel or channel regulator (Gaedeke et al., 2001).

The Arabidopsis *NRT1.1* (*CHL1*) gene encodes a dual-affinity nitrate transporter that contributes to both low- and high-affinity uptake in roots of Arabidopsis seedlings (Tsay et al., 1993; Touraine and Glass, 1997; Wang et al., 1998; Liu et al., 1999). Recent studies have shown that *CHL1* is expressed preferentially in proliferating regions of roots and shoots (e.g., lateral root primordia and young leaves) and contributes to the growth of nascent organs (Guo et al., 2001). Further analysis of *CHL1* has revealed a surprising result:

CHL1 is expressed in guard cells (see below). This observation led us to examine possible functions for *CHL1* in stomatal movements and function. Because *CHL1* is a nitrate transporter, we examined stomatal opening and gas exchange in the presence or absence of nitrate. The results from these experiments are described below.

RESULTS

***CHL1* Functions in Light-Induced Stomatal Opening and Nitrate**

Accumulation in Guard Cells. Recent studies of *CHL1* showed only low levels of *CHL1* expression in mature shoot organs and root tissues using transgenic plants containing *CHL1*- β -glucuronidase/green fluorescent protein (*GUS/GFP*) fusion constructs (Guo et al., 2001). Close examination of shoots from these lines, however, revealed strong *CHL1* expression in guard cells of mature leaves (Figure D-1A) and hypocotyls (Figure D-1B). Strong GUS staining also was found in guard cells of floral organs (data not shown). Immunolocalization experiments with affinity-purified anti-*CHL1* antibody confirmed these findings, showing high levels of *CHL1* protein in guard cells (Figures D-1C and 1D; staining with preimmune serum is shown in Figures D-1E and 1F).

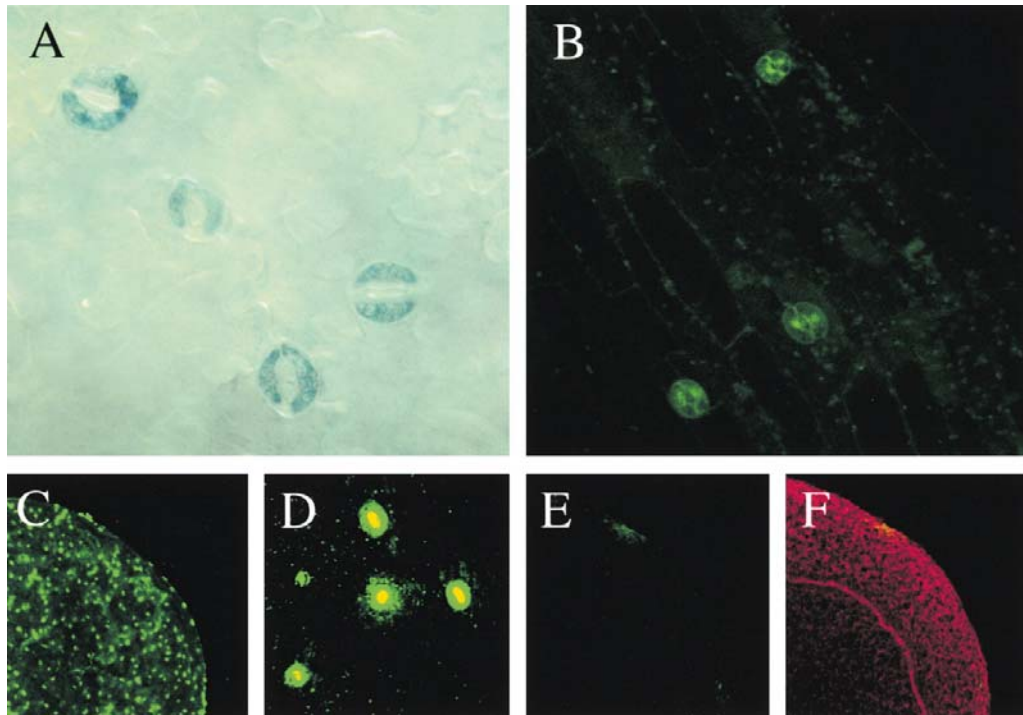


Figure D-1: Localization of *CHL1* Expression and Protein in Guard Cells.

(A) Portion of a leaf from a plant carrying the Haell *CHL1-GUS* fusion construct (Guo et al., 2001). Strong GUS staining indicative of *CHL1* expression is found in guard cells. (B) Section of a hypocotyl from a 7-day-old transgenic plant carrying the Haell *CHL1-GFP* construct (Guo et al., 2001). Strong GFP signals are found only in guard cells using confocal laser scanning microscopy. (C) Immunofluorescence from a portion of a leaf stained with anti-*CHL1* antibody. Whole-mount assays were performed with affinity-purified anti-*CHL1* antibody and Alexa Fluor 488–conjugated secondary antibody (Molecular Probes) using confocal laser scanning microscopy (Guo et al., 2001). (D) Higher magnification of a section of the image in (C) showing immunofluorescence from individual stomata. (E) Control experiment using preimmune serum showing little immunofluorescence from a leaf. (F) Outline of the leaf shown in (E) by propidium iodide staining.

The finding of strong *CHL1* expression in guard cells suggests that *CHL1* may play a role in stomatal function. Because *CHL1* is a nitrate transporter, stomatal function was examined in the presence or absence of nitrate in wild-

type and *chl1* mutant plants. Light-induced stomatal opening was examined first. *chl1* mutants (two alleles tested) were impaired significantly (reduced to one-third the wild-type level) in stomatal opening in white light when detached leaves were incubated with 30 mM KNO₃ (Figure D-2A). This deficiency was dependent on nitrate, because no significant difference ($P < 0.05$ by *t* test) in stomatal opening was observed between mutant and wild-type cells if NO₃⁻ was replaced with Cl⁻ (Figure D-2A). Thus, *CHL1* contributes substantially to light-induced opening of stomates when nitrate is the anion but is dispensable for light-induced opening when chloride is the anion.

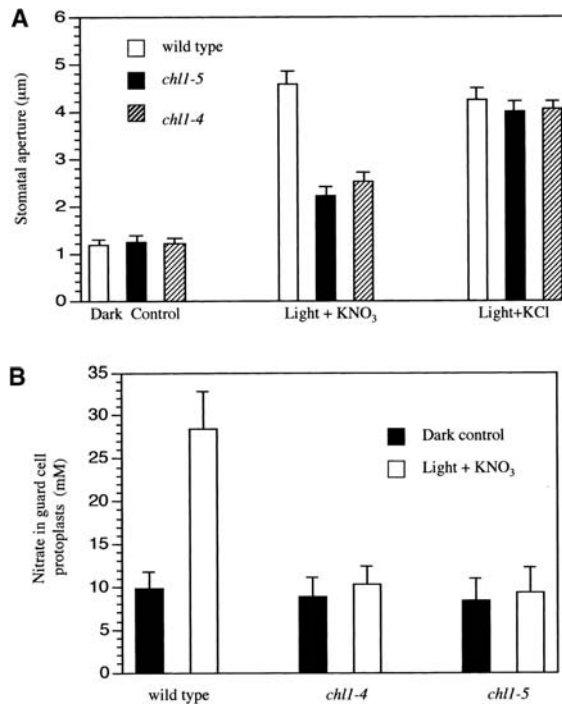


Figure D-2: CHL1 Functions in Light-Induced Stomatal Opening. (A) Stomatal apertures were determined for wild-type and *chl1* mutant plants (*chl1-4* and *chl1-5*) undergoing light-induced stomatal opening. Data were averaged from three separate experiments; $n = 40$ aperture measurements per experiment. Error bars represent standard deviations. (B) Nitrate accumulation was measured in guard cell protoplasts isolated from detached leaves of wild-type and *chl1* mutant plants during light-induced stomatal opening in the presence of nitrate. Error bars represent standard deviations ($n = 4$).

One explanation for these results is that CHL1 mediates nitrate uptake into guard cells. Because nitrate is an anion, it could serve as a counter-ion for K^+ influx during stomatal opening. Nitrate accumulation in guard cells was measured during light-induced opening in wild-type and mutant plants. In wild-type guard cells, nitrate concentrations increased nearly threefold after 3 h of

light treatment (Figure D-2B). *chl1* mutant guard cells, however, showed no significant increase in nitrate accumulation during the same treatment (Figure D-2B). These results show that net nitrate influx occurs during stomatal opening and that this influx is dependent on CHL1.

CHL1 Supports Stomatal Function in Intact Plants. The experiments described above were performed with detached leaves floating on liquid medium. To examine the role of CHL1 in stomatal function further, stomatal apertures and gas exchange were examined for leaves on intact plants. Plants were grown in a 16-h-light/8-h-dark cycle with a continuous supply of nitrate (i.e., in organic peat soil or with vermiculite irrigated with NH_4NO_3). During the middle of the light period, stomatal apertures were found to be 35 to 45% greater in wild-type plants than in *chl1* mutants (Figure D-3). For plants deprived of nitrate for 10 days, there was little difference between wild-type and mutant plants as a result of the decrease in stomatal aperture in wild-type plants (Figure D-3).

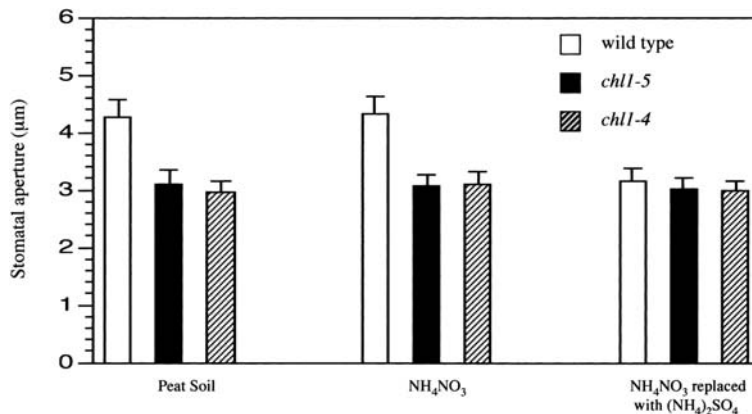


Figure D-3: Stomatal Apertures in Intact Plants. Stomatal apertures were determined for leaves from intact plants during the middle of the light period (16 h of light and 8 h of dark) as described in Methods. Data were averaged from three separate experiments; $n = 40$ aperture measurements per experiment.

One explanation for these results is that the reductions in stomatal apertures observed in the mutants are attributable to indirect and detrimental effects of *chl1* mutations on photosynthetic activity, which could increase intercellular CO₂ levels and cause stomates to close. To test this possibility, stomatal conductance was measured in mature leaves of wild-type and *chl1* mutant plants in the dark, when no photosynthesis occurs. When stomates were induced to open by decreasing CO₂ levels (treating plants with CO₂-free air), *chl1* mutants (two alleles tested) showed much reduced increases in stomatal conductance (Figure D-4A) and stomatal aperture (Figure D-4B, measured at 40 min after CO₂ depletion) compared with the wild type. Thus, *CHL1* functions

to increase stomatal aperture in plants treated continuously with nitrate, and this function is not mediated by an indirect effect on intercellular CO₂ levels.

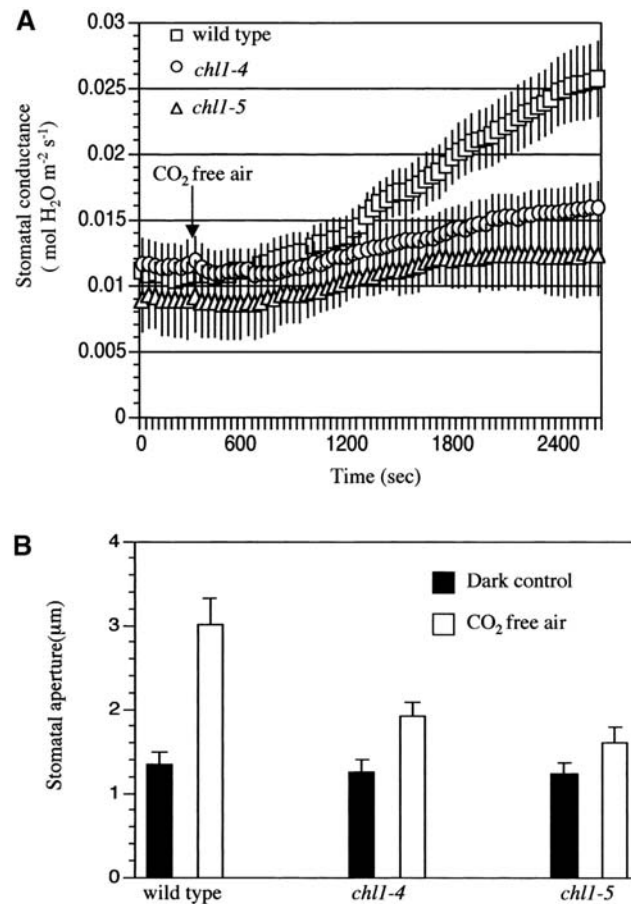


Figure D-4: Stomatal Conductance and Apertures in Plants Depleted of CO₂ in the Dark. (A) Stomatal conductance was measured in wild-type and *chl1* mutant plants in the dark when CO₂ levels (400 mL/L) were decreased to 0 mL/L (CO₂-free air). Squares, wild type ($n = 6$); circles, *chl1-4* ($n = 5$); triangles, *chl1-5* ($n = 5$). Error bars represent standard deviations. (B) Stomatal apertures in leaves of the wild type and *chl1* mutants after 40 min of treatment with CO₂-free air. Error bars represent standard deviations ($n = 5$).

***chl1* Mutations Do Not Affect Abscisic Acid–Induced Stomatal Closing or Abscisic Acid Inhibition of Stomatal Opening.** One explanation for the

effect of *chl1* mutations on stomatal aperture is that they affect stomatal responses to abscisic acid. Abscisic acid induces stomates to close. To determine if *chl1* mutants are altered in abscisic acid–induced stomatal closing, leaves from wild-type and mutant plants were placed in the light with a solution of 30 mM KCl to open the stomates and then treated with 1 and 10 μ M abscisic acid to induce closing. After 2 h, wild-type and mutant stomates closed to the same extent (Figure D-5A). As another test of abscisic acid response, light-induced stomatal opening was measured in the presence of abscisic acid, which inhibits opening. Both mutant and wild-type plants showed similar inhibition of stomatal opening by abscisic acid (Figure D-5B). We conclude that the reduced stomatal aperture in *chl1* mutants is not the result of effects on abscisic acid responses.

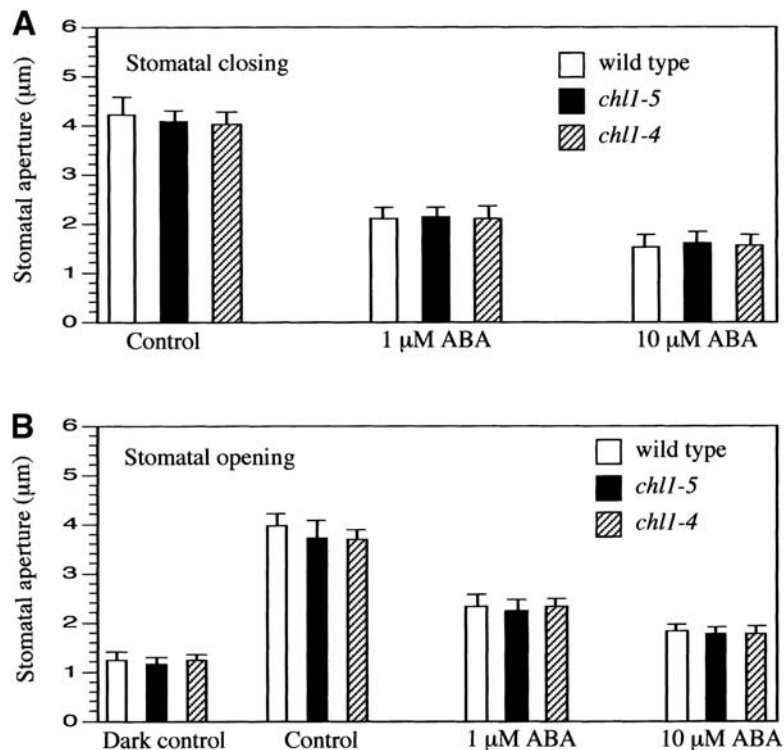


Figure D-5: Abscisic Acid Effects on Stomatal Opening and Closing of Wild-Type and *chl1* Mutant Plants. (A) Stomatal apertures were determined for wild-type and *chl1* mutant plants (*chl1-4* and *chl1-5*) undergoing abscisic acid (ABA)–induced stomatal closing as described in Methods. Data were averaged from three separate experiments; $n = 40$ aperture measurements per experiment. Error bars represent standard deviations. (B) Light-induced stomatal opening was measured in the wild type and *chl1* mutants with or without abscisic acid treatment. Dark control data represent stomatal apertures from leaves taken from seedlings kept in the dark for 5 h. Data were averaged from three separate experiments; $n = 40$ aperture measurements per experiment. Error bars represent standard deviations.

Nitrate Induces Depolarization in Wild-Type but Not *chl1* Mutant Guard

Cells. Further confirmation that CHL1 functions in guard cells was obtained by examining changes in membrane potential in guard cells in response to nitrate. In roots, CHL1 functions as an electrogenic nitrate transporter that depolarizes

the plasma membrane during nitrate uptake (Tsay et al., 1993; Wang et al., 1998). Thus, changes in membrane potential are indicative of nitrate uptake into the cell. To test for such activity in guard cells, the voltage-sensitive dye bis-oxonol was used to examine changes in membrane potential induced by nitrate. This dye has been used to examine membrane potential changes in potato leaves (Hedrich et al., 2001) and animal cells (Dall'Asta et al., 1997). When epidermal strips from wild-type plants were exposed to 100 mM NO_3^- , fluorescence signals from guard cells increased dramatically (indicating depolarization) and reached a peak after 30 s (Figures D-6A and 6E). Fluorescence increases also were observed with lower concentrations of NO_3^- : 30-s peak values were 80 for 10 mM NO_3^- and 120 for 50 mM NO_3^- . No significant increase in fluorescence was found in mutant guard cells (two *chl1* alleles tested) exposed to 100 mM NO_3^- (Figures D-6B and 6E) or 10 and 50 mM NO_3^- (data not shown). Cs^+ was used as the counter-ion in these experiments to minimize the effect of cation-induced depolarization (Tsay et al., 1993; Ichida et al., 1997). To show that fluorescence signals obtained with CsNO_3 were in the range observed with KCl, wild-type guard cells were treated with 100 mM KCl. The resulting fluorescence signals showed a similar time course of induction, but peak levels were a bit lower compared with those recorded at 100 mM CsNO_3 (Figures D-6C and 6E). *chl1* mutant guard cells showed an almost identical response to wild-type cells with 100 mM KCl (Figures D-6D and 6E). To demonstrate that these fluorescence increases

were caused by depolarization of the cellular membrane, wild-type and *chl1* mutant guard cells were depolarized with 50 μ M dinitrophenol (a H⁺ ionophore) in the presence of the bis-oxonol dye and found to display increased fluorescence (data not shown). These data show that nitrate induces *CHL1*-dependent membrane depolarization in guard cells, indicative of nitrate uptake into these cells.

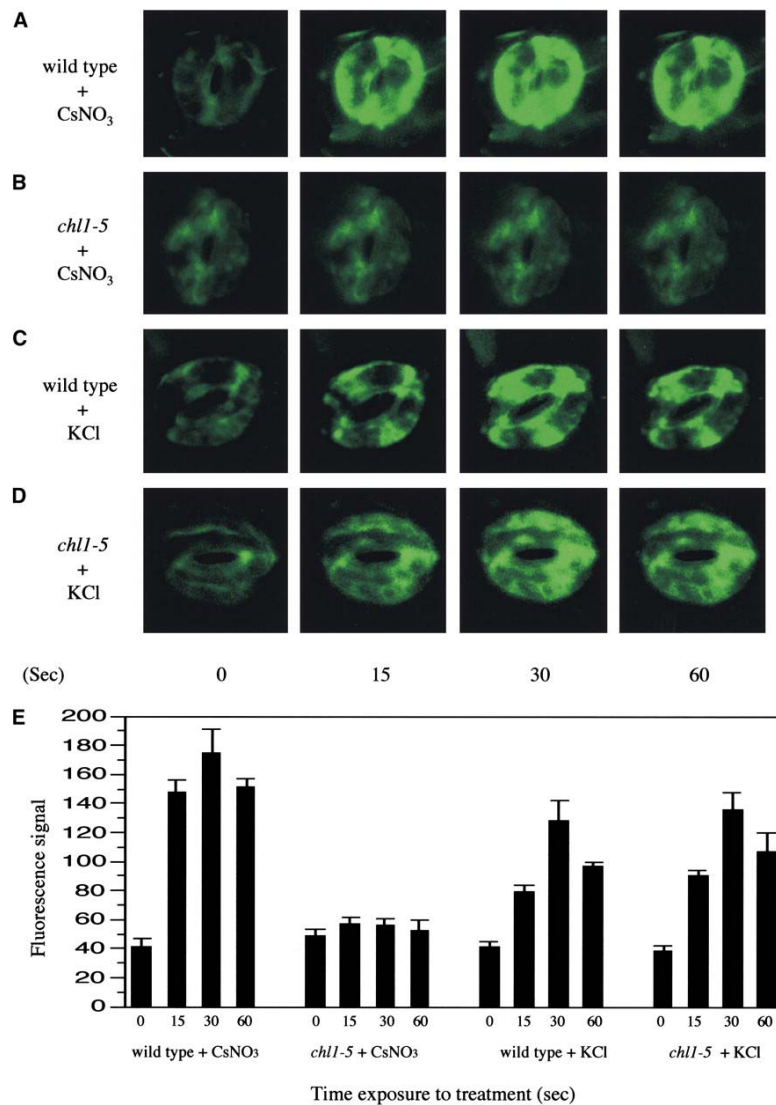


Figure D-6: Nitrate Induces Depolarization of Membrane Potential in Guard Cells of Wild-Type but Not *chl1* Plants. Depolarization of membrane potentials is represented as an increase in fluorescence. (A) Fluorescence from a representative wild-type guard cell at 0, 15, 30, and 60 s after adding CsNO₃ to a final concentration of 100 mM. (B) Fluorescence from a representative mutant (*chl1-5*) guard cell at 0, 15, 30, and 60 s after adding CsNO₃ to a final concentration of 100 mM. (C) Fluorescence from a representative wild-type guard cell at 0, 15, 30, and 60 s after adding KCl to a final concentration of 100 mM. (D) Fluorescence from a representative mutant (*chl1-5*) guard cell at 0, 15, 30, and 60 s after adding KCl to a final concentration of 100 mM. (E) Quantified fluorescence signals from the stomates for each genotype or treatment. Error bars represent standard deviations ($n = 5$).

***chl1* Mutant Plants Have Reduced Water Loss and Are Drought Tolerant.**

Given that *chl1* mutations affect stomatal aperture, one would expect these mutations to also affect transpiration and water loss in whole plants. To assess *CHL1* function in these processes, water loss was measured by two methods. First, the fresh weight of detached leaves was determined for wild-type and *chl1* plants during desiccation. For plants treated continuously with nitrate, water loss was faster in wild-type compared with mutant leaves (Figure D-7A, left and middle), whereas no significant difference was found between leaves from wild-type and mutant plants deprived of nitrate for 10 days (Figure D-7A, right). Second, water loss from mature plants undergoing drought stress for 20 days was measured. After 5 days of drought treatment, the rosette leaves in wild-type plants showed severe wilting and chlorosis, whereas the leaves of *chl1* mutants were turgid and remained green (Figure D-7B). Measurements of soil water content showed that water loss was faster from pots containing wild-type plants compared with pots containing mutants during the first 12 days of desiccation (Figure D-7C).

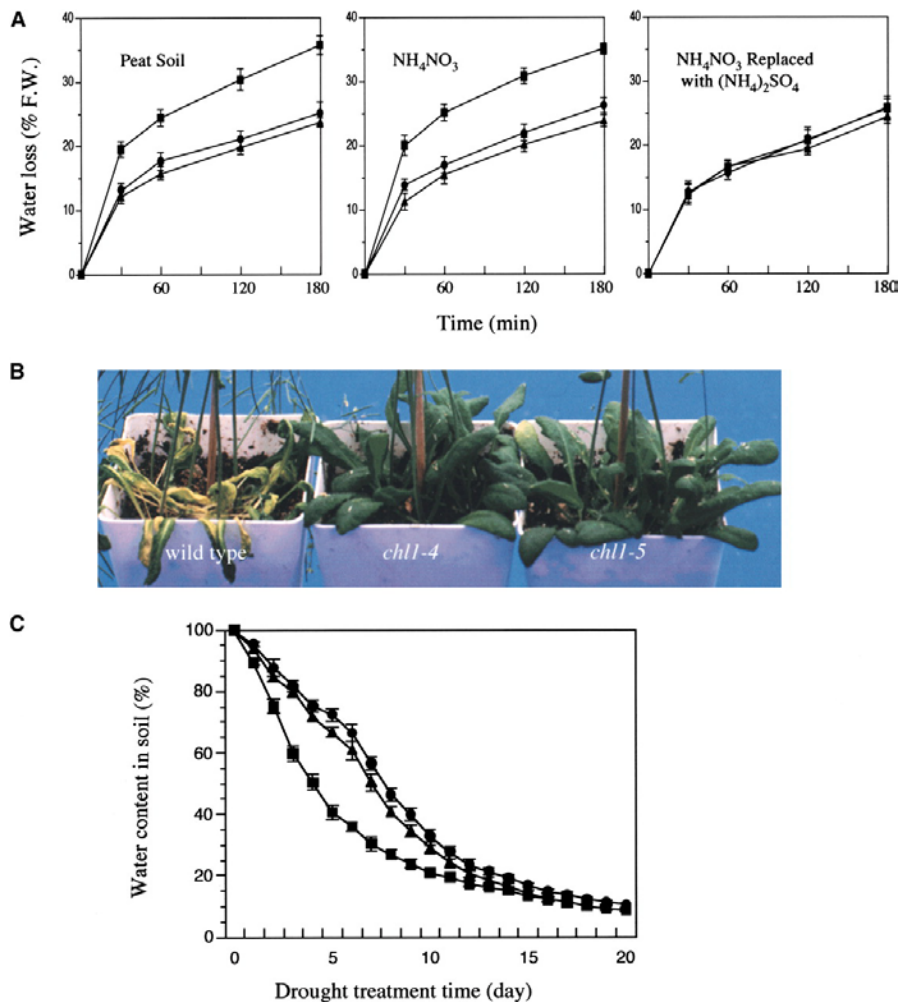


Figure D-7: *Chl1* Mutants Are More Drought Tolerant than Wild-Type Plants under Drought Stress. (A) Water loss from the leaves of wild-type and *chl1* plants grown with the indicated nitrogen sources. Data show percentage of initial fresh weight (F.W.) lost from leaves from three individual plants per genotype. Results from one of three experiments are shown. Squares, wild type; circles, *chl1-4*; triangles, *chl1-5*. Error bars represent standard deviations. (B) Wild-type and *chl1* mutant plants after 5 days of drought stress. Plants were irrigated for 22 days with nitrate-containing medium and then drought stressed by terminating irrigation. Ten pots per genotype were examined in one of three separate experiments. (C) Soil water contents were determined by weighing pots and plotted as a percentage of initial fresh weight in *chl1* and wild-type pots during desiccation. Pots were covered to minimize soil evaporation. Squares, wild type; circles, *chl1-4*; triangles, *chl1-5*. Error bars represent standard deviations.

DISCUSSION

Work on nitrate transporters in plants has focused on nitrate uptake into roots (reviewed by Crawford and Glass, 1998; Forde, 2000; Glass et al., 2001; Crawford and Forde, 2002). Some nitrate transporters are expressed in shoots, but there have been no indications that they function in guard cells. The results described here show that *CHL1* is expressed in guard cells and functions as a nitrate transporter and promotes stomatal opening when nitrate is the sole anion. Because *chl1* mutants grown with nitrate medium have reduced stomatal apertures and transpiration, *CHL1* is involved in these processes as well. Our results suggest that it is the impaired uptake of nitrate into guard cells of the mutant that results in reduced opening of stomates and in reduced stomatal aperture and transpiration. However, the relative importance of nitrate uptake compared with chloride uptake or malate accumulation in guard cells of *Arabidopsis* plants grown in soil is not known. At present, there is no evidence for an obligate role for nitrate/*CHL1* in stomatal function. However, it is possible that nitrate, chloride, and malate all play roles of different importance depending on the environmental conditions (such as the external nitrate and chloride concentrations and the time of day). In addition, reduced stomatal aperture and transpiration in the mutants could involve effects mediated by reduced nitrate uptake in the roots or nascent

organs in the mutants. Further experiments are needed to address these issues.

We performed some experiments to exclude any indirect effects of *chl1* mutations on transpiration. We examined stomatal distribution and density in leaves of *chl1* mutants and found no difference between wild-type and mutant plants (data not shown). These findings are consistent with results reported for lettuce, which when grown in N-limited medium has equivalent numbers of adaxial and abaxial stomata compared with plants supplied with NO_3^- (Broadley et al., 2001). It also appears that CHL1 does not serve as a general anion transporter because *chl1* mutations have little effect on stomatal opening when chloride is the only anion in the bath solution. We measured conductance in stomates induced to open in the dark by the depletion of CO_2 and found that *chl1* mutations impaired stomatal opening, showing that the effect from the *chl1* mutations is not dependent on an indirect effect on photosynthesis and intercellular CO_2 levels. Finally, we examined abscisic acid-induced responses on stomates and found no difference between the wild type and the mutants.

The findings reported here identify an anion transporter gene that functions in stomatal opening and indicate that nitrate can play a role in this process. These results were surprising because there has been little mention of nitrate in stomatal movements and no reports of a nitrate transporter being expressed or functioning in guard cells. Previous work had focused on Cl^- and

malate, which are well known as primary anions that counterbalance the influx of K^+ during stomatal opening, leading to models proposing that Cl^- transporters provide for anion transport during stomatal opening (Raschke and Fellows, 1971; Allaway, 1973; Raschke and Schnabl, 1978; Blatt, 2000; Assmann and Wang, 2001; Dietrich et al., 2001). However, there are data in the literature that have implicated nitrate as being important in stomatal movements. KNO_3 supports the opening of stomates as well as KCl in *Vicia* epidermal strips (Humble and Hsiao, 1969). In addition, the anion channels that mediate stomatal closure show their highest selectivity for nitrate. The R-type GCAC1 channel is fourfold more selective (Hedrich and Marten, 1993), and the S-type anion channels are 21 times more permeable to nitrate than to chloride (Schmidt and Schroeder, 1994). It would make sense that anion channels mediating stomatal closure would have a preference for nitrate if nitrate were important in mediating stomatal opening, as indicated by our results.

The results from our work also suggest that the presence or absence of nitrate in the growth environment can influence stomatal conductance and that this effect is mediated in part by the *CHL1* transporter. We found that water loss was greater for wild-type plants in nitrate-containing soil than for wild-type plants in soil depleted of nitrate or for *chl1* mutant plants in nitrate-replete soil (Figures D-7A and 7C). In addition, wild-type plants were more drought sensitive than *chl1* mutants, which are defective in nitrate uptake into guard

cells (Figure D-7B). Consistent with these findings are reports indicating that higher nitrate levels correlate with greater stomatal conductance in plants. Nitrate-fed soybeans have a higher transpiration rate per unit leaf area than nitrogen-fixing seedlings when both are under water stress (Ines Minguéz and Sau, 1989). A dramatic reduction in stomatal conductance is observed in lettuce plants when NH_4NO_3 is replaced in hydroponic medium with an equivalent concentration of CaSO_4 (Broadley et al., 2001). In cotton, stomates show increased sensitivity to water stress (close at higher water potentials) with decreasing levels of supplied nitrate (Radin and Ackerson, 1981). In addition, NH_4NO_3 -sufficient common beans were reported to suffer more drought-induced senescence than control plants grown under conditions of N_2 fixation after 10 days of desiccation stress (Lodeiro et al., 2000). These studies could not distinguish between general nitrogen effects and specific effects of nitrate. The finding that CHL1 functions as a nitrate transporter and supports stomatal opening provides evidence for a role for nitrate and provides insights into the relationship between stomatal conductance and nitrate.

METHODS

Plant Material and Growth. Wild-type and *chl1* mutant plants of *Arabidopsis thaliana* ecotype Columbia were grown in peat soil (Sun Gro Horticulture, Bellevue, WA) with fertilizer (Pete's 20-10-20; McConkey, Sumner, WA) or on

vermiculite irrigated with nutrient solution (pH 5.5, 6 mM NH_4NO_3 , 0.5 mM $\text{K}_2\text{HPO}_4\text{-KH}_2\text{PO}_4$, 0.2 mM MgSO_4 , 0.1 mM CaCl_2 , 0.05 mM $\text{FeSO}_4\text{-EDTA}$, 50 μM H_3BO_3 , 12 μM MnSO_4 , 1 μM ZnCl_2 , 1 μM CuSO_4 , and 0.2 μM Na_2MoO_4) for 18 days under a light cycle of 16 h of light and 8 h of dark at 24°C. The vermiculite-grown plants then were flushed five times with 400 mL of double-distilled water with a repeat treatment the next day. Half of the pots (16 total) then were irrigated with the same NH_4NO_3 nutrient solution described above; the other half were irrigated with the same solution except that the NH_4NO_3 was replaced with 6 mM $(\text{NH}_4)_2\text{SO}_4$. Both sets of plants grew and appeared the same after 10 days of treatment.

The *chl1-4* and *chl1-5* mutants were generated by γ -irradiation (Tsay et al., 1993). *chl1-4* has reduced levels of apparently full-length mRNA, but *chl1-5* has a deletion that results in no detectable mRNA (Tsay et al., 1993).

Constructs and Plant Transformation. CHL1 promoter- β -glucuronidase/green fluorescent protein fusion constructs and plant transformation were generated as described (Guo et al., 2001).

Light and Confocal Microscopy. Histochemical localization of β -glucuronidase was performed and observed using light microscopy as described (Guo et al., 2001). Green fluorescent protein and immunolocalization (using antibodies raised against the N-terminal 15 amino

acids of CHL1) were analyzed using a confocal laser scanning microscope as described (Guo et al., 2001).

Stomatal Aperture Measurements. Plants were grown for 4 weeks in peat soil and then placed in the dark overnight to close the stomata. Detached leaves then were floated in 30 mM KNO₃ or KCl solutions (with 0.1 mM CaCl₂ and 5 mM Mes-KOH, pH 6.15) under light (80 $\mu\text{mol}\cdot\text{m}^{-2}\cdot\text{s}^{-1}$) for 3 h to induce stomatal opening, which was measured as aperture width (Pei et al., 1997; Szyroki et al., 2001). For plants grown in different nitrogen sources or treated with CO₂-free air, detached leaves were blended and the resulting epidermal fragments were taken to examine stomatal aperture immediately (Pei et al., 1997; Szyroki et al., 2001). To measure stomatal closing, detached leaves were floated in 30 mM KCl solution as described above under light for 2 h. After 2 h, abscisic acid (Sigma) was added to the buffer solution. After an additional 2 h, leaves were blended and apertures were measured. To measure abscisic acid effect on stomatal opening, 4-week-old seedlings were kept in the dark for 5 h to close the stomata. Detached leaves were floated in 30 mM KCl solution with or without abscisic acid for 2 h under light. Detached leaves then were blended and stomatal apertures were measured.

Stomatal Conductance Measurements. Stomatal conductance was measured using the infrared gas analyzer technique (Hedrich et al., 2001) with

the LI-6400 Portable Photosynthesis System (Li-Cor, Lincoln, NE). Plants were grown on vermiculite and irrigated with NH_4NO_3 nutrient solution as described above. Four-week-old plants were transferred from pots to 10-mL flasks with 8 mL of NH_4NO_3 nutrient solution, grown for 12 h under continuous light at 24°C , and then kept in the dark for 5 h to close the stomates. The fully expanded leaves of wild-type and *chl1* mutant plants were used to examine stomatal conductance in the dark at 24°C . Gas flow through the cuvette was 500 mL/min. The CO_2 level was switched from 400 to 0 mL/L (CO_2 -free air) when the leaf showed a stable gas-exchange rate and stomatal conductance was measured. Detached leaves were taken to examine stomatal aperture after 40 min of CO_2 -free air treatment, as described (Pei et al., 1997; Szyroki et al., 2001).

Water Loss and Drought Tolerance Measurements. Water loss from the leaves of wild-type and *chl1* plants grown with the indicated nitrogen sources was determined as described (Figure D-7A; Leung et al., 1997; Wang et al., 2001). Plants were irrigated for 22 days and then drought stressed by terminating irrigation, as described previously (Vartanian et al., 1994; Pei et al., 1998).

Guard Cell Protoplast Isolation and Nitrate Measurements. Guard cell protoplasts were isolated as described (Miedema and Assmann, 1996) with some modifications. After 3 h of incubation in 30 mM KNO_3 solution, as

described above, detached leaves were blended for 1 min and filtered through a 100- μm nylon mesh. Harvested epidermal peels were transferred to a conical flask containing 50 mL of digestion solution 1 (0.7% [w/v] Cellulysin [Calbiochem, La Jolla, CA], 0.1% [w/v] PVP40 [Sigma], and 0.25% [w/v] BSA in basic medium [5 mM MES, pH 5.5, 0.5 mM CaCl_2 , 0.5 mM MgCl_2 , 10 mM KH_2PO_4 , 0.5 mM ascorbic acid, 450 mM sorbitol]) and digested for up to 2 h in a vigorously shaking water bath. When all mesophyll cells were digested, the peels were filtered and transferred to digestion solution 2 (1.3% [w/v] Cellulase RS [Yakult Honsha, Tokyo, Japan], 0.0075% [w/v] Pectolyase Y-23 [Seishin, Tokyo, Japan], and 0.25% [w/v] BSA in basic medium). Peels were examined for lack of intact guard cells. When digested, protoplasts were filtered through a 10- μm nylon mesh folded into four layers and washed with the basal medium. Guard cell protoplasts were harvested by filtering with a 10- μm nylon mesh. Cells were collected by centrifugation at 200g for 4 min. Cell numbers were counted in the samples using a hemacytometer (Hausser Scientific, Horsham, PA). The purity of guard cell protoplasts was ~92% (1000 cells counted). An average diameter of 6 μm was used to calculate the volume of a protoplast. The cells ($\sim 1 \times 10^8$) were ground frozen into a powder. Distilled water (0.5 mL) was added to the ground pellet; this was boiled for 5 min and then spun. The supernatant was used to measure nitrate concentration by HPLC (Thayer and Huffaker, 1980).

Imaging Membrane Potential Changes in Intact Guard Cells. Epidermal strips from detached leaves were made as described (Pei et al., 1997) and then incubated in loading buffer (5 mM Mes-KOH, pH 5.7, 0.25 mM KCl, and 1 mM CaCl₂). Peels were mounted onto a copper mesh as described (Allen et al., 1999) and then incubated with 200 μ L of loading buffer containing 1 μ M dye [bis-(1,3-dibutylbarbituric acid)trimethine oxonol (B-438; Molecular Probes, Eugene, OR)] for 10 min. B-438 fluorescent signals were detected using a confocal laser scanning microscope (MRC-600; Bio-Rad). The dye was excited using a fluorescein isothiocyanate filter set (488 nm), and images were collected using an emission filter (530 \pm 15 nm). The images were collected at 0, 15, 30, and 60 s after adding CsNO₃ or KCl solutions. Signal intensities were quantified using Photoshop (Adobe Systems, San Jose, CA).

ACKNOWLEDGEMENTS

We thank June Kwak, Nathalie Leonhardt, Gethyn Allen, and Julian Schroeder for their invaluable technical advice and assistance with guard cell measurements, and Rongchen Wang and Rudi Tischner for their advice in measuring nitrate by HPLC. This work was supported by National Institutes of Health Grant GM40672.

REFERENCES CITED

Allaway, W.G. (1973). Accumulation of malate in guard cells of *Vicia faba* during stomatal opening. *Planta* 110, 63–70.

Allen, G.J., Kuchitsu, K., Chu, S.P., Murata, Y., and Schroeder, J.I. (1999). *Arabidopsis abi1-1* and *abi2-1* mutations impair abscisic acid induced cytosolic calcium rises in guard cells. *Plant Cell* 11, 1785–1798.

Assmann, S.M., and Wang, X.-Q. (2001). From milliseconds to millions of years: Guard cells and environmental responses. *Curr. Opin. Plant Biol.* 4, 421–428.

Blatt, M.R. (2000). Cellular signaling and volume control in stomatal movements in plants. *Annu. Rev. Cell Dev. Biol.* 16, 221–241.

Broadley, M.R., Escobar-Gutierrez, A.J., Burns, A., and Burns, I.G. (2001). Nitrogen-limited growth of lettuce is associated with lower stomatal conductance. *New Phytol.* 152, 97–106.

Crawford, N.M., and Forde, B.G. (2002). Molecular and developmental biology of inorganic nitrogen nutrition. In *The Arabidopsis Book*, E. Meyerowitz and C. Somerville, eds (Rockville, MD: American Society of Plant Biologists).

Crawford, N.M., and Glass, A.D.M. (1998). Molecular and physiological aspects of nitrate uptake in plants. *Trends Plant Sci.* 3, 389–395.

Dall'Asta, V., Gatti, R., Orlandini, G., Rossi, P.A., Rotoli, B.M., Sala, R., Bussolati, O., and Gazzola, G.C. (1997). Membrane potential changes visualized in complete growth media through confocal laser scanning microscopy of bis-oxonol-loaded cells. *Exp. Cell Res.* 231, 260–268.

Dietrich, P., and Hedrich, R. (1994). Interconversion of fast and slow gating modes of GCAC1, a guard cell anion channel. *Planta* 195, 301–304.

Dietrich, P., Sanders, D., and Hedrich, R. (2001). The role of ion channels in light-dependent stomatal opening. *J. Exp. Bot.* 52, 1959–1967.

Forde, B.G. (2000). Nitrate transporters in plants: Structure, function and regulation. *Biochim. Biophys. Acta* 1465, 219–235.

Gaedeke, N., Klein, M., Kolukisaoglu, U., Forestier, C., Muller, A., Ansoerge, M., Becker, D., Mamnun, Y., Kuchler, K., Schulz, B., Mueller-Roeber, B., and Martinoia, E. (2001). The *Arabidopsis thaliana* ABC transporter *AtMRP5* controls root development and stomata movement. *EMBO J.* 20, 1875–1887.

Glass, A.D.M., Brito, D.T., Kaiser, B.N., Kronzucker, H.J., Kumar, A., Okamoto, M., Rawat, S.R., Siddiqi, M.Y., Silim, S.M., Vidmar, J.J., and Zhuo, D. (2001). Nitrogen transport in plants, with an emphasis on the regulation of fluxes to match plant demand. *J. Plant Nutr. Soil Sci.* 164, 199–207.

Guo, F.-Q., Wang, R., Chen, M., and Crawford, N.M. (2001). The Arabidopsis dual-affinity nitrate transporter gene *AtNRT1.1* (*CHL1*) is activated and functions in nascent organ development during vegetative and reproductive growth. *Plant Cell* 13, 1761–1777.

Hedrich, R., and Marten, I. (1993). Malate-induced feedback regulation of plasma membrane anion channels could provide a CO₂ sensor to guard cells. *EMBO J.* 12, 897–901.

Hedrich, R., Spidola, N., Savchenko, G., Felle, H.H., Kaiser, W.M., and Heber, U. (2001). Changes in apoplastic pH and membrane potential in leaves in relation to stomatal responses to CO₂, malate, abscisic acid or interruption of water supply. *Planta* 213, 594–601.

Humble, G.D., and Hsiao, T.C. (1969). Specific requirement of potassium for light-activated opening of stomata in epidermal strips. *Plant Physiol.* 44, 230–234.

Ichida, A.M., Pei, Z.M., Baizabal-Aguirre, V.M., Turner, K.J., and Schroeder, J.I. (1997). Expression of a Cs⁺-resistant guard cell K⁺ channel confers Cs⁺-resistant, light-induced stomatal opening in transgenic Arabidopsis. *Plant Cell* 9, 1843–1857.

Ines Minguez, M., and Sau, F. (1989). Response of nitrate-fed and nitrogen-fixing soybeans to progressive water stress. *J. Exp. Bot.* 213, 497–502.

Kwak, J., Murata, Y., Baizabal-Aguirre, V.M., Merrill, J., Wang, M., Kemper, A., Hawke, S.D., Tallman, G., and Schroeder, J.I. (2001). Dominant negative guard cell K⁺ channel mutants reduce inward-rectifying K⁺ currents and light-induced stomatal opening in Arabidopsis. *Plant Physiol.* 127, 473–485.

Leonhardt, N., Bazin, I., Richaud, P., Marin, E., Vavasseur, A., and Forestier, C. (2001). Antibodies to the CFTR modulate the turgor pressure of guard cell protoplasts via slow anion channels. *FEBS Lett.* 494, 15–18.

Leonhardt, N., Marin, E., Vavasseur, A., and Forestier, C. (1997). Evidence for the existence of a sulfonyleurea-receptor-like protein in plants: Modulation of stomatal movements and guard cell potassium channels by sulfonyleureas and potassium channel openers. *Proc. Natl. Acad. Sci. USA* 94, 14156–14161.

- Leonhardt, N., Vavasseur, A., and Forestier, C. (1999). ATP binding cassette modulators control abscisic acid-regulated slow anion channels in guard cells. *Plant Cell* 11, 1141–1152.
- Leung, J., Merlot, S., and Giraudat, J. (1997). The Arabidopsis *ABSCISIC ACID-INSENSITIVE2 (ABI2)* and *ABI1* genes encode homologous protein phosphatases 2C involved in abscisic acid signal transduction. *Plant Cell* 9, 759–771.
- Liu, K.-H., Huang, C.-Y., and Tsay, Y.-F. (1999). CHL1 is a dual-affinity nitrate transporter of Arabidopsis involving multiple phases of nitrate uptake. *Plant Cell* 11, 865–874.
- Lodeiro, A.R., Gonzalez, P., Hernandez, A., Balague, L.J., and Favelukes, G. (2000). Comparison of drought tolerance in nitrogen-fixing and inorganic nitrogen-grown common beans. *Plant Sci.* 154, 31–41.
- Miedema, H., and Assmann, S.M. (1996). A membrane-delimited effect of internal pH on the K⁺ outward rectifier of *Vicia faba* guard cells. *J. Membr. Biol.* 154, 227–237.
- Pei, Z.M., Ghassemian, M., Kwak, C.M., McCourt, P., and Schroeder, J.I. (1998). Role of farnesyltransferase in ABA regulation of guard cell anion channels and plant water loss. *Science* 282, 287–290.
- Pei, Z.M., Kuchitsu, K., Ward, J.M., Schwarz, M., and Schroeder, J.I. (1997). Differential abscisic acid regulation of guard cell slow anion channels in Arabidopsis wild type and *abi1* and *abi2* mutants. *Plant Cell* 9, 409–423.
- Pilot, G., Lacombe, B., Gaymard, F., Cherel, I., Boucherez, J., Thibaud, J.-B., and Sentenac, H. (2001). Guard cell inward K⁺ channel activity in *Arabidopsis* involves expression of the twin channel subunits KAT1 and KAT2. *J. Biol. Chem.* 276, 3215–3221.
- Radin, J.W., and Ackerson, R.C. (1981). Water relations of cotton plants under nitrogen deficiency. III. Stomatal conductance, photosynthesis, and abscisic acid accumulation during drought. *Plant Physiol.* 67, 115–119.
- Raschke, K., and Fellows, M.P. (1971). Stomatal movement in *Zea mays*: Shuttle of potassium and chloride between guard cells and subsidiary cells. *Planta* 101, 296–316.
- Raschke, K., and Schnabl, H. (1978). Availability of chloride affects the balance between potassium chloride and potassium malate in guard cells of *Vicia faba* L. *Plant Physiol.* 62, 84–87.

Roelfsema, M.R.G., and Hedrich, R. (2002). Studying guard cells in the intact plant: Modulation of stomatal movement by apoplastic factors. *New Phytol.* 153, 425–431.

Schmidt, C., and Schroeder, J.I. (1994). Anion selectivity of slow anion channels in the plasma membrane of guard cells: Large nitrate permeability. *Plant Physiol.* 106, 383–391.

Schroeder, J.I., Allen, G.J., Hugouvieux, V., Kwak, J.M., and Waner, D. (2001). Guard cell signal transduction. *Annu. Rev. Plant Physiol. Plant Mol. Biol.* 52, 627–658.

Schroeder, J.I., and Keller, B.U. (1992). Two types of anion channel currents in guard cells with distinct voltage regulation. *Proc. Natl. Acad. Sci. USA* 89, 5025–5029.

Szyroki, A., Ivashikina, N., Dietrich, P., Roelfsema, M.R., Ache, P., Reintanz, B., Deeken, R., Godde, M., Felle, H., Steinmeyer, R., Palme, K., and Hedrich, R. (2001). KAT1 is not essential for stomatal opening. *Proc. Natl. Acad. Sci. USA* 98, 2917–2921.

Talbott, L.-D., and Zeiger, E. (1998). The role of sucrose in guard cell osmoregulation. *J. Exp. Bot.* 49, 329–337.

Thayer, J.R., and Huffaker, R.C. (1980). Determination of nitrate and nitrite by HPLC: Comparison with other methods for nitrate determination. *Anal. Biochem.* 102, 110–119.

Touraine, B., and Glass, A.D.M. (1997). NO_3^- and ClO_3^- fluxes in the *chl1-5* mutant of *Arabidopsis thaliana*: Does the *CHL1-5* gene encode a low-affinity NO_3^- transporter? *Plant Physiol.* 114, 137–144.

Tsay, Y.-F., Schroeder, J.I., Feldmann, K.A., and Crawford, N.M. (1993). A herbicide sensitivity gene *CHL1* of *Arabidopsis* encodes a nitrate-inducible nitrate transporter. *Cell* 72, 705–713.

Vartanian, N., Marcotte, L., and Giraudat, J. (1994). Drought rhizogenesis in *Arabidopsis thaliana*: Differential responses of hormonal mutants. *Plant Physiol.* 104, 761–767.

Wang, R., Liu, D., and Crawford, N.M. (1998). The *Arabidopsis CHL1* protein plays a major role in high affinity nitrate uptake. *Proc. Natl. Acad. Sci. USA* 95, 15134–15139.

Wang, X.Q., Hemayet, U., Jones, A.M., and Assmann, S.M. (2001). G protein regulation of ion channels and abscisic acid signaling in *Arabidopsis* guard cells. *Science* 292, 2070–2072.

The text of Section D of the Appendix is a reprint of the material as it appears in *The Plant Cell*, Guo, F.-Q., Young, J., Crawford, N.M. (2003). I contributed to the data for Figure D-4A.